Novel Roles for Heterochromatin and Nuclear RNAi in *C. elegans* Dosage Compensation

by

Michael Bradly Davis

A dissertation submitted in partial fulfillment
of the requirements for the degree of
Doctor of Philosophy
(Molecular, Cellular, and Developmental Biology)
in The University of Michigan
2021

Doctoral Committee:

Associate Professor Györgyi Csankovszki, Chair
Associate Professor Laura Buttitta
Professor Kenneth M. Cadigan
Associate Professor Sundeep Kalantry

Michael B. Davis

mbradlyd@umich.edu

ORCID iD: 0000-0003-3416-3038

Acknowledgements

I would like to thank Dr. Györgyi Csankovszki and the Csankovszki lab, as well as my thesis committee members Dr. Laura Buttitta, Dr. Sundeep Kalantry, Dr. Ken Cadigan for all their help throughout the process. I would also thank my wife Molly Davis and my family for all their support.

Table of Contents

Chapter 3: Dual Roles for Nuclear RNAi in *C. elegans* Dosage Compensation

Chapter 4: Conclusions and Future Directions

List of Figures

List of Tables

Abstract

Dosage compensation involves chromosome-wide gene regulatory mechanisms which impact higher order chromatin structure and are crucial for organismal health. Dosage compensation in *C. elegans* hermaphrodites is initiated by the silencing of *xol-1* and subsequent activation of the Dosage Compensation Complex (DCC) which compacts both hermaphrodite X chromosomes and reduces transcriptional output by twofold. While it is known that the DCC is responsible for dosage compensation in *C. elegans*, the full complement of DCC-mediated mechanisms contributing to X chromosome repression is still unknown. In this thesis I describe two conserved chromatin and gene regulatory pathways which act in conjunction with the DCC to promote dosage compensation. The H3K9me3 histone methyltransferases (*met-2, set-25*) and two genes encoding nuclear lamina localized proteins (*cec-4, lem-2)* constitute a pathway which anchors the hermaphrodite X chromosomes to the nuclear lamina to facilitate dosage compensation. The nuclear RNAi Argonautes *hrde-1* and *nrde-3,* as well as the piRNA Argonaute *prg-1* also contribute to dosage compensation. These Argonaute genes repress *xol-1* transcripts, while also fulfilling a *xol-1*-independent role which includes compaction of the X chromosomes. These data indicate novel endogenous roles and physiological significance for the H3K9me3 heterochromatin and Argonaute pathways in *C. elegans* dosage compensation.

CHAPTER 1

Introduction to Dosage Compensation and Nuclear RNAi

The evolution of sex chromosomes and sex chromosome dosage compensation

The evolution of sex chromosomes has allowed for species with distinct sexes to confer sexual dimorphism through differences in the genetic content of one set of chromosomes. Sex chromosomes are designated as XX and XY in species where the males are heterogametic (XY), or ZZ and ZW in species where the females are heterogametic (ZW) (for a review, see Bull, 1983). The evolution of sex chromosomes is initiated when a pair of autosomes acquire a sex-determining gene (Charlesworth, 1991). After a sex-determining gene is acquired by a chromosome, there is reduced meiotic recombination between the sex determination gene-bearing chromosome and its partner (Rice, 1996; Charlesworth, 1996). In the heterogametic sex, (XY males in humans) this lack of recombination contributes to the degradation of the sex-determination gene-bearing Y chromosome to the point at which it eventually contains only the sex determining factor along with a small complement of genes (Muller, 1918; Charlesworth, 1978). However, with the evolutionary development of sex chromosomes and the heterogametic (XY) state, the XY sex is also faced with the emergence of hemizygosity for the entire X chromosome (Ohno, 1967). In other words, where the ancestral species and homogametic sex are XX and thus contain two copies of X-linked genes, the newly evolved heterogametic XY sex only contains one copy of the X-linked genes.

The 2-1 difference in the ratio of X chromosome gene dose between XX-XY (or Z chromosome gene dose in ZZ-ZW) sexes presents the problem of hemizygosity (Ohno, 1967). This problem is reflected in the fact that human monosomies for all autosomes are lethal, except for rare instances of chromosome 21 monosomy, in which case just 9 living children have been identified (Nguyen, *et al.,* 2009). At a molecular level, the balancing of sex chromosome gene expression is crucial to diploid organisms as there are many X-linked genes encoding proteins which function in complexes with autosomal protein gene-products, the stoichiometry of which is sensitive to gene dose (Rice and McLysaght, 2017). Moreover, when a diploid organism is missing a copy of an entire chromosome, X-linked recessive mutations can present a disease state which would normally be masked by a healthy allele on the partner chromosome (Fisher, 1935). Thus, while sex determination has carved out sex chromosome mechanisms to efficiently develop sexual dimorphism, X-linked gene dose must also be accounted for, such that male X chromosome gene expression at dose-sensitive loci remains similar to the ancestral or female (XX) state (Ohno, 1967). The balancing of sex chromosome gene expression between sexes is thus referred to as dosage compensation.

X chromosome dosage compensation mechanisms are widely variable across vertebrates. In many cases the sex chromosome gene expression is incompletely balanced, and in some cases the balancing is sparse. In eutherian (placental) mammals such as mice and humans, the XX females will inactivate one X chromosome at random, so in every cell a sole random maternal or paternal X chromosome is active and X chromosome gene expression is balanced between the sexes (Loda, 2019; Graves *et al.,* 2015). On the other hand, Marsupial mammals always silence the paternal X chromosome to accomplish similar levels of complete dosage compensation (Cooper *et al.,* 1993). Both Marsupial and placental mammals utilize different long noncoding

RNAs as the main driver of silencing a single X chromosome (Grant *et al.,* 2012; Graves *et al.,* 2015). Monotreme egg-laying mammals like the platypus have 5 copies of the X and Y sex chromosomes and rather than a global silencing mechanism a very partial gene-by-gene dosage compensation mechanism appears to be adopted (Murtagh, 1977; Julien *et al.,* 2012). The ZZ-male ZW-female sex chromosomes of chickens also exhibit partial dosage compensation, with the ZZ-ZW Z-linked gene expression ratio about 1.33 (Julien *et al.,* 2012). With many Z-linked genes completely uncompensated and some equally expressed in both sexes a gene-by-gene mechanism for dosage compensation is the current model for chickens (Julien *et al.,* 2012; Loda, 2019). Fish exhibit a partial dosage compensation in ZZ males which appears to be characterized by a region with high DNA methylation (Shao *et al.,* 2014). Although not many studies have been conducted on reptilian dosage compensation several species of snake appear to be completely devoid of dosage compensation with partial dosage compensation being a theme in some still (Vicoso *et al.,* 2013). While sex determination and dosage compensation mechanisms differ across metazoans, the two processes are inextricably linked in many closely examined vertebrate with fish being a notable exception (Chen *et al.,* 2014). The mechanistic details of sex chromosome dosage compensation have been best described in four of the most widely studied genetic systems; mice, human cells, the fruit fly *Drosophila* and the nematode *C. elegans* (For a summary, see figure 1.1). In these systems, the complete annotation of sex-linked and autosomal genes has allowed for more accurate genome-wide expression studies to more accurately assess the effects of dosage compensation mutations on the precise balance of sex chromosome to autosome gene expression (Gu and Walters, 2017).

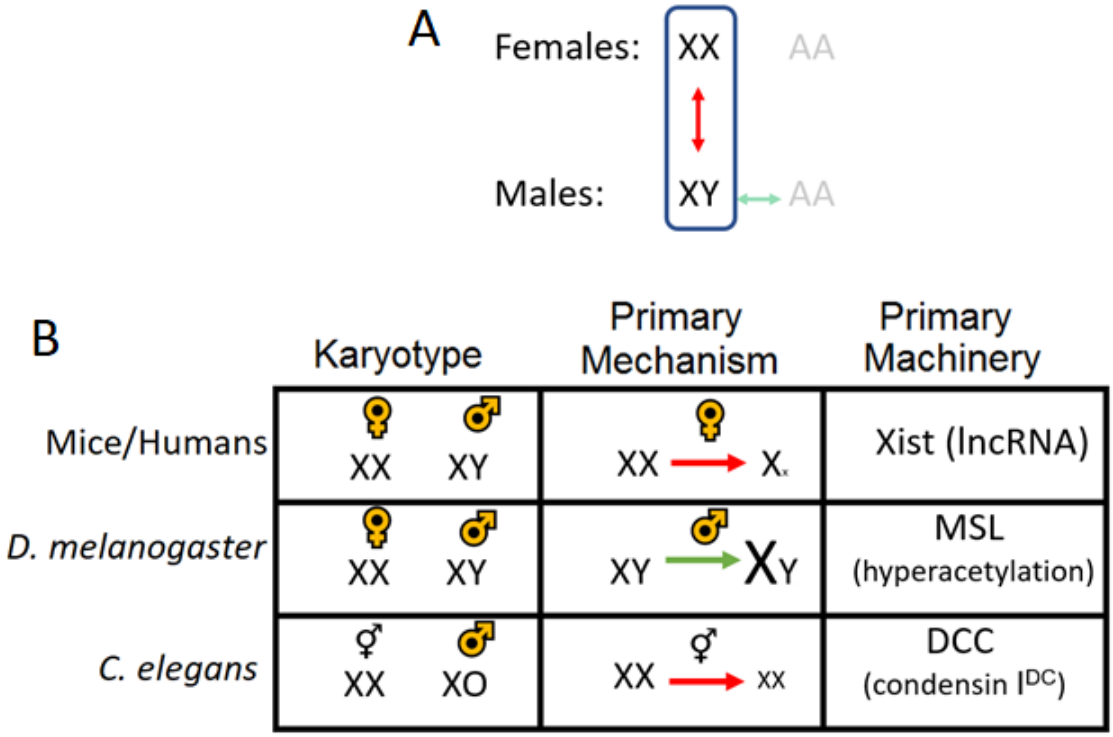

Figure 1.1 Diverse Mechanisms Achieve Dosage Compensation in Metazoans A. The balancing of sex chromosome gene expression is achieved by dosage compensation. B. The Karyotype and sexes of each of the three most widely studied model systems. Female mice/humans dosage compensate via random inactivation of a single X chromosome, mediated by the lncRNA *xist.* Male *Drosophila* dosage compensate via the two-fold upregulation of their single X chromosome, mediated by the MSL complex through hyperacetylation of gene bodies. Hermaphrodite *C. elegans* dosage compensate via the downregulation of both X chromosomes by two-fold, mediated by condensin-containing DCC.

Moreover, as the paradigm of sex chromosome dosage compensation involves chromosome-wide gene regulatory systems, studies employing chromosome capture techniques to dosage compensated chromosomes have provided a high-resolution chromosome scale view on how sex chromosomes are differentially organized from autosomes. The Hi-C technique is a high-throughput experimental approach which provides a genome-wide view of the frequency of interactions between all regions of every chromosome (Belton *et al.,* 2012). This technique has been applied to mammalian cells, *Drosophila,* and *C. elegans* within the context of sex chromosome dosage compensation. The remainder of this section will the summarize key

findings regarding dosage compensation in these model systems, where such a wealth of data has been compiled from various genetic, molecular, and high-throughput approaches.

Sex determination and dosage compensation in mice and humans

In eutherian mammals, females have two X chromosomes and males have a single X chromosome and a Y chromosome. The conserved SRY gene on the Y chromosome of males is sufficient to produce the male sex (Koopman, *et al.,* 1991). The primary mode of sex chromosome dosage compensation (X chromosome inactivation or XCI) entails the random inactivation of a single X chromosome in females (Lyon, 1961). XCI in humans results in repression of ~80-88% of X-linked genes and possibly 93-97% of X-linked genes in mice (Balaton *et al.,* 2015; Berlech *et al.,* 2015). The fact that more human X-Y gene pairs are expressed from both sex chromosomes than mice may account for the relatively increased tolerance of the XO state in mice, which unlike humans, presents fewer of the phenotypes associated with Turner syndrome (Bellot *et al.,* 2014).

Mammalian XCI is coordinated by an ~800KB region termed the X inactivation center (XIC) (Nora *et al.,* 2012). Several long noncoding RNAs (lncRNAs) are encoded at this locus, which are responsible for the initiation of X chromosome inactivation (Anguera *et al.,* 2011; Ogawa *et al.,* 2003; Stavropoulos *et al.,* 2005; Chureau *et al.,* 2011; Sun *et al.,* 2013; Tian *et al.,* 2010; Furlan *et al.,* 2018; Nora *et al.,* 2012). The *Xist* lncRNA ultimately serves the most important role, acting *in cis* to trigger the transcriptional repression and heterochromatinization of the X chromosome to be silenced (Penny *et al.,* 1996; Loda, 2019). The *Tsix* lncRNA, which plays a larger role in mice than humans overlaps with the *Xist* locus, but is transcribed in the opposite direction and encompasses a larger genomic region (Lee *et al.,* 1999). *Tsix* lncRNA serves as a

negative regulator of *Xist,* and when female humans lose on functional copy of *Tsix* the X chromosome with the functional copy is consistently inactivated (Lee *et al.,* 1999).

Within the ~17KB *Xist* lncRNA itself there are repetitive elements termed A-F tandem repeats (Brockdorf *et al.,* 1992). The A-F repeats are conserved in both mice and humans (Brown *et al.,* 1992). Studies in mice deleting the individual elements from a transgenic *Xist* sequence and measuring the effect on gene silencing and *Xist* localization have highlighted specific functional roles of each element. The 5' most situated element is the A repeat, which is required for gene silencing, the B and C elements are required for PRC-1 recruitment, which promotes histone modifications on the inactive X, and the E element is required for the spreading of *Xist* along the length of the X chromosome (Wutz *et al.,* 2002; Yamada *et al.,* 2015; Almeida *et al.,* 2017; Loda *et al.,* 2017; Pintacuda *et al.,* 2017; Colognori *et al.,* 2019). A number of heterochromatin marks are coordinately enriched regionally on the inactivated X, including H3K27me3, H4K20me1, and H3K9me3 and H2A ubiquitylation (Plath *et al.,* 2003; Silva *et al.,* 2003; Wang *et al.,* 2004; Napoles *et al.,* 2007; Kohlmaier, *et al.,* 2004). The inactive X is also depleted of histone acetylation marks which would typically be found on active chromatin (Mikami *et al.,* 2014). Moreover, CpG islands which are typically found near gene promoters to be hypomethylated at active genes exhibit high levels of DNA methylation on the inactivate X (Gendrel *et al.,* 2012) Thus, a chromatin landscape emerges on the inactive X that is consistent with a heterochromatin state.

As mammalian dosage compensation is mediated through *XIST*, there have been numerous studies to determine the various proteins which physically interact with this lncRNA. Since the activation of *XIST* results in a heterochromatinized inactive X chromosome which is almost completely silent, these studies have been important to understand the multiple repressive

mechanisms which *Xist* facilitates. Indeed, *Xist* promotes the recruitment of several factors mediating histone deacetylation, histone methylation, X chromosome subnuclear localization changes, and *Xist* RNA methylation all of which in part effect silencing of the X chromosome. In 2015 multiple efforts were made to identify protein interactors of the *Xist* lncRNA, and subsequent work has characterized several key proteins (Chu *et al.,* 2015; McHugh, *et al.,* 2015; Minajigi *et al.,* 2015).

The SPEN protein is one *Xist*-interactor which is crucial for *Xist*-mediated gene silencing (Monfort *et al.,* 2015). The model for SPEN function in XCI involves activation of the SMRT protein which activates the HDAC3 histone deacetylase, resulting in widespread histone deacetylation on the X chromosome contributing to gene silencing (Guenther *et al.,* 2001; Shi *et al.,* 2001; You *et al.,* 2013; Mikami *et al.,* 2013; Chu *et al.,* 2015; McHugh *et al.,* 2015; Monfort *et al.,* 2015). The RBM15 and its paralog RBM15b also interact with *Xist* (Chu *et al.,* 2015; McHugh *et al.,* 2015; Minajigi *et al.,* 2015). These proteins are part of the RNA A6 methylation complex and are required for RNA A6 methylation of *Xist* at 78 residues (Patil *et al.,* 2016). Although the function of RNA methylation with respect to gene repression is incompletely understood, deletion of the 78 sites which are A6 methylated on *Xist* results in mild X de-repression, which indicates that this process contributes to XCI but to a relatively minor degree (Patil *et al.,* 2016). A third interactor of *Xist* is hnRNP K (heterogenous nuclear ribonucleoprotein K) (Chu *et al.,* 2015; McHugh *et al.,* 2015; Minajigi *et al.,* 2015). hnRNP K recruits PRC-1 to the X chromosome, which in turn recruits PRC-2 (Almeida *et al.,* 2017; Pintacuda *et al.,* 2017). The PRC-1 and PRC-2 proteins represent the polycomb proteins which mediate histone 3 lysine 27 trimethylation (H3K27me3) and histone 2A Lysine 119 Ubiquitylation (H2AK119ub), -two heterochromatin modifications enriched on the inactive X

chromosome (Wang *et al.,* 2001; Plath *et al.,* 2003; Silva *et al.,* 2003; Napoles *et al.,* 2004). The LBR (Lamina B Receptor) protein is localized to the nuclear lamina and also interacts with *Xist* through a specific domain on the lncRNA (Gruenbaum *et al.,* 2005). However, it has been shown that the active X chromosomes of both male and female cells are both recruited to the nuclear lamina, and the level of X-linked gene derepression in LBR mutants is relatively minor (Dyer *et al.,* 1989; Nesterova *et al.,* 2018). Thus, while subnuclear re-localization of the inactive X to the nuclear lamina is a feature in XCI, it appears not to be a major driver of silencing (Nesterova *et al.,* 2018).

Global chromatin structure is also affected by X inactivation in mammals (Giorgetti *et al.,* 2016; Gdula *et al.,* 2019). Mammalian autosomes and active X chromosomes contain topologically associating domains (TADs) which are stretches of several hundred thousand base pairs exhibiting a high degree of interaction frequency (Nora *et al.,* 2012; Dixon *et al.,* 2012). The regions of high intra-chromosomal interaction are separated by domain boundaries such that the region within a single TAD interacts with itself to a greater extent than regions outside of the TAD. On the inactivated X chromosome these TADs are largely absent, and instead the chromosome forms two 'mega-domains' (Giorgetti *et al.,* 2016). Moreover, depletion of the Structural Maintenance of Chromosome (SMC) protein SMCHD1 reverts the structure of the inactive X chromosome to that of an active X or autosome with semi-regularly spaced TAD structures emerging (Gdula *et al.,* 2016). The Smchd1 gene is required for silencing of many genes in the context of XCI, however the role of global chromosome structure in mammalian XCI is the topic of ongoing research (Gendrel *et al.,* 2013; Mould *et al.,* 2013; Brockdorff *et al.,* 2020). Studies to identify the precise mechanism through which SMCHD1 selectively represses

the formation of TADs on the inactive X chromosome will likely provide additional insight to how these global chromosome structural changes manifest (Gdula *et al.,* 2019).

Sex determination and dosage compensation in *Drosophila*

In *Drosophila* sex is determined by the ratio of X chromosomes to autosomes, with X:AA conferring the male sex and XX:AA conferring the female sex (Bridges, 1916; Muller, 1932). The mechanism of sex chromosome dosage compensation is male-specific in this species, with the single X of males being transcriptionally upregulated two-fold to balance the output of the female X's (Mukherjee and Beermann, 1965; Lakhotia and Mukherjee 1969, 1970; Belote and Lucchesi 1980). Sex chromosome dosage compensation, or X-upregulation (as it is more commonly referred to in *Drosophila* research) is achieved by an RNA/protein complex called MSL (Male specific lethal) containing the MSL1, MSL2, MSL3, MLE, and MOF proteins, along with two non-coding RNAs (ncRNAs) Rox1 and Rox2 (For a review, see Gelbert and Kuroda, 2009). This complex facilitates H4K16ac enrichment on the single male X chromosome via the histone acetyltransferase activity of MOF, which leads to two-fold upregulation of X-linked transcripts to achieve dosage compensation (Hilfiker *et al.,* 1997; Smith *et al.,* 2000; Akhtar and Becker, 2000; Thomas and Voss, 2007, Gelbart *et al.,* 2009). While H4K16ac is found on the X chromosomes and autosomes of both male and females, males display a specific enrichment of this mark at the gene bodies of X-linked genes (Smith *et al.,* 2000). Targeting of the MSL complex to the X chromosomes is achieved by the MSL2 protein (Straub *et al.,* 2005). Furthermore, although the genes encoding the proteins in the MSL complex are transcriptionally active in both sexes, the Sxl (Sex lethal) gene is responsible for preventing MSL-mediated X-upregulation from occurring in females (Reviewed in Penalva and Sánchez, 2003). First, the SXL proteins targets *msl2* pre-mRNA transcripts and prevents splicing from removing an intron

with SXL binding sites (Merendino *et al.,* 1999; Forch *et al.,* 2001). When the *msl2* mRNA is exported to the cytoplasm containing SXL binding sites, the SXL protein binds to the 5' and 3' ends of the *msl2* mRNA (Bashaw and Baker, 1997; Kelley *et al.,* 1997; Gebauer *et al.,* 1999). At the 3' end, SXL recruits the UNR protein which blocks ribosome pre-initiation complex assembly, and at the 5' end, SXL prevents the stability of the small ribosomal subunit (Beckmann *et al.,* 2005; Abaza *et al.,* 2006; Duncan *et al.,* 2006, 2009; Medenbach *et al.,* 2011). The SXL-mediated repression of *msl2* is thus a crucial female-specific regulatory output to robustly ensure that the two X chromosomes *Drosophila* are not inappropriately upregulated.

The major activating chromatin modification directed by the MSL complex, H4K16ac has been linked to nucleosome repositioning and chromatin decondensation (Turner *et al.,* 1992; Bone *et al.,* 1994; Shogren-Knaak *et al.,* 2006; Robinson *et al.,* 2008). The incorporation of H4K16ac onto nucleosome arrays *in vitro* prevents the formation of compact chromatin fibers and nucleosome sliding (Shogren-Knaak, *et al.,* 2006). With MOF-directed H4K16ac via the MSL complex being implicated strongly in x-upregulation, another key question in the field is the precise degree to which the acetylation of H4K16 is responsible for the full two-fold up-regulation of X-linked transcripts, or whether additional MSL-mediated functions are responsible in part for the X-upregulation. Copur, *et al.,* 2018 investigated mutants for H4 acetylation as well as MOF mutants and characterized their dosage compensation phenotypes. They determined that a lack of maternal and zygotic MOF leads to complete lethality in males but not females (Copur *et al.,* 2018). Additionally, an H4K16R mutation which is not capable of being acetylated recapitulated this male-specific lethality characterized by arrest in gastrulation (Copur *et al.* 2018). These findings highlighted the crucial role MSL-directed H4K16ac in dosage compensation in male *Drosophila.*

RNA-seq analysis of transgenic flies with MSL binding to specific autosomal locations have shown that the recruitment of the MSL locally increases gene expression even at these autosomal locations (Park *et al.,* 2010). Several studies have attempted to identify the precise step(s) of transcription modulated by the MSL complex. Larschan *et al.,* 2011 conducted GRO-seq assays which showed an MSL-dependent increase in RNA pol II occupancy at X-linked gene bodies, arguing for a model in which transcriptional elongation is more efficiently promoted in X-upregulating male *Drosophila*. Conversely, Conrad *et al.,* 2012 showed that there is an increased recruitment of RNA pol II to X-linked gene promoters as well as short-promoter proximal RNA production, which argues for RNA pol II recruitment as the key transcriptional step underlying X up-regulation. Ferrari *et al.,* 2013 further proposed a "Jumpstart and gain" model for transcriptional regulation by MSL whereby H4K16ac facilitates faster release of RNA pol II from 5' promoter pausing and/or increased RNA pol II processivity. Thus, the MSL-mediated X-upregulation in *Drosophila* dosage compensation is likely due to increased transcriptional elongation efficiency driven by H4K16ac on dosage compensated gene bodies.

Similar to mammals, the *Drosophila* male X chromosome also takes on a unique global chromosome structure. Hi-C data indicate that the single *Drosophila* male X chromosome differs from the paired females X chromosomes in that it exhibits an increased frequency of intrachromosomal contacts over middle or long-range distances (between 500kb and 1Mb) (Koustav *et al.,* 2019). Importantly, the increased contacts in the male were not clustered to specific regions, but rather random. The Hi-C data on the *Drosophila* male X chromosome have shown that the boundary domains of TADs in the fruitfly, which are mediated by BEAF-32 and CP190, were significantly weaker than females (Koustav *et al.,* 2019). Taken together, the Hi-C data show a dosage compensated X chromosome which is less restricted by interaction

boundaries and more easily able to interact with itself at longer distances. While the mammalian and *Drosophila* sex chromosomes both show unique global chromosome structure, the TAD boundaries are weaker than autosomal ones on the upregulated *Drosophila* X and completely replaced by two giant mega-domains on the inactive mammalian X.

Sex determination and dosage compensation in *C. elegans*

The activation of *C. elegans* dosage compensation is closely linked with sex determination (See Figure 1.2). The ratio of X chromosomes to autosomes determines whether or not *xol-1* is transcribed in the early embryo (Miller *et al.,* 1998). *Xol-1* is a master switch gene which is sufficient for male sex determination and negative regulation of dosage compensation (Miller *et al.,* 1998). A number of genes on the X chromosome and autosomes called X-signal elements (XSEs) and autosomal signal elements (ASEs) respectively are transcribed in both sexes (Akerib and Meyer, 1994; Hodgkin *et al.,* 1994; Nicoll *et al.,* 1997; Carmi *et al.,* 1998; Powell *et al.,* 2005; Gladden *et al.,* 2007). The XSEs encode *sex-1, sex-2, fox-1,* and *ceh*-39 which repress *xol-1* and ASEs encode *sea-1* and *sea*-2 which activate *xol-1* (Gladden and Meyer, 2007). Both the XSE's and ASE's largely regulate *xol*-1 at the transcriptional level, however the RNA-binding protein FOX-1 encoded by an additional XSE represses *xol-1* post-transcriptionally via inhibition of pre-mRNA splicing (Nicoll *et al.,* 1997). In the context of *xol-1* regulation, XO-AA karyotype males contain an XSE:ASE ratio of 1:2, thus, the ASE's outcompete the XSE's, ultimately promoting *xol-1* activation. In XX:AA karyotype hermaphrodites contain an XSE:ASE ratio of 1:1, which is a strong enough gene dose for the XSEs to outcompete the ASEs ultimately repressing *xol-1* expression. Once the sex chromosome ploidy of the animal is communicated in the context of *xol-1* regulation, the proper sexual fate and dosage compensation programs are adopted.

Immediately downstream of *xol-1* activation in males, the XOL-1 protein represses *sdc-1, sdc-2,* and *sdc-3*, to prevent Dosage Compensation Complex (DCC) loading (Rhind *et al.,* 1995). *xol-1* activation in males also represses downstream hermaphrodite-promoting sex determination factors (Goodwin and Ellis, 2002). In hermaphrodites, *xol-1* remains repressed, and the *sdc-1, sdc-2,* and *sdc-3* genes are activated to promote dosage compensation and hermaphrodite sexual fate. Although a wealth of genetic data exists on the sex determination and dosage compensation activation pathway in *C. elegans*, some major questions are unaddressed. The crystal structure of XOL-1 was determined to be most similar to a GHMP kinase, with ~10% amino acid sequence similarity. GHMP kinases are conserved from archaea and bacteria to higher eukaryotes, and while they have known roles in metabolism, they have never been implicated in a developmental process (Luz *et al.,* 2003). GHMP kinases are predicted to bind ATP, although *xol-1*'s mechanism in negatively regulating the *sdc-1, sdc-2, sdc-3* genes remains elusive (Luz *et al.,* 2003). Furthermore, although Gladden *et al*., 2007 refined the relative contribution of each XSE to dosage compensation, the strongest XSE and nuclear hormone receptor superfamily homolog, *sex-1*, also promotes dosage compensation in a separate role downstream of *xol-1* through an unknown mechanism (Gladden *et al.,* 2007).

The *C. elegans* dosage compensation complex (DCC)

Sometime no earlier than the 30-50 cell stage in embryonic development, shortly after the *sdc-1,2,3* genes are activated in hermaphrodites, they promote the assembly of and take part in the Dosage Compensation Complex (DCC). The *C. elegans* DCC consists of a ten-protein complex encoded by 9 maternally contributed genes: *dpy-21, dpy-26, dpy-27, dpy-28, dpy-30, mix-1, capg-1, sdc-1, sdc-3* and 1 zygotically expressed gene: *sdc-2* (Reviewed in Meyer, 2005).

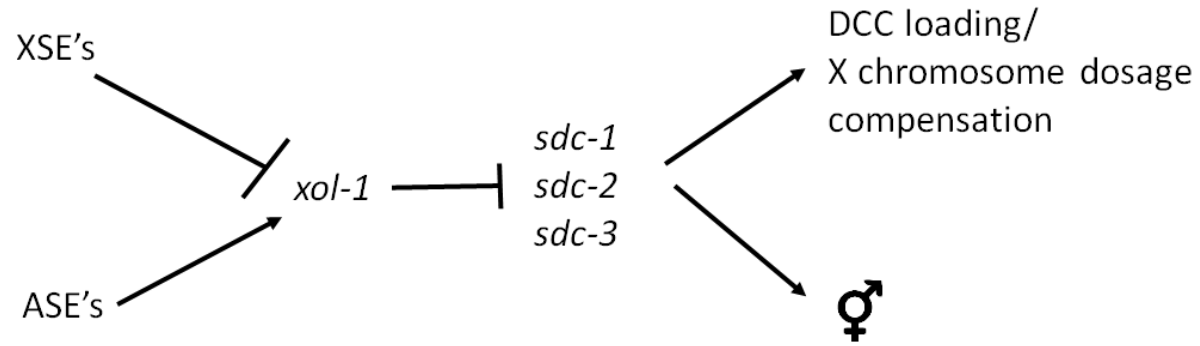

Figure 1.2 Sex Determination and Dosage Compensation in *C. elegans*
The autosomal signal elements (ASE's) and x signal elements (XSE's) communicate the sex chromosome karyotype of the animal via competition for *xol-1* regulation. In XX hermaphrodites, *xol-1* is repressed, relieving the repression of *sdc-1, sdc-2,* and *sdc-3.* The SDC-1, SDC-2, and SDC-3 proteins in turn assemble the dosage compensation complex onto the X chromosomes and promote the hermaphrodite sexual fate. This figure is modified from Hodgkin, *et al.,* 1992.

Five of these genes encode proteins which form a *bona fide* condensin complex (DPY-26, DPY-27, DPY-28, CAPG-1, and MIX-1) (Csankovszki *et al.,* 2009). The other five proteins which interact with the condensin complex are accessory proteins. These proteins aid in targeting the condensin to the dosage compensated X chromosomes and serve additional roles in promoting downregulation of the sex chromosomes (Chu *et al.,* 2002; Hsu and Meyer, 1994; Meneely and Wood, 1984; Gladden *et al.,* 2007). The DCC binds to X recognition sites on hermaphrodite chromosomes called *rex* sites which are enriched for a 12 base pair consensus motif required for DCC binding (Jans *et al.,* 2009). However, the targeting specificity of the DCC is more complex than just X chromosome sequence specificity. Indeed, sumoylation of several DCC proteins (DPY-27, DPY-28, and SDC-3) promotes DCC binding to the X chromosomes (Pferdehirt and Meyer, 2013). Moreover, while DPY-28 is one of the four proteins participating in both Condensin I and Condensin I^{dc}, it is only given a SUMO tag during its dosage compensation role when Condensin I^{dc} binds to the X chromosomes (Pferdehirt and Meyer, 2013). The fact that condensin I and condensin I^{dc} differ in only the 1 subunit (SMC-4/DPY-27), suggests that the

biochemical features of condensin's activity in cell division and interphase may also be conserved.

Condensin compacts chromosomes and aids in chromosome segregation in mitosis and meiosis

Widely conserved across metazoan life, condensins are pentameric complexes which play essential roles in mitosis and meiosis (Paul *et al.,* 2019). Yeast contain a single condensin complex, while higher Eukaryotes contain two condensins (condensin I and condensin II) (Hirano, 2016). The conserved structural elements of condensin consist of two SMC (structural maintenance of chromosome) proteins and three CAP (chromosome-associated polypeptide) proteins (Hirano, 2016). Condensin has been shown to hydrolyze ATP *in vitro* and produce positive DNA supercoiling in an ATP-dependent manner, which is thought to be a mechanism central to its role in condensing chromosomes (Kimura and Hirano, 1997). The model for condensin-mediated chromosome compaction entails the formation of chromosomal loops (Paul *et al.,* 2019). Condensin II entraps the DNA to form a larger loop and sets up the axis of the chromosome, while Condensin I binds at several points along the Condensin II's large loop, effectively thickening the axis (See Figure 1.3) (Paul *et al.,* 2019). The SMC proteins contain conserved ATPase head subunits which form a heterodimer capable of hydrolyzing ATP (Jessberger *et al.,* 2002). SMC-2 and SMC-4 are featured in this role in most vertebrate condensin structures (Reviewed in Hirano, 2002). In contrast, the CAP proteins exhibit a wider range of diversity in peptide sequence across distinct condensin complexes and do not contain ATPase modules (Swedlow and Hirano, 2003). RNAi and mutant analyses have highlighted the importance of all five subunits for these condensin complexes at the cellular level for proper chromosome segregation and compaction, and also at the organismal level, with varying degrees

of lethality and developmental arrest associated with disruption in each subunit (Meyer and Casson, 1986; Villeneuve and Meyer, 1987; Nusbaum and Meyer, 1989; DeLong *et al.,* 1993; Hsu and Meyer, 1994).

Mitosis and meiosis are contexts in which condensins have been studied for several decades. However, studies to determine the gene regulatory capacity of condensin during interphase are complicated by the fact that most condensin mutations disrupt the vital process of cell division. The fact that *C. elegans* dosage compensation employs a condensin complex (Condensin I^{dc}) uniquely dedicated to orchestrating chromosome-wide gene repression in interphase cells is a distinguishing feature of the worm. The *C. elegans* DCC thus provides a

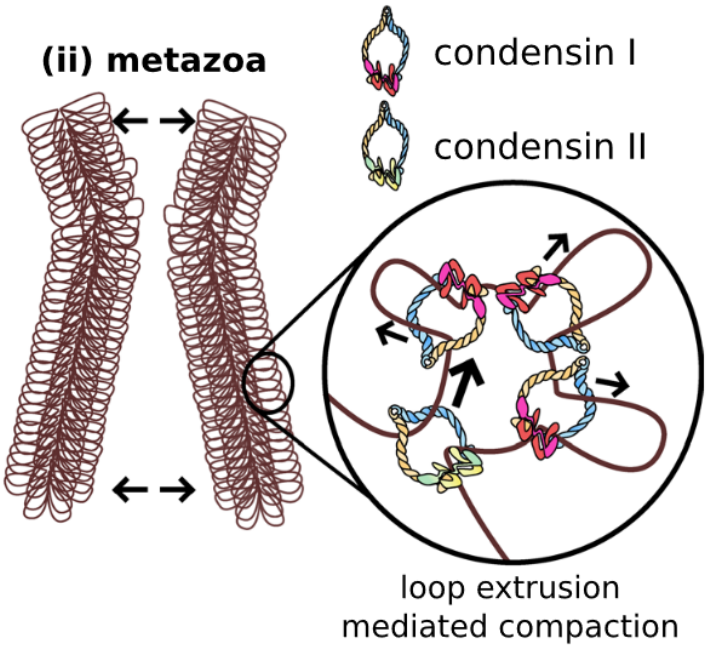

Figure 1.3 Model for Condensin-mediated compaction of chromosomes. Condensin II entraps the DNA at two distinct regions and pushes the DNA through its SMC ring, setting up the axis of the chromosome. Condensin I entraps the DNA at multiple locations within each Condensin II-mediated loop, forming several smaller loops, thickening the chromosomal axis. This figure is modified from Paul *et al.,* 2019.

niche opportunity to understand how condensins function in a largely unexplored context: interphase gene regulation.

Condensin complexes in *C. elegans*

In *C. elegans*, condensin II is nuclear-localized and responsible for condensing chromosomes in prophase, as well as facilitating chromosome segregation in anaphase, which mirrors their vertebrate condensin homologs (Reviewed in Skibbens, 2019). Condensin I is also required for anaphase segregation, however, only associates with chromatids after nuclear envelope breakdown (Gerlich *et al.,* 2006).

C. elegans is unique in that it also contains a third condensin, condensin I^{DC} which functions distinctly in interphase gene regulation in the context of X chromosome dosage compensation (Csankovszki *et al.,* 2009). Interestingly, condensin I^{DC} differs from condensin I in just one subunit, as SMC-4 is replaced by DPY-27 (See Figure 1.4) (Hagstrom *et al.,* 2002). Mutations in genes like *capg-1* and *mix-1* which encode proteins participating in both condensin I and condensin I^{DC} exhibit early lethality, likely due to loss of condensin I function leading to chromosome segregation errors, which preclude analysis of the dosage compensation roles of these subunits (Lieb *et al.,* 1998; Csankovszki *et al.,* 2009). However, dosage compensation complex accessory proteins which confer targeting of condensin I^{DC} to dosage compensated chromosomes are useful in that mutants for genes encoding these proteins like *dpy-21* exhibit dosage compensation phenotypes with no apparent mitotic or meiotic defects.

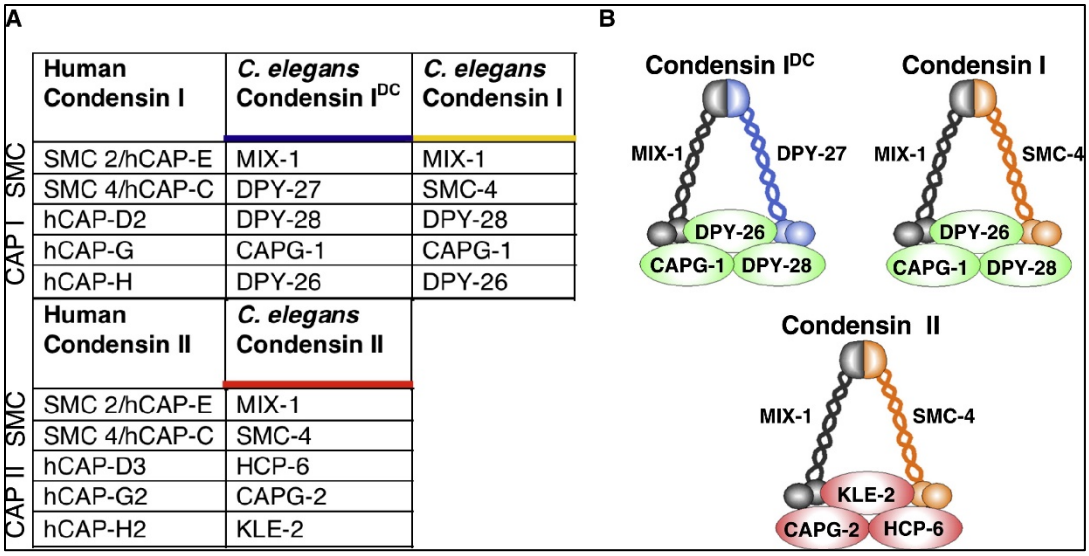

Figure 1.4 Condensin complexes in humans and *C. elegans* Humans have two condensins and *C. elegans* have 3 distinct condensins, with condensin I^{dc} differing from Condensin I in just a single subunit: DPY-27/MIX-1. This figure is from Csankovszki *et al.,* 2009.

Condensin functions in interphase gene regulation

While condensin's role in cell division is well-characterized, the evidence is also mounting for interphase condensin function in various gene regulatory contexts. In aging (senescent) human cells, condensin helps compartmentalize the genome into active (A) and inactive (B) compartments (Iwasaki *et al.,* 2019). In this context, condensin binds to the A compartment regions of the genome and promotes expression of senescence associated secretory phenotype (SASP) genes to help the cell deal with aging (Iwasaki *et al.,* 2019). The sole condensin in yeast also has interphase roles. Yeast tRNA genes are found throughout all chromosomes and spread through the genome, but condensin helps to physically orient them into clusters and promote RNA polymerase III activity to transcribe them (Haeusler and Pratt-Hyatt, 2008). In *Drosophila*, the condensin II protein Cap-H2 also plays a role in interphase by compacting chromatin (Wallace *et al.,* 2015).

Studies using post-mitotic (non-dividing) cell types as well as conditional condensin depletions are a work-around for this issue. Unfortunately, these restraints still limit the scope of what contexts interphase condensin gene regulatory roles can be assessed. The existence of a dedicated interphase condensin (I^{DC}) unique to *C. elegans* presents a niche opportunity to uncover the modulatory gene expression capacity of condensin in an endogenous role (Csankovszki *et al.,* 2009). The next section will explore the features and regulatory landscape orchestrated by condensin I^{DC} as part of the DCC.

DCC-mediated repressive mechanisms and other features of *C. elegans* dosage compensation

Despite the fact that hermaphrodite X chromosomes account for ~18% of the total genomic content of the worm in a cell, the DCC compacts the X chromosome such that they occupy ~10% of the nucleus (Figure 1.5) (Lau *et al.,* 2014). In various mutants for dosage compensation promoting genes the volume of the X chromosomes expands to ~15% or greater (Lau *et al.,* 2014; Snyder *et al.,* 2016). The DCC also coordinates enrichment of the H4K20me1 repressive chromatin mark (Figure 1.5) (Vielle *et al.,* 2012; Wells *et al.,* 2012). While the SET-1 methyltransferase and its homolog PR-Set7 are responsible for producing H4K20me1 on all chromosomes, the SET-4 protein is responsible for converting the mark to H4K20me2/3 on all chromosomes with the exception of the X (Rice *et al.,* 2002; Oda *et al.,* 2009). In addition, the DCC component DPY-21 is a histone demethylase that acts on H4K20me2/3 to ensure that converts H4K20me2/3 to H4K20me1 on the X chromosomes to coordinate this enrichment during interphase (Brejc *et al.,* 2017). At a global chromatin scale, the DCC is also responsible for the formation of Topologically Associating Domains (TADs) on the hermaphrodite X chromosomes (Crane *et al.,* 2015). These TADs are spaced at semiregular ~1Mb intervals along

the 17Mb X chromosome. A strong DCC mutation such as *sdc*-2, where the DCC fails to load to the X chromosomes results in the loss of 9 of 17 X chromosome TADs (Crane *et al.,* 2015). However, these experiments were conducted on mixed stage embryos, so the effect may be greater in adult worms but a strong DCC mutation like *sdc-2* is so lethal that the question cannot be assessed. The subnuclear localization of hermaphrodite X chromosomes is also regulated in the context of dosage compensation (Snyder *et al.,* 2016). This pathway will be the topic of chapter 2, but briefly, the X chromosomes are sequestered to the nuclear periphery via nuclear lamina localized proteins binding to H3K9me3 residues on the X chromosomes. This nuclear lamina localization of the X chromosomes also contributes to X-linked gene repression but to a smaller degree than DCC mutations (Snyder *et al.,* 2016).

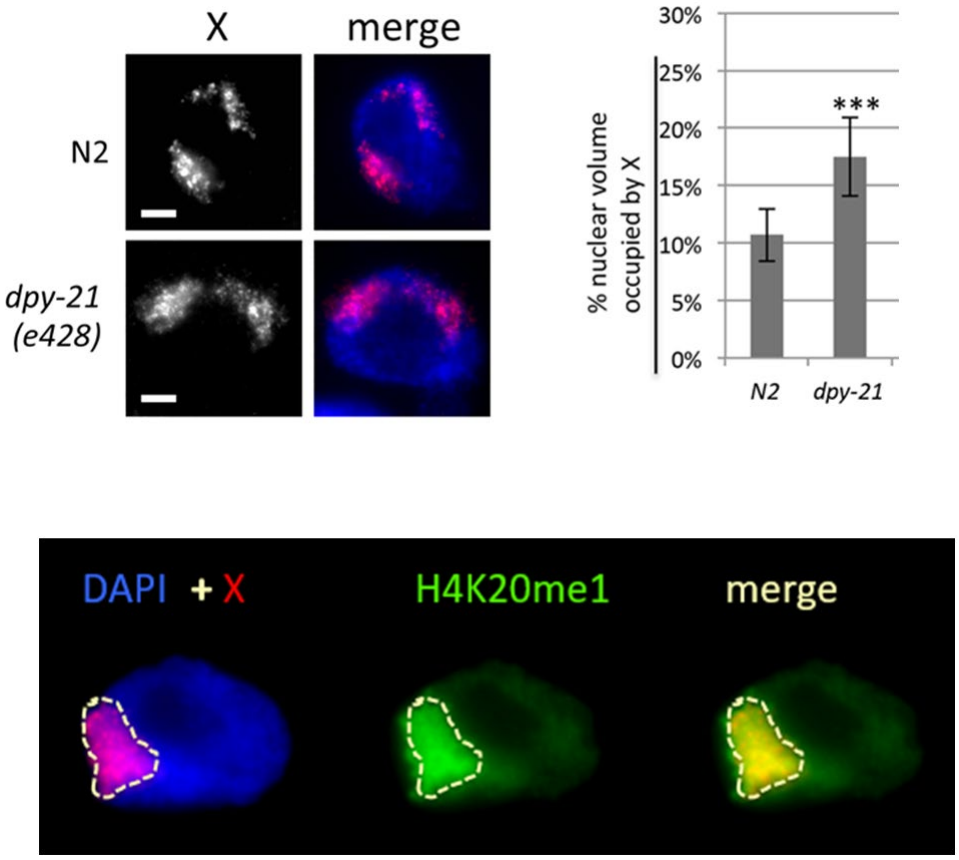

Figure 1.5 The DCC Mediates X Chromosome Compaction and Facilitates H4K20me1 Enrichment on Hermaphrodite X Chromosomes Top: Wild Type (N2) X chromosomes in *C. elegans* hermaphrodites occupy ~10% volume of each nucleus, while DCC mutant (*dpy-21*) X chromosomes occupy 17% volume of each nucleus. Bottom: In wild type hermaphrodite nuclei, the X chromosome (pink) also displays enrichment of the repressive H4K20me1 mark (green). Co-localization of X and H4K20me1 shown in merge. Figure modified from Lau *et al.,* 2014 (top) and Wells *et al.,* 2012 (bottom).

Identifying Additional Regulators of *C. elegans* Dosage Compensation

As indicated from the Hi-C TAD experiments noted above, loss of function mutations for the zygotically expressed DCC gene *sdc-2* encoding a worm-specific protein present the most consequential dosage compensation-specific phenotype: the DCC fails to activate in *sdc-2(null)* hermaphrodites, resulting in strong embryonic lethality and X-linked gene de-repression (Nusbaum and Meyer, 1989). In contrast, mutations affecting genes implicated in a single aspect of a DCC-mediated gene repression mechanism like *set-1* or *set-4* in which the H4K20me1 histone methylation enrichment on the X chromosomes is lost, the level of X chromosome gene de-repression is less than half of that of *sdc-2(null)* mutants (Kramer *et al.,* 2015). Mutations in other DCC subunits confer various levels of X-linked gene de-repression, however the accompanying molecular phenotypes (e.g. mis-regulated X chromosome compaction) are not enough to explain the sum of all the repressive mechanisms orchestrated by the DCC to coordinate the two-fold gene expression change which defines X chromosome dosage compensation (Jans *et al.* 2009). In this vein, our lab has sought to identify additional pathways and processes facilitating DCC function.

In brief, our screening strategy to identify novel regulators of dosage compensation entails employing a *xol-1(null)* mutation to force on dosage compensation inappropriately in male worms. The ectopic loading of the DCC to the single X chromosome in males results in complete XO lethality. In this background, if genes promoting dosage compensation are knocked down via RNAi, dosage compensation is disrupted to a variable degree and a corresponding number of males will be rescued. This screening strategy is particularly compelling, in that we use a null mutation in a master switch gene *xol-1* to activate dosage compensation with 100% efficacy, yet despite being such a crucial gene in development, XOL-1 protein's function is

completely unknown. This strategy has uncovered an additional gene regulatory network in *C. elegans* which we have implicated in dosage compensation: the nuclear RNAi pathway. For more than twenty years, RNAi has generated a lot of research interest in *C. elegans* biology, experimental gene manipulation techniques, and even gene therapeutics. The remaining contents of this introductory chapter will explore the endogenous RNAi pathways in *C. elegans,*

Introduction to RNAi

RNAi is an endogenous gene silencing pathway conserved across eukaryotes. Early studies on transgenic plants demonstrated the phenomenon of posttranscriptional gene silencing. When researchers attempted to introduce extra copies of flower pigmentation genes into the *Petunia Hybrida* genome they observed a subset of transformants with severely reduced pigmentation (van der Krol *et al.,* 1990). They speculated that the transcribed product of the integrated transgene was triggering the silencing of its own element and the endogenous counterpart (van der Krol *et al.,* 1990). This RNA-mediated process whereby silencing of genes or transposons occurs due to the target genes having significant sequence homology to the transgene RNA continued to be studied and speculated on in plants (Baulcombe 1996).

The metazoan version of the RNAi phenomenon was first discovered in *C. elegans* by Andrew Fire and Craig Mello in 1998. Since its initial characterization highlighted that the pathway could be manipulated to knock down specific genes in various organisms, the method has been utilized for temporal and tissue-specific gene silencing through a variety of iterations of the technique. It was shortly after determined that HeLa (Human) cells and human embryonic kidney cells can also be transfected with a construct expressing an siRNA encoding a dsRNA to target an endogenous transcript for repression (Elbashir *et al*., 2001). RNAi as an experimental technique has been streamlined for well over a decade. *Drosophila* strain libraries with

transgenic encoded *Gal4-UAS*-driven tissue-specific expression of small hairpin RNA constructs targeting most of the genome are a common implementation (Dietzl *et al*., 2007). In this iteration, fly strains bearing a transgenic *tissue-specific promoter-Gal4* construct are mated to flies bearing a transgenic *UAS-dsRNA* construct to target a specific gene in a specific tissue. In *C. elegans*, the most commonly utilized RNAi procedure leverages a peculiarity of the species' ability to induce RNAi by feeding the worm a bacterial strain expressing the dsRNA targeting a gene of interest (Timmons *et al*., 2001). The use of RNAi as a laboratory technique has allowed for widespread reverse genetic screens in a multitude of organisms and the subsequent discovery of many novel genes implicated in disease and development. However, despite the vast number of mechanistic studies detailing the features of RNAi pathways in almost every model organism from yeast to mice, the role and relevance of the endogenous RNAi pathway to organismal development and physiology are less understood.

Small RNAs in *C. elegans*

Small RNAs in *C. elegans* can be classified into 3 categories consisting of microRNAs, siRNAs, and piRNAs. The first class, microRNAs, are largely implicated in the translational inhibition of developmental genes (For a review, see Vella and Slack, 2005). The second and third classes utilize a significantly overlapping subset of conserved and nematode-specific RNAi machinery in worms. The second class is comprised of ubiquitously expressed siRNAs which target ~550 endogenous genes (and transposons, and pseudogenes) and the third class is comprised of germline enriched piRNAs which largely target transposons and repetitive elements (Asikainen *et al.,* 2008; Bagijn *et al.,* 2012). The endogenously expressed siRNA class of small RNAs constitute the endogenous RNAi pathway, while the viral or experimentally induced siRNAs constitute the exogenous RNAi pathway. This distinction is important in that

there are some shared components, such as the DCR-1 protein, which has important RNA processing roles in both RNAi pathways, as well as microRNA processing, but also many proteins exist which function specifically in the endogenous or exogenous RNAi pathway (Ketting *et al.,* 2001; Knight & Bass, 2001).

Exogenous RNAi and downstream amplification pathway in *C. elegans*

Foreign dsRNA species are processed by DCR-1 into 26 nucleotide primary siRNAs, which are bound by the argonaute RDE-1 (Ketting *et al.,* 2001, Tabara *et al.*, 1999). The siRNA complexed with RDE-1 then target complementary mRNA transcripts. A ribonuclease protein RDE-8 is then recruited to argonaute-targeted transcripts to cleave them in half (Tsai *et al.,* 2015). The 3' end of the cleaved transcript is then targeted for amplification of silencing via secondary siRNA generation by one of two partially redundant RNA-dependent RNA polymerases: EGO-1 (enriched in the germline) or RRF-1 (enriched in the soma) (Gu *et al.,* 2009, Gent *et al.,* 2009). These secondary siRNAs are characterized as 22G (22 nucleotides long with a 5' guanosine bias) and are complementary to various regions throughout the 3' cleaved target transcript (Ambros *et al.,* 2003, Gu *et al.,* 2009). For each primary siRNA that is synthesized to target a specific mRNA, many distinct secondary siRNAs targeting the same transcript are generated (Aoki, *et al.,* 2007). Furthermore, *rrf-1* is required for exo-RNAi in the soma, highlighting the importance of the generating of these secondary siRNAs to effect RNAi silencing (Sijen *et al*., 2001). Secondary siRNAs complex with a subset of partially redundant WAGOs, or "worm-specific Argonautes", which effect posttranscriptional silencing in the cytoplasm and co-transcriptional silencing in the nucleus (For a review, see Billi, Fischer, and Kim 2014).

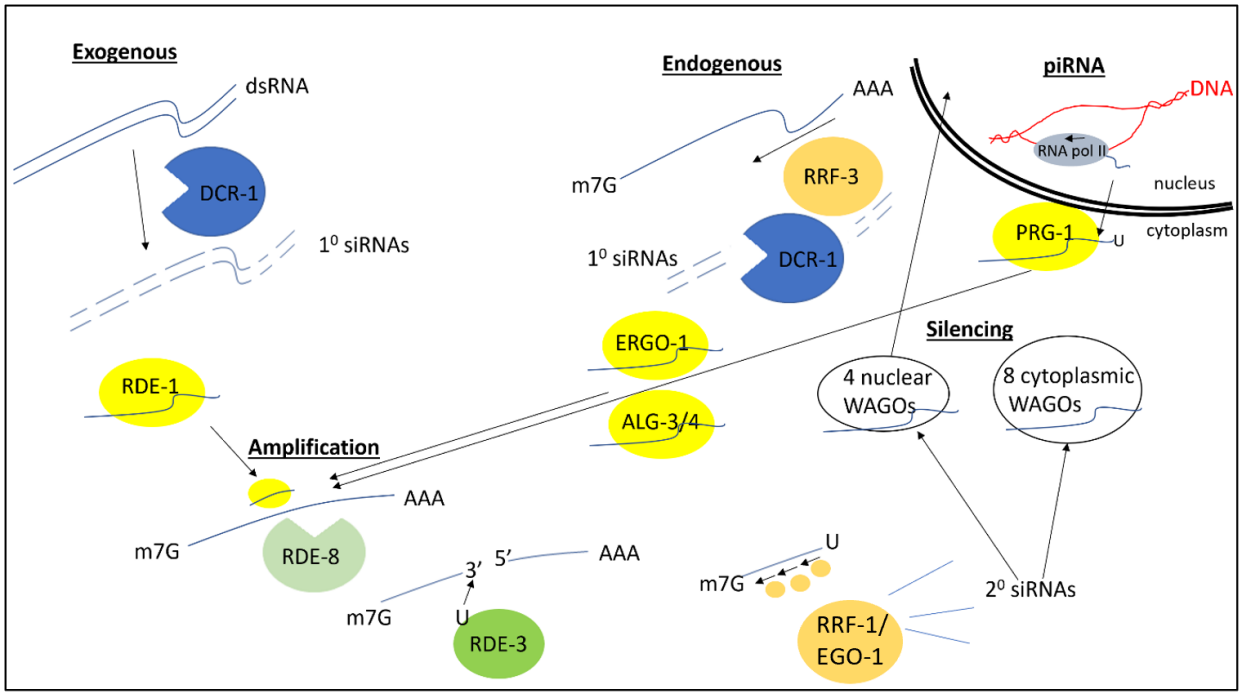

Figure 1.6 Convergence of RNAi pathways in *C. elegans* The exogenous, endogenous, and piRNA pathways have unique upstream components and converge on the amplification of their respective primary siRNAs/piRNAs into secondary siRNAs. They also share a subset of WAGO's to mediate silencing in the cytoplasm and/or nucleus.

Endogenous RNAi pathway in *C. elegans*

Endogenous RNAi target transcripts are templated for the generation of a dsRNA by distinct RNA-dependent RNA polymerase RRF-3, which DCR-1 processes into primary siRNAs (Bernstein *et al.,* 2001; Gent *et al*., 2009). These endogenous siRNAs are bound by redundant Argonautes ALG-3/4 in the spermatogenic gonad, and ERGO-1 in the soma and oogenic gonad (Han *et al*., 2009; Conine *et al.,* 2010; Vasale *et al*., 2010). These siRNAs complexed with the Argonaute then target endogenous mRNAs and feed into the same amplification pathway as the exo-siRNAs, consisting of the RDRP-mediated secondary siRNA generation and downstream WAGO effectors (Gent *et al.,* 2010).

piRNA pathway in *C. elegans*

Genomically encoded piRNAs are 21 base pairs in length with a 5' uridine bias (Ambros *et al.,* 2003, Ruby *et al.,* 2006, Das *et al.,* 2008, Batista *et al.,* 2008). These RNA pol II transcribed small RNAs are complexed with the PIWI protein PRG-1, enriched in the germline and target mostly transposons, repetitive elements and a small number of endogenous genes (Bagijn, *et al.,* 2012, Lee *et al.,* 2012, Ashe *et al.,* 2012, Gu *et al.,* 2012, Billi *et al.,* 2013). Mechanistically, the PRG-1 protein complexed with the piRNA feeds into the same amplification step of the downstream RNAi pathway utilizing 22G secondary siRNAs and a shared subset of WAGO proteins to effect silencing (Bagijn *et al.,* 2012, Lee *et al.,* 2012). Progressive transgenerational sterility, is a hallmark phenotype of *prg-1* (piRNA) mutants (Yigit *et al.,* 2006). As the majority of piRNA targets are transposons and repetitive elements, it was long speculated that de-repression of these elements in the germline are causal to progressive transgenerational sterility. However, a recent publication from Barucci *et al*., 2020 has dismantled this hypothesis. They show that *prg-1* mutants do not exhibit widespread de-repression of transposons and repetitive elements. Strikingly, of ~60,000 repetitive elements examined, less than 100 were upregulated in *prg-1* mutants. Additionally in *prg-1* mutants many ectopic 22G siRNAs mapping to replicative histone genes were identified. Analysis of the corresponding histone genes showed that transcription, protein expression and incorporation into chromatin was progressively diminished in *prg-1* mutants, and removal of a 22G biogenesis factor *mut-16* in these animals restored fertility. Thus, this hallmark phenotype of *prg-1* (PIWI mutants) is explained by a level of histone gene downregulation that becomes increasingly detrimental to reproduction at restrictive temperatures, despite the siRNAs in the PIWI-functional pathway targeting mostly transposons and repetitive elements (Barucci *et al*., 2020).

22G secondary siRNAs and amplification of RNAi-mediated silencing

Since the initial discovery of RNAi in 1998 by Fire and Mello, the existence of an internal silencing amplification mechanism was speculated. The careful work of this initial landmark publication demonstrated that titrating dsRNA triggers to very low concentrations was still capable of strongly silencing genes, arguing against a strict stoichiometric ratio whereby every injected dsRNA molecule corresponds to silencing of an individual mRNA target transcript (Fire *et al.*, 1998). Sijen *et al*., 2001 later identified 22G secondary siRNAs as a pool of small RNAs that were complementary to the mRNA target but not to the corresponding 26G primary siRNAs. Additionally, they demonstrated that the RNA-dependent RNA polymerase RRF-1 was required for the generation of secondary siRNAs and silencing, however the 26G siRNAs were still maintained for a given dsRNA trigger. Thus, the generation of 22G secondary siRNAs represent an amplificatory step in RNAi whereby many silencing 22G siRNAs are generated from a single mRNA transcript which is targeted by a single 26G primary siRNA (Gent *et al.,* 2010).

RNAi-mediated posttranscriptional silencing in the cytoplasm

As secondary 22G siRNAs interact with WAGOs (worm specific Argonautes) to effect gene silencing, it was a peculiar finding that WAGO Argonautes proteins lack the catalytic residues required for cleaving RNA commonly observed in some primary Argonautes in *C. elegans* as well as Argonautes in many other species (Yigit *et al*., 2006). While it is not known what precise mechanism ultimately lead to WAGO-mediated mRNA degradation in *C. elegans* RNAi, the RDE-10/RDE-11 complex was shown to associate with target mRNA being degraded by exo-RNAi treatment (Yang *et al*., 2012). Furthermore, RDE-11 is required for the degradation of the target mRNA and RNAi depletion of both *rde-10/rde*-11 results in a no production of

secondary 22G siRNAs despite primary 26G siRNAs persisting for the target transcript (Yang *et al.,* 2012). RDE-10 and RDE-11 are divergent, worm specific proteins, and RDE-10 has no conserved domains, however RDE-11 has a RING-type Zinc Finger domain, which is required for its interaction with RDE-10 and depletion of target mRNA transcripts (Yang *et al*., 2012). There may be additional factors which are recruited to the siRNA/Argonaute complex in an RDE-10/RDE-11-dependent manner which promote target mRNA repression through endonuclease activity or exosome degradation of target mRNA transcripts, however the RDE-10/RDE-11 complex could also function in directly targeting mRNA for de-adenylation and subsequent exosome-mediated degradation (Yang *et al*., 2012).

Nuclear RNAi in *C. elegans*

Bosher *et al.,* 1999 presented early evidence for a nuclear silencing component to RNAi in *C. elegans* through analysis of a bicistronic mRNA containing the *lir-1* and *lin-26* genes. About 15% of *C. elegans* genes are arranged into operons, multi-gene co-transcriptional units most commonly observed in bacteria (Blumenthal, 2018). Given that null mutations in *lin*-26 but not in *lir-1* result in embryonic lethality, it was surprising that *lir-1*(RNAi) treatment resulted in strong embryonic lethality and *lin-26* repression. Furthermore, RNAi constructs targeting intron sequences in the *lir-1/lin-26* bicistron were still effective in silencing both genes as well as producing the embryonic lethality phenotype observed with *lin-26* null mutation. These results suggested that the experimental RNAi is capable of targeting pre-mRNAs in the nucleus (Bosher *et al.,* 1999).

The *C. elegans* nuclear RNAi silencing machinery was initially described by Guang *et al.,* 2008, who conducted a forward screen to identify mutations that prevent experimental RNAi from silencing a nuclear-localized mRNA transcript. NRDE-3 was identified as a positive hit

from this screen which contains a PIWI and PAZ domain, classifying it as an Argonaute. Interestingly, NRDE-3 also contains a nuclear localization signal (NLS), but siRNAs are required for NRDE-3 to exhibit strong nuclear localization, suggesting that the NRDE-3/siRNA complex formation may expose the Argonaute's NLS to allow for nuclear translocation (Guang *et al.,* 2008). In a forward screen to identify mutations which prevent the heritable transmission of experimental-induced RNAi silencing, Buckley *et al.,* 2012 identified HRDE-1 as an Argonaute protein, which like NRDE-3 contains a PIWI, PAZ and NLS domains and likewise directs siRNAs to the nucleus, however these two nuclear Argonautes differ in their expression patterns. GFP fusion proteins to NRDE-3 and HRDE-1 which rescue defective nuclear RNAi silencing showed that NRDE-3 is expressed in somatic cells after the ~80 cell stage in embryogenesis, while HRDE-1 is expressed in the germlines of both sexes (Guang *et al.,* 2008, Buckley *et al.,* 2012).

Forward screens for additional nuclear RNAi defective mutations identified the *nrde-1, nrde-2,* and *nrde-3* genes whose proteins are nuclear localized and required for reduced transcription at targeted nuclear RNAi loci. (Burkhart *et al.,* 2011, Guang *et al.,* 2010). NRDE-1, NRDE-2, and NRDE-4 are not required for NRDE-3 to associate with siRNAs and thus function downstream of siRNA/NRDE-3 complex formation (Burkhart *et al.,* 2011). NRDE-1 and NRDE-2 associate with the pre-mRNA of NRDE-3 target genes and NRDE-1 additionally associates with chromatin of the target gene in a NRDE-4-dependent manner. These nematode specific proteins thus constitute a core nuclear Nrde complex, with a hierarchical recruitment that ultimately associates the NRDE-3/siRNA complex with both the target pre-mRNA and underlying target chromatin region (Burkhart *et al.,* 2011, Guang *et al.,* 2010). This nuclear Nrde complex is also utilized in the HRDE-1-mediated germline version of this silencing. In somatic

cells, NRDE-3 and the nuclear Nrde complex of NRDE-1,2,4 are required for the accumulation of the repressive chromatin marks H3K9me3 and H3K27me3 at many target loci (Burton *et al.,* 2012, Gu *et al,* 2012, Mao *et al.,* 2015). Additionally, the H3K9me2/3 histone methyltransferases SET-32 and SET-25 are required for the initiation of HRDE-1-mediated germline nuclear RNAi silencing (Kalinava, *et al.,* 2018, Woodhouse *et al.,* 2018). Thus, silencing of target genes via nuclear RNAi in all tissues is accompanied by a canonical heterochromatin signature directed by the Nrde complex.

The piRNA pathway regulates *xol-1* expression in *C. elegans*

Tang *et al.,* 2018 identified an X chromosome piRNA, 21ux-1 which is responsible for repressing *xol-1.* This link between the piRNA pathway and dosage compensation is interesting in that *xol-1* is significantly de-repressed in *prg*-1 and *21ux-1* mutants at the mRNA and protein level in L4 and adult hermaphrodites. The 22G secondary siRNAs corresponding to *21ux-1* were enriched in immunoprecipitated HRDE-1 samples, thus the canonical piRNA regulatory pathway utilizing PRG-1 as a primary Argonaute and HRDE-1 as a 22G-associating effector Argonaute are implicated in repression of *xol-1* transcription in hermaphrodites to promote dosage compensation activation. There have been no studies to date that address the possibility of a role for the piRNA pathway or other Argonaute proteins in regulating dosage compensation downstream of *xol-1.*

Summary of research efforts

The goal of this thesis was to identify and describe additional genes promoting dosage compensation in *C. elegans.* In chapter two we describe a genetic pathway encoding several proteins which are responsible for depositing the H3K9me3 heterochromatin modification on

chromosomes and tethering the hermaphrodite X chromosomes to the nuclear lamina to help reinforce dosage compensation. In chapter three we describe the contribution of three genes encoding Argonaute proteins which contribute to *xol-1* repression and X chromosome compaction in dosage compensation. The research described in these chapters indicate that existing gene regulatory programs which promote heterochromatin modifications also contribute to *C. elegans* dosage compensation. The last chapter of this thesis summarizes these findings and offers potential explanations for how these pathways could be promoting DCC function.

References

Abaza, Irina, Olga Coll, Solenn Patalano, and Fátima Gebauer. "Drosophila UNR Is Required for Translational Repression of Male-Specific Lethal 2 MRNA during Regulation of X-Chromosome Dosage Compensation." *Genes & Development* 20, no. 3 (2006): 380–89.

Akerib, Chantal Christ, and Barbara J. Meyer. "Identification of X Chromosome Regions in Caenorhabditis Elegans That Contain Sex-Determination Signal Elements." *Genetics* 138, no. 4 (1994): 1105–25.

Akhtar, Asifa, and Peter B. Becker. "Activation of Transcription through Histone H4 Acetylation by MOF, an Acetyltransferase Essential for Dosage Compensation in Drosophila." *Molecular Cell* 5, no. 2 (2000): 367–75.

Almeida, Mafalda, Greta Pintacuda, Osamu Masui, Yoko Koseki, Michal Gdula, Andrea Cerase, David Brown, Arne Mould, Cassandravictoria Innocent, Manabu Nakayama, Lothar Schermelleh, Tatyanna B. Nesterova, Haruhiko Koeski, and Neil Brockdorff. "PCGF3/5–PRC1 Initiates Polycomb Recruitment in X Chromosome Inactivation." *Science* 356, no. 6342 (2017): 1081–84.

Ambros, Victor, Rosalind C. Lee, Ann Lavanway, Peter T. Williams, and David Jewell. "MicroRNAs and Other Tiny Endogenous RNAs in C. Elegans." *Current Biology* 13, no. 10 (2003): 807–18.

Anguera, Montserrat C., Weiyuan Ma, Danielle Clift, Satoshi Namekawa, Raymond J. Kelleher III, and Jeannie T. Lee. "Tsx Produces a Long Noncoding RNA and Has General Functions in the Germline, Stem Cells, and Brain." *PLoS Genetics* 7, no. 9 (2011): e1002248.

Aoki, Kazuma, Hiromi Moriguchi, Tomoko Yoshioka, Katsuya Okawa, and Hiroaki Tabara. “In Vitro Analyses of the Production and Activity of Secondary Small Interfering RNAs in C. Elegans.” *The EMBO Journal* 26, no. 24 (2007): 5007–19.

Ashe, Alyson, Alexandra Sapetschnig, Eva-Maria Weick, Jacinth Mitchell, Marloes P. Bagijn, Amy C. Cording, Anna-Lisa Doebley, Leonard D. Goldstein, Nicolas J. Lehrbach, and Jérémie Le Pen, Greta Pintacuda, Aisa Sakaguchi, Peter Sarkies, Shawn Ahmed and Eric A. Miska. “PiRNAs Can Trigger a Multigenerational Epigenetic Memory in the Germline of C. Elegans.” *Cell* 150, no. 1 (2012): 88–99.

Asikainen, Suvi, Liisa Heikkinen, Garry Wong, and Markus Storvik. “Functional Characterization of Endogenous SiRNA Target Genes in Caenorhabditis Elegans.” *BMC Genomics* 9, no. 1 (2008): 1–10.

Bagijn, Marloes P., Leonard D. Goldstein, Alexandra Sapetschnig, Eva-Maria Weick, Samir Bouasker, Nicolas J. Lehrbach, Martin J. Simard, and Eric A. Miska. “Function, Targets, and Evolution of Caenorhabditis Elegans PiRNAs.” *Science* 337, no. 6094 (2012): 574–78.

Balaton, Bradley P., Allison M. Cotton, and Carolyn J. Brown. “Derivation of Consensus Inactivation Status for X-Linked Genes from Genome-Wide Studies.” *Biology of Sex Differences* 6, no. 1 (2015): 1–11.

Barucci, Giorgia, Eric Cornes, Meetali Singh, Blaise Li, Martino Ugolini, Aleksei Samolygo, Celine Didier, Florent Dingli, Damarys Loew, Piergiuseppe Quarato, and Germano Cecere. “Small-RNA-Mediated Transgenerational Silencing of Histone Genes Impairs Fertility in PiRNA Mutants.” *Nature Cell Biology* 22, no. 2 (2020): 235–45.

Bashaw, Greg J., and Bruce S. Baker. “The Regulation of the Drosophila Msl-2 Gene Reveals a Function for Sex-Lethal in Translational Control.” *Cell* 89, no. 5 (1997): 789–98.

Batista, Pedro J., J. Graham Ruby, Julie M. Claycomb, Rosaria Chiang, Noah Fahlgren, Kristin D. Kasschau, Daniel A. Chaves, Weifeng Gu, Jessica J. Vasale, and Shenghua Duan, Darryl Conte, Jr., Shunjun Luo, Gary P. Scroth, James C. Carrington, David P. Bartel, and Craig C. Mello. "PRG-1 and 21U-RNAs Interact to Form the PiRNA Complex Required for Fertility in C. Elegans." *Molecular Cell* 31, no. 1 (2008): 67–78.

Baulcombe, David C. "RNA as a Target and an Initiator of Post-Transcriptional Gene Silencing in Trangenic Plants." *Post-Transcriptional Control of Gene Expression in Plants*, 1996, 79–88.

Beckmann, Karsten, Marica Grskovic, Fátima Gebauer, and Matthias W. Hentze. "A Dual Inhibitory Mechanism Restricts Msl-2 MRNA Translation for Dosage Compensation in Drosophila." *Cell* 122, no. 4 (2005): 529–40.

Bellott, Daniel W., Jennifer F. Hughes, Helen Skaletsky, Laura G. Brown, Tatyana Pyntikova, Ting-Jan Cho, Natalia Koutseva, Sara Zaghlul, Tina Graves, and Susie Rock, etc, *et al.,* David C. Page. "Mammalian Y Chromosomes Retain Widely Expressed Dosage-Sensitive Regulators." *Nature* 508, no. 7497 (2014): 494–99.

Belote, John M., and John C. Lucchesi. "Male-Specific Lethal Mutations of Drosophila Melanogaster." *Genetics* 96, no. 1 (1980): 165–86.

Belton, Jon-Matthew, Rachel Patton McCord, Johan Harmen Gibcus, Natalia Naumova, Ye Zhan, and Job Dekker. "Hi–C: A Comprehensive Technique to Capture the Conformation of Genomes." *Methods* 58, no. 3 (2012): 268–76.

Berletch, Joel B., Wenxiu Ma, Fan Yang, Jay Shendure, William S. Noble, Christine M. Disteche, and Xinxian Deng. "Escape from X Inactivation Varies in Mouse Tissues." *PLoS Genetics* 11, no. 3 (2015): e1005079.

Bernstein, Emily, Amy A. Caudy, Scott M. Hammond, and Gregory J. Hannon. “Role for a Bidentate Ribonuclease in the Initiation Step of RNA Interference.” *Nature* 409, no. 6818 (2001): 363–66.

Billi, Allison C., Sylvia EJ Fischer, and John K. Kim. “Endogenous RNAi Pathways in C. Elegans.” *WormBook: The Online Review of C. Elegans Biology [Internet]*, 2018.

Billi, Allison C., Mallory A. Freeberg, Amanda M. Day, Sang Young Chun, Vishal Khivansara, and John K. Kim. “A Conserved Upstream Motif Orchestrates Autonomous, Germline-Enriched Expression of Caenorhabditis Elegans PiRNAs.” *PLoS Genetics* 9, no. 3 (2013): e1003392.

Blumenthal, Thomas. “Trans-Splicing and Operons in C. Elegans.” *WormBook: The Online Review of C. Elegans Biology [Internet]*, 2018.

Bone, James R., J. Lavender, Ron Richman, Melanie J. Palmer, Bryan M. Turner, and Mitzi I. Kuroda. “Acetylated Histone H4 on the Male X Chromosome Is Associated with Dosage Compensation in Drosophila.” *Genes & Development* 8, no. 1 (1994): 96–104.

Bosher, Julia M., Pascale Dufourcq, Satis Sookhareea, and Michel Labouesse. “RNA Interference Can Target Pre-MRNA: Consequences for Gene Expression in a Caenorhabditis Elegans Operon.” *Genetics* 153, no. 3 (1999): 1245–56.

Brejc, Katjuša, Qian Bian, Satoru Uzawa, Bayly S. Wheeler, Erika C. Anderson, David S. King, Philip J. Kranzusch, Christine G. Preston, and Barbara J. Meyer. “Dynamic Control of X Chromosome Conformation and Repression by a Histone H4K20 Demethylase.” *Cell* 171, no. 1 (2017): 85-102. e23.

Bridges, Calvin B. “Non-Disjunction as Proof of the Chromosome Theory of Heredity (Concluded).” *Genetics* 1, no. 2 (1916): 107.

Brockdorff, Neil, Alan Ashworth, Graham F. Kay, Veronica M. McCabe, Dominic P. Norris, Penny J. Cooper, Sally Swift, and Sohaila Rastan. “The Product of the Mouse Xist Gene Is a 15 Kb Inactive X-Specific Transcript Containing No Conserved ORF and Located in the Nucleus.” *Cell* 71, no. 3 (1992): 515–26.

Brockdorff, Neil, Joseph S. Bowness, and Guifeng Wei. “Progress toward Understanding Chromosome Silencing by Xist RNA.” *Genes & Development* 34, no. 11–12 (2020): 733–44.

Brown, Carolyn J., Brian D. Hendrich, Jim L. Rupert, Ronald G. Lafreniere, Yigong Xing, Jeanne Lawrence, and Huntington F. Willard. “The Human XIST Gene: Analysis of a 17 Kb Inactive X-Specific RNA That Contains Conserved Repeats and Is Highly Localized within the Nucleus.” *Cell* 71, no. 3 (1992): 527–42.

Buckley, Bethany A., Kirk B. Burkhart, Sam Guoping Gu, George Spracklin, Aaron Kershner, Heidi Fritz, Judith Kimble, Andrew Fire, and Scott Kennedy. “A Nuclear Argonaute Promotes Multigenerational Epigenetic Inheritance and Germline Immortality.” *Nature* 489, no. 7416 (2012): 447–51.

Bull, James J. *Evolution of Sex Determining Mechanisms.* The Benjamin/Cummings Publishing Company, Inc., 1983.

Burkhart, Kirk B., Shouhong Guang, Bethany A. Buckley, Lily Wong, Aaron F. Bochner, and Scott Kennedy. “A Pre-MRNA–Associating Factor Links Endogenous SiRNAs to Chromatin Regulation.” *PLoS Genetics* 7, no. 8 (2011): e1002249.

Burton, Nick O., Kirk B. Burkhart, and Scott Kennedy. “Nuclear RNAi Maintains Heritable Gene Silencing in Caenorhabditis Elegans.” *Proceedings of the National Academy of Sciences* 108, no. 49 (2011): 19683–88.

Carmi, Ilil, Jennifer B. Kopczynski, and Barbara J. Meyer. “The Nuclear Hormone Receptor SEX-1 Is an X-Chromosome Signal That Determines Nematode Sex.” *Nature* 396, no. 6707 (1998): 168–73.

Charlesworth, Brian. “Model for Evolution of Y Chromosomes and Dosage Compensation.” *Proceedings of the National Academy of Sciences* 75, no. 11 (1978): 5618–22.

Charlesworth, Brian. “The Evolution of Sex Chromosomes.” *Science* 251, no. 4997 (1991): 1030–33.

Chen, Songlin, Guojie Zhang, Changwei Shao, Quanfei Huang, Geng Liu, Pei Zhang, Wentao Song, Na An, Domitille Chalopin, and Jean-Nicolas Volff, etc, *et al.,* Jun Wang. “Whole-Genome Sequence of a Flatfish Provides Insights into ZW Sex Chromosome Evolution and Adaptation to a Benthic Lifestyle.” *Nature Genetics* 46, no. 3 (2014): 253–60.

Chu, Ci, Qiangfeng Cliff Zhang, Simão Teixeira Da Rocha, Ryan A. Flynn, Maheetha Bharadwaj, J. Mauro Calabrese, Terry Magnuson, Edith Heard, and Howard Y. Chang. “Systematic Discovery of Xist RNA Binding Proteins.” *Cell* 161, no. 2 (2015): 404–16.

Chu, Diana S., Heather E. Dawes, Jason D. Lieb, Raymond C. Chan, Annie F. Kuo, and Barbara J. Meyer. “A Molecular Link between Gene-Specific and Chromosome-Wide Transcriptional Repression.” *Genes & Development* 16, no. 7 (2002): 796–805.

Chureau, Corinne, Sophie Chantalat, Antonio Romito, Angélique Galvani, Laurent Duret, Philip Avner, and Claire Rougeulle. “Ftx Is a Non-Coding RNA Which Affects Xist Expression and Chromatin Structure within the X-Inactivation Center Region.” *Human Molecular Genetics* 20, no. 4 (2011): 705–18.

Colognori, David, Hongjae Sunwoo, Andrea J. Kriz, Chen-Yu Wang, and Jeannie T. Lee. “Xist Deletional Analysis Reveals an Interdependency between Xist RNA and Polycomb

Complexes for Spreading along the Inactive X." *Molecular Cell* 74, no. 1 (2019): 101-117. e10.

Conine, Colin C., Pedro J. Batista, Weifeng Gu, Julie M. Claycomb, Daniel A. Chaves, Masaki Shirayama, and Craig C. Mello. "Argonautes ALG-3 and ALG-4 Are Required for Spermatogenesis-Specific 26G-RNAs and Thermotolerant Sperm in Caenorhabditis Elegans." *Proceedings of the National Academy of Sciences* 107, no. 8 (2010): 3588–93.

Conrad, Thomas, Florence MG Cavalli, Juan M. Vaquerizas, Nicholas M. Luscombe, and Asifa Akhtar. "Drosophila Dosage Compensation Involves Enhanced Pol II Recruitment to Male X-Linked Promoters." *Science* 337, no. 6095 (2012): 742–46.

Cooper, D. W., P. G. Johnston, J. M. Watson, and J. A. M. Graves. "X-Inactivation in Marsupials and Monotremes." In *Seminars in Developmental Biology*, 4:117–28. Elsevier, 1993.

Copur, Ömer, Andrey Gorchakov, Katja Finkl, Mitzi I. Kuroda, and Jürg Müller. "Sex-Specific Phenotypes of Histone H4 Point Mutants Establish Dosage Compensation as the Critical Function of H4K16 Acetylation in Drosophila." *Proceedings of the National Academy of Sciences* 115, no. 52 (2018): 13336–41.

Crane, Emily, Qian Bian, Rachel Patton McCord, Bryan R. Lajoie, Bayly S. Wheeler, Edward J. Ralston, Satoru Uzawa, Job Dekker, and Barbara J. Meyer. "Condensin-Driven Remodelling of X Chromosome Topology during Dosage Compensation." *Nature* 523, no. 7559 (2015): 240–44.

Csankovszki, Gyorgyi, Karishma Collette, Karin Spahl, James Carey, Martha Snyder, Emily Petty, Uchita Patel, Tomoko Tabuchi, Hongbin Liu, and Ian McLeod, James Thompson, Ali Sarkeshik, John Yates, Barbara J. Meyer, and Kristin Hagstrom. "Three Distinct Condensin

Complexes Control C. Elegans Chromosome Dynamics." *Current Biology* 19, no. 1 (2009): 9–19.

Das, Partha P., Marloes P. Bagijn, Leonard D. Goldstein, Julie R. Woolford, Nicolas J. Lehrbach, Alexandra Sapetschnig, Heeran R. Buhecha, Michael J. Gilchrist, Kevin L. Howe, Rory Stark, etc., *et al.,* Eric A. Miska. "Piwi and PiRNAs Act Upstream of an Endogenous SiRNA Pathway to Suppress Tc3 Transposon Mobility in the Caenorhabditis Elegans Germline." *Molecular Cell* 31, no. 1 (2008): 79–90.

De Napoles, Mariana, Tatyana Nesterova, and Neil Brockdorff. "Early Loss of Xist RNA Expression and Inactive X Chromosome Associated Chromatin Modification in Developing Primordial Germ Cells." *PloS One* 2, no. 9 (2007): e860.

DeLong, L., J. D. Plenefisch, R. D. Klein, and B. J. Meyer. "Feedback Control of Sex Determination by Dosage Compensation Revealed through Caenorhabditis Elegans Sdc-3 Mutations." *Genetics* 133, no. 4 (1993): 875–96.

Dietzl, Georg, Doris Chen, Frank Schnorrer, Kuan-Chung Su, Yulia Barinova, Michaela Fellner, Beate Gasser, Kaolin Kinsey, Silvia Oppel, and Susanne Scheiblauer, etc., *et al.,* Barry J. Dickson. "A Genome-Wide Transgenic RNAi Library for Conditional Gene Inactivation in Drosophila." *Nature* 448, no. 7150 (2007): 151–56.

Dixon, Jesse R., Siddarth Selvaraj, Feng Yue, Audrey Kim, Yan Li, Yin Shen, Ming Hu, Jun S. Liu, and Bing Ren. "Topological Domains in Mammalian Genomes Identified by Analysis of Chromatin Interactions." *Nature* 485, no. 7398 (2012): 376–80.

Duncan, Kent E., Claudia Strein, and Matthias W. Hentze. "The SXL-UNR Corepressor Complex Uses a PABP-Mediated Mechanism to Inhibit Ribosome Recruitment to Msl-2 MRNA." *Molecular Cell* 36, no. 4 (2009): 571–82.

Duncan, Kent, Marica Grskovic, Claudia Strein, Karsten Beckmann, Ricarda Niggeweg, Irina Abaza, Fátima Gebauer, Matthias Wilm, and Matthias W. Hentze. “Sex-Lethal Imparts a Sex-Specific Function to UNR by Recruiting It to the Msl-2 MRNA 3′ UTR: Translational Repression for Dosage Compensation.” *Genes & Development* 20, no. 3 (2006): 368–79.

Dyer, K. A., T. K. Canfield, and S. M. Gartler. “Molecular Cytological Differentiation of Active from Inactive X Domains in Interphase: Implications for X Chromosome Inactivation.” *Cytogenetic and Genome Research* 50, no. 2–3 (1989): 116–20.

Elbashir, Sayda M., Jens Harborth, Winfried Lendeckel, Abdullah Yalcin, Klaus Weber, and Thomas Tuschl. “Duplexes of 21-Nucleotide RNAs Mediate RNA Interference in Cultured Mammalian Cells.” *Nature* 411, no. 6836 (2001): 494–98.

Ferrari, Francesco, Annette Plachetka, Artyom A. Alekseyenko, Youngsook L. Jung, Fatih Ozsolak, Peter V. Kharchenko, Peter J. Park, and Mitzi I. Kuroda. “‘Jump Start and Gain’ Model for Dosage Compensation in Drosophila Based on Direct Sequencing of Nascent Transcripts.” *Cell Reports* 5, no. 3 (2013): 629–36.

Fire, Andrew, SiQun Xu, Mary K. Montgomery, Steven A. Kostas, Samuel E. Driver, and Craig C. Mello. “Potent and Specific Genetic Interference by Double-Stranded RNA in Caenorhabditis Elegans.” *Nature* 391, no. 6669 (1998): 806–11.

Fisher, R. A. “The Sheltering of Lethals.” *The American Naturalist* 69, no. 724 (1935): 446–55.

Förch, Patrik, Livia Merendino, Concepción Martínez, and Juan Valcárcel. “Modulation of Msl-2 5′ Splice Site Recognition by Sex-Lethal.” *Rna* 7, no. 9 (2001): 1185–91.

Förch, P., and J. Valcarcel. “Molecular Mechanisms of Gene Expression Regulation by the Apoptosis-Promoting Protein TIA-1.” *Apoptosis* 6, no. 6 (2001): 463–68.

Furlan, Giulia, Nancy Gutierrez Hernandez, Christophe Huret, Rafael Galupa, Joke Gerarda van Bemmel, Antonio Romito, Edith Heard, Céline Morey, and Claire Rougeulle. “The Ftx Noncoding Locus Controls X Chromosome Inactivation Independently of Its RNA Products.” *Molecular Cell* 70, no. 3 (2018): 462-472. e8.

Gdula, Michal R., Tatyana B. Nesterova, Greta Pintacuda, Jonathan Godwin, Ye Zhan, Hakan Ozadam, Michael McClellan, Daniella Moralli, Felix Krueger, and Catherine M. Green, etc., *et al.,* Neil Brockdorff. “The Non-Canonical SMC Protein SmcHD1 Antagonises TAD Formation and Compartmentalisation on the Inactive X Chromosome.” *Nature Communications* 10, no. 1 (2019): 1–14.

Gebauer, Fatima, Davide FV Corona, Thomas Preiss, Peter B. Becker, and Matthias W. Hentze. “Translational Control of Dosage Compensation in Drosophila by Sex-lethal: Cooperative Silencing via the 5′ and 3′ UTRs of Msl-2 MRNA Is Independent of the Poly (A) Tail.” *The EMBO Journal* 18, no. 21 (1999): 6146–54.

Gelbart, Marnie E., and Mitzi I. Kuroda. “Drosophila Dosage Compensation: A Complex Voyage to the X Chromosome,” 2009.

Gelbart, Marnie E., Erica Larschan, Shouyong Peng, Peter J. Park, and Mitzi I. Kuroda. “Drosophila MSL Complex Globally Acetylates H4K16 on the Male X Chromosome for Dosage Compensation.” *Nature Structural & Molecular Biology* 16, no. 8 (2009): 825–32.

Gendrel, Anne-Valerie, Anwyn Apedaile, Heather Coker, Ausma Termanis, Ilona Zvetkova, Jonathan Godwin, Y. Amy Tang, Derek Huntley, Giovanni Montana, and Steven Taylor, Eleni Giannolatou, Edith Heard, Irina Stancheva, and Neil Brockdorff. “Smchd1-Dependent and-Independent Pathways Determine Developmental Dynamics of CpG Island Methylation on the Inactive X Chromosome.” *Developmental Cell* 23, no. 2 (2012): 265–79.

Gendrel, Anne-Valerie, Y. Amy Tang, Masako Suzuki, Jonathan Godwin, Tatyana B. Nesterova, John M. Greally, Edith Heard, and Neil Brockdorff. “Epigenetic Functions of Smchd1 Repress Gene Clusters on the Inactive X Chromosome and on Autosomes.” *Molecular and Cellular Biology* 33, no. 16 (2013): 3150–65.

Gent, Jonathan I., Ayelet T. Lamm, Derek M. Pavelec, Jay M. Maniar, Poornima Parameswaran, Li Tao, Scott Kennedy, and Andrew Z. Fire. “Distinct Phases of SiRNA Synthesis in an Endogenous RNAi Pathway in C. Elegans Soma.” *Molecular Cell* 37, no. 5 (2010): 679–89.

Gent, Jonathan I., Mara Schvarzstein, Anne M. Villeneuve, Sam Guoping Gu, Verena Jantsch, Andrew Z. Fire, and Antoine Baudrimont. “A Caenorhabditis Elegans RNA-Directed RNA Polymerase in Sperm Development and Endogenous RNA Interference.” *Genetics* 183, no. 4 (2009): 1297–1314.

Gerlich, Daniel, Toru Hirota, Birgit Koch, Jan-Michael Peters, and Jan Ellenberg. “Condensin I Stabilizes Chromosomes Mechanically through a Dynamic Interaction in Live Cells.” *Current Biology* 16, no. 4 (2006): 333–44.

Giorgetti, Luca, Bryan R. Lajoie, Ava C. Carter, Mikael Attia, Ye Zhan, Jin Xu, Chong Jian Chen, Noam Kaplan, Howard Y. Chang, Edith Heard and Job Dekker. “Structural Organization of the Inactive X Chromosome in the Mouse.” *Nature* 535, no. 7613 (2016): 575–79.

Gladden, John M., Behnom Farboud, and Barbara J. Meyer. “Revisiting the X: A Signal That Specifies Caenorhabditis Elegans Sexual Fate.” *Genetics* 177, no. 3 (2007): 1639–54.

Gladden, John M., and Barbara J. Meyer. “A ONECUT Homeodomain Protein Communicates X Chromosome Dose to Specify Caenorhabditis Elegans Sexual Fate by Repressing a Sex Switch Gene.” *Genetics* 177, no. 3 (2007): 1621–37.

Goodwin, Elizabeth B., and Ronald E. Ellis. “Turning Clustering Loops: Sex Determination in Caenorhabditis Elegans.” *Current Biology* 12, no. 3 (2002): R111–20.

Grant, Jennifer, Shantha K. Mahadevaiah, Pavel Khil, Mahesh N. Sangrithi, Hélène Royo, Janine Duckworth, John R. McCarrey, John L. VandeBerg, Marilyn B. Renfree, and Willie Taylor, etc., *et al.,* James M. A. Taylor. “Rsx Is a Metatherian RNA with Xist-like Properties in X-Chromosome Inactivation.” *Nature* 487, no. 7406 (2012): 254–58.

Graves, Jennifer A. Marshall. “Evolution of Vertebrate Sex Chromosomes and Dosage Compensation.” *Nature Reviews Genetics* 17, no. 1 (2016): 33–46.

Gruenbaum, Yosef, Ayelet Margalit, Robert D. Goldman, Dale K. Shumaker, and Katherine L. Wilson. “The Nuclear Lamina Comes of Age.” *Nature Reviews Molecular Cell Biology* 6, no. 1 (2005): 21–31.

Gu, Luiqi, and James R. Walters. “Evolution of Sex Chromosome Dosage Compensation in Animals: A Beautiful Theory, Undermined by Facts and Bedeviled by Details.” *Genome Biology and Evolution* 9, no. 9 (2017): 2461–76.

Gu, Sam Guoping, Julia Pak, Shouhong Guang, Jay M. Maniar, Scott Kennedy, and Andrew Fire. “Amplification of SiRNA in Caenorhabditis Elegans Generates a Transgenerational Sequence-Targeted Histone H3 Lysine 9 Methylation Footprint.” *Nature Genetics* 44, no. 2 (2012): 157–64.

Gu, Weifeng, Heng-Chi Lee, Daniel Chaves, Elaine M. Youngman, Gregory J. Pazour, Darryl Conte Jr, and Craig C. Mello. “CapSeq and CIP-TAP Identify Pol II Start Sites and Reveal Capped Small RNAs as C. Elegans PiRNA Precursors.” *Cell* 151, no. 7 (2012): 1488–1500.

Gu, Weifeng, Masaki Shirayama, Darryl Conte Jr, Jessica Vasale, Pedro J. Batista, Julie M. Claycomb, James J. Moresco, Elaine M. Youngman, Jennifer Keys, and Matthew J. Stoltz,

etc., *et al.,* Craig C. Mello. “Distinct Argonaute-Mediated 22G-RNA Pathways Direct Genome Surveillance in the C. Elegans Germline.” *Molecular Cell* 36, no. 2 (2009): 231–44.

Guang, Shouhong, Aaron F. Bochner, Kirk B. Burkhart, Nick Burton, Derek M. Pavelec, and Scott Kennedy. “Small Regulatory RNAs Inhibit RNA Polymerase II during the Elongation Phase of Transcription.” *Nature* 465, no. 7301 (2010): 1097–1101.

Guang, Shouhong, Aaron F. Bochner, Derek M. Pavelec, Kirk B. Burkhart, Sandra Harding, Jennifer Lachowiec, and Scott Kennedy. “An Argonaute Transports SiRNAs from the Cytoplasm to the Nucleus.” *Science* 321, no. 5888 (2008): 537–41.

Guenther, Matthew G., O. R. R. Barak, and Mitchell A. Lazar. “The SMRT and N-CoR Corepressors Are Activating Cofactors for Histone Deacetylase 3.” *Molecular and Cellular Biology* 21, no. 18 (2001): 6091–6101.

Haeusler, Rebecca A., Matthew Pratt-Hyatt, Paul D. Good, Theresa A. Gipson, and David R. Engelke. “Clustering of Yeast TRNA Genes Is Mediated by Specific Association of Condensin with TRNA Gene Transcription Complexes.” *Genes & Development* 22, no. 16 (2008): 2204–14.

Hagstrom, Kirsten A., Victor F. Holmes, Nicholas R. Cozzarelli, and Barbara J. Meyer. “C. Elegans Condensin Promotes Mitotic Chromosome Architecture, Centromere Organization, and Sister Chromatid Segregation during Mitosis and Meiosis.” *Genes & Development* 16, no. 6 (2002): 729–42.

Han, Ting, Arun Prasad Manoharan, Tim T. Harkins, Pascal Bouffard, Colin Fitzpatrick, Diana S. Chu, Danielle Thierry-Mieg, Jean Thierry-Mieg, and John K. Kim. “26G Endo-SiRNAs

Regulate Spermatogenic and Zygotic Gene Expression in Caenorhabditis Elegans." *Proceedings of the National Academy of Sciences* 106, no. 44 (2009): 18674–79.

Hilfiker, Andres, Denise Hilfiker-Kleiner, Antonio Pannuti, and John C. Lucchesi. "Mof, a Putative Acetyl Transferase Gene Related to the Tip60 and MOZ Human Genes and to the SAS Genes of Yeast, Is Required for Dosage Compensation in Drosophila." *The EMBO Journal* 16, no. 8 (1997): 2054–60.

Hirano, Tatsuya. "Condensin-Based Chromosome Organization from Bacteria to Vertebrates." *Cell* 164, no. 5 (2016): 847–57.

Hirano, Tatsuya. "The ABCs of SMC Proteins: Two-Armed ATPases for Chromosome Condensation, Cohesion, and Repair." *Genes & Development* 16, no. 4 (2002): 399–414.

Hodgkin, Jonathan, Jonathan D. Zellan, and Donna G. Albertson. "Identification of a Candidate Primary Sex Determination Locus, Fox-1, on the X Chromosome of Caenorhabditis Elegans." *Development* 120, no. 12 (1994): 3681–89.

Hsu, David R., and Barbara J. Meyer. "The Dpy-30 Gene Encodes an Essential Component of the Caenorhabditis Elegans Dosage Compensation Machinery." *Genetics* 137, no. 4 (1994): 999–1018.

Iwasaki, Osamu, Hideki Tanizawa, Kyoung-Dong Kim, Andrew Kossenkov, Timothy Nacarelli, Sanki Tashiro, Sonali Majumdar, Louise C. Showe, Rugang Zhang, and Ken-ichi Noma. "Involvement of Condensin in Cellular Senescence through Gene Regulation and Compartmental Reorganization." *Nature Communications* 10, no. 1 (2019): 1–20.

Jans, Judith, John M. Gladden, Edward J. Ralston, Catherine S. Pickle, Agnès H. Michel, Rebecca R. Pferdehirt, Michael B. Eisen, and Barbara J. Meyer. "A Condensin-like Dosage

Compensation Complex Acts at a Distance to Control Expression throughout the Genome." *Genes & Development* 23, no. 5 (2009): 602–18.

Jessberger, Rolf. "The Many Functions of SMC Proteins in Chromosome Dynamics." *Nature Reviews Molecular Cell Biology* 3, no. 10 (2002): 767–78.

Julien, Philippe, David Brawand, Magali Soumillon, Anamaria Necsulea, Angélica Liechti, Frédéric Schütz, Tasman Daish, Frank Grützner, and Henrik Kaessmann. "Mechanisms and Evolutionary Patterns of Mammalian and Avian Dosage Compensation." *PLoS Biology* 10, no. 5 (2012): e1001328.

Kalinava, Natallia, Julie Zhouli Ni, Zoran Gajic, Matthew Kim, Helen Ushakov, and Sam Guoping Gu. "C. Elegans Heterochromatin Factor SET-32 Plays an Essential Role in Transgenerational Establishment of Nuclear RNAi-Mediated Epigenetic Silencing." *Cell Reports* 25, no. 8 (2018): 2273-2284. e3.

Kelley, Richard L., Jiwu Wang, Leslie Bell, and Mitzi I. Kuroda. "Sex Lethal Controls Dosage Compensation in Drosophila by a Non-Splicing Mechanism." *Nature* 387, no. 6629 (1997): 195–99.

Ketting, René F., Sylvia EJ Fischer, Emily Bernstein, Titia Sijen, Gregory J. Hannon, and Ronald HA Plasterk. "Dicer Functions in RNA Interference and in Synthesis of Small RNA Involved in Developmental Timing in C. Elegans." *Genes & Development* 15, no. 20 (2001): 2654–59.

Kimura, Keiji, and Tatsuya Hirano. "ATP-Dependent Positive Supercoiling of DNA by 13S Condensin: A Biochemical Implication for Chromosome Condensation." *Cell* 90, no. 4 (1997): 625–34.

Knight, Scott W., and Brenda L. Bass. “A Role for the RNase III Enzyme DCR-1 in RNA Interference and Germ Line Development in Caenorhabditis Elegans.” *Science* 293, no. 5538 (2001): 2269–71.

Kohlmaier, Alexander, Fabio Savarese, Monika Lachner, Joost Martens, Thomas Jenuwein, Anton Wutz, and Peter Becker. “A Chromosomal Memory Triggered by Xist Regulates Histone Methylation in X Inactivation.” *PLoS Biology* 2, no. 7 (2004): e171.

Koopman, Peter, John Gubbay, Nigel Vivian, Peter Goodfellow, and Robin Lovell-Badge. “Male Development of Chromosomally Female Mice Transgenic for Sry.” *Nature* 351, no. 6322 (1991): 117–21.

Kramer, Maxwell, Anna-Lena Kranz, Amanda Su, Lara H. Winterkorn, Sarah Elizabeth Albritton, and Sevinc Ercan. “Developmental Dynamics of X-Chromosome Dosage Compensation by the DCC and H4K20me1 in C. Elegans.” *PLoS Genetics* 11, no. 12 (2015): e1005698.

Lakhotia, S. C., and A. S. Mukherjee. “Chromosomal Basis of Dosage Compensation in Drosophila: I. Cellular Autonomy of Hyperactivity of the Male X-Chromosome in Salivary Glands and Sex Differentiation.” *Genetics Research* 14, no. 2 (1969): 137–50.

Lakhotia, S. C., and A. S. Mukherjee. “CHROMOSOMAL BASIS OF DOSAGE COMPENSATION IN DROSOPHILA: III. Early Completion of Replication by the Polytene X-Chromosome in Male: Further Evidence and Its Implications.” *The Journal of Cell Biology* 47, no. 1 (1970): 18–33.

Larschan, Erica, Eric P. Bishop, Peter V. Kharchenko, Leighton J. Core, John T. Lis, Peter J. Park, and Mitzi I. Kuroda. “X Chromosome Dosage Compensation via Enhanced Transcriptional Elongation in Drosophila.” *Nature* 471, no. 7336 (2011): 115–18.

Lau, Alyssa C., Kentaro Nabeshima, and Györgyi Csankovszki. “The C. Elegans Dosage Compensation Complex Mediates Interphase X Chromosome Compaction.” *Epigenetics & Chromatin* 7, no. 1 (2014): 1–16.

Lee, Heng-Chi, Weifeng Gu, Masaki Shirayama, Elaine Youngman, Darryl Conte Jr, and Craig C. Mello. “C. Elegans PiRNAs Mediate the Genome-Wide Surveillance of Germline Transcripts.” *Cell* 150, no. 1 (2012): 78–87.

Lee, Jeannie, Lance S. Davidow, and David Warshawsky. “Tsix, a Gene Antisense to Xist at the X-Inactivation Centre.” *Nature Genetics* 21, no. 4 (1999): 400–404.

Lieb, Jason D., Michael R. Albrecht, Pao-Tien Chuang, and Barbara J. Meyer. “MIX-1: An Essential Component of the C. Elegans Mitotic Machinery Executes X Chromosome Dosage Compensation.” *Cell* 92, no. 2 (1998): 265–77.

Loda, Agnese, Johannes H. Brandsma, Ivaylo Vassilev, Nicolas Servant, Friedemann Loos, Azadeh Amirnasr, Erik Splinter, Emmanuel Barillot, Raymond A. Poot, Edith Heard and Joost Gribnau. “Genetic and Epigenetic Features Direct Differential Efficiency of Xist-Mediated Silencing at X-Chromosomal and Autosomal Locations.” *Nature Communications* 8, no. 1 (2017): 1–16.

Loda, Agnese, and Edith Heard. “Xist RNA in Action: Past, Present, and Future.” *PLoS Genetics* 15, no. 9 (2019): e1008333.

Luz, John Gately, Christian A. Hassig, Catherine Pickle, Adam Godzik, Barbara J. Meyer, and Ian A. Wilson. “XOL-1, Primary Determinant of Sexual Fate in C. Elegans, Is a GHMP Kinase Family Member and a Structural Prototype for a Class of Developmental Regulators.” *Genes & Development* 17, no. 8 (2003): 977–90.

Lyon, Mary F. “Gene Action in the X-Chromosome of the Mouse (Mus Musculus L.).” *Nature* 190, no. 4773 (1961): 372–73.

Mao, Hui, Chengming Zhu, Dandan Zong, Chenchun Weng, Xiangwei Yang, Hui Huang, Dun Liu, Xuezhu Feng, and Shouhong Guang. “The Nrde Pathway Mediates Small-RNA-Directed Histone H3 Lysine 27 Trimethylation in Caenorhabditis Elegans.” *Current Biology* 25, no. 18 (2015): 2398–2403.

McHugh, Colleen A., Chun-Kan Chen, Amy Chow, Christine F. Surka, Christina Tran, Patrick McDonel, Amy Pandya-Jones, Mario Blanco, Christina Burghard, Annie Moradian, etc., *et al.,* Mitchell Guttman. “The Xist LncRNA Interacts Directly with SHARP to Silence Transcription through HDAC3.” *Nature* 521, no. 7551 (2015): 232–36.

Medenbach, Jan, Markus Seiler, and Matthias W. Hentze. “Translational Control via Protein-Regulated Upstream Open Reading Frames.” *Cell* 145, no. 6 (2011): 902–13.

Meneely, Philip M., and William B. Wood. “An Autosomal Gene That Affects X Chromosome Expression and Sex Determination in Caenorhabditis Elegans.” *Genetics* 106, no. 1 (1984): 29–44.

Merendino, Livia, Sabine Guth, Daniel Bilbao, Concepción Martínez, and Juan Valcárcel. “Inhibition of Msl-2 Splicing by Sex-Lethal Reveals Interaction between U2AF 35 and the 3′ Splice Site AG.” *Nature* 402, no. 6763 (1999): 838–41.

Meyer, Barbara J. “X-Chromosome Dosage Compensation.” *WormBook: The Online Review of C. Elegans Biology [Internet]*, 2005.

Meyer, Barbara J., and Lawrence P. Casson. “Caenorhabditis Elegans Compensates for the Difference in X Chromosome Dosage between the Sexes by Regulating Transcript Levels.” *Cell* 47, no. 6 (1986): 871–81.

Mikami, Suzuka, Teppei Kanaba, Naoki Takizawa, Ayaho Kobayashi, Ryoko Maesaki, Toshinobu Fujiwara, Yutaka Ito, and Masaki Mishima. “Structural Insights into the Recruitment of SMRT by the Corepressor SHARP under Phosphorylative Regulation.” *Structure* 22, no. 1 (2014): 35–46.

Miller, Leilani M., John D. Plenefisch, Lawrence P. Casson, and Barbara J. Meyer. “Xol-1: A Gene That Controls the Male Modes of Both Sex Determination and X Chromosome Dosage Compensation in C. Elegans.” *Cell* 55, no. 1 (1988): 167–83.

Minajigi, Anand, John E. Froberg, Chunyao Wei, Hongjae Sunwoo, Barry Kesner, David Colognori, Derek Lessing, Bernhard Payer, Myriam Boukhali, Wilhelm Haas, and Jeannie T. Lee. “A Comprehensive Xist Interactome Reveals Cohesin Repulsion and an RNA-Directed Chromosome Conformation.” *Science* 349, no. 6245 (2015).

Monfort, Asun, Giulio Di Minin, Andreas Postlmayr, Remo Freimann, Fabiana Arieti, Stéphane Thore, and Anton Wutz. “Identification of Spen as a Crucial Factor for Xist Function through Forward Genetic Screening in Haploid Embryonic Stem Cells.” *Cell Reports* 12, no. 4 (2015): 554–61.

Mould, Arne W., Zhenyi Pang, Miha Pakusch, Ian D. Tonks, Mitchell Stark, Dianne Carrie, Pamela Mukhopadhyay, Annica Seidel, Jonathan J. Ellis, and Janine Deakin, Matthew J. Wakefield, Lutz Krause, Marnie Blewitt, and Graham F. Kay. “Smchd1 Regulates a Subset of Autosomal Genes Subject to Monoallelic Expression in Addition to Being Critical for X Inactivation.” *Epigenetics & Chromatin* 6, no. 1 (2013): 1–16.

Mukherjee, Ardhendu S., and Wolfgang Beermann. “Synthesis of Ribonucleic Acid by the X-Chromosomes of Drosophila Melanogaster and the Problem of Dosage Compensation.” *Nature* 207, no. 4998 (1965): 785–86.

Muller, Hermann J. “Genetic Variability, Twin Hybrids and Constant Hybrids, in a Case of Balanced Lethal Factors.” *Genetics* 3, no. 5 (1918): 422.

Muller, Hermann Joseph. “Some Genetic Aspects of Sex.” *The American Naturalist* 66, no. 703 (1932): 118–38.

Murtagh, Carolyn E. “A Unique Cytogenetic System in Monotremes.” *Chromosoma* 65, no. 1 (1977): 37–57.

Napoles, Mariana de, Jacqueline E. Mermoud, Rika Wakao, Y. Amy Tang, Mitusuhiro Endoh, Ruth Appanah, Tatyana B. Nesterova, Jose Silva, Arie P. Otte, and Miguel Vidal. “Polycomb Group Proteins Ring1A/B Link Ubiquitylation of Histone H2A to Heritable Gene Silencing and X Inactivation.” *Developmental Cell* 7, no. 5 (2004): 663–76.

Nesterova, Tatyana B., Guifeng Wei, Heather Coker, Greta Pintacuda, Joseph S. Bowness, Tianyi Zhang, Mafalda Almeida, Bianca Bloechl, Benoit Moindrot, and Emma J. Carter, etc., *et al.,* Neil Brockdorff. “Systematic Allelic Analysis Defines the Interplay of Key Pathways in X Chromosome Inactivation.” *Nature Communications* 10, no. 1 (2019): 1–15.

Nguyen, H. P., A. Riess, Maren Krüger, P. Bauer, S. Singer, M. Schneider, H. Enders, and A. Dufke. “Mosaic Trisomy 21/Monosomy 21 in a Living Female Infant.” *Cytogenetic and Genome Research* 125, no. 1 (2009): 26–32.

Ni, Julie Zhouli, Esteban Chen, and Sam Guoping Gu. “Complex Coding of Endogenous SiRNA, Transcriptional Silencing and H3K9 Methylation on Native Targets of Germline Nuclear RNAi in C. Elegans.” *BMC Genomics* 15, no. 1 (2014): 1–14.

Nicoll, Monique, Chantal C. Akerib, and Barbara J. Meyer. “X-Chromosome-Counting Mechanisms That Determine Nematode Sex.” *Nature* 388, no. 6638 (1997): 200–204.

Nora, Elphège P., Bryan R. Lajoie, Edda G. Schulz, Luca Giorgetti, Ikuhiro Okamoto, Nicolas Servant, Tristan Piolot, Nynke L. Van Berkum, Johannes Meisig, etc., *et al.,* Job Dekker and Edith Heard. "Spatial Partitioning of the Regulatory Landscape of the X-Inactivation Centre." *Nature* 485, no. 7398 (2012): 381–85.

Nusbaum, Chad, and Barbara J. Meyer. "The Caenorhabditis Elegans Gene Sdc-2 Controls Sex Determination and Dosage Compensation in XX Animals." *Genetics* 122, no. 3 (1989): 579–93.

Oda, Hisanobu, Ikuhiro Okamoto, Niall Murphy, Jianhua Chu, Sandy M. Price, Michael M. Shen, Maria Elena Torres-Padilla, Edith Heard, and Danny Reinberg. "Monomethylation of Histone H4-Lysine 20 Is Involved in Chromosome Structure and Stability and Is Essential for Mouse Development." *Molecular and Cellular Biology* 29, no. 8 (2009): 2278–95.

Ogawa, Yuya, and Jeannie T. Lee. "Xite, X-Inactivation Intergenic Transcription Elements That Regulate the Probability of Choice." *Molecular Cell* 11, no. 3 (2003): 731–43.

Ohno, Susumu. *Sex Chromosomes and Sex-Linked Genes*. Vol. 1. Springer Science & Business Media, 2013.

Pal, Koustav, Mattia Forcato, Daniel Jost, Thomas Sexton, Cédric Vaillant, Elisa Salviato, Emilia Maria Cristina Mazza, Enrico Lugli, Giacomo Cavalli, and Francesco Ferrari. "Global Chromatin Conformation Differences in the Drosophila Dosage Compensated Chromosome X." *Nature Communications* 10, no. 1 (2019): 1–16.

Park, Seung-Won, Hyangyee Oh, Yuh-Ru Lin, and Yongkyu Park. "MSL Cis-Spreading from RoX Gene up-Regulates the Neighboring Genes." *Biochemical and Biophysical Research Communications* 399, no. 2 (2010): 227–31.

Patil, Deepak P., Chun-Kan Chen, Brian F. Pickering, Amy Chow, Constanza Jackson, Mitchell Guttman, and Samie R. Jaffrey. “M 6 A RNA Methylation Promotes XIST-Mediated Transcriptional Repression.” *Nature* 537, no. 7620 (2016): 369–73.

Paul, Matthew Robert, Andreas Hochwagen, and Sevinç Ercan. “Condensin Action and Compaction.” *Current Genetics* 65, no. 2 (2019): 407–15.

Penalva, Luiz OF, and Lucas Sánchez. “RNA Binding Protein Sex-Lethal (Sxl) and Control of Drosophila Sex Determination and Dosage Compensation.” *Microbiology and Molecular Biology Reviews* 67, no. 3 (2003): 343–59.

Penny, Graeme D., Graham F. Kay, Steven A. Sheardown, Sohaila Rastan, and Neil Brockdorff. “Requirement for Xist in X Chromosome Inactivation.” *Nature* 379, no. 6561 (1996): 131–37.

Pferdehirt, Rebecca R., and Barbara J. Meyer. “SUMOylation Is Essential for Sex-Specific Assembly and Function of the Caenorhabditis Elegans Dosage Compensation Complex on X Chromosomes.” *Proceedings of the National Academy of Sciences* 110, no. 40 (2013): E3810–19.

Pintacuda, Greta, Alexander N. Young, and Andrea Cerase. “Function by Structure: Spotlights on Xist Long Non-Coding RNA.” *Frontiers in Molecular Biosciences* 4 (2017): 90.

Plath, Kathrin, Jia Fang, Susanna K. Mlynarczyk-Evans, Ru Cao, Kathleen A. Worringer, Hengbin Wang, C. Cecile, Arie P. Otte, Barbara Panning, and Yi Zhang. “Role of Histone H3 Lysine 27 Methylation in X Inactivation.” *Science* 300, no. 5616 (2003): 131–35.

Powell, Jennifer R., Margaret M. Jow, and Barbara J. Meyer. “The T-Box Transcription Factor SEA-1 Is an Autosomal Element of the X: A Signal That Determines C. Elegans Sex.” *Developmental Cell* 9, no. 3 (2005): 339–49.

Rhind, Nicholas R., Leilani M. Miller, Jennifer B. Kopczynski, and Barbara J. Meyer. “Xo1-1 Acts as an Early Switch in the C. Elegans Male/Hermaphrodite Decision.” *Cell* 80, no. 1 (1995): 71–82.

Rice, Alan M., and Aoife McLysaght. “Dosage Sensitivity Is a Major Determinant of Human Copy Number Variant Pathogenicity.” *Nature Communications* 8, no. 1 (2017): 1–11.

Rice, Judd C., Kenichi Nishioka, Kavitha Sarma, Ruth Steward, Danny Reinberg, and C. David Allis. “Mitotic-Specific Methylation of Histone H4 Lys 20 Follows Increased PR-Set7 Expression and Its Localization to Mitotic Chromosomes.” *Genes & Development* 16, no. 17 (2002): 2225–30.

Rice, William R. “Evolution of the Y Sex Chromosome in Animals.” *Bioscience* 46, no. 5 (1996): 331–43.

Robinson, Philip JJ, Woojin An, Andrew Routh, Fabrizio Martino, Lynda Chapman, Robert G. Roeder, and Daniela Rhodes. “30 Nm Chromatin Fibre Decompaction Requires Both H4-K16 Acetylation and Linker Histone Eviction.” *Journal of Molecular Biology* 381, no. 4 (2008): 816–25.

Ruby, J. Graham, Calvin Jan, Christopher Player, Michael J. Axtell, William Lee, Chad Nusbaum, Hui Ge, and David P. Bartel. “Large-Scale Sequencing Reveals 21U-RNAs and Additional MicroRNAs and Endogenous SiRNAs in C. Elegans.” *Cell* 127, no. 6 (2006): 1193–1207.

Shi, Yanhong, Michael Downes, Wen Xie, Hung-Ying Kao, Peter Ordentlich, Chih-Cheng Tsai, Michelle Hon, and Ronald M. Evans. “Sharp, an Inducible Cofactor That Integrates Nuclear Receptor Repression and Activation.” *Genes & Development* 15, no. 9 (2001): 1140–51.

Shogren-Knaak, Michael, Haruhiko Ishii, Jian-Min Sun, Michael J. Pazin, James R. Davie, and Craig L. Peterson. “Histone H4-K16 Acetylation Controls Chromatin Structure and Protein Interactions.” *Science* 311, no. 5762 (2006): 844–47.

Sijen, Titia, Jamie Fleenor, Femke Simmer, Karen L. Thijssen, Susan Parrish, Lisa Timmons, Ronald HA Plasterk, and Andrew Fire. “On the Role of RNA Amplification in DsRNA-Triggered Gene Silencing.” *Cell* 107, no. 4 (2001): 465–76.

Silva, Jose, Winifred Mak, Ilona Zvetkova, Ruth Appanah, Tatyana B. Nesterova, Zoe Webster, Antoine HFM Peters, Thomas Jenuwein, Arie P. Otte, and Neil Brockdorff. “Establishment of Histone H3 Methylation on the Inactive X Chromosome Requires Transient Recruitment of Eed-Enx1 Polycomb Group Complexes.” *Developmental Cell* 4, no. 4 (2003): 481–95.

Skibbens, Robert V. “Condensins and Cohesins–One of These Things Is Not like the Other!” *Journal of Cell Science* 132, no. 3 (2019): jcs220491.

Smith, Edwin R., Antonio Pannuti, Weigang Gu, Arnd Steurnagel, Richard G. Cook, C. David Allis, and John C. Lucchesi. “The Drosophila MSL Complex Acetylates Histone H4 at Lysine 16, a Chromatin Modification Linked to Dosage Compensation.” *Molecular and Cellular Biology* 20, no. 1 (2000): 312–18.

Snyder, Martha J., Alyssa C. Lau, Elizabeth A. Brouhard, Michael B. Davis, Jianhao Jiang, Margarita H. Sifuentes, and Györgyi Csankovszki. “Anchoring of Heterochromatin to the Nuclear Lamina Reinforces Dosage Compensation-Mediated Gene Repression.” *PLoS Genetics* 12, no. 9 (2016): e1006341.

Stavropoulos, Nicholas, Rebecca K. Rowntree, and Jeannie T. Lee. “Identification of Developmentally Specific Enhancers for Tsix in the Regulation of X Chromosome Inactivation.” *Molecular and Cellular Biology* 25, no. 7 (2005): 2757–69.

Straub, Tobias, Gregor D. Gilfillan, Verena K. Maier, and Peter B. Becker. "The Drosophila MSL Complex Activates the Transcription of Target Genes." *Genes & Development* 19, no. 19 (2005): 2284–88.

Sun, Sha, Brian C. Del Rosario, Attila Szanto, Yuya Ogawa, Yesu Jeon, and Jeannie T. Lee. "Jpx RNA Activates Xist by Evicting CTCF." *Cell* 153, no. 7 (2013): 1537–51.

Swedlow, Jason R., and Tatsuya Hirano. "The Making of the Mitotic Chromosome: Modern Insights into Classical Questions." *Molecular Cell* 11, no. 3 (2003): 557–69.

Tabara, Hiroaki, Madathia Sarkissian, William G. Kelly, Jamie Fleenor, Alla Grishok, Lisa Timmons, Andrew Fire, and Craig C. Mello. "The Rde-1 Gene, RNA Interference, and Transposon Silencing in C. Elegans." *Cell* 99, no. 2 (1999): 123–32.

Tang, Wen, Meetu Seth, Shikui Tu, En-Zhi Shen, Qian Li, Masaki Shirayama, Zhiping Weng, and Craig C. Mello. "A Sex Chromosome PiRNA Promotes Robust Dosage Compensation and Sex Determination in C. Elegans." *Developmental Cell* 44, no. 6 (2018): 762-770. e3.

Thomas, Tim, and Anne K. Voss. "The Diverse Biological Roles of MYST Histone Acetyltransferase Family Proteins." *Cell Cycle* 6, no. 6 (2007): 696–704.

Tian, Di, Sha Sun, and Jeannie T. Lee. "The Long Noncoding RNA, Jpx, Is a Molecular Switch for X Chromosome Inactivation." *Cell* 143, no. 3 (2010): 390–403.

Timmons, Lisa, Donald L. Court, and Andrew Fire. "Ingestion of Bacterially Expressed DsRNAs Can Produce Specific and Potent Genetic Interference in Caenorhabditis Elegans." *Gene* 263, no. 1–2 (2001): 103–12.

Tsai, Hsin-Yue, Chun-Chieh G. Chen, Darryl Conte Jr, James J. Moresco, Daniel A. Chaves, Shohei Mitani, John R. Yates III, Ming-Daw Tsai, and Craig C. Mello. "A Ribonuclease

Coordinates SiRNA Amplification and MRNA Cleavage during RNAi." *Cell* 160, no. 3 (2015): 407–19.

Turner, Bryan M., Andrew J. Birley, and Jayne Lavender. "Histone H4 Isoforms Acetylated at Specific Lysine Residues Define Individual Chromosomes and Chromatin Domains in Drosophila Polytene Nuclei." *Cell* 69, no. 2 (1992): 375–84.

Van der Krol, Alexander R., Leon A. Mur, Marcel Beld, J. N. Mol, and Antoine R. Stuitje. "Flavonoid Genes in Petunia: Addition of a Limited Number of Gene Copies May Lead to a Suppression of Gene Expression." *The Plant Cell* 2, no. 4 (1990): 291–99.

Vasale, Jessica J., Weifeng Gu, Caroline Thivierge, Pedro J. Batista, Julie M. Claycomb, Elaine M. Youngman, Thomas F. Duchaine, Craig C. Mello, and Darryl Conte. "Sequential Rounds of RNA-Dependent RNA Transcription Drive Endogenous Small-RNA Biogenesis in the ERGO-1/Argonaute Pathway." *Proceedings of the National Academy of Sciences* 107, no. 8 (2010): 3582–87.

Vella, Monica C., and Frank J. Slack. "C. Elegans MicroRNAs." *WormBook: The Online Review of C. Elegans Biology [Internet]*, 2005.

Vicoso, Beatriz, J. J. Emerson, Yulia Zektser, Shivani Mahajan, and Doris Bachtrog. "Comparative Sex Chromosome Genomics in Snakes: Differentiation, Evolutionary Strata, and Lack of Global Dosage Compensation." *PLoS Biology* 11, no. 8 (2013): e1001643.

Vielle, Anne, Jackie Lang, Yan Dong, Sevinc Ercan, Chitra Kotwaliwale, Andreas Rechtsteiner, Alex Appert, Q. Brent Chen, Andrea Dose, and Thea Egelhofer, etc., *et al.,* Julie Ahringer. "H4K20me1 Contributes to Downregulation of X-Linked Genes for C. Elegans Dosage Compensation," 2012.

Villeneuve, Anne M., and Barbara J. Meyer. “Sdc-1: A Link between Sex Determination and Dosage Compensation in C. Elegans.” *Cell* 48, no. 1 (1987): 25–37.

Wallace, Heather A., Joseph E. Klebba, Thomas Kusch, Gregory C. Rogers, and Giovanni Bosco. “Condensin II Regulates Interphase Chromatin Organization through the Mrg-Binding Motif of Cap-H2.” *G3: Genes, Genomes, Genetics* 5, no. 5 (2015): 803–17.

Wang, Hengbin, Liangjun Wang, Hediye Erdjument-Bromage, Miguel Vidal, Paul Tempst, Richard S. Jones, and Yi Zhang. “Role of Histone H2A Ubiquitination in Polycomb Silencing.” *Nature* 431, no. 7010 (2004): 873–78.

Wang, Jianbo, Jesse Mager, Yijing Chen, Elizabeth Schneider, James C. Cross, Andras Nagy, and Terry Magnuson. “Imprinted X Inactivation Maintained by a Mouse Polycomb Group Gene.” *Nature Genetics* 28, no. 4 (2001): 371–75.

Wells, Michael B., Martha J. Snyder, Laura M. Custer, and Gyorgyi Csankovszki. “Caenorhabditis Elegans Dosage Compensation Regulates Histone H4 Chromatin State on X Chromosomes.” *Molecular and Cellular Biology* 32, no. 9 (2012): 1710–19.

Woodhouse, Rachel M., Gabriele Buchmann, Matthew Hoe, Dylan J. Harney, Jason KK Low, Mark Larance, Peter R. Boag, and Alyson Ashe. “Chromatin Modifiers SET-25 and SET-32 Are Required for Establishment but Not Long-Term Maintenance of Transgenerational Epigenetic Inheritance.” *Cell Reports* 25, no. 8 (2018): 2259-2272. e5.

Wutz, Anton, Theodore P. Rasmussen, and Rudolf Jaenisch. “Chromosomal Silencing and Localization Are Mediated by Different Domains of Xist RNA.” *Nature Genetics* 30, no. 2 (2002): 167–74.

Yamada, Norishige, and Yuya Ogawa. “Mechanisms of Long Noncoding Xist RNA-Mediated Chromosome-Wide Gene Silencing in X-Chromosome Inactivation.” In *Long Noncoding RNAs*, 151–71. Springer, 2015.

Yang, Huan, Ying Zhang, Jim Vallandingham, Hau Li, Laurence Florens, and Ho Yi Mak. “The RDE-10/RDE-11 Complex Triggers RNAi-Induced MRNA Degradation by Association with Target MRNA in C. Elegans.” *Genes & Development* 26, no. 8 (2012): 846–56.

Yigit, Erbay, Pedro J. Batista, Yanxia Bei, Ka Ming Pang, Chun-Chieh G. Chen, Niraj H. Tolia, Leemor Joshua-Tor, Shohei Mitani, Martin J. Simard, and Craig C. Mello. “Analysis of the C. Elegans Argonaute Family Reveals That Distinct Argonautes Act Sequentially during RNAi.” *Cell* 127, no. 4 (2006): 747–57.

You, Seo-Hee, Hee-Woong Lim, Zheng Sun, Molly Broache, Kyoung-Jae Won, and Mitchell A. Lazar. “Nuclear Receptor Co-Repressors Are Required for the Histone-Deacetylase Activity of HDAC3 in Vivo.” *Nature Structural & Molecular Biology* 20, no. 2 (2013): 182–87.

CHAPTER 2

Anchoring of Heterochromatin to the Nuclear Lamina Helps Stabilize Dosage Compensation-Mediated Gene Repression

This chapter was published as Snyder M , Lau AC, Brouhard EA, Davis M, *et al.* (2016) in PLoS Genetics as "Anchoring of heterochromatin to the nuclear lamina helps stabilize dosage compensation-mediated gene repression" I conducted the FISH experiments, imaging and analyses for all of Figure 2.5, the FISH experiments, imaging and analyses for Figure 2.6, parts D, E, F. I also assisted with scoring the worm counts for Figure 2.12 and the proofreading and editing of this manuscript. All other figures are the work of A. Lau, M. Snyder, E. Brouhard, J. Jiang, M. Sifuentes, and G. Csankovszki.

ABSTRACT

Higher order chromosome structure and nuclear architecture can have profound effects on gene regulation. We analyzed how compartmentalizing the genome by tethering heterochromatic regions to the nuclear lamina affects dosage compensation in the nematode *C. elegans*. In this organism, the dosage compensation complex (DCC) binds both X chromosomes of hermaphrodites to repress transcription two-fold, thus balancing gene expression between XX hermaphrodites and XO males. X chromosome structure is disrupted by mutations in DCC subunits. Using X chromosome paint fluorescence microscopy, we found that X chromosome structure and subnuclear localization are also disrupted when the mechanisms that anchor heterochromatin to the nuclear lamina are defective. Strikingly, the heterochromatic left end of

the X chromosome is less affected than the gene-rich middle region, which lacks heterochromatic anchors. These changes in X chromosome structure and subnuclear localization are accompanied by small, but significant levels of derepression of X-linked genes as measured by RNA-seq, without any observable defects in DCC localization and DCC-mediated changes in histone modifications. We propose a model in which heterochromatic tethers on the left arm of the X cooperate with the DCC to compact and peripherally relocate the X chromosomes, contributing to gene repression.

AUTHOR SUMMARY

DNA isolated from the nucleus of a single human cell, if stretched out, would be 3 meters long. This amount of DNA must be packaged into a nucleus, which is orders of magnitude smaller. DNA of active genes tends to be loosely packed and localized internally within the nucleus, while DNA of inactive genes tends to be tightly packed and localized near the nuclear periphery. We studied the effects of DNA compaction and nuclear localization on gene expression levels using regulation of the X chromosomes in the nematode *Caenorhabditis elegans* as a model. In this organism, hermaphrodites have two X chromosomes, and males have only one. Genes on the two X chromosomes in hermaphrodites are expressed at half the level compared to the male X, such that the two Xs together express as much gene products as the single X in males. We found that silent regions at the left end of hermaphrodite X chromosomes are tethered to the nuclear periphery, and these tethers are used to build a compact chromosome structure. If this process is defective, gene expression levels are elevated, but less than two-fold. These results indicate that chromosome compaction and nuclear localization contribute to influencing gene expression levels, but other mechanisms must also contribute.

INTRODUCTION

Expression of genes must be tightly regulated both spatially and temporarily to ensure normal development. While our understanding of gene regulation at the level of transcription factor binding and modulation of chromatin structure is supported by an abundance of data, the contribution of the spatial organization of the nucleus to regulation of gene expression is not well understood. Regulation of sex chromosome-linked gene expression in the process of dosage compensation provides an excellent model to dissect the influence of different gene regulatory mechanisms on chromosome-wide modulation of gene activity. In the nematode *C. elegans*, dosage compensation downregulates expression of genes on the otherwise highly expressed X chromosomes of hermaphrodites, such that transcript levels from the two hermaphrodite X chromosomes are brought down to match transcript levels from the single X in males (Lau and Csankovszki, 2015; Strome *et al.,* 2014). A complex of proteins called the dosage compensation complex (DCC) binds the length of both hermaphrodite X chromosomes to regulate transcription. The DCC contains a subcomplex, condensin I^{DC}, which is homologous to condensin complexes in all eukaryotes responsible for compaction and segregation of chromosomes in mitosis and meiosis (Chuang *et al.,* 1994; Csankovszki *et a.,* 2009; Mets and Meyer, 2009).

Although a number of studies in recent years uncovered molecular mechanisms of DCC action, how these alterations in X chromosome structure repress gene expression remains unknown. Consistent with a similarity to mitotic condensins, DCC binding leads to compaction of hermaphrodite X chromosomes in interphase (Lau and Csankovszki, 2014; Sharm *et al.,* 2014). The DCC also remodels the X chromosomes into topologically associating domains

(TADs) with more regular spacing and stronger boundaries than those found on autosomes (Crane *et al.,* 2015). At the level of chromatin organization, posttranslational modifications of histones are also altered in a DCC-dependent manner: monomethylation of histone H4 lysine 20 (H4K20me1) becomes enriched, and acetylation of histone H4 lysine 16 (H4K16ac) becomes depleted on dosage compensated Xs as compared to autosomes (Vielle *et al.,* 2012; Wells *et al.,* 2012). Analysis of gene expression in H4K20 histone methyltransferase (HMT) mutants revealed that changes in H4K20me1 levels contribute to DCC-mediated repression, but are not fully responsible for the observed two-fold repression (Kramer *et al.,* 2015). The relative contributions of chromosome condensation and partitioning of the chromosome into TADs are unclear. To date, no correlation has been found between genes being subjected to DCC-mediated repression and regions of the chromosome bound by the DCC (Jans *et al.,* 2009; Kruesi *et al.,* 2013), DCC-induced changes in TADs (Crane *et al.,* 2017) or posttranslational histone modifications (Wells *et al.,* 2012). These observations led to the suggestion that the DCC regulates gene expression not on a gene-by-gene basis, but rather in a chromosome-wide manner.

A model of DCC-mediated chromosome-wide repression is consistent with the idea of the formation of a repressive nuclear compartment. Organization of chromosomes within the nucleus is not random, but rather active and inactive portions of the genome are clustered together and separated into spatially distinct compartments Bickmore and van Steensel, 2013; Ciabrelli and Cavalli, 2015; Van Borle and Corces, 2012). One prominent feature of nuclear organization is positioning heterochromatic regions at the nuclear periphery or near the nucleolus (Akhtar and Gasser, 2007; Kind and van Steensel, 2010; Talamas and Capelson, 2015). An open question is to what extent this level of organization influences gene activity, rather than being a consequence of it. In this study we investigated the role of nuclear organization, particularly the

tethering of heterochromatic regions to the nuclear lamina, in regulating genes on dosage compensated X chromosomes in *C. elegans*.

Genome-nuclear lamina interactions change dynamically during cellular differentiation and development and are known to influence gene activity. In *C. elegans*, tissue specific promoters are localized randomly in nuclei of undifferentiated cells, reflecting the pluripotent state of these cells. As cells commit to specific fates and differentiate, active promoters move toward the nuclear interior, while repressed promoters move toward the nuclear periphery (Miester *et al.,* 2010). Disruption of nuclear lamina anchoring by depletion of lamin (LMN-1) or lamin-interacting proteins leads to derepression of otherwise silent transgenes, demonstrating the relevance of the anchoring process to gene repression, at least in the context of transgenes (Mattout *et al.,* 2011). Anchoring of these heterochromatic transgenic arrays to the nuclear lamina requires trimethylation of histone H3 lysine 9 (H3K9me3) by the HMTs MET-2 and SET-25, as well as the chromodomain protein CEC-4 (Gonzalez-Sandoval *et al.,* 2015; Towbin *et al.,* 2012). The relevance of this process to the regulation of endogenous gene expression is less clear. Gene expression does not change dramatically in the absence of H3K9me3 or CEC-4, but repression induced by heterochromatic anchoring does help restrict alternate cell fates in development (Gonzalez-Sandoval *et al.,* 2015; Towbin *et al.,* 2012). These observations indicate that likely multiple mechanisms contribute to repression of genes not expressed in a given cell type, and the contribution of lamina anchoring to gene regulation may only become apparent in sensitized backgrounds. Similar results were obtained in other organisms. For example, in differentiating mouse embryonic stem cells, genome-nuclear lamina interactions are remodeled such that some, but not all, genes move away from the nuclear lamina when activated (Peric-Hupkes *et al.,* 2010).

Consistent with a generally repressive environment, regions of the genome associated with the nuclear lamina (lamina associated domains, or LADs) are depleted of active chromatin marks and are enriched for repressive marks such as H3K9 and H3K27 methylation in a variety of organisms (Peric-Hupkes *et al.,* 2010; Guelen *et al.,* 2008; Ikegami *et al.,* 2010; Pickersgill *et al.,* 2006). These silencing marks, and the enzymes that deposit them, are required for peripheral localization of heterochromatic transgenes and some developmentally regulated endogenous sequences (Towbin *et al.,* 2012; Bian *et al.,* 2013; Harr *et al.,* 2015; Kind *et al.,* 2013). Artificial tethering of genes to the nuclear lamina leads to repression of some, but not all, genes Dialynas *et al.,* 2010; Finlan *et al.,* 2008; Kumaran *et al.,* 2008; Reddy *et al.,* 2008). These observations are consistent with the idea that the vicinity of the nuclear lamina is a repressive environment, yet it is not incompatible with transcription. Therefore, subnuclear compartmentalization may not be a primary driver of gene expression levels, but rather serve as a mechanism to stabilize existing transcriptional programs (Gonzalez-Sandoval *et al.,* 2015).

Here we show that anchoring of heterochromatic regions to the nuclear lamina contributes to shaping the higher order structure and nuclear localization of dosage-compensated X chromosomes. These X chromosome-specific phenotypes were observed in multiple tissues, and thus appear to be inherent to the chromosome and not any cell-type specific differentiation program. We show that heterochromatin integrity and its nuclear lamina anchors are required for spatial organization of the nucleus and dosage compensation mediated condensation of the X chromosome. In mutant strains that lack these anchors, despite normal DCC localization to the X chromosome, we observe a small, but significant level of X derepression, consistent with the idea that anchoring contributes to stabilizing gene repression. Remarkably, tethering of heterochromatic regions of the X chromosome to the nuclear lamina affects the entire

chromosome, not only the tethered domain. We propose a model in which the tethered domain nucleates formation of a peripherally localized compact structure, which facilitates the action of the DCC to compact the entire X chromosome.

MATERIALS AND METHODS

C. elegans strains

Strains were maintained as described (Nabeshima *et al.,* 2011). Strains include: N2 Bristol strain (wild type); MT16973 *met-1(n4337)* I; VC967 *set-32(ok1457)* I; VC1317 *lem-2(ok1807)* II; MT13293 *met-2(n4256)* III; PFR40 *hpl-2(tm1489)* III; MT17463 *set-25(n5021)* III; EKM104 *set-25(n5021)* III; *him-8(mn253)* IV; EKM99 *met-2(n4256) set-25(n5021)* III; RB2301 *cec-4(ok3124)* IV; TY4403 *him-8(e1489)* IV; *xol-1(y9) sex-1(y263)* X; TY1072 *her-1(e1520)* V; *sdc-2(y74*) X; EKM71 *dpy-21(e428)* V; RB1640 *set-20(ok2022)* X; VC2683 *set-6(ok2195)* X; PFR60 *hpl-1(tm1624)* X. Males were obtained from strains that carry a mutation in *him-8*, a gene required for the segregation of the X chromosome in meiosis, mutations in which lead to high incidence of males, but do not affect the soma. All strains were fed OP50 and grown at 15°C to avoid temperature sensitive sterility associated with some mutations in some the strains.

RNA Interference (RNAi)

E. coli HT115 bacteria cells carrying plasmids that express double stranded RNAi corresponding to the gene of interest, were grown from a single colony for 8–10 hours at 37°C and 125 µL were plated onto NGM plates supplemented with IPTG (0.2% w/v) and Ampicillin (1ug/ml) and allowed to dry overnight. For imaging experiments, worms were grown on RNAi plates for two generations at 15°C as follows: L1 worms were placed on a plate and allowed to feed until they reached L4 stage whereby 2–3 L4 worms were moved to a new plate and allowed

to lay eggs for 24 hours. F1 worms were grown to 24 hours post L4 for fixation. The male rescue RNAi screen was described in detail in (Petty *et al.,* 2009). Briefly, *him-8(e1489)IV; xol-1(y9) sex-1(y263) X* worms were treated with RNAi as before. For results shown on Figure 2.1, L4 worms from the P0 generation were allowed to lay eggs for 24hr at 20°C, the parents were removed, and embryos were counted. For results shown on Figure 2.12, P0 worms were fed RNAi food for an additional day, until they reached young adult stage before egg collection began. Worms were grown at 20°C and males were counted and removed for 2–4 days after eggs were laid. Male rescue was calculated by dividing the number of observed males by the number of expected males. The *him-8(e1489)IV* strain consistently yields 38% male progeny so the expected number of males was assumed to be 38% of the embryos laid. Male rescue was calculated as: (Observed number of males)/ (0.38 x number of eggs laid).

Antibodies

The following antibodies were used: rabbit anti-H3K9me3 (Active Motif #39766), rabbit anti-H4K20me1 (Abcam ab9051), rabbit anti-DPY-27 [4], rabbit anti-beta tubulin (Novus NB600-936). Anti-CAPG-1 antibodies were raised in goat using the same epitope as in [4]. Secondary anti-rabbit and anti-goat antibodies were purchased from Jackson Immunoresearch.

Immunofluorescence

Immunofluorescence experiments were performed as described (Csankovszki *et al.,* 2009). Young adult worms were dissected in 1X sperm salts (50 mM Pipes pH 7, 25 mM KCl, 1 mM MgSO4, 45 mM NaCl and 2 mM CaCl2, supplemented with 1 mM levamisole), fixed in 2% paraformaldehyde in 1X sperm salts for 5 minutes and frozen on dry-ice for 10 minutes. For anti-H4K20me1 and anti-CAPG-1 staining, worms were fixed in 1% PFA. After fixation, slides were

frozen on a dry ice block for 20–30 minutes, washed three times in PBS with 0.1% Triton X-100 (PBST) before incubation with diluted primary antibodies in a humid chamber, overnight at room temperature. Slides were then washed three times with PBST, incubated for 4 hours with diluted secondary antibody at room temperature, washed again twice for 10 minutes each with PBST, and once for 10 minutes with PBST plus DAPI. Slides were mounted with Vectashield (Vector Labs). Antibodies were used at the following concentrations: CAPG-1, 1:1000; DPY-27, 1:100; H4K20me1, 1:200; H3K9me3, 1:500.

Fluorescence In Situ Hybridization (FISH)

Slides were prepared as for immunofluorescence through the PBST washes following fixation. Slides were then dehydrated with sequential 2 minute washes in 70%, 80%, 95% and 100% ethanol before being allowed to air dry for 5 minutes at room temperature. Full X-paint probe and chromosome I paint probe preparation was described in detail in (Lau *et al.,* 2014; Nabeshima *et al.,* 2011). The X-left probe contained DNA amplified from the following YACs: Y35H6, Y47C4, Y51E2, Y02A12, Y105G12, Y97B8, Y76F7, Y40,H5, Y43D5, Y18F11, Y89H11 (covers the region from 0.1Mb to 4.2 Mb of the chromosome). The X-mid probe contained DNA amplified from the following YACs: Y18C11, Y50C2, Y70G9, Y44D2, Y102D2, Y97D4, Y97D9 (covers the region from 7.4Mb to 11.0 Mb). The X-right probe contained DNA amplified from the following YACs: Y31A8, Y52C11, Y42D5, Y53A6, Y7A5, Y46E1, Y50B3, Y25B5, Y43F3, Y52F1, Y68A3 (covers the region from 14.0 Mb to 17.6 Mb of the chromosome). The Chromosome I left probe was made from the following YACs: Y73F10, Y50C1, Y65B4, Y18H1, Y73A3, Y34D9, Y48G8, Y52D1, Y71G12, Y102E12, Y71F9, Y115A10, Y44E3, Y74A12, Y74A11, Y39E12, Y40G6, Y110A7 (covers the region from the 0.2–4.6 Mb of the chromosome); chromosome I middle probe was made from the following

YACs: Y70C6, Y46D1, Y54B12, Y101C10, Y39A9, Y53F1, Y97F9, Y97D1, Y97E2, Y43C3, Y43E2, Y49G9, Y102E5, Y106G6 (covering the region from 4.6 Mb—10.1 Mb); the chromosome I right probe was made form the following YACs: Y71B8, Y19G12, Y37F4, Y95D11, Y53A2, Y47H9, Y47H10, Y45E10, Y91F4, Y50A7, Y43D10, Y40B1, Y63D3, Y112D2, Y54E5 (covering the region fro 10.1–15.07 Mb). 10 microliters of probe was added to each slide, covered with a coverslip and placed on a 95°C heat block for 5 minutes. The heat block was then cooled to 37°C slowly and the slides were moved to a 37°C incubator in a humid chamber and incubated overnight. Slides were washed as follows: 3 washes of 2X SSC/50% formamide for 5 minutes each; 3 washes of 2X SSC for 5 minutes each; 1 wash of 1X SSC for 10 minutes. All washes were performed in a 39°C water bath. Finally, the slides were washed once with PBST containing DAPI for 10 minutes at room temperature before mounting with Vectashield.

Quantification

Volume Quantification: Chromosome volumes were quantified as in (Lau *et al.,* 2014). Briefly, using the Mask: Segment function of Slidebook, a user-defined threshold is determined that separates signal from background and auto-fluorescence. The same level of background was used for all nuclei based on observed background. Masks were calculated for each channel with DAPI being the primary mask and the X paint being the secondary mask. Nuclear volume was calculated by taking the number of voxels (volumetric pixels) for the DAPI channel to determine total DNA content (morphology: volume (voxels)). The overlapping voxels between the X and the DAPI was determined by using a cross mask of the DAPI and X paint signals (cross mask: mask overlaps) in Slidebook. The percent nuclear volume occupied by the X was determined by dividing the number of X voxels by the total number of DAPI voxels.

Three-zone assay quantification: Concentric ovals of equal area were drawn over one focal plane from the center of the Z stack that contained the largest amount of X FISH signal. Masks were made from each of these zones using the Advanced operations > Convert regions to mask objects function in Slidebook. A single plane from the X chromosome mask set for volume quantification was used here. The amount of X signal in each of the zones was calculated using the cross mask: mask overlap function in Slidebook where the zone mask was the primary mask and the X mask was the secondary mask. The total voxels for all three zones were summed and the voxels in each zone were divided by the total to determine what percentage of the X signal was located in each zone.

mRNA-seq

Worms were synchronized by bleaching gravid adults to isolate embryos and allowing worms to hatch overnight. Newly hatched L1 larval worms were plated and grown for 3 hours on NGM plates with OP50. To the worm pellet, ten volumes of Trizol were added and RNA was extracted and precipitated using the manufacturer's instructions. Total RNA was cleaned using the Qiagen RNeasy kit. Non-stranded mRNA-seq libraries were prepared using TruSeq RNA Library Preparation Kit. Single-end 50-bp sequencing was performed using Illumina HiSeq-2000. Reads were trimmed for quality using the TrimGalore program from Babraham Bioinformatics (http://www.bioinformatics.babraham.ac.uk/projects/trim_galore/) and aligned to the *C. elegans* genome version WS235 with Tophat v 2.0.13 (Trapnell et. al. 2012). Default parameters allow up to 20 hits for each read. Gene expression was quantified using Cufflinks v2.2.1 with use of “rescue method” for multi-reads and supplying gene annotation for WS235. Gene count estimation was performed using HTSeq-count tool v0.6.0 in the default “union” mode (Anders et. al. 2014). Differential expression analysis was performed using DESeq2 v1.6.3

in R version 3.2.3 (Anders and Huber 2010; R Development Core Team 2012). All analyses were performed with genes that had average expression level above 1 RPKM (fragments per kilobase per million, as calculated by Cufflinks).

Western blot

From the worm suspension collected for RNA-seq experiments, 50 µL of L1s were used for protein analysis. For CAPG-1 antibody validation, 50 µL of mixed stage worms were used. Equal volume of sample buffer was added (0.1 M Tris pH 6.8, 7.5 M urea, 2% SDS, 100mM β-ME, 0.05% bromophenol blue), the suspension was heated to 65°C for 10 minutes, sonicated for 30-seconds twice, heated to 65°C for 5 minutes, 95°C for 5 minutes, then kept at 37°C until loading onto SDS-PAGE gel. Proteins were transferred to nitrocellulose and probed with the appropriate antibodies.

RESULTS

In order to identify chromatin modifying genes that influence dosage compensation, we previously performed a targeted RNAi screen to analyze genes implicated in chromatin regulation, including histone variants, as well as genes containing chromo, bromo, or set domains (Petty *et al.,* 2009). The assay is based on rescue of males that inappropriately turn on dosage compensation. The DCC assembles on the X chromosome of *xol-1(y9) sex-1(y263)* males, leading to insufficient expression of genes from the single X chromosome and thus lethality. RNAi-mediated disruption of dosage compensation can rescue a proportion of these males. Control vector RNAi leads to background level of rescue (about 1.5%), while RNAi of a component of the DCC rescues over 25% of males. We previously described the screen in detail, as well as the role of one of the hits from the screen, the histone H2A variant HTZ-1 (Petty *et al.,* 2009). In this study we characterize the remaining genes identified in this screen that led to low but reproducible levels of male rescue. These genes include the histone methyltransferases *met-2*, *set-32*, *set-20*, *set-6*, *set-25*, and the chromodomain protein *cec-4* (Figure 2.1). All of these histone methyltransferases are known (*met-2*, *set-25*, (Towbin *et al.,* 2012)) or predicted (*set-6*, *set-20*, *set-32* (Anderson and Horvitz, 2007)) to modify H3K9. H3K9 methylation and the chromodomain protein CEC-4 were previously shown to work together in regulating nuclear organization and anchoring heterochromatic transgenic arrays to the nuclear lamina (Gonzalez-Mattout *et al.,* 2011; Sandoval *et al.,* 2015; Towbin *et al.,* 2010). We therefore included in our analysis LEM-2 (hMAN1), a non-essential component of the nuclear lamina. RNAi of the single *C. elegans* lamin gene LMN-1 leads to embryonic lethality (Liu *et al.,* 2000), precluding this type of analysis. However, RNAi-depletion of LEM-2 led to male rescue comparable to, or higher than, the rescue caused by depletion of the HMTs or CEC-4 (Figure 2.1). Chi square test

of the data indicated that all genes rescued significantly more males than vector RNAi (Figure 2.1B). To ensure that the rescue is reproducible, we also performed the rescue assay with a subset of the identified genes in four independent biological replicates and analyzed the results using Student's t-test. In this analysis, all genes identified in the screen with the exception of *set-6* and *set-20* rescued significantly more males than vector RNAi (2.12).

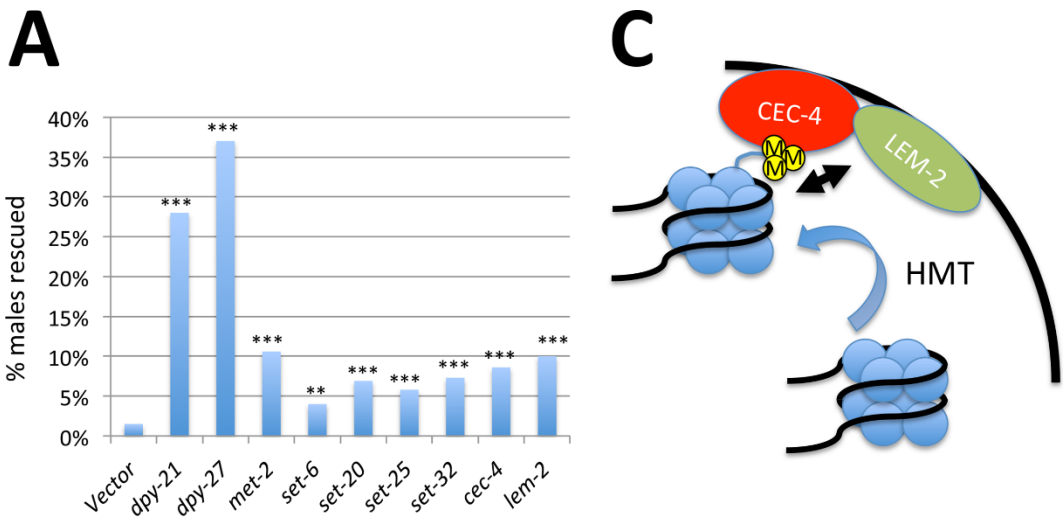

B

			OBSERVED		EXPECTED	
RNAi	n	total males	live males	dead	live males	dead
Vector	2165	822	12	810	12	810
dpy-21	503	191	54	137	3	188
dpy-27	1248	474	175	299	7	467
met-2	1657	629	67	562	9	620
set-32	1229	467	34	433	7	460
set-20	836	317	22	295	5	312
set-6	801	304	12	292	5	299
set-25	1575	599	35	564	9	590
cec-4	1814	689	59	630	10	679
lem-2	1072	407	41	366	6	401

Figure 2.1 RNAi screen to identify genes that promote dosage compensation. (A) Male rescue assay. RNAi-mediated depletion of the indicated genes in the *him-8 xol-1 sex-1* background led to rescue of the indicated percentage of males. Depleting DCC components DPY-21 and DPY-27 rescues a larger percentage of males than depletion of the other genes identified in this screen Asterisks indicate statistical significance based on Chi square test analysis of results, with expected rescue being equivalent to vector RNAi. * = $p<0.05$, ** = $p<0.01$, *** = $p<0.001$. (B) Raw data and expected table used in Chi square analysis. (C) Proposed mechanism of anchoring heterochromatic regions to the nuclear lamina. HMTs methylate H3K9. The chromodomain protein CEC-4 binds to this chromatin mark. Bound genomic regions are enriched for interaction with the nuclear lamina protein LEM-2.

X chromosome decondensation in mutants

The finding of H3K9 methyltransferases, CEC-4, and LEM-2, in this screen suggested that nuclear organization, and specifically anchoring of chromosomal regions to the nuclear lamina (Figure 2.1C), might affect dosage compensation. To investigate X chromosome morphology and its location in the nucleus in the absence of these proteins, we performed X chromosome paint fluorescence *in situ* hybridization (FISH) in the various mutant backgrounds. First we investigated the 32-ploid nuclei of the intestine, because their large size facilitates visualization of chromosome territories. In wild type (N2) hermaphrodite worms, the X chromosome territories are kept compact by the action of the DCC (Lau *et al.,* 2014) and the territory is found near the nuclear lamina (Figure 2.2A). Visual inspection of the X chromosome territories in *met-2(n4256)*, *set-6(ok2195)*, *set-20(ok2022)*, *set-25(n5021)*, *set-32(ok1457)*, *cec-4(ok1324)*, and *lem-2(ok1807)* hermaphrodites revealed that the nuclear territory occupied by the X chromosomes became larger. As a control, we also analyzed the X chromosomes in *met-1(n4337)*, *hpl-1(tm1624)* and *hpl-2(tm1489)* mutants. MET-1 is an unrelated HMT, while HPL-1 and HPL-2 are homologs of the highly conserved heterochromatin protein and H3K9me3 binding protein HP-1 (Schott *et al.,* 2006) (Figure 2.2A). To quantify X chromosome condensation, we measured the volumes of X chromosome territories, as in (Lau *et al.,* 2014). Briefly, we generated intensity threshold-based 3D masks for the X chromosome (X paint signal) and for the nucleus (DAPI signal). We then calculated the volume of the X chromosome and of the nucleus, and determined the portion of the nucleus occupied by the X chromosome. Normalization to total nuclear volume was necessary due to the large variability in nuclear size after the harsh treatments involved in FISH. Quantification of the volume of the X chromosome territory showed that in the H3K9 HMT mutants, as well as in *cec-4* and *lem-2* mutants, the X

chromosome occupied a much larger portion of the nucleus than in control wild type, or *met-1*, *hpl-1* or *hpl-2* mutant hermaphrodites. Lack of X chromosome condensation defects in *hpl-1* and *hpl-2* mutants are consistent with a previous study that reported no defects in nuclear lamina anchoring of heterochromatic transgenic arrays in *hpl-1* or *hpl-2* mutants (Gonzalez-Sandoval *et al.,* 2015). In nuclei of wild type worms the X chromosome occupied about 10% of the nuclear volume, compared to an average of up to 20% percent in mutants ($p<0.001$, Student's t-test, for all comparisons between a mutant and wild type) (Figure 2.2B). In fact, the degree of decondensation in *set-25(n5021)* mutants is even larger than in DCC mutant or RNAi-depleted hermaphrodites (*dpy-21(e428)* and *dpy-27(RNAi)* (Lau *et al.,* 2014)) ($p = 0.0251$ for comparison with *dpy-21*, and $p = 0.00442$ for comparison with *dpy-27;* other differences were not statistically significant) (Figure 2.2). We conclude that the X chromosome is decondensed to a significant degree in worms carrying mutations in DCC subunits, as well as in H3K9 HMT, *cec-4* and *lem-2* mutants.

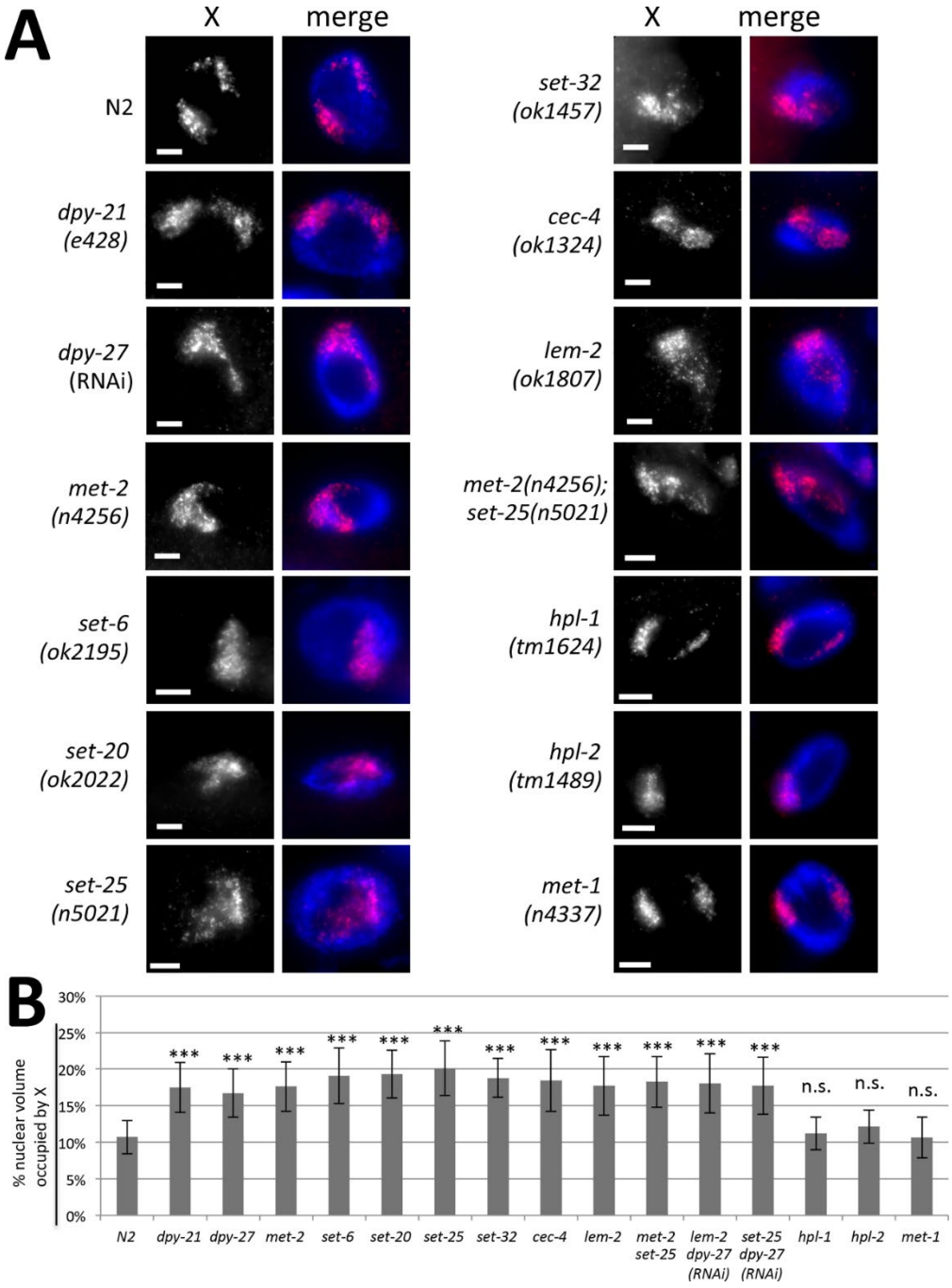

Figure 2.2 X chromosome decondensation in mutants. (A) X chromosome paint FISH (red) in representative images of intestinal nuclei (DAPI, blue) of hermaphrodite adult worms in each genotype. The X chromosomes are compact and peripherally localized in wild type (N2), *hpl-1, hpl-2* and *met-1* mutant hermaphrodites, but are decondensed and more centrally located in the other mutants. Scale bar, 5 mm. (B) Quantification of X chromosome volumes normalized to nuclear size (n=20 nuclei). Error bars indicate standard deviation. n.s. = $p>0.05$ not significant, *** = $p<0.001$ by Student's t-test (N2 compared to appropriate mutant).

SET-25 and MET-2 are the only well characterized HMTs among the ones we identified. MET-2 introduces H3K9 mono- and dimethylation, while SET-25 introduces H3K9 trimethylation. Complete lack of H3K9 methylation, and loss of anchoring of heterochromatic arrays, are only observed in the *met-2 set-25* double mutants and not in *set-25* or *met-2* single mutants (Towbin *et al.,* 2012). We therefore analyzed X chromosome structure in the *met-2(n4256) set-25(n5021)* double mutant strain and found that the X chromosome morphology is comparable to single mutants without an obvious additive effect ($p = 0.56$ for *met-2* compared to *met-2 set-25*; $p = 0.11$ for *set-25* compared to *met-2 set-25*) (Figure 2.2A and 2.2B). For the rest of this study we concentrated on *lem-2*, *set-25 or met-2 set-25*, *and cec-4* mutants, and we will refer to them collectively as "tethering mutants".

One possible explanation for X decondensation phenotype is that the tethering defects diminish the ability of the DCC to condense the X chromosome. For example, the DCC may use these heterochromatic tethers as nucleation sites for a more compact chromosomal organization. An alternative possibility is that lack of tethering leads to chromosome decondensation independent of the DCC. We tested whether simultaneous disruptions of tethering and the DCC lead to increased levels of decondensation by measuring X chromosome volumes in *set-25* and *lem-2* mutants that were depleted of DPY-27 using RNAi (Figure 2.2B). X chromosomes of nuclei in *dpy-27(RNAi*) treated *lem-2* mutants were significantly different from wild type, but statistically indistinguishable from either *lem-2* mutants ($p = 0.77$, Student's t-test) or *dpy-27(RNAi)* ($p = 0.26$). Similarly, X chromosomes of nuclei in *dpy-27(RNAi)* treated *set-25* mutants were significantly different from wild type, but statistically indistinguishable from *set-25* mutants ($p = 0.052$) and *dpy-27(RNAi)* ($p = 0.39$). Therefore, at this resolution, we cannot detect any additional defects when tethering mutations are combined with DCC depletion,

consistent with the hypothesis that the DCC and tethering genes work together, and are both required, to condense the X chromosomes.

To determine whether the phenotype is specific to the 32-ploid intestinal nuclei, we also examined diploid tail tip hypodermal cells hyp 8–11. Results were comparable to intestinal cells. In wild type cells, the X chromosome occupies about 10% of the nucleus, while it occupies a much larger portion of the nucleus in anchoring mutants ($p<0.001$ for all mutant comparisons to wild type) (Figure 2.13).

The dosage compensated X chromosome relocates to a more central position in tethering mutants

Previous studies showed that tethering mutants have a defect in anchoring heterochromatic transgenic arrays to the nuclear lamina (Mattout *et al.,* 2011; Gonzalez-Sandoval *et al.,* 2015; Towbin *et al.,* 2012). Similarly, visual inspection of our images suggested that tethering mutants have a defect in subnuclear positioning of the X chromosome resulting in the X occupying a more central position (Figure 2.2). To quantify this defect, we performed an analysis similar to the three-zone assay used in (Miester *et al.,* 2010). We selected nuclei that were spherical or ellipsoid shaped. From the Z-stacks generated during imaging, we selected the optical section toward the middle of the nucleus with the largest and brightest X-paint signal. This optical section was divided into three-zones of equal area, and the portion of the X signal located in each zone was quantified (Figure 2.3A). The percentage of nuclei in each genotype that can be quantified using this assay is shown in (Supplemental Figure 2.14). Representative irregularly shaped nuclei are also shown to illustrate that the X chromosome appeared qualitatively similar to the X chromosomes in round or ellipsoid shaped nuclei: compact and peripherally located in N2 hermaphrodites, and larger and more centrally located in tethering

mutants. The three-zone assay showed that in wild type (N2) nuclei only about 20% of the X chromosome signal was located in the central zone, while in tethering mutants over 40% of the X signal was located in this zone, suggesting that the X chromosome relocates to a more central position within the nucleus (Figure 2.3B). Comparisons of the portions of the X chromosome located in the central zone revealed statistically significant differences in all tethering mutants. As for volume measurement, the three-zone assay again failed to reveal additional defects in *met-2 set-25* double mutants compared to *set-25* single mutants. We then compared this effect to mutating or depleting a subunit of the DCC by RNAi. The three-zone assay showed less significant relocation of the X toward the center in *dpy-27* RNAi-treated hermaphrodites compared to tethering mutants. In *dpy-21* mutants, although the portion of the X in the central zone increased from 24% to 34%, the difference did not reach statistical significance (Figure 2.3B). One possible reason for the less significant relocation in dosage compensation mutants is the fact that *dpy-27(RNAi)* or a mutation in *dpy-21* does not completely disrupt dosage compensation function. Complete lack of DCC activity would be lethal to hermaphrodites, precluding this type of analysis (see analysis of the male X below).

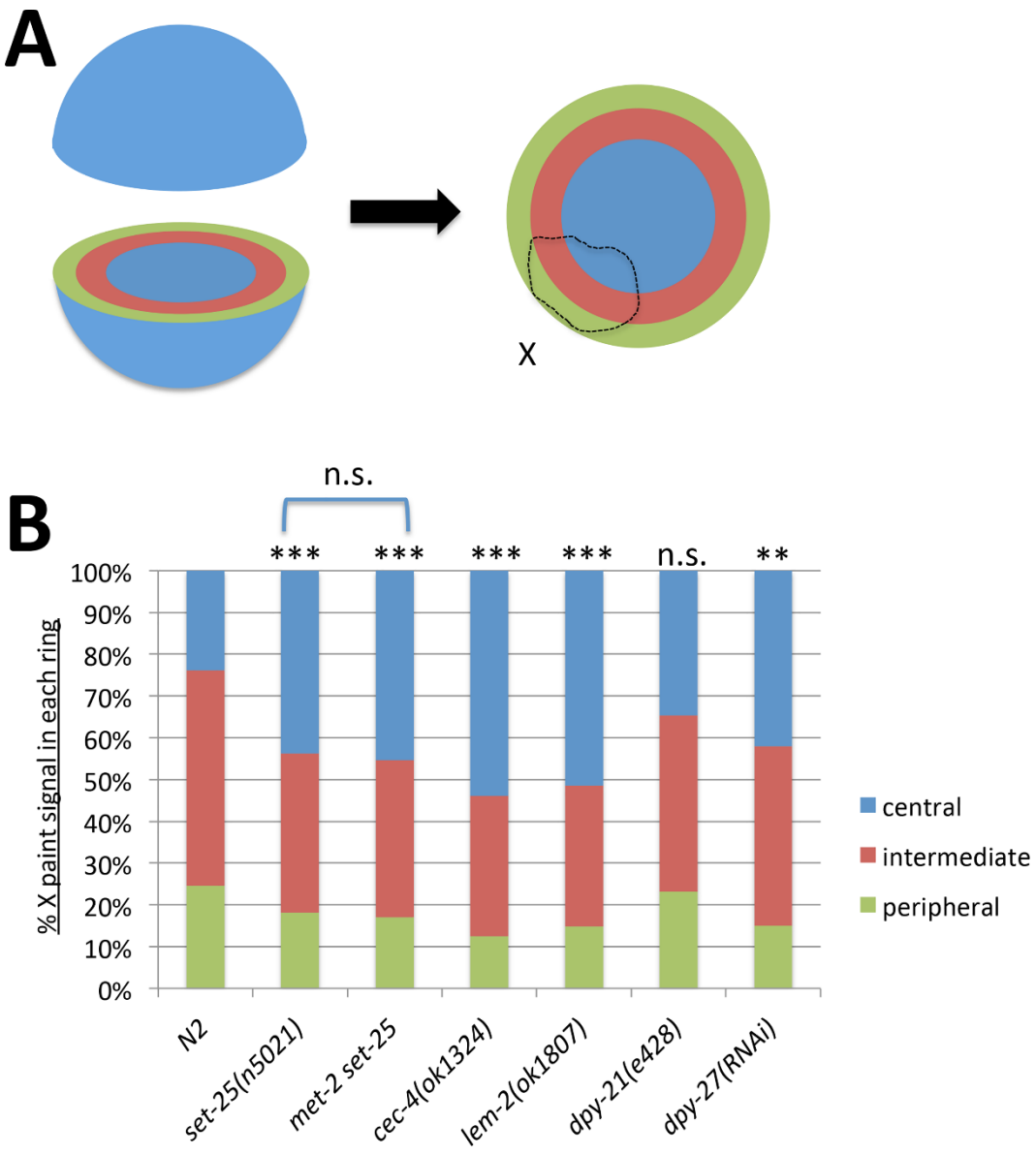

Figure 2.3 The X chromosome relocates centrally in the nucleus. (A) A diagram of the three-zone assay. An optical section from the middle of the nucleus was divided into three concentric rings of equal area. The proportion of the X chromosome paint signal in each zone (peripheral-intermediate-central) was quantified. (B) Results of quantification of the three-zone assay using whole X paint FISH probes in hermaphrodite intestinal nuclei (n=10). In tethering mutants, a larger portion of the X chromosome is located in the central zone compared to wild type hermaphrodites. Relocation to a central region is less significant in DCC mutants or DCC-depleted hermaphrodites. Asterisks indicate statistical analysis (Student's t-test) of the centrally located portion of the X chromosome (shown in blue). n.s. = $p>0.05$, * = $p<0.05$, ** = $p<0.01$, *** = $p<0.001$. See Table 2.1 for statistical data.

H3K9me3 is generally found in heterochromatic regions of the genome. In *C. elegans*, several megabase regions at both ends of autosomes and the left end of the X chromosome are enriched for this mark (Liu *et al.,* 2011). These H3K9me3-enriched domains also coincide with nuclear lamina-associated domains, as assessed by ChIP (Ikegami *et al.,* 2010) or DamID (Towbin *et al.,* 2012). Together these results suggest a model in which both arms of autosomes and the left of arm of the X chromosome are tethered to the nuclear lamina (Towbin *et al.,* 2012; Ikegami *et al.,* 2010; Gonzalez-Sandoval *et al.,* 2013; Miester *et al.,* 2013; Towbin *et al.,* 2013) (Figure 2.4A). Peripheral localization of heterochromatic chromosomal regions may be mediated by CEC-4, as is the case for heterochromatic transgenes (Gonzalez-Sandoval *et al.,* 2015).

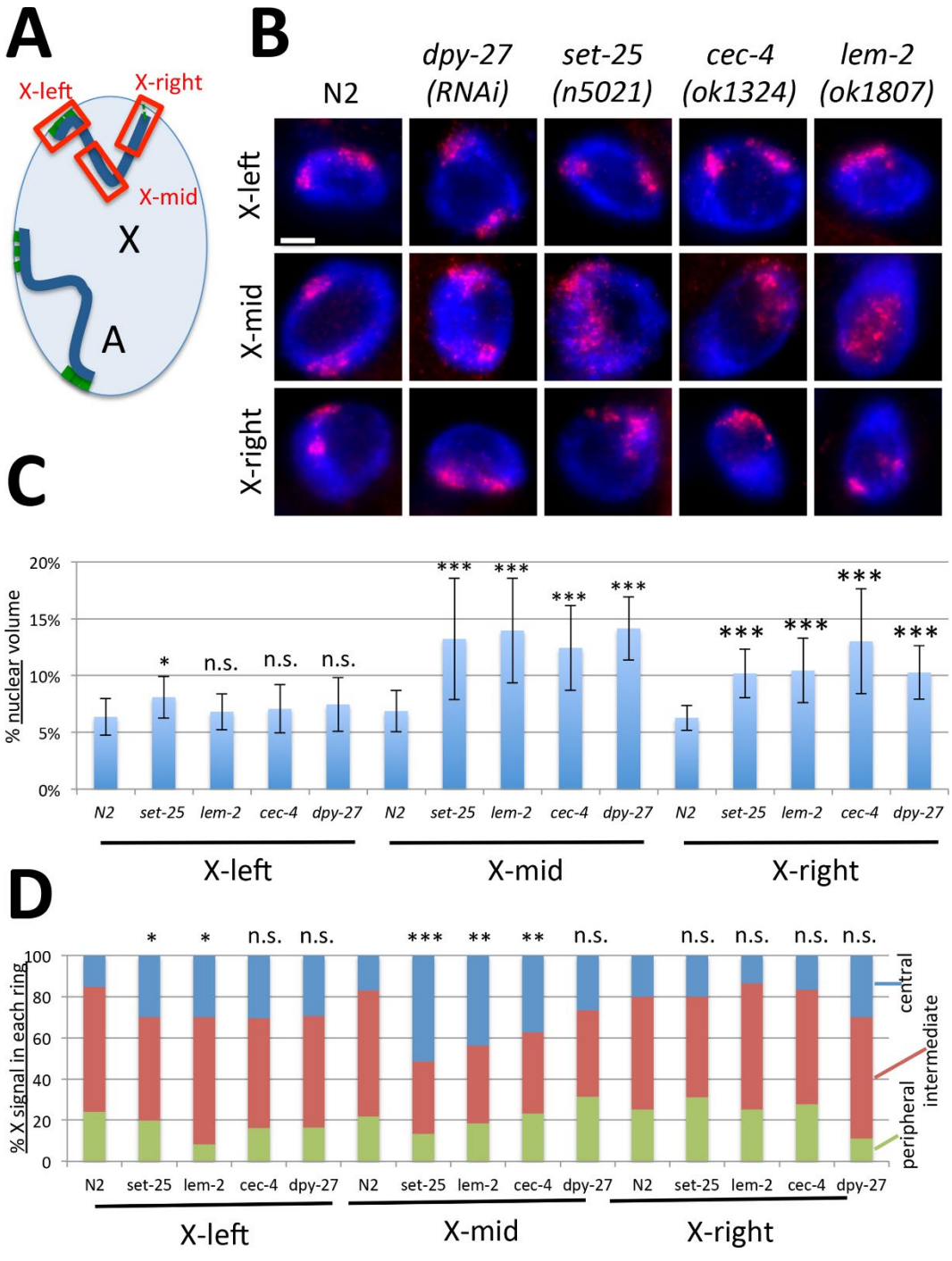
A
X-left
X-right
X-mid
X
A
B
N2
dpy-27 (RNAi)
set-25 (n5021)
cec-4 (ok1324)
lem-2 (ok1807)
X-left
X-mid
X-right
C
% nuclear volume
20%
15%
10%
5%
0%
*
n.s.
n.s.
n.s.
***
***
***
***
***
***
***
***
N2
set-25
lem-2
cec-4
dpy-27
X-left
X-mid
X-right
D
% X signal in each ring
100
80
60
40
20
0
*
*
n.s.
n.s.
***
**
**
n.s.
n.s.
n.s.
n.s.
n.s.
central
intermediate
peripheral
N2
set-25
lem-2
cec-4
dpy-27
X-left
X-mid
X-right

Figure 2.4 The middle region of the X chromosome is most affected in the absence of heterochromatic tethers. (A) Autosomes are anchored to the nuclear lamina at both chromosome arms (anchors shown in green), while the X chromosome only has a significant anchored domain at the left end. Probes used in FISH analysis are indicated in red. Each probe covered an approximately 3-4 Mb genomic region. (B) Representative images of X-left, X-mid, X-right FISH analysis in each genotype. The mid-X region appears most decondensed and most centrally located in mutants. Scale bar, 5 mm. (C) Quantification of volumes occupied by the indicated FISH probes, normalized to nuclear size (n=12 nuclei). Error bars indicate standard deviation. The greatest degree of decondensation in mutants is observed for the mid-X probe. (D) Three zone assay for each probe (n=12 nuclei). The greatest degree of central relocation is observed for the mid-X probe. Asterisks indicate statistical analysis of mutant to wild type comparisons of volumes in (C) and centrally located portion of the X in (D) using Student's t-test. n.s. = $p>0.05$, * = $p<0.05$, ** = $p<0.01$, *** = $p<0.001$. See Table 2.1 for statistical data.

To examine whether heterochromatic segments of the X chromosomes are affected differently than other chromosomal regions, we prepared probes to approximately 3–4 Mb regions of the chromosome. The X-left probe covers a region enriched for H3K9me3 and LEM-2, the X-mid probe covers a gene-rich portion of the chromosome with very little H3K9me3 and LEM-2, and the X-right probe covers a region with intermediate levels of H3K9me3 and LEM-2 (Figure 2.4A and 2.4B). We then assessed the level of decondensation of each of these regions by measuring the proportion of the nuclear volume occupied by this region of the X chromosome (Figure 2.4C). Surprisingly, the left end of the X chromosome was least affected and remained condensed both in tethering mutants and in DCC-depleted hermaphrodites. We only observed a mild level of decondensation in *set-25* mutants. By contrast, the gene-rich middle portion of the chromosome was most affected and was significantly decondensed in all tethering mutants. The right end of the chromosome, which contains some LEM-2 and H3K9me3 peaks, but fewer than the left end, exhibited an intermediate phenotype.

The gene-rich middle portion of the X chromosome was not only decondensed but also appeared to exhibit the greatest degree of central relocation. To quantify this effect, we again performed the three-zone assay and found that indeed the mid-X region was most affected (Figure 2.4D). While on average only 17% of the X-mid probe was located in the central zone in wild type nuclei, up to 50% of the same region was found in this zone in tethering mutants. Relocation to a central position was less obvious for the left end of the chromosome and was not detectable for the right end. These results were at first unexpected. However, they are consistent with previous observations that have hinted at the existence of redundant tethering mechanisms in differentiated cells. The tethering mechanism mediated by heterochromatin is only essential for anchoring of heterochromatic arrays in embryonic cells, and the arrays remain anchored in differentiated tissues even in the absence of SET-25 and MET-2 (Towbin *et al.,* 2012). Similarly, CEC-4 is required for anchoring in embryos, but other, yet unknown, mechanisms can compensate for the lack of CEC-4 protein in differentiated cells (Gonzalez-Sandoval *et al.,* 2015). We note that all of our analyses were performed in terminally differentiated postmitotic cells of adult animals. Our results suggest that regions of the left end of the X chromosome are anchored to the nuclear periphery by an additional mechanism that is independent of SET-25, CEC-4, and LEM-2, and loss of H3K9me3-lamina mediated anchoring mechanism is not sufficient to significantly relocate this region. The lack of heterochromatic anchoring mechanism affects the middle of the chromosome disproportionately, even though this region is depleted of H3K9me3 and LEM-2 interactions. One possible interpretation of this result is that the few H3K9me3 sites and LEM-2-bound regions present in the middle of the chromosome represent the only anchoring mechanism present in this region. In the absence of these tethers, the mid-X region is free to relocate more centrally, while redundant anchors maintain tethering to a greater

degree at the two chromosome ends. The other interpretation, which is not mutually exclusive, is that heterochromatic anchors at the left end of the chromosome are used to nucleate a compact structure, which is required to be able to pull the rest of the X chromosome toward the periphery and compact it efficiently (see Discussion).

Defects in DCC function had a somewhat different effect. The mid-X region was more decondensed after *dpy-27(RNAi)* than the right end, and the left end was unaffected, similar to the decondensation defects seen in tethering mutants. Less significant decompaction of the left end may be related to the somewhat lower levels of DCC binding in this region (Liu *et al.,* 2011; Kranz *et al.,* 2013). Alternatively, nuclear lamina tethers at the left end may be sufficient to compact this region even in the absence of the DCC. Although the portion of the mid-X region in the central domain increased in *dpy-27* RNAi, the difference did not reach statistical significance, suggesting again insufficient disruption of dosage compensation (Figure 2.4C and 2.4D).

Chromosomal phenotypes are dosage compensation dependent

To examine these X chromosomal phenotypes in the complete absence of DCC activity, we analyzed the X chromosome in males and in XO animals that develop as hermaphrodites due to a mutation in the *her-1* gene required for male development (Hodgkin, 1980) (Figure 2.5). The XO hermaphrodites also carry a null mutation in the dosage compensation gene *sdc-2* to ensure that all XX progeny die due to dosage compensation defects and only XO animals survive (Dawes *et al.,* 1999). The DCC is XX hermaphrodite-specific and does not bind to the male X or the X chromosome in XO hermaphrodites, therefore these backgrounds allow us to examine X chromosome structure in the complete absence of the DCC, but in the presence of heterochromatic anchors. In wild type males and in XO hermaphrodites, the single X occupied

an large proportion of the nucleus, about 16%, as we previously observed, which is significantly different from the 10% seen in wild type hermaphrodites (Lau *et al.,* 2014) (Figure 2.5A and 2.5B). It is also different from what was seen previously in nuclei of young embryos, possibly due to the differences in stage of development and differentiation status (Sharma *et al.,* 2014). Note that the level of decondensation in males and XO hermaphrodites is greater than in tethering mutants. In XO animals, the single X chromosome occupies 16% of the nucleus, compared to the two Xs occupying 18–20% in tethering mutant hermaphrodites. However, in *set-25* mutant males, the X did not decondense further compared to normal males (Figure 2.5A and 2.5B). In addition, the three-zone assay revealed that the X chromosome is located significantly more centrally in XO hermaphrodites and males, compared to wild type hermaphrodites (Figure 2.5C). Irregularly shaped nuclei that cannot be quantified using this assay also appeared to have large centrally located X chromosomes (Figure 2.14. While in *set-25* mutant males a slightly higher proportion of the X chromosome was located in the central zone, this difference was not statistically significant (Figure 2.5C). These results indicate that the activity of the DCC is required to condense and peripherally relocate the X chromosome, and that the lack of both DCC function and heterochromatic tethers (in *set-25* males) does not lead to additional defects.

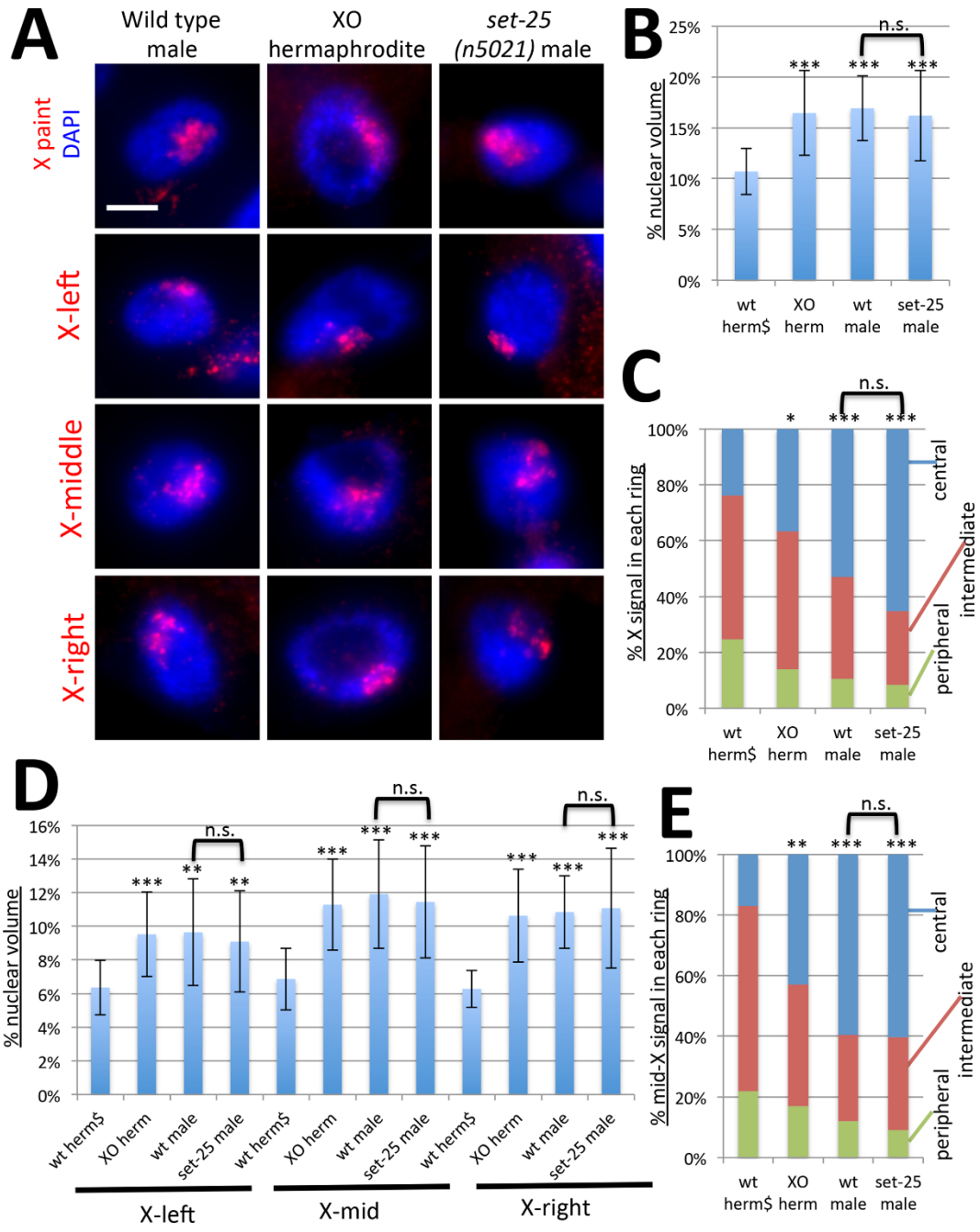

Figure 2.5 The X chromosome is decondensed and centrally located in the absence of dosage compensation in XO animals. (A) Chromosome paint FISH (red) in intestinal nuclei (DAPI, blue) of male adult worms, XO hermaphrodites and *set-25* mutant males using whole X paint probe, and probes to the left, middle, and right domains of the X chromosome. The X chromosome, and the middle region of the X chromosome, appear large and diffuse and are located more toward the nuclear interior. *set-25* mutations do not have additional effects on X chromosome morphology in males. Scale bar, 5 mm. (B) Quantification of volumes occupied by the X paint probe (n=20 nuclei). The N2 hermaphrodite data point (wt herm) is repeated from Figure 3.2B and is marked by $ sign. (C) Three-zone assay for the whole chromosome X paint

probe (n=10). Wt herm$ data point is repeated from Figure 3.3B. (D) Quantification of volumes occupied by the X-left, X-mid, and X-right probes normalized to nuclear size (n=20). Wt herm$ data points are repeated from Figure 3.4C. (E) Three zone assay for the mid-X probe (n=10). wt herm$ data point is repeated from Figure 3.4D. Error bars in (B) and (D) indicate standard deviation. Asterisks indicate statistical analysis compared to wild type hermaphrodites for volumes in (B) and (D) and centrally located portion of the X or mid-X (C) and (E), using Student's t-test. wt male and *set-25* male comparisons are also shown as indicated. n.s. = $p>0.05$, * = $p<0.05$, ** =$p<0.01$, *** = $p<0.001$. See Table 2.1 for statistical data.

We next analyzed the left, middle and right regions of the X chromosome in XO animals (Figure 2.5A, 2.5D and 2.5E). All regions of the X chromosome were decondensed in XO animals, compared to hermaphrodites, but mutations in *set-25* did not lead to any further decondensation (Figure 2.5D). Furthermore, the mid-X region was more centrally located in XO animals than in hermaphrodites, but again mutations in *set-25* did not lead to additional central relocation. While we cannot exclude the possibility that the X chromosome is affected in tethering mutant males, we conclude that hermaphrodite X chromosomes are more severely affected by these mutations than male X chromosomes.

Chromosomal phenotypes are X specific

To determine whether the chromosomal phenotypes are specific to the X chromosome, we analyzed the structure and localization of a similarly sized autosome, chromosome I (Figure 2.6A). Chromosome I occupies about 15% of the nucleus in wild type hermaphrodites, closely correlated with its genome content, indicating lack of condensation beyond genomic average (Lau *et al.,* 2014). As we found previously for dosage compensation mutants (Lau *et al.,* 2014), the volume of chromosome I appeared unaffected in tethering mutants (Figure 2.6B). In addition, the three-zone assay revealed that a significant portion of chromosome I signal is located in the central zone in wild type hermaphrodites (39%) (Figure 2.6C). This value is significantly different from the value obtained for the X chromosome in wild type hermaphrodites (23%,

Figure 2.3, p = 0.035, Student's t-test), and more similar to the X chromosome in tethering mutants (ranging from 43% to 55%, Figure 2.3). In addition, mutations in tethering mutants did not lead to any further central relocation of chromosome I compared to the same chromosome in wild type hermaphrodites (Figure 2.6C). These results suggest that the X chromosome is more sensitive to the loss of heterochromatic tethers than the autosomes.

To confirm these results, we further examined different domains of chromosome I (Figure 2.6D). Chromosome I has two anchored heterochromatic domains, one at each end (left and right), while the middle region lacks significant interactions with the nuclear lamina (Towbin *et al.,* 2012; Ikegami *et al.,* 2010; Lui *et al.,* 2011). Our FISH analysis is consistent with these earlier observations. The left and right domains of the chromosome were located near the nuclear periphery, while the middle region was more centrally located. Neither volume measurements (Figure 2.6E), nor the three-zone analysis (Figure 2.6F) showed any significant differences between wild type (N2) and *set-25* mutant hermaphrodites. A significantly greater portion of the chromosome I middle domain was located in the central zone (36%) in wild type hermaphrodites compared to the X chromosome (17%, Figure 2.4, p = 0.018, Student's t-test), and this value was more comparable to the centrally located portion of the mid-X region in tethering mutants (ranging from 37% to 51%, Figure 2.4). These results indicate that in wild type hermaphrodites, the two ends of chromosome I are peripherally located, while the middle domain is more centrally located. Furthermore, we conclude that this organization does not change significantly in the absence of heterochromatic tethers, and that the observed chromosomal phenotypes are specific to the dosage compensated X chromosome.

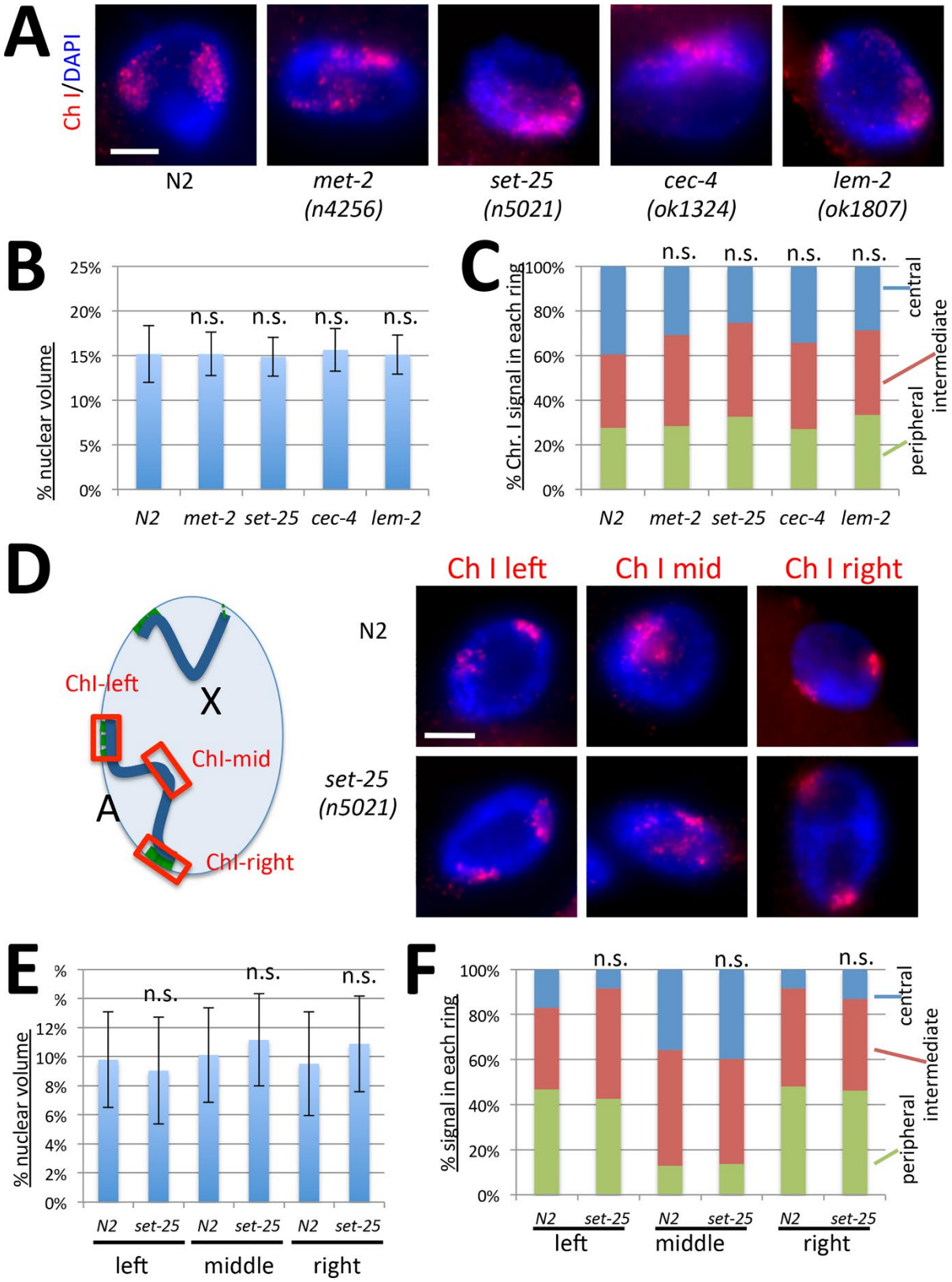
A
Ch I/DAPI
N2
met-2 (n4256)
set-25 (n5021)
cec-4 (ok1324)
lem-2 (ok1807)
B
% nuclear volume
25%
20%
15%
10%
5%
0%
n.s.
N2
met-2
set-25
cec-4
lem-2
C
% Chr. I signal in each ring
100%
80%
60%
40%
20%
0%
n.s.
central
intermediate
peripheral
D
ChI-left
X
ChI-mid
A
ChI-right
Ch I left
Ch I mid
Ch I right
N2
set-25 (n5021)
E
% nuclear volume
12%
10%
8%
6%
4%
2%
0%
n.s.
N2
set-25
left
middle
right
F
% signal in each ring
100%
80%
60%
40%
20%
0%
n.s.
central
intermediate
peripheral
N2
set-25
left
middle
right

Figure 2.6 Chromosome I structure and organization is not affected in tethering mutants. (A) Chromosome I paint FISH (red) in representative images of intestinal nuclei (DAPI, blue) of hermaphrodite adult worms. Chromosome I appears comparably sized in each background. Scale bar, 5 mm. (B) Quantification of chromosome I volumes normalized to nuclear size (n=12 nuclei). Error bars indicate standard deviation. (C) Three-zone assay for whole Chr I paint (n=10 nuclei). The chromosome did not relocate to a more central position in any of the mutants (D) FISH analysis of the left, middle and right regions of Chr I in wild type (N2) and *set-25(n5021)* mutant hermaphrodites. Diagram (left) indicates locations of probes, representative images are shown on the right. The left and right ends of the chromosome are peripherally located, but the middle appears more centrally located in both backgrounds. (E) Quantification of volumes occupied by Chr I domains (n=20 nuclei). Error bars indicate standard deviation (F) Three-zone assay for the left, middle and right domains of Chr I (n=10 nuclei). The middle domain is more centrally located than the left and right arms in both genotypes. Student's t-test did not reveal any statistically significant differences for volume measurements in (B) and (E), or for the portion of chromosome located in the central zone in (C) and (F), mutant compared to wild type. n.s. = $p > 0.05$. See Table 2.2 for statistical data.

The distribution of H3K9me3 within the nucleus

Previous ChIP-chip analysis showed that H3K9me3 is enriched at both ends of autosomes and at the left end of the X chromosome, although peaks can be found elsewhere on the X as well (Liu *et al.,* 2011). To determine how this signal is distributed in the nucleus, we performed immunofluorescence microscopy (IF) with H3K9me3 specific antibodies in wild type cells and in tethering mutants (Figure 2.7). Antibodies specific to DCC subunit CAPG-1 were used as staining controls and to mark the territories of the X chromosomes. S4 Fig shows specificity of this newly developed antibody to CAPG-1. In wild type cells, the H3K9me3 signal was distributed all over the nucleus, with no obvious enrichment at the nuclear periphery, except for the presence of some peripherally located bright foci. Both the overall staining and the bright foci are H3K9me3-specific, as they were absent in *set-25* mutants. Sites of exceptionally high levels of H3K9me3 signal were not observed by ChIP (Liu *et al.,* 2011). Therefore, we interpret these bright foci as three-dimensional clustering of multiple H3K9me3 enriched loci. The X chromosome territory almost always contained, or was directly juxtaposed to one of these bright

foci (Figure 2.7, top row). In rare cases, the X was not associated with the brightest foci, but foci of lesser intensity were still visible in the X territory (Figure 2.7, second row). H3K9me3 staining was comparable to wild type in *cec-4* and *lem-2* mutants, suggesting that the defects in tethering in these mutants are not related to lack of H3K9me3.

Notably, H3K9me3 was not absent in *met-2* mutants. In fact, *met-2* mutants were indistinguishable from wild type. This is in contrast to what was previously observed in *met-2* mutant embryos, where H3K9me3 levels were greatly reduced (Towbin *et al.,* 2012). However, it is similar to what was observed in the germline, where *met-2* was reported to be dispensable for H3K9me3 (Bessler *et al.,* 2010), and similar to what we reported previously in intestinal nuclei of *met-2* mutants (Jack *et al.,* 2013). These results suggest tissue specific differences in the use of HMTs to deposit H3K9me3. Despite near-normal levels and distribution of H3K9me3 in *met-2* mutants, the X chromosomes were decondensed, suggesting that *met-2* contributes to the regulation of X chromosome structure in ways other than H3K9me3.

We also note that *set-32* mutants contained two types of nuclei. Some nuclei were indistinguishable from wild type (Figure 2.7, row 5) and some had reduced levels of H3K9me3 (Figure 2.7, row 6). The two *set-32* mutant nuclei depicted on Figure 2.7 come from the same worm, illustrating cell-to-cell variation within a single animal in this genetic background. These observations suggest that in contrast to what is seen in embryos (Towbin *et al.,* 2012), in differentiated cells, enzymes other than SET-25 contribute to the deposition of H3K9me3.

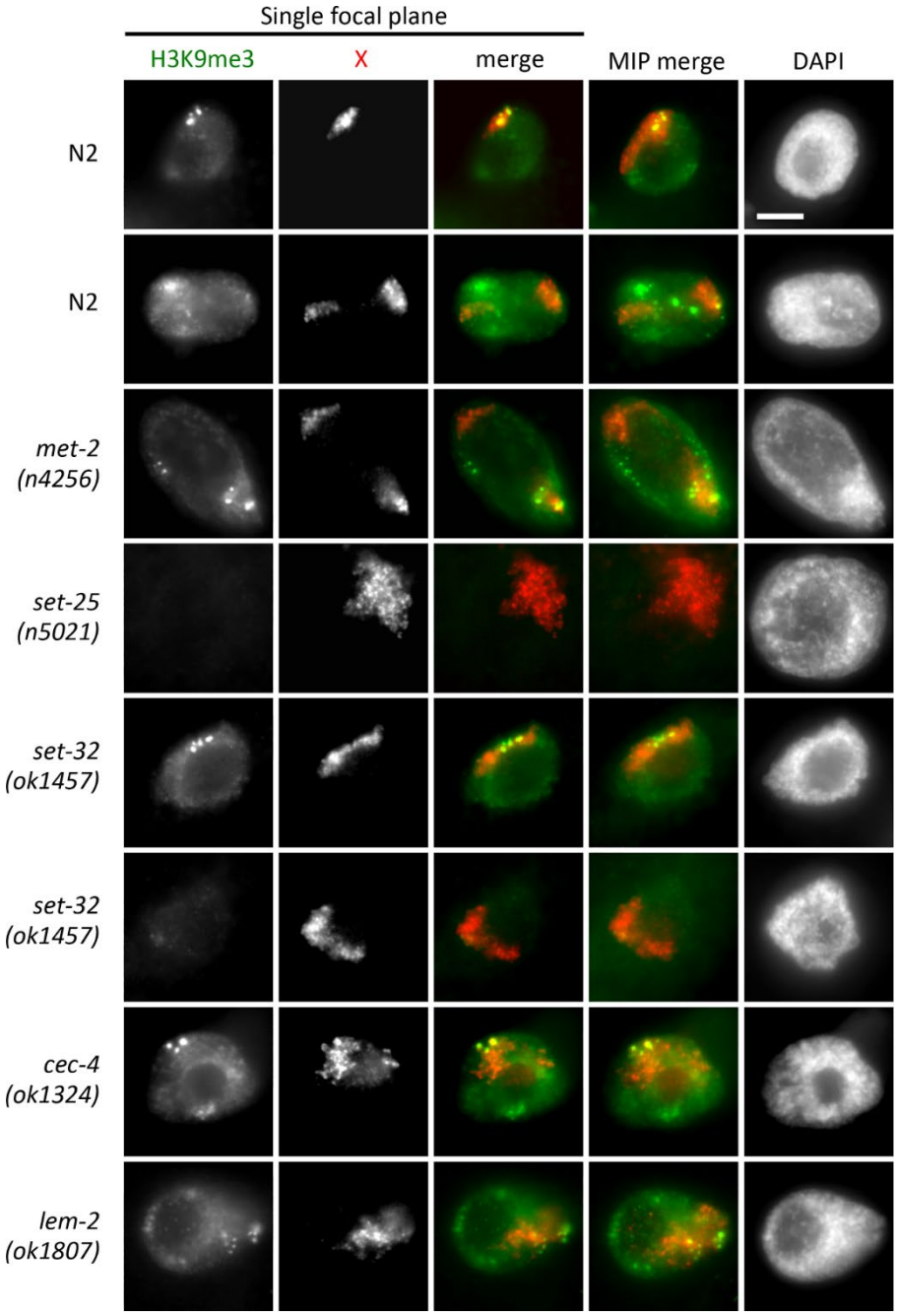

Figure 2.7 Analysis of H3K9me3 levels. Immunofluorescence analysis with antibodies specific to H3K9me3 (green), combined with antibodies specific to DCC subunit CAPG-1 (red) to mark the location of the X chromosomes. To illustrate the spatial proximity of the bright H3K9me3 foci to the X territory, single focal planes are shown. Maximum intensity projections of whole nuclei are shown for reference (right, MIP). The H3K9me3 signal is distributed diffusely in the nucleus with some peripherally localized bright foci. H3K9me3 signal intensity is only affected in *set-25* and *set-32* mutants. Scale bar, 5 μm.

The DCC remains X-bound and the X chromosomes maintain enrichment for H4K20me1

A possible explanation for the dosage compensation defects in tethering mutants (Figure 2.1) is disruption of DCC localization. To test this possibility we stained worms with X-paint FISH probe followed by immunofluorescence using antibodies specific to the DCC subunit DPY-27. Despite changes in X chromosome morphology, we observed normal localization of the DCC to X chromosomes (Figure 2.8A). While we cannot exclude minor changes in DCC distribution along the X chromosome, we conclude that the DCC does associate with the X chromosomes in tethering mutants.

An alternative explanation for defects in dosage compensation in these mutants is that DCC function is disrupted. Previously characterized molecular functions of the DCC include condensation of the X chromosome (Sharma *et al.,* 2014; Lau *et al.,* 2014), altering chromosome topology (Crane *et al.,* 2015), and leading to a different distribution of posttranslational histone modifications, particularly H4K20me1 and H4K16ac (Vielle *et al.,* 2012; Wells *et al.,* 2012). To test whether mutations in tethering genes affect the ability of the DCC to lead to enrichment of H4K20me1 on the X, we co-stained worms with antibodies specific to the DCC (to mark the location of the X) and antibodies specific to H4K20me1. Results showed that this chromatin mark continues to be enriched on the X chromosomes (Figure 2.8B). Therefore, at least some aspects of DCC function remain intact in tethering mutants. Although wild type level of enrichment of H4K20me1 on the X appears to be required for X chromosome condensation (Lau *et al.,* 2014), our results indicate that it is not sufficient.

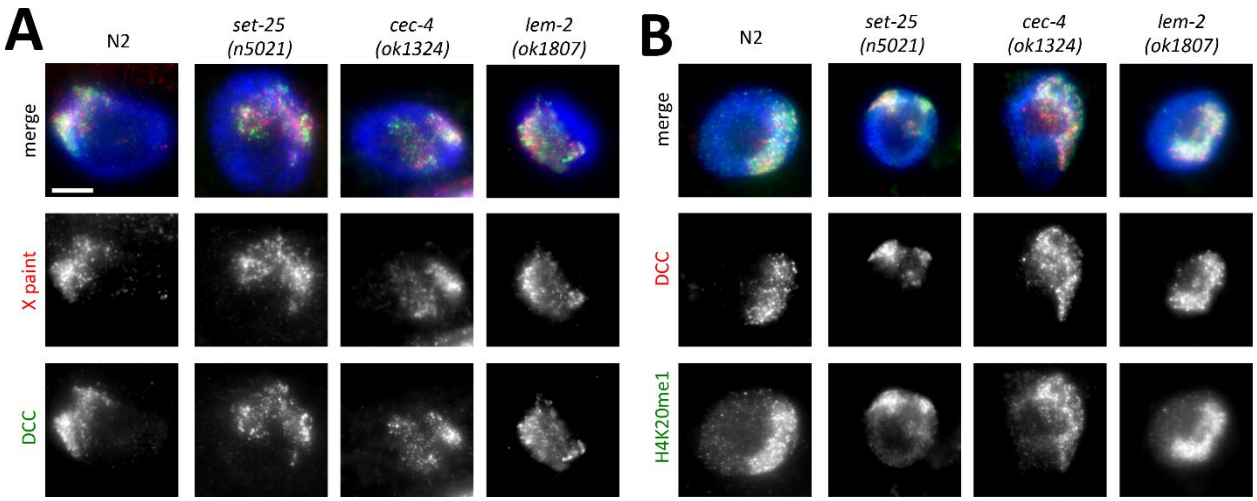

Figure 2.8 DCC localization and H4K20me1 enrichment in tethering mutants. (A) Combined X paint fluorescence in situ hybridization (red) and immunofluorescence with antibodies specific to DCC component DPY-27 (green). The DCC remains localized on the decondensed X chromosomes of tethering mutants. (B) Immunofluorescence images with antibodies specific to H4K20me1 (green) and DCC component CAPG-1 (red) to mark the location of the X chromosome. H4K20me1 remains enriched on DCC-bound X chromosomes. Scale bar, 5 μm.

Derepression of X-linked genes in tethering mutants

To test how loss of heterochromatic anchoring affects gene expression, we performed mRNA-seq analysis (Figure 2.9). We performed this analysis in L1 stage larval hermaphrodites. By this stage, somatic cells are differentiated, dosage compensation-mediated chromatin marks are fully established (Vielle *et al.,* 2012; Custer *et al.,* 2015), and gene expression differences resulting from DCC function are easily detectable using RNA-seq (Kramer *et al.,* 2011). Based on the low level of male rescue observed upon RNAi-depletion of tethering genes (Figure 2.1), we did not expect major disruptions of regulation of X-linked genes. Therefore, to compare gene expression changes in tethering mutants to gene expression changes resulting from moderate

changes in DCC function, we generated a data set using L1 hermaphrodite worms in which the DCC subunit DPY-27 was partially depleted by RNAi. Note that even though DPY-27 levels were significantly reduced in these worms (Figure 2.15), there was very little lethality associated with the RNAi treatment, indicating that DCC function was only partially disrupted.

Under these mild *dpy-27(RNAi)* conditions, we observed a small increase in average X-linked gene expression compared to gene expression changes on autosomes. These results are qualitatively similar to previously reported analysis of dosage compensation mediated gene expression changes (Crane *et al.,* 2015; Kramer *et al.,* 2015; Jans *et al.,* 2009), but the magnitude of change is smaller, indicating that this data is an appropriate representation of gene expression changes when DCC function is partially disrupted. The median $\log_2$ ratio of expression between *dpy-27(RNAi)* worms and control vector RNAi treated worms was significantly higher on the X (0.062) compared to autosomes (-0.059) (for all expressed genes) (Figure 2.9A, one-sided Wilcoxon rank-sum test $p = 3.09 \times 10^{-78}$), consistent with a small degree of X depression. Strains carrying mutations in *cec-4(ok3124)* or *met-2(n4256) set-25(n5021)* showed similar X chromosome derepression compared to *dpy-27(RNAi)*. The median $\log_2$ ratio of expression between *cec-4(ok3124)*/control or *met-2(n4256) set-25(n5021)*/control was significantly higher on the X (0.095 and 0.057 respectively) compared to autosomes (-0.042 and -0.057 respectively) (Figure 2.9B and 2.9C, one sided Wilcoxon rank-sum test $p = 8.07 \times 10^{-42}$ and $p = 8.48 \times 10^{-18}$).

To examine whether the observed differences in gene expression might reflect random variations between chromosomes, we examined the average gene expression change on each autosome compared to the rest of the genome (Figure 2.9A–2.9C). Small gene expression change differences were in fact observed between any autosome and the rest of the genome, and many of these differences were statistically significant (two-sided Wilcoxon rank sum test). However, for

chromosomes I, II, III, and IV, the autosome was downregulated, not upregulated, compared to the rest of the genome (Figure 2.9A–2.9C). Chromosome V was the only autosome that appeared upregulated compared to genomic average, both in *dpy-27(RNAi)* and in tethering mutants, and this derepression was mild compared the derepression observed for the X chromosome (Figure 2.9A–2.9C).

We then compared expression changes on the X chromosome to each autosome individually (Figure 2.9D–2.9F). Again we observed a small yet statistically greater level of derepression on the X than any of the autosomes in all three backgrounds. Importantly, the X chromosome was significantly more upregulated than chromosome V, the only autosome that is derepressed compared to the genomic average (Figure 2.9D–2.9F, one sided Wilcoxon rank-sum test $p = 8.35 \times 10^{-24}$ in *dpy-27(RNAi)*, $p = 0.00126$ in *cec-4*, and $p = 0.000468$ in *met-2 set-25*). These analyses indicate that the greatest degree of derepression is seen on the X chromosome. Furthermore, the trends were the same in *dpy-27(RNAi)* and in *cec-4* and *met-2 set-25* mutants, indicating again that gene expression changes in tethering mutants are comparable to gene expression changes in partial DCC depletion conditions. These results suggest that lack of CEC-4, or MET-2 and SET-25 function leads to similar gene expression changes as a partial depletion of the DCC.

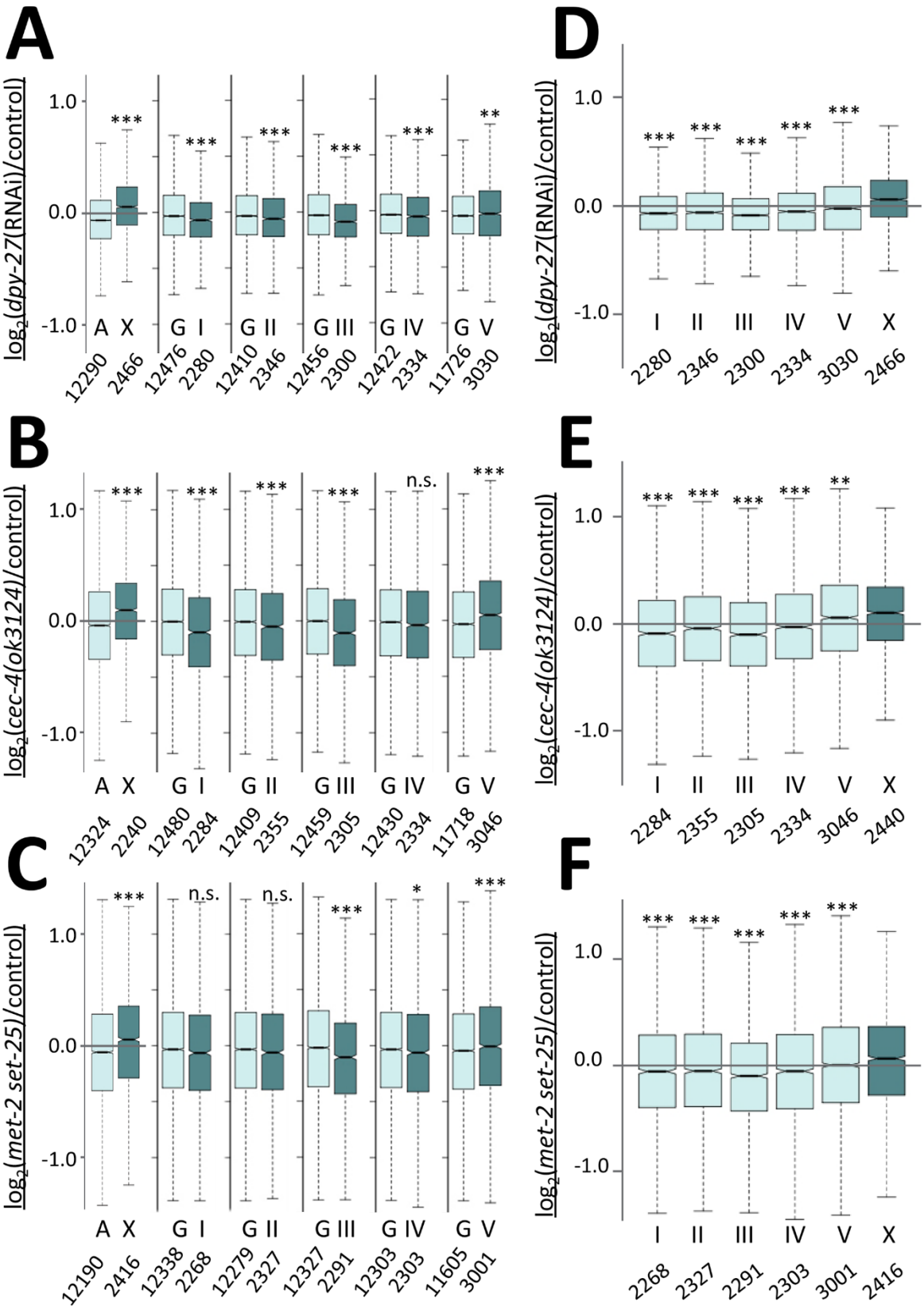
A
log2(dpy-27(RNAi)/control)
1.0
0.0
-1.0
***
***
***
***
***
**
A X
G I
G II
G III
G IV
G V
12290
2466
12476
2280
12410
2346
12456
2300
12422
2334
11726
3030
D
log2(dpy-27(RNAi)/control)
***
***
***
***
***
I
II
III
IV
V
X
2280
2346
2300
2334
3030
2466
B
log2(cec-4(ok3124)/control)
***
***
***
***
n.s.
***
A X
G I
G II
G III
G IV
G V
12324
2240
12480
2284
12409
2355
12459
2305
12430
2334
11718
3046
E
log2(cec-4(ok3124)/control)
***
***
***
***
**
I
II
III
IV
V
X
2284
2355
2305
2334
3046
2440
C
log2(met-2 set-25)/control)
***
n.s.
n.s.
***
*
***
A X
G I
G II
G III
G IV
G V
12190
2416
12338
2268
12279
2327
12327
2291
12303
2303
11605
3001
F
log2(met-2 set-25)/control)
***
***
***
***
***
I
II
III
IV
V
X
2268
2327
2291
2303
3001
2416

Figure 2.9 RNA-seq analysis of gene expression changes in tethering mutants. (A-C) Boxplots show the distribution of log2 expression ratios on the X and autosome between dpy-27(RNAi) and control RNAi, *cec-4(ok3124)* mutant and control, and *met-2(n4256) set-25(n5021)* mutant and control. The X chromosome was significantly derepressed compared to autosomes (each autosome individually, or as a group) in *dpy-27(RNAi)* (A), *cec-4(ok3124)* mutants (B), and *met-2(n4256) set-25(n5021)* mutants (C). Increased expression from the X was tested between the X and all autosomes (left), or the X and individual autosomes (right) by one-sided Wilcoxon rank-sum test (** = $p < 0.01$, *** = $p < 0.001$).

To complement our analysis of average gene expression, we also looked at genes whose expression changed significantly using DESeq2 analysis (Figure 2.16). Consistent with previous gene expression studies (Gonzalez-Sandoval *et al.,* 2015), expression of very few genes changed significantly in *cec-4* mutants. However, the same was true for *dpy-27(RNAi)*. In both cases, a slightly higher percentage of X-linked genes were upregulated than the percentage of upregulated autosomal genes, and a slightly higher percentage of X-linked genes were upregulated than downregulated. There were more genes with significant changes in gene expression in *met-2 set25* mutants, consistent with a dosage-compensation-independent gene regulatory role for these genes (Gonzalez-Sandoval *et al.,* 2015). The percentage of X-linked genes that met the statistical criteria for significant upregulation was not greater than the percentage of downregulated X-linked genes in this background (Figure 2.16). Perhaps the subtle changes caused by mild dosage compensation defects are not sufficient to show statistically significant changes in expression (based on 3 or 4 biological replicates) at the individual gene level.

To further determine whether there is a correlation between the degree of gene expression change in the tethering mutants and the degree of gene expression change in worms with a partial

defect in DCC function, we plotted the $\log_2$ ratio of expression of the tethering mutants and control worms against the $\log_2$ ratio of expression of *dpy-27(RNAi)* and control vector worms (Figure 2.10A and 2.10B). With a $\log_2$ cutoff of 0.1 (10%) for upregulation, the largest percentage of X-linked genes fell in the quadrant of derepression in both *dpy-27(RNAi)* and tethering mutants (32–34% versus 3–19% on other quadrants). For autosomal genes the opposite was true, and the largest percentage fell in the quadrant of downregulation in both backgrounds (30–32%, compared to 4–20% in other quadrants). These results indicate a bias toward upregulation of a common set of X-linked genes in DCC-deficient worms and in tethering mutants. A similar degree of correlation was observed when comparing *cec-4* to *met-2 set-25* (Figure 2.10C), and again the correlation was higher for X-linked genes than autosomal genes. There is a population of genes on autosomes whose expression is repressed by MET-2 and SET-25 independent of DCC-mediated changes (Figure 2.10B, red circle), or independent of CEC-4 (Figure 2.10C, red circle), consistent with a previous study (Gonzalez-Sandoval *et al.,* 2015).

To examine correlations between gene expression changes, we performed regression analysis, which showed a moderate positive correlation between tethering mutants and *dpy-27(RNAi)* $\log_2$ ratios for both X and autosomal genes (R-squared values ranged from 0.34 and 0.49, Pearson correlation values between 0.58 and 0.7) (Figure 2.10D). Additionally, X-linked genes had slightly higher R-squared and Pearson correlation values compared to autosomal genes. Correlations of gene expression changes on the X indicate that the genes whose expression is most affected by depletion of the DCC are also the genes whose expression is most affected in tethering mutants. Correlations on autosomes may be explained by the observation that defects in DCC activity affect not only X-linked gene expression, but indirectly also contribute to modulating autosomal gene expression (Jans *et al.,* 2009). A control analysis, gene

expression changes in *dpy-27(RNAi)* correlated with gene expression changes in an unrelated condition (*lsm-1* mutants, (Therizols *et al.,* 2014)), showed lower R-squared values and lower Pearson correlation values on all chromosomes (Figure 2.10D).

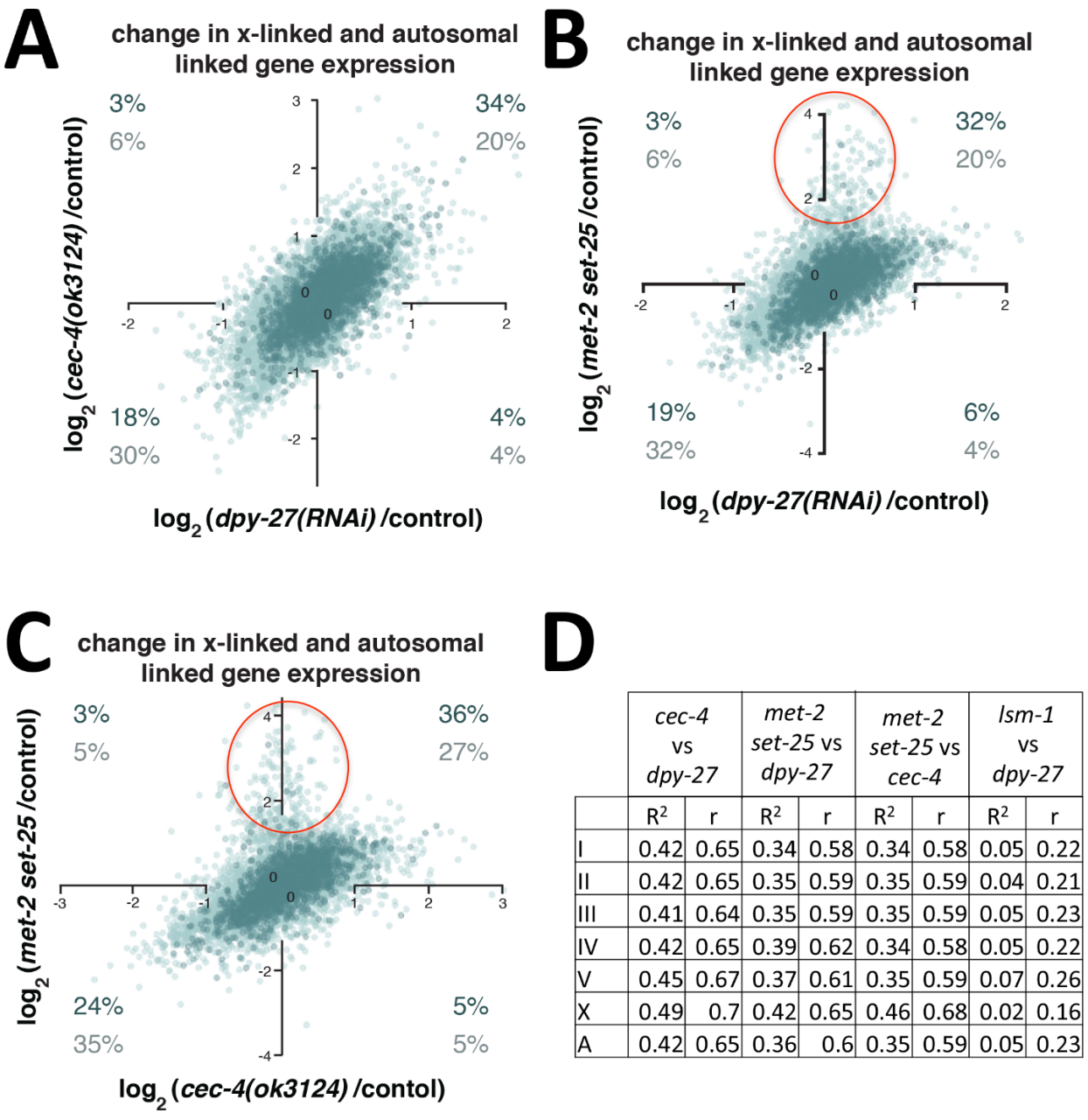

D

	cec-4 vs *dpy-27*		*met-2 set-25* vs *dpy-27*		*met-2 set-25* vs *cec-4*		*lsm-1* vs *dpy-27*	
	R^2	r	R^2	r	R^2	r	R^2	r
I	0.42	0.65	0.34	0.58	0.34	0.58	0.05	0.22
II	0.42	0.65	0.35	0.59	0.35	0.59	0.04	0.21
III	0.41	0.64	0.35	0.59	0.35	0.59	0.05	0.23
IV	0.42	0.65	0.39	0.62	0.34	0.58	0.05	0.22
V	0.45	0.67	0.37	0.61	0.35	0.59	0.07	0.26
X	0.49	0.7	0.42	0.65	0.46	0.68	0.02	0.16
A	0.42	0.65	0.36	0.6	0.35	0.59	0.05	0.23

Figure 2.10 Comparison of gene expression changes in tethering mutants and partial DCC depletions. The magnitude of log2 expression ratios of X-linked (dark) and autosomal linked genes (light) between *cec-4(ok3124)* mutant and control plotted against *dpy-27(RNAi)* and control RNAi (A), *met-2(n4256) set-25(n5021)* mutant and control plotted against *dpy-27(RNAi)*

and control RNAi (B), and *met-2(n4256) set-25(n5021)* mutant and control plotted against *cec-4(ok3124)* mutant and control (C). Red circles indicate a group of genes that are repressed by MET-2 and SET-25 independent of dosage compensation or *cec-4* function. Percent of X-linked (dark numbers) and autosomal genes (light numbers) with greater than 10% (log2 of 0.1) change in expression are indicated in each quadrant. (D) The R-squared of each regression and the Pearson correlation values are shown for X-linked (X) and autosomal genes (A) for each comparison.

To determine whether gene expression changes correlate with chromosomal changes, we compared $\log_2$ ratios of genes located at X chromosome left, middle, and right regions. Regions were designated based on LEM-2 ChIP-chip signals domains (Ikegami *et al.,* 2010). The region 0 Mb—4 Mb was designated "left", 4 Mb—15.75 Mb was designated "middle", and 15.75 Mb—17 Mb was designated "right". Since the middle region of the X chromosome is subject to the greatest level of decondensation and relocation in tethering and DCC mutants (Figure 2.4), we hypothesized that genes in the middle of the X would be more derepressed compared to the right and left arms. However, when examining the distribution of $\log_2$ ratios in *dpy-27(RNAi)/*control, *cec-4(ok3124)/*control, and *met-2(n4256) set-25(n5021)/*control, the X chromosome regions did not show significant differences by two-sided Wilcoxon rank-sum test (Figure 2.16, median $\log_2$ ratio between 0.047 and 0.099 and p-values ranged from 0.09 and 0.90). While surprising, these observations are consistent with the model that DCC induced changes in X chromosome structure modulate gene expression chromosome-wide rather than locally (Crane *et al.,* 2015; Kramer *et al.,* 2015; Jans *et al.,* 2009; Kruesi *et al.,* 2013).

DISCUSSION

In a screen to identify genes with roles in X chromosome dosage compensation, we identified a group of genes with previously known roles in anchoring heterochromatic domains to the nuclear lamina: H3K9 HMTs, the chromodomain protein CEC-4, and the nuclear lamina protein LEM-2. These genes are collectively required to compact the X chromosomes and tether them to the nuclear periphery. Compartmentalization of the nucleus in this way may restrict availability of transcriptional activators for the X chromosomes, thus creating a repressive compartment to modulate X-linked gene expression. Although H3K9me and nuclear lamina interactions are enriched at the left end of the X chromosomes, we find that these mutations disproportionately affect compaction and subnuclear localization of the gene-rich middle portion. Large-scale changes in chromosome morphology are accompanied by only modest changes in gene expression, suggesting that while nuclear architecture does contribute to modulating gene expression, it is not the primary determinant.

Models of the effect of heterochromatic anchors on X chromosome morphology

The observation that the middle of the X chromosome is more sensitive to loss of heterochromatic anchors (Figure 2.4), can be explained by postulating the existence of redundant anchors, previously proposed to exist in differentiated cells (Gonzalez-Sandoval *et al.,* 2015; Towbin *et al.,* 2012) (Figure 2.11, model 1). In this model, two types of anchors maintain peripheral localization of the X chromosome. Heterochromatic tethers are enriched at the left end of the X (Towbin *et al.,* 2012; Ikegami *et al.,* 2010), but the rest of the chromosome must also be weakly tethered. Additional anchors also tether the left end. When heterochromatic anchors are lost, the left end remains near the periphery due to the additional anchors, but the rest of the X chromosome decondenses and relocates centrally. However, if we assume that these tethers are

not sex- and chromosome-specific, the model fails to explain why the X chromosome in males (Figure 2.5) and the autosomes in hermaphrodites (Figure 2.6) are not sensitive to the loss of heterochromatic tethers. To explain why only the DCC-bound X is affected, we propose an alternative model (Figure 2.11, model 2): (1) heterochromatic anchors at the left end of the X nucleate a compact chromatin structure, and (2) the activity of the DCC propagates this structural organization to encompass the entire chromosome. In the absence of the DCC, but in the presence of heterochromatic tethers (for example, the male X), the left end maintains its compact structure and peripheral localization. However, the rest of the chromosome decondenses and moves more centrally. In the presence of the DCC, but without heterochromatic anchors (tethering mutants), redundant anchors keep the left end at the periphery, but the DCC is unable to compact the rest of the chromosome and bring it to the periphery. Since autosomes are not bound by the DCC, they are not affected by the loss of heterochromatic tethers.

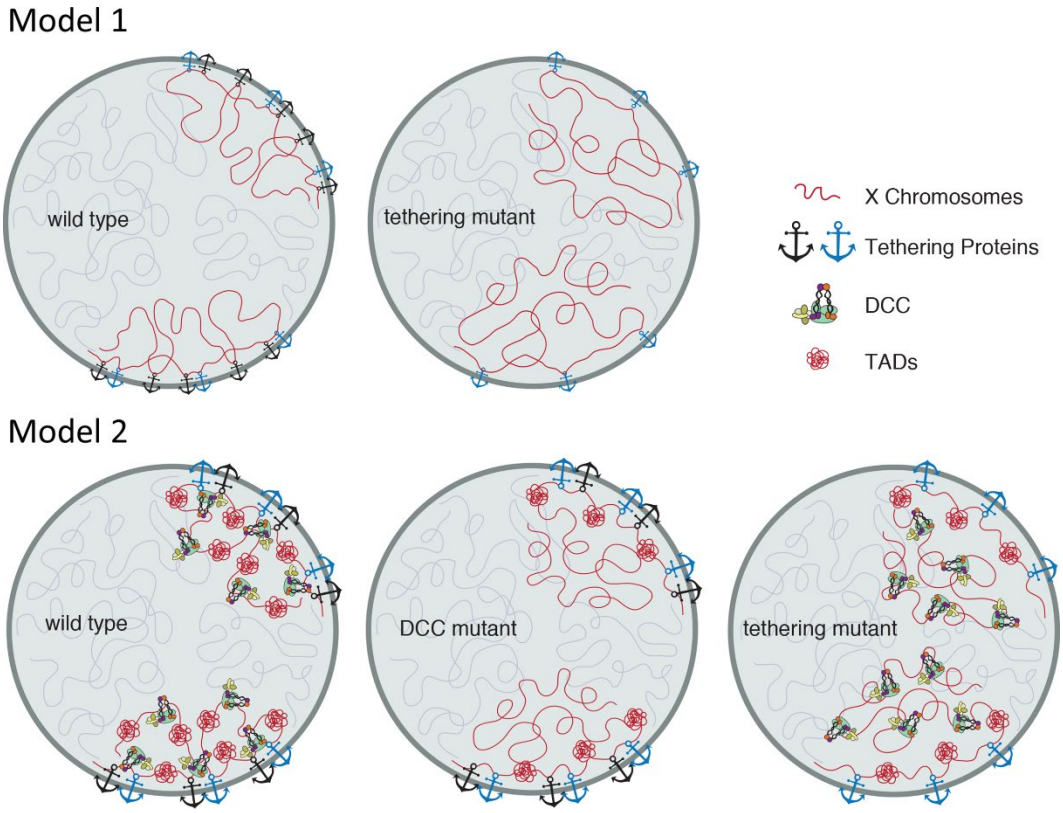

Figure 2.11 Model showing the effects of tethering and DCC function on X chromosome compaction and nuclear localization. In differentiated cells, multiple anchoring mechanisms tether the left end of the X chromosome to the nuclear lamina (black and blue anchors). In wild type cells, the DCC organizes the X chromatin into topologically associating domains (TADs) and uses heterochromatin anchors to compact the X chromosome and bring it to the nuclear periphery. In the absence of the DCC, the left end of the X remains peripheral and compact due to the action of the tethering proteins, and its TAD structure is maintained. The rest of the X chromosome loses its TAD organization, decondenses and moves more internally. When heterochromatic tethers (black anchors) are lost, redundant tethers (blue) keep the left end of the X near the nuclear lamina. Without the heterochromatic anchors, the DCC is unable to compact the rest of the chromosome and bring it near the periphery. Therefore, the rest of the X chromosome decondenses and relocates away from the nuclear lamina.

Correlation between compaction, subnuclear localization and gene expression

Chromatin compaction and subnuclear localization are believed to be coordinated with gene expression levels to a certain degree (Bickmore and van Steensel, 2013; Ciabrelli and Cavalli, 2015; Van Bortle and Corces, 2012). We analyzed chromatin condensation, subnuclear localization, and gene expression changes in DCC-depleted animals and in tethering mutants. We observed elevated levels of X-linked gene expression (Figure 2.9), decreased compaction (Figures 2.2 and 2.4), and relocation to a more central position (Figures 2.3, 2.4 and 2.5), both in the absence of the DCC and in tethering mutants, providing support for the hypothesis that these processes are coordinated. However, the correlation is not perfect. The degree of gene expression change did not correlate well with the degree of decondensation and/or subnuclear relocation. At the whole chromosome level, the X chromosomes in tethering mutants decondensed to a degree comparable to DCC mutants (Figure 2.2). Similarly, the degree of relocation was greater in tethering mutants than in partial loss-of-function DCC mutant, and comparable to the positioning in XO animals that completely lack DCC function (Figures 2.3 and 2.5). However, gene expression changes in tethering mutants are much less significant than in DCC mutants (Figure 2.9). Similar conclusions were reached when we analyzed different regions of the X chromosome: relocation and decondensation was most significant in the middle of the X chromosome (Figure 2.4), but gene expression changes were comparable in all regions of the chromosome (Figure 2.16). A higher resolution study may reveal a stronger correlation, but at the level of whole chromosomes, or large chromosomal domains, the correlation between gene expression change, chromosome decondensation and subnuclear localization is limited. A recent study showed that chromatin decondensation, even in the absence of transcriptional activation, is sufficient to drive nuclear reorganization (Bauer *et al.,* 2012). Similarly, in *cec-4* mutants,

decondensation of transgenic arrays is coupled to their relocation within the nucleus, but it is accompanied by only minimal changes in gene expression (Gonzalez-Sandoval *et al.,* 2015). This is reminiscent of our results, where chromatin decondensation and relocation in general correlate, but the degree of condensation does not reflect the degree of gene expression change.

We believe these results reflect that fact that repression by the DCC involves multiple mechanisms, and disruption of condensation and subnuclear localization is not sufficient to cause major changes in gene expression. Other DCC-mediated changes, for example enrichment of H4K20me1 on the X chromosome, are intact in tethering mutants (Figure 2.8), and are sufficient to maintain repression. However, it should be emphasized that loss of tethers (and/or the accompanying change in X chromosome packaging and nuclear organization) does result in gene expression changes that are biologically significant. While the gene expression change is modest (Figures 2.9 and 2.10), it is sufficient to rescue a significant proportion of males in our genetic assay (Figures 2.1 and 2.12). Thus, chromatin condensation, subnuclear localization, and tethering to the nuclear periphery, may not be the primary determinants of gene expression change, or may act redundantly with other factors, but they do contribute to stabilizing gene expression programs in development (Gonzalez-Sandoval *et al.,* 2015) and during dosage compensation (this study).

The role of condensin in interphase nuclear organization

Condensin has been implicated previously in chromosome territory organization in a variety of organisms (Lau *et al.,* 2014; Buster *et al.,* 2013; Iwasaki *et al.,* 2015). In condensin mutant fission yeast, disruption of condensin-dependent intrachromosomal interactions disturbed chromosome territory organization (Csankovszki *et al.,* 2004). We previously showed that the dosage compensation condensin complex is required for compaction of the X chromosomes in

interphase in *C. elegans* (Lau *et al.,* 2014). Our current data reveal that interphase chromosome compaction requires not only the DCC, but also nuclear lamina anchors. We favor the interpretation that heterochromatic tethers and the DCC cooperate to compact the X chromosomes (Figure 2.11, model 2). Although low resolution, our FISH analysis supports this hypothesis. The X chromosomes appear compact and in a well-defined peripheral territory only when tethered and DCC-bound. In both DCC and tethering mutants, the X paint signal becomes more diffuse with less well-defined borders (Figure 2.2, (Lau *et al.,* 2014)). Chromosome I paint signals in wild type worms qualitatively are more comparable to X paint signals in DCC mutants or tethering mutants than to X paint signals in wild type (Figure 2.6). The two ends of chromosome I are anchored to the nuclear periphery, and remain anchored in tethering mutants, while the middle domain is more centrally located even in wild type worms, reminiscent of the organization of X chromosome in tethering mutants and in males (Figure 2.6, (Lau *et al.,* 2014)). Overall, these observations suggest that the DCC and heterochromatic anchors work together to compact and peripherally relocate the middle domain of the X chromosomes not directly tethered to the nuclear periphery.

It is interesting to note that we observe significant chromosome decondensation despite normal DCC binding to the chromosome (Figure 2.8). Current models of DCC binding to the X include a recruitment step to *rex* sites (Jans *et al.,* 2009; McDonel *et al.,* 2006; Ercan *et al.,* 2007), which have very high levels of DCC binding (Jans *et al.,* 2009; Solovei *et al.,* 2013), and tend to define TAD boundaries (Crane *et al.,* 2015). From these *rex* sites to DCC spreads to *dox* sites enriched at promoter regions (Jans *et al.,* 2009; Solovei *et al.,* 2013). From our low-resolution immunofluorescence analysis, DCC binding seems unaffected in tethering mutants. Yet, despite

near normal levels of DCC, the X chromosome is not compacted, indicating that in the absence of heterochromatic tethers, DCC function appears to be compromised.

Our results also reveal parallels with recent genome-wide chromosome conformation capture (Hi-C) analysis of dosage compensated X chromosomes (Crane *et al.,* 2015). Hermaphrodite X chromosomes are packaged into a structure with regularly spaced boundaries between topologically associated domains (TADs). In the absence of the DCC, boundaries become less well defined and TAD organization weakens, except at the left end of the X, which is the domain that is tethered to the nuclear lamina (Crane *et al.,* 2015) (Figure 2.11, model 2). This parallels our observations that in DCC mutants the left end of the X chromosome remains less affected than the rest of the chromosome. It is likely that the observed changes in TAD formation (Crane *et al.,* 2015) and chromosome compaction and subnuclear localization (Figures 2.2–2.5, (Lau *et al.,* 2014)) in the absence of the condensin-like DCC reflect the same underlying changes in chromosome structure analyzed at different resolutions and using different methods.

If TAD formation, chromatin condensation, and subnuclear localization indeed correlate, our results would predict that TADs at the left of the X chromosome would also be less disrupted in tethering mutants than along the rest of the X chromosome. These results and predictions would suggest that nuclear lamina anchors (both the anchors mediated by H3K9me3 and the yet uncharacterized anchors) are able to impose this level of organization (TAD formation) on the tethered portion of the chromosome. Autosomes in general lack regularly spaced TADs, except at the tethered ends of chromosome arms (Crane *et al.,* 2015). This observation is consistent with our observations of peripherally located chromosome I arms (Figure 2.6), and our suggestion that nuclear lamina anchors are sufficient to form regularly spaced TADs in the anchored domain.

Changes in nuclear organization during cellular differentiation and development

The mechanisms of anchoring appear to be different in embryonic cells compared to differentiated cells. Repetitive heterochromatic arrays require H3K9 methylation and CEC-4 for peripheral localization in embryonic cells but not in differentiated cells, suggesting that differentiated cells have other mechanisms in place for tethering genomic regions to the nuclear envelope (Gonzalez-Sandoval *et al.,* 2015; Towbin *et al.,* 2012). Whether heterochromatin and CEC-4 mediated anchors continue to function in differentiated cells remained unclear Gonzalez-Sandoval *et al.,* 2015), yet our results are consistent with this possibility. The left end of the X chromosome remains in the vicinity of the nuclear lamina in the absence of H3K9me3, LEM-2, or CEC-4 in fully differentiated cells, suggesting the existence of additional anchors (Figure 2.4). However, X chromosome morphology does change in the absence of these proteins, indicating that tethers mediated by them continue to influence chromosome structure in differentiated cells.

Our results are reminiscent of the findings in differentiating mouse cells Zuleger *et al.,* 2013). In early development, lamin B receptor (*Lbr*) is the predominant mediator of interactions with the nuclear lamina. Later in development, lamin-A/C-dependent tethers appear, sometimes accompanied by the loss of *Lbr*-mediated mechanisms. Loss of peripheral localization of heterochromatin is only observed when both types of tethers are absent (Zuleger *et al.,* 2013). It will be interesting to uncover the nature of the additional anchors in differentiated *C. elegans* tissues and how these anchors affect X chromosome morphology and dosage compensation. However, it is possible that the additional anchors will be cell-type specific, consistent with the observation in mammalian cells where various tissue-specific transmembrane proteins are used to anchor genomic regions to the nuclear lamina (Helbling-Leclerc *et al.,* 2002). Tissue-specific differences between anchoring mechanisms are also consistent with observations that point

mutations in lamin can exhibit tissue-specific defects in humans (Brenner, 1974) as in *C. elegans* (Mattout *et al.,* 2011).

ACKNOWLEDGEMENTS

We thank members of the Csankovszki lab for helpful project discussions. This work was supported by National Science Foundation grant MCB 1021013 (to Gyorgyi Csankovszki). Some nematode strains used in this work were provided by the Caenorhabditis Genetics Center, which is funded by the NIH National Center for Research Resources. The *set-1(tm1821)* allele was provided by the Mitani laboratory through the National Bioresource Project of the MEXT, Japan.

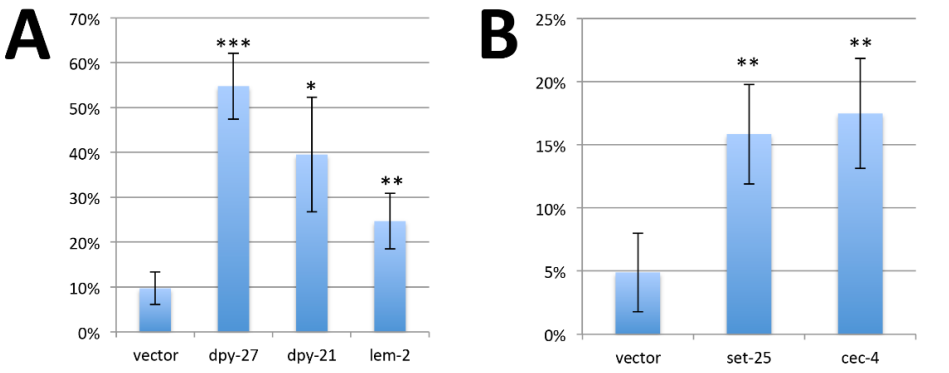

RNAi	n values in each replicate	t-test
vector	628, 660, 670, 511	
dpy-27	696, 658, 518, 756	0.000244383
dpy-21	596, 819, 548, 430	0.014998157
lem-2	654, 716, 743, 607	0.009565229

RNAi	n values in each replicate	t-test
vector	486, 399, 247, 592	
set-25	726, 436, 476, 512	0.005411048
cec-4	599, 458, 617, 552	0.004266121

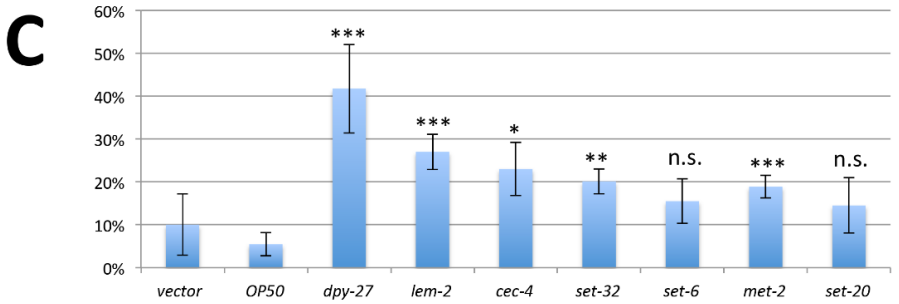

RNAi	n values in each replicate	t-test compared to vector
vector	524, 398, 717, 526, 689, 478, 338, 618	
OP50	438, 427, 610, 680	
dpy-27	232, 493, 356, 357, 449, 515, 488, 471	9.55966E-06
lem-2	469, 511, 504, 493	0.000454673
cec-4	496, 511, 504, 493	0.013910958
set-32	589, 544, 612, 494	0.006103465
set-6	267, 468, 339, 357	0.165680185
met-2	258, 418, 570, 214	0.000274968
set-20	663, 750, 643, 670	0.308095616

Figure 2.12 Additional male rescue analysis. A limited number of genes were analyzed in each experiment (A, B, and C), but using four independent biological replicates. Note that RNAi feeding of parents was extended by 24 hours compared to the experiment shown on Figure 3.1. This led to higher levels of male rescue overall, but the trend remained the same. OP50 is the normal bacterial food source, without any plasmid to produce RNA. With the exception of *set-6* and *set-20*, RNAi of all genes rescued significantly more males than control vector RNAi. It is important to point out that the few males rescued on vector RNAi plates were small and sickly, while the males rescued using RNAi of the other genes appeared more normal size and had better mobility. Error bars indicate standard deviation based on four replicates. Asterisks indicate statistical significance using Student t-test, n.s. = $p>0.05$, * = $p<0.05$, ** = $p<0.01$, *** = $p<0.001$. Numbers of embryos counted and p-values (compared to vector RNAi) are shown in the table below each graph.

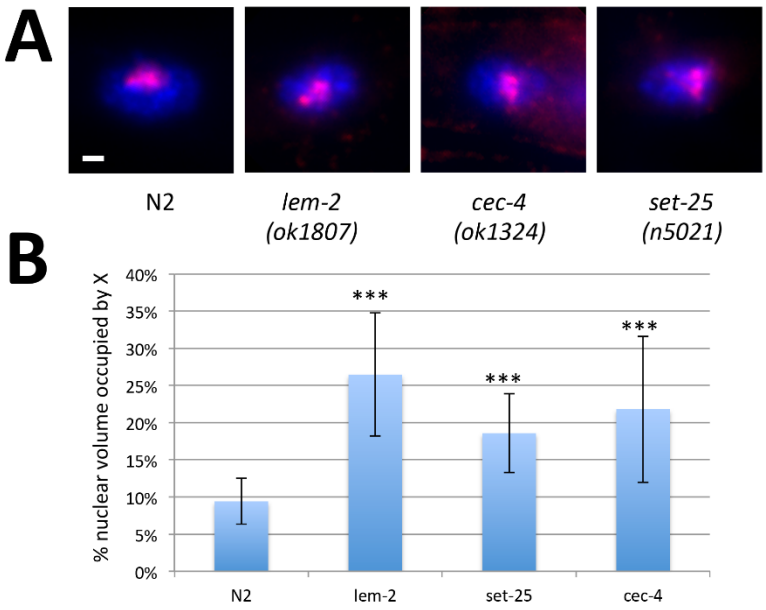

Figure 2.13 Chromosome volume measurements in hypodermal nuclei of hermaphrodites. (A) X chromosome paint FISH (red) in diploid tail tip hypodermal nuclei (DAPI, blue) of hermaphrodite adult worms. The X chromosomes are compact and peripherally localized in wild type (N2), but are decondensed and more centrally located in mutants. Scale bar, 1 mm. (B) Quantification of X chromosome volumes normalized to nuclear size (n=17-26 nuclei). Error bars indicate standard deviation. *** = $p<0.001$ by Student's t-test (N2 compared to appropriate mutant)

A

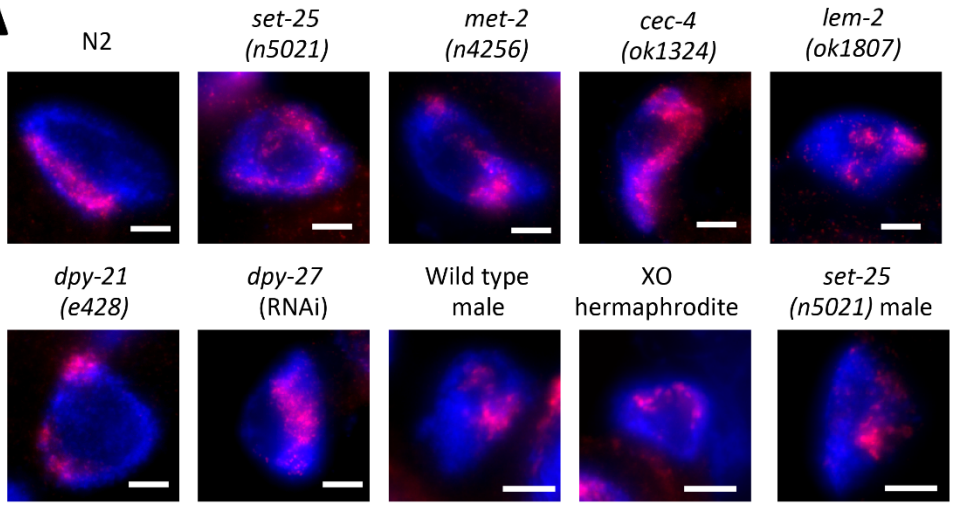

B

genotype	sex	n	% round or ellipsoid
n2	hermaphrodite	31	68%
set-25	hermaphrodite	23	70%
met-2	hermaphrodite	54	57%
cec-4	hermaphrodite	42	61%
lem-2	hermaphrodite	23	87%
dpy-21	hermaphrodite	54	48%
dpy-27(RNAi)	hermaphrodite	31	65%
him-8 (wild type)	male	107	80%
him8;set-25	male	77	86%
her-1; sdc-2, XO	hermaphrodite	109	74%

Figure 2.14 X paint FISH images in irregularly-shaped nuclei. (A) Representative irregularly shaped nuclei in the various backgrounds. The X is compact and peripherally located in N2 hermaphrodites and is decondensed and more centrally located in tethering mutants and in males. (B) Table indicating the percent of nuclei in each background that were suitable for analysis using the three-zone assay.

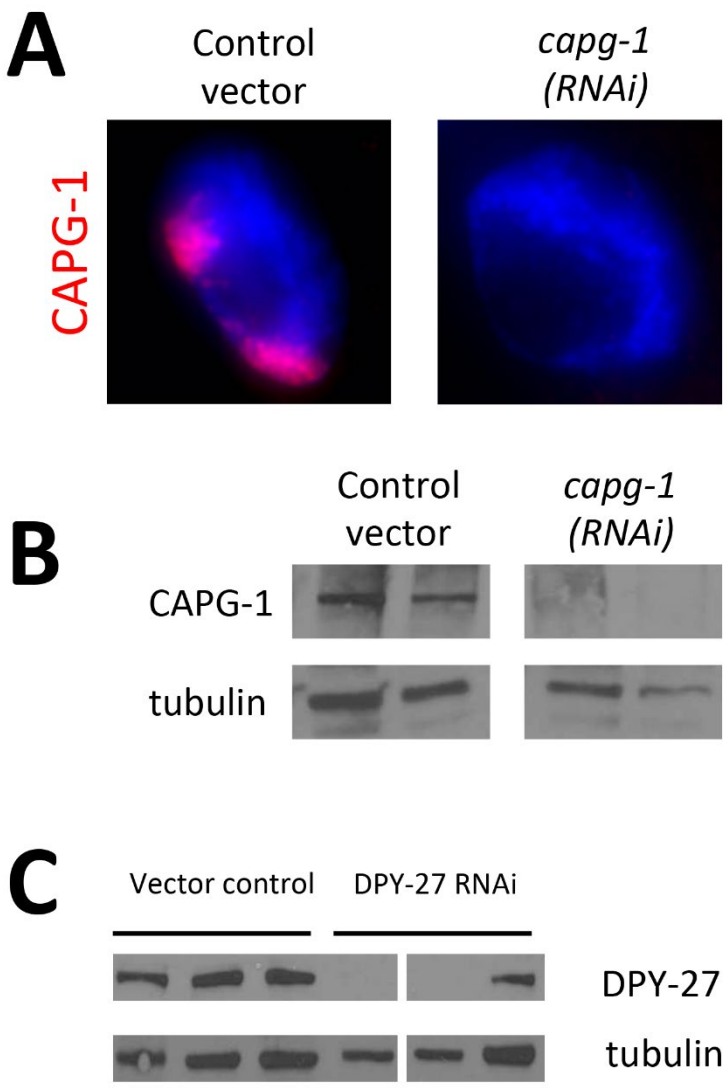

Figure 2.15 Antibody validation and RNAi-depletion control.
(A) Immunofluorescence analysis of the newly developed CAPG-1 antibody in nuclei of control vector RNAi-treated worms shows two territories corresponding to the X chromosomes. In capg-1(RNAi) nuclei, the signal is below level of detection, similar to what has been observed previously with other antibodies to DCC components. (B) On a western blot, the antibody recognizes a protein of the predicted size (131 kD) in control vector RNAi treated worms, but not in CAPG-1 RNAi treated worms. Tubulin was used as loading control. (C) Western blot analysis of three control and three *dpy-27(RNAi)* samples, indicating levels of DPY-27 depletion. Tubulin is shown as a loading control.

A

		X total	X up	% up	X down	% down	A total	A up	% up	A down	% down
padj=.1	*dpy-27(RNAi)*	2466	54	2.19%	15	0.61%	12290	163	1.33%	183	1.49%
	cec-4	2240	80	3.57%	44	1.96%	12324	356	2.89%	972	7.89%
	met-2 set-25	2416	72	2.98%	101	4.18%	12190	507	4.16%	829	6.80%
padj=.05	*dpy-27(RNAi)*	2466	25	1.01%	3	0.12%	12290	90	0.73%	87	0.71%
	cec-4	2240	44	1.96%	28	1.25%	12324	205	1.66%	629	5.10%
	met-2 set-25	2416	39	1.61%	62	2.57%	12190	369	3.03%	450	3.69%

B

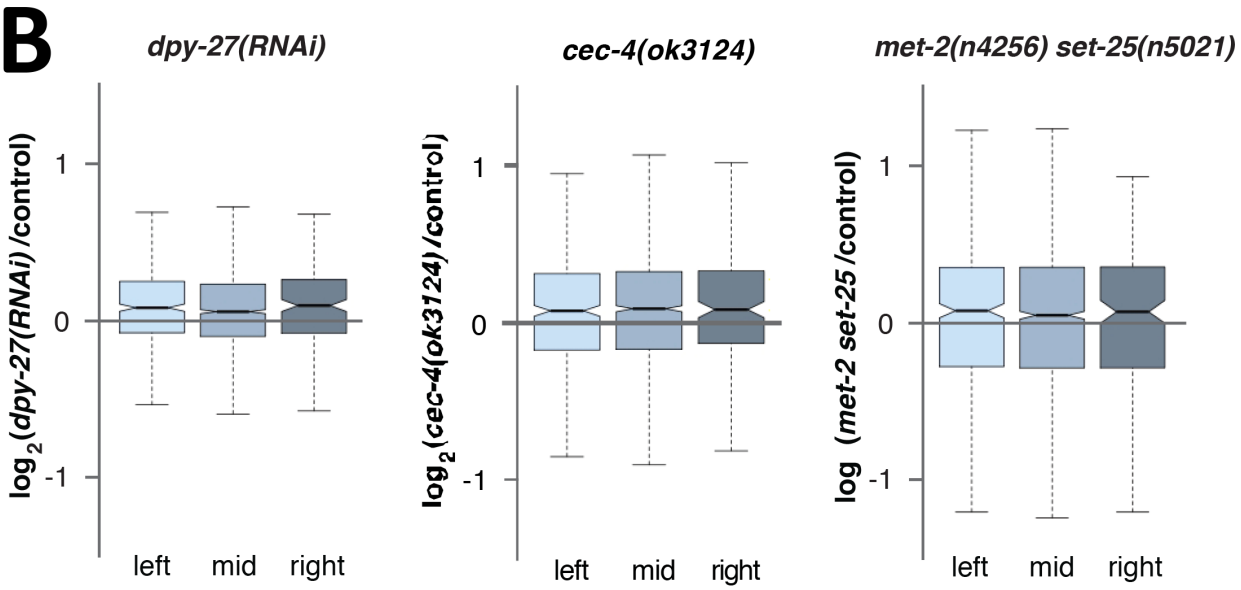

Figure 2.16 Additional comparison gene expression changes on individual chromosomes. (A-C) Boxplots show the distribution of log2 expression ratios on each autosomes (I, II, III, IV, and V) and the rest of the genome (labeled G) between dpy-27(RNAi) and control (A), cec-4(ok3124) mutant and control (B), and met-2(n4256) set-25(n5021) mutant and control. The only autosome that showed derepression compared to the rest of the genome is chromosome V. Differences in gene expression changes between the given chromosome and the rest of the genome were tested by two-sided Wilcoxon rank-sum test (n.s. = $p>0.05$, * = $p < 0.05$, ** = $p<0.01$, *** = $p < 0.001$).

whole X paint

	N2	*set-25*	*met-2 set-25*	*cec-4*	*lem-2*	*dpy-21*	*dpy-27(RNAi*	XO herm	wt male	set-25 male
n	10	10	10	10	10	10	10	10	10	10
peripheral %	0.2460166	0.18108734	0.17100431	0.12483749	0.14885454	0.23171619	0.15055586	0.14006767	0.10578356	0.08473489
st dev	0.12317077	0.08394753	0.09806461	0.07869138	0.08338365	0.17584326	0.10072818	0.06415232	0.07645738	0.07217885
intermed %	0.51555485	0.38185777	0.37545447	0.33605121	0.33670623	0.42227491	0.42842662	0.49212446	0.36320889	0.26202141
st dev	0.11855283	0.05666637	0.08394526	0.08337165	0.06486988	0.12696711	0.09175781	0.09170447	0.08244027	0.12066364
central %	0.23842855	0.43705489	0.45354122	0.5391113	0.51443923	0.3460089	0.42101753	0.36780787	0.53100755	0.6532437
st dev	0.09564744	0.10651531	0.13278119	0.11776565	0.11001907	0.22261633	0.1343343	0.126949	0.13926637	0.17946691
t-test of central ring compared to N2 hermaphrodite										
		0.00085208	0.00070257	9.5192E-06	2.3491E-05	0.18809096	0.00320924	0.02177761	5.6208E-05	3.7175E-06
t-test of central ring compared to set-25 hermaphrodite								t-test compared to wt male		
			0.76784616							0.09960997

left X probe

	N2	set-25	lem-2	cec-4	dpy-27(RNAi)
n	12	12	12	12	12
peripheral %	0.24059006	0.19880636	0.08421264	0.16131613	0.16444175
st dev	0.12888683	0.16120025	0.08460705	0.13741298	0.17310133
intermed %	0.60562542	0.50227208	0.6161937	0.53208363	0.54276048
st dev	0.06694305	0.12348118	0.15840007	0.18913377	0.18914569
central %	0.15378454	0.29892157	0.29959368	0.30660023	0.29279777
st dev	0.13005938	0.14996516	0.20293387	0.25018588	0.24752464
t-test of central ring compared to N2 hermaphrodite					
		0.01895785	0.04995183	0.07821709	0.10355896

Middle X probe

	N2	set-25	lem-2	cec-4	dpy-27(RNAi	XO herm	wt male	set-25 male
n	12	12	12	12	12	10	10	10
peripheral %	0.219341	0.13426402	0.18524328	0.23265349	0.31545998	0.17023531	0.12021431	0.09025599
st dev	0.17906491	0.10996228	0.12817088	0.08833383	0.2030099	0.12669977	0.07361085	0.08042172
intermed %	0.61054607	0.35300007	0.37657471	0.39334755	0.41918957	0.40027687	0.28490383	0.30690104
st dev	0.16494192	0.08933676	0.14280516	0.08937391	0.09451049	0.18146025	0.17001368	0.16435189
central %	0.17011293	0.51273591	0.43818202	0.37399896	0.26535045	0.42948782	0.59488186	0.60284297
st dev	0.14102809	0.17738852	0.24039562	0.13893657	0.22160637	0.25248608	0.21750042	0.21740858
t-test of central ring compared to N2 hermaphrodite								
		4.3012E-05	0.0040592	0.00221382	0.23182446	0.00718188	9.0914E-05	7.4828E-05
							t-test with wt male	
								0.93565866

Right X probe

	N2	set-25	lem-2	cec-4	dpy-27(RNAi)
n	12	12	12	12	12
peripheral %	0.25088158	0.3116153	0.25253889	0.27816668	0.11216881
st dev	0.14277669	0.20004045	0.15345298	0.16198887	0.10510497
intermed %	0.54939892	0.48653712	0.61143382	0.55403456	0.58685975
st dev	0.09645279	0.14703048	0.0966098	0.15558981	0.20696769
central %	0.19971952	0.20184757	0.13602729	0.16779875	0.3009714
st dev	0.16839145	0.18234042	0.12730597	0.24469094	0.2564932
t-test of central ring compared to N2 hermaphrodite					
		0.97657508	0.30811983	0.71370518	0.26718607

Table 2.1 Statistical analysis of X chromosome FISH data using the three-zone assay. n indicates number of nuclei analyzed. Average % of paint signal in each ring and standard deviations are shown. Results of statistical analysis using Student's t test on the portion of the signal in the central ring are below each data set.

Whole chr I paint					
	N2	*met-2*	*set-25*	*cec-4*	*lem-2*
n	10	10	10	10	10
peripheral %	0.27498174	0.28393391	0.32433095	0.27035885	0.33438014
st dev	0.15508742	0.1178846	0.15313704	0.12927037	0.08154668
intermed %	0.32962194	0.40729479	0.42261037	0.38715812	0.37789169
st dev	0.06548054	0.07281563	0.07054663	0.06638567	0.04499781
central %	0.39539632	0.3087713	0.25305867	0.34248303	0.28772817
st dev	0.19366442	0.12723365	0.16203304	0.17888866	0.09688504
t-test of central ring compared to N2 hermaphrodite					
		0.25490246	0.09205845	0.53367557	0.13946616
t-test of central ring compared to X chromosome paint central ring					
	0.03985768				

Left chr I paint		
	N2	*set-25*
n	10	10
peripheral %	0.46685393	0.42616007
st dev	0.17003909	0.15502068
intermed %	0.3625494	0.4885656
st dev	0.10119311	0.1273334
central %	0.17059667	0.08527433
st dev	0.10999698	0.08684983
t-test of central ring compared to N2		
		0.07102638

Middle chr I paint		
	N2	*set-25*
n	10	10
peripheral %	0.12857949	0.13774714
st dev	0.12385027	0.0527957
intermed %	0.51425098	0.46450183
st dev	0.14121135	0.13704882
central %	0.35716953	0.39775103
st dev	0.19140075	0.1152638
t-test of central ring compared to N2		
		0.57436305
t-test of central ring compared to X-mid central ring in N2		
	0.01802029	

Right chr I paint		
	N2	*set-25*
n	10	10
peripheral %	0.48173491	0.46238507
st dev	0.14179603	0.22371649
intermed %	0.4352292	0.40681055
st dev	0.08409888	0.12059219
central %	0.08303589	0.13080437
st dev	0.0771285	0.17828623
t-test of central ring compared to N2		
		0.45154159

Table 2.2. Statistical analysis of chromosome I FISH with the three zone assay. n indicates number of nuclei analyzed. Average % of paint signal in each ring and standard deviations are shown. Results of statistical analysis using Student's t test on the portion of the signal in the central ring are below each data set.

REFERENCES

Akhtar, Asifa, and Susan M. Gasser. “The Nuclear Envelope and Transcriptional Control.” *Nature Reviews Genetics* 8, no. 7 (2007): 507–17.

Andersen, Erik C., and H. Robert Horvitz. “Two C. Elegans Histone Methyltransferases Repress Lin-3 EGF Transcription to Inhibit Vulval Development,” 2007.

Bauer, Christopher R., Tom A. Hartl, and Giovanni Bosco. “Condensin II Promotes the Formation of Chromosome Territories by Inducing Axial Compaction of Polyploid Interphase Chromosomes,” 2012.

Bessler, Jessica B., Erik C. Andersen, and Anne M. Villeneuve. “Differential Localization and Independent Acquisition of the H3K9me2 and H3K9me3 Chromatin Modifications in the Caenorhabditis Elegans Adult Germ Line.” *PLoS Genetics* 6, no. 1 (2010): e1000830.

Bian, Qian, Nimish Khanna, Jurgis Alvikas, and Andrew S. Belmont. “β-Globin Cis-Elements Determine Differential Nuclear Targeting through Epigenetic Modifications.” *Journal of Cell Biology* 203, no. 5 (2013): 767–83.

Bickmore, Wendy A., and Bas van Steensel. “Genome Architecture: Domain Organization of Interphase Chromosomes.” *Cell* 152, no. 6 (2013): 1270–84.

Brenner, Sydney. “The Genetics of Caenorhabditis Elegans.” *Genetics* 77, no. 1 (1974): 71–94.

Buster, Daniel W., Scott G. Daniel, Huy Q. Nguyen, Sarah L. Windler, Lara C. Skwarek, Maureen Peterson, Meredith Roberts, Joy H. Meserve, Tom Hartl, and Joseph E. Klebba, David Bilder, Giovanni Bosco, and Gregory C. Rogers. “SCFSlimb Ubiquitin Ligase Suppresses Condensin II–Mediated Nuclear Reorganization by Degrading Cap-H2.” *Journal of Cell Biology* 201, no. 1 (2013): 49–63.

Chuang, Pao-Tien, Donna G. Albertson, and Barbara J. Meyer. “DPY-27: A Chromosome Condensation Protein Homolog That Regulates C. Elegans Dosage Compensation through Association with the X Chromosome.” *Cell* 79, no. 3 (1994): 459–74.

Ciabrelli, Filippo, and Giacomo Cavalli. “Chromatin-Driven Behavior of Topologically Associating Domains.” *Journal of Molecular Biology* 427, no. 3 (2015): 608–25.

Crane, Emily, Qian Bian, Rachel Patton McCord, Bryan R. Lajoie, Bayly S. Wheeler, Edward J. Ralston, Satoru Uzawa, Job Dekker, and Barbara J. Meyer. “Condensin-Driven Remodelling of X Chromosome Topology during Dosage Compensation.” *Nature* 523, no. 7559 (2015): 240–44.

Csankovszki, Gyorgyi, Karishma Collette, Karin Spahl, James Carey, Martha Snyder, Emily Petty, Uchita Patel, Tomoko Tabuchi, Hongbin Liu, and Ian McLeod, etc., *et al.,* Kristen Hagstrom. “Three Distinct Condensin Complexes Control C. Elegans Chromosome Dynamics.” *Current Biology* 19, no. 1 (2009): 9–19.

Csankovszki, Györgyi, Patrick McDonel, and Barbara J. Meyer. “Recruitment and Spreading of the C. Elegans Dosage Compensation Complex along X Chromosomes.” *Science* 303, no. 5661 (2004): 1182–85.

Custer, Laura M., Martha J. Snyder, Kerry Flegel, and Györgyi Csankovszki. “The Onset of C. Elegans Dosage Compensation Is Linked to the Loss of Developmental Plasticity.” *Developmental Biology* 385, no. 2 (2014): 279–90.

Dawes, Heather E., Dorit S. Berlin, Denise M. Lapidus, Chad Nusbaum, Tamara L. Davis, and Barbara J. Meyer. “Dosage Compensation Proteins Targeted to X Chromosomes by a Determinant of Hermaphrodite Fate.” *Science* 284, no. 5421 (1999): 1800–1804.

Dialynas, George, Sean Speese, Vivian Budnik, Pamela K. Geyer, and Lori L. Wallrath. "The Role of Drosophila Lamin C in Muscle Function and Gene Expression." *Development* 137, no. 18 (2010): 3067–77.

Ercan, Sevinc, Paul G. Giresi, Christina M. Whittle, Xinmin Zhang, Roland D. Green, and Jason D. Lieb. "X Chromosome Repression by Localization of the C. Elegans Dosage Compensation Machinery to Sites of Transcription Initiation." *Nature Genetics* 39, no. 3 (2007): 403–8.

Finlan, Lee E., Duncan Sproul, Inga Thomson, Shelagh Boyle, Elizabeth Kerr, Paul Perry, Bauke Ylstra, Jonathan R. Chubb, and Wendy A. Bickmore. "Recruitment to the Nuclear Periphery Can Alter Expression of Genes in Human Cells." *PLoS Genetics* 4, no. 3 (2008): e1000039.

Gonzalez-Sandoval, Adriana, Benjamin D. Towbin, and Susan M. Gasser. "The Formation and Sequestration of Heterochromatin during Development: Delivered on 7 September 2012 at the 37th FEBS Congress in Sevilla, Spain." *The FEBS Journal* 280, no. 14 (2013): 3212–19.

Gonzalez-Sandoval, Adriana, Benjamin D. Towbin, Veronique Kalck, Daphne S. Cabianca, Dimos Gaidatzis, Michael H. Hauer, Liqing Geng, Li Wang, Teddy Yang, and Xinghao Wang, etc., *et al.,* Susan M. Gasser. "Perinuclear Anchoring of H3K9-Methylated Chromatin Stabilizes Induced Cell Fate in C. Elegans Embryos." *Cell* 163, no. 6 (2015): 1333–47.

Guelen, Lars, Ludo Pagie, Emilie Brasset, Wouter Meuleman, Marius B. Faza, Wendy Talhout, Bert H. Eussen, Annelies De Klein, Lodewyk Wessels, Wouter De Laat, and Bas van

Steensel. “Domain Organization of Human Chromosomes Revealed by Mapping of Nuclear Lamina Interactions.” *Nature* 453, no. 7197 (2008): 948–51.

Harr, Jennifer C., Teresa Romeo Luperchio, Xianrong Wong, Erez Cohen, Sarah J. Wheelan, and Karen L. Reddy. “Directed Targeting of Chromatin to the Nuclear Lamina Is Mediated by Chromatin State and A-Type Lamins.” *Journal of Cell Biology* 208, no. 1 (2015): 33–52.

Helbling-Leclerc, Anne, Gisèle Bonne, and Ketty Schwartz. “Emery-Dreifuss Muscular Dystrophy.” *European Journal of Human Genetics* 10, no. 3 (2002): 157–61.

Hodgkin, Jonathan. “More Sex-Determination Mutants of Caenorhabditis Elegans.” *Genetics* 96, no. 3 (1980): 649–64.

Ikegami, Kohta, Thea A. Egelhofer, Susan Strome, and Jason D. Lieb. “Caenorhabditis Elegans Chromosome Arms Are Anchored to the Nuclear Membrane via Discontinuous Association with LEM-2.” *Genome Biology* 11, no. 12 (2010): 1–20.

Iwasaki, Osamu, Christopher J. Corcoran, and Ken-ichi Noma. “Involvement of Condensin-Directed Gene Associations in the Organization and Regulation of Chromosome Territories during the Cell Cycle.” *Nucleic Acids Research* 44, no. 8 (2016): 3618–28.

Jack, Antonia PM, Silva Bussemer, Matthias Hahn, Sebastian Pünzeler, Martha Snyder, Michael Wells, Gyorgyi Csankovszki, Irina Solovei, Gunnar Schotta, and Sandra B. Hake. “H3K56me3 Is a Novel, Conserved Heterochromatic Mark That Largely but Not Completely Overlaps with H3K9me3 in Both Regulation and Localization.” *PloS One* 8, no. 2 (2013): e51765.

Jans, Judith, John M. Gladden, Edward J. Ralston, Catherine S. Pickle, Agnès H. Michel, Rebecca R. Pferdehirt, Michael B. Eisen, and Barbara J. Meyer. “A Condensin-like Dosage

Compensation Complex Acts at a Distance to Control Expression throughout the Genome." *Genes & Development* 23, no. 5 (2009): 602–18.

Kind, Jop, Ludo Pagie, Havva Ortabozkoyun, Shelagh Boyle, Sandra S. De Vries, Hans Janssen, Mario Amendola, Leisha D. Nolen, Wendy A. Bickmore, and Bas van Steensel. "Single-Cell Dynamics of Genome-Nuclear Lamina Interactions." *Cell* 153, no. 1 (2013): 178–92.

Kind, Jop, and Bas van Steensel. "Genome–Nuclear Lamina Interactions and Gene Regulation." *Current Opinion in Cell Biology* 22, no. 3 (2010): 320–25.

Kramer, Maxwell, Anna-Lena Kranz, Amanda Su, Lara H. Winterkorn, Sarah Elizabeth Albritton, and Sevinc Ercan. "Correction: Developmental Dynamics of X-Chromosome Dosage Compensation by the DCC and H4K20me1 in C. Elegans." *PLoS Genetics* 12, no. 2 (2016): e1005899.

Kranz, Anna-Lena, Chen-Yu Jiao, Lara Heermans Winterkorn, Sarah Elizabeth Albritton, Maxwell Kramer, and Sevinç Ercan. "Genome-Wide Analysis of Condensin Binding in Caenorhabditis Elegans." *Genome Biology* 14, no. 10 (2013): 1–15.

Kruesi, William S., Leighton J. Core, Colin T. Waters, John T. Lis, and Barbara J. Meyer. "Condensin Controls Recruitment of RNA Polymerase II to Achieve Nematode X-Chromosome Dosage Compensation." *Elife* 2 (2013): e00808.

Kumaran, R. Ileng, and David L. Spector. "A Genetic Locus Targeted to the Nuclear Periphery in Living Cells Maintains Its Transcriptional Competence." *The Journal of Cell Biology* 180, no. 1 (2008): 51–65.

Lau, Alyssa C., and Györgyi Csankovszki. "Balancing up and Downregulation of the C. Elegans X Chromosomes." *Current Opinion in Genetics & Development* 31 (2015): 50–56.

Lau, Alyssa C., and Györgyi Csankovszki. “Condensin-Mediated Chromosome Organization and Gene Regulation.” *Frontiers in Genetics* 5 (2015): 473.

Lau, Alyssa C., Kentaro Nabeshima, and Györgyi Csankovszki. “The C. Elegans Dosage Compensation Complex Mediates Interphase X Chromosome Compaction.” *Epigenetics & Chromatin* 7, no. 1 (2014): 1–16.

Liu, Jun, Tom Rolef Ben-Shahar, Dieter Riemer, Millet Treinin, Perah Spann, Klaus Weber, Andrew Fire, and Yosef Gruenbaum. “Essential Roles for Caenorhabditis Elegans Lamin Gene in Nuclear Organization, Cell Cycle Progression, and Spatial Organization of Nuclear Pore Complexes.” *Molecular Biology of the Cell* 11, no. 11 (2000): 3937–47.

Liu, Tao, Andreas Rechtsteiner, Thea A. Egelhofer, Anne Vielle, Isabel Latorre, Ming-Sin Cheung, Sevinc Ercan, Kohta Ikegami, Morten Jensen, and Paulina Kolasinska-Zwierz, etc., *et al.,* X Shirley Liu. “Broad Chromosomal Domains of Histone Modification Patterns in C. Elegans.” *Genome Research* 21, no. 2 (2011): 227–36.

Mattout, Anna, Brietta L. Pike, Benjamin D. Towbin, Erin M. Bank, Adriana Gonzalez-Sandoval, Michael B. Stadler, Peter Meister, Yosef Gruenbaum, and Susan M. Gasser. “An EDMD Mutation in C. Elegans Lamin Blocks Muscle-Specific Gene Relocation and Compromises Muscle Integrity.” *Current Biology* 21, no. 19 (2011): 1603–14.

McDonel, Patrick, Judith Jans, Brant K. Peterson, and Barbara J. Meyer. “Clustered DNA Motifs Mark X Chromosomes for Repression by a Dosage Compensation Complex.” *Nature* 444, no. 7119 (2006): 614–18.

Meister, Peter, and Angela Taddei. “Building Silent Compartments at the Nuclear Periphery: A Recurrent Theme.” *Current Opinion in Genetics & Development* 23, no. 2 (2013): 96–103.

Meister, Peter, Benjamin D. Towbin, Brietta L. Pike, Aaron Ponti, and Susan M. Gasser. “The Spatial Dynamics of Tissue-Specific Promoters during C. Elegans Development.” *Genes & Development* 24, no. 8 (2010): 766–82.

Mets, David G., and Barbara J. Meyer. “Condensins Regulate Meiotic DNA Break Distribution, Thus Crossover Frequency, by Controlling Chromosome Structure.” *Cell* 139, no. 1 (2009): 73–86.

Nabeshima, Kentaro, Susanna Mlynarczyk-Evans, and Anne M. Villeneuve. “Chromosome Painting Reveals Asynaptic Full Alignment of Homologs and HIM-8–Dependent Remodeling of X Chromosome Territories during Caenorhabditis Elegans Meiosis.” *PLoS Genetics* 7, no. 8 (2011): e1002231.

Peric-Hupkes, Daan, Wouter Meuleman, Ludo Pagie, Sophia WM Bruggeman, Irina Solovei, Wim Brugman, Stefan Gräf, Paul Flicek, Ron M. Kerkhoven, Maarten van Lohuizen, Marcel Reinders, Lodewyk Wessels, and Bas van Steensel. “Molecular Maps of the Reorganization of Genome-Nuclear Lamina Interactions during Differentiation.” *Molecular Cell* 38, no. 4 (2010): 603–13.

Petty, Emily L., Karishma S. Collette, Alysse J. Cohen, Martha J. Snyder, and Györgyi Csankovszki. “Restricting Dosage Compensation Complex Binding to the X Chromosomes by H2A. Z/HTZ-1.” *PLoS Genetics* 5, no. 10 (2009): e1000699.

Pickersgill, Helen, Bernike Kalverda, Elzo De Wit, Wendy Talhout, Maarten Fornerod, and Bas van Steensel. “Characterization of the Drosophila Melanogaster Genome at the Nuclear Lamina.” *Nature Genetics* 38, no. 9 (2006): 1005–14.

Reddy, K. L., J. M. Zullo, E. Bertolino, and H. Singh. “Transcriptional Repression Mediated by Repositioning of Genes to the Nuclear Lamina.” *Nature* 452, no. 7184 (2008): 243–47.

Schott, Sonia, Vincent Coustham, Thomas Simonet, Cecile Bedet, and Francesca Palladino. "Unique and Redundant Functions of C. Elegans HP1 Proteins in Post-Embryonic Development." *Developmental Biology* 298, no. 1 (2006): 176–87.

Sharma, Rahul, Daniel Jost, Jop Kind, Georgina Gómez-Saldivar, Bas van Steensel, Peter Askjaer, Cédric Vaillant, and Peter Meister. "Differential Spatial and Structural Organization of the X Chromosome Underlies Dosage Compensation in C. Elegans." *Genes & Development* 28, no. 23 (2014): 2591–96.

Solovei, Irina, Audrey S. Wang, Katharina Thanisch, Christine S. Schmidt, Stefan Krebs, Monika Zwerger, Tatiana V. Cohen, Didier Devys, Roland Foisner, and Leo Peichl, etc., *et al.,* Boris Joffe. "LBR and Lamin A/C Sequentially Tether Peripheral Heterochromatin and Inversely Regulate Differentiation." *Cell* 152, no. 3 (2013): 584–98.

Strome, Susan, William G. Kelly, Sevinc Ercan, and Jason D. Lieb. "Regulation of the X Chromosomes in Caenorhabditis Elegans." *Cold Spring Harbor Perspectives in Biology* 6, no. 3 (2014): a018366.

Talamas, Jessica A., and Maya Capelson. "Nuclear Envelope and Genome Interactions in Cell Fate." *Frontiers in Genetics* 6 (2015): 95.

Therizols, Pierre, Robert S. Illingworth, Celine Courilleau, Shelagh Boyle, Andrew J. Wood, and Wendy A. Bickmore. "Chromatin Decondensation Is Sufficient to Alter Nuclear Organization in Embryonic Stem Cells." *Science* 346, no. 6214 (2014): 1238–42.

Towbin, Benjamin D., Cristina González-Aguilera, Ragna Sack, Dimos Gaidatzis, Véronique Kalck, Peter Meister, Peter Askjaer, and Susan M. Gasser. "Step-Wise Methylation of Histone H3K9 Positions Heterochromatin at the Nuclear Periphery." *Cell* 150, no. 5 (2012): 934–47.

Towbin, Benjamin D., Adriana Gonzalez-Sandoval, and Susan M. Gasser. “Mechanisms of Heterochromatin Subnuclear Localization.” *Trends in Biochemical Sciences* 38, no. 7 (2013): 356–63.

Towbin, Benjamin Daniel, P. Meister, B. L. Pike, and S. M. Gasser. “Repetitive Transgenes in C. Elegans Accumulate Heterochromatic Marks and Are Sequestered at the Nuclear Envelope in a Copy-Number-and Lamin-Dependent Manner.” In *Cold Spring Harbor Symposia on Quantitative Biology*, sqb. 2010.75. 041. Cold Spring Harbor Laboratory Press, 2011.

Van Bortle, Kevin, and Victor G. Corces. “Nuclear Organization and Genome Function.” *Annual Review of Cell and Developmental Biology* 28 (2012): 163–87.

Vielle, Anne, Jackie Lang, Yan Dong, Sevinc Ercan, Chitra Kotwaliwale, Andreas Rechtsteiner, Alex Appert, Q. Brent Chen, Andrea Dose, and Thea Egelhofer, etc., *et al.,* Julie Ahringer. “H4K20me1 Contributes to Downregulation of X-Linked Genes for C. Elegans Dosage Compensation,” 2012.

Wells, Michael B., Martha J. Snyder, Laura M. Custer, and Gyorgyi Csankovszki. “Caenorhabditis Elegans Dosage Compensation Regulates Histone H4 Chromatin State on X Chromosomes.” *Molecular and Cellular Biology* 32, no. 9 (2012): 1710–19.

Zuleger, Nikolaj, Shelagh Boyle, David A. Kelly, Jose I. de Las Heras, Vassiliki Lazou, Nadia Korfali, Dzmitry G. Batrakou, K. Natalie Randles, Glenn E. Morris, and David J. Harrison, Wendy A. Bickmore, and Eric C. Schirmer. “Specific Nuclear Envelope Transmembrane Proteins Can Promote the Location of Chromosomes to and from the Nuclear Periphery.” *Genome Biology* 14, no. 2 (2013): 1–20.

CHAPTER 3

Dual Roles of Nuclear RNAi in *C. elegans* Dosage Compensation

This chapter was submitted to the journal *Genetics* on 7/29/21 as Davis MB, *et al.,* (2021) "Dual Roles for Nuclear RNAi in *C. elegans* Dosage Compensation" I conducted all the FISH experiments, mating experiments, and hermaphrodite viability assays. The qPCR experiment and figure 3.3 was conducted by Eshna Jash and the Immunofluorescence experiment and figure 3.7 was conducted by Bahaar Chawla. Figure 3.1 was conducted by Lilian Tushman. The rest of the paper is my work.

ABSTRACT

Dosage compensation involves chromosome-wide gene regulatory mechanisms which impact higher order chromatin structure and are crucial for organismal health. Using a genetic approach, we identified Argonaute genes which promote dosage compensation in *C. elegans.* Dosage compensation in *C. elegans* hermaphrodites is initiated by the silencing of *xol-1* and subsequent activation of the Dosage Compensation Complex (DCC) which binds to both hermaphrodite X chromosomes and reduces transcriptional output by twofold. A hallmark phenotype of dosage compensation mutants is decondensation of the X chromosomes. We characterized this phenotype in Argonaute mutants using X chromosome paint probes and fluorescence microscopy. We found that while nuclear Argonaute mutants *hrde-1* and *nrde-3* exhibit de-repression of *xol-1* transcripts, they also affect X chromosome condensation in a *xol-1*-independent manner. We also characterized the physiological contribution of Argonaute genes

to dosage compensation using genetic assays and find that *hrde-1* and *nrde-3*, together with the piRNA Argonaute *prg-1,* contribute to healthy dosage compensation both upstream and downstream of *xol-1*.

INTRODUCTION

The evolution of sexual dimorphism facilitated the emergence of sex chromosomes in metazoans (Ohno, 1967; Rice, 1984). While the autosomal source of the ancestral sex chromosomes can be divergent between species, a defining factor of sex chromosomes is a difference in the genetic content between the sexes. However, sex chromosomes also bring about the problem of one sex containing half of the gene dose from that chromosome (Ohno, 1967). The problem of haploinsufficiency is evidenced by numerous documented cases of lethality in monosomic conditions (Torres *et al.,* 2008). However, the difference in gene dose associated with sex chromosomes is alleviated by the evolution of dosage compensation (Ohno, 1967). In various organisms, the enormous undertaking of dosage compensation features the regulation of an entire chromosome such that a viable balance of sex chromosome gene expression between the sexes is met. In *C. elegans,* dosage compensation is achieved by a ten-protein complex named the Dosage Compensation Complex (DCC) (For a review, see Lau and Csankovszki, 2015 and Albritton and Ercan, 2018). The DCC is comprised of a pentameric condensin complex, an H4K20me2/3 demethylase (*dpy-21)* and several proteins which confer X chromosome binding specificity (Chuang *et al.,* 1994; Csankovszki *et al.,* 2009; Pferdehirt *et al.,* 2011; Brejc *et al.,* 2017). The DCC downregulates the transcriptional output of both hermaphrodite X chromosomes in interphase cells by two-fold (Kruesi *et al.,* 2013). This system affords a niche opportunity to study the regulatory and functional capacity of condensin in the context of gene regulation.

Indeed, many insights into this unique condensin within the context of the DCC have been discovered. The DCC compacts the X chromosomes, restricting their volume within the

nucleus, and facilitates the formation of TADs (topologically associating domains) spaced in ~1Mb intervals along the 17Mb X chromosome (Lau *et al.,* 2014, Crane *et al.,* 2017). The complex is also required for X enrichment of the repressive H4K20me1 mark and loss of the activating H4K16ac mark in interphase (Vielle *et al.,* 2012; Wells *et al.,* 2012; Brejc *et al.,* 2017). Loss of function mutations for the zygotically expressed DCC gene *sdc-2* result in a complete failure for the DCC to load, severe lethality and de-repression of X-linked genes (Dawes *et al.,* 1999). While mutations in the H4K20 histone methyltransferase and demethylase genes lead to significant X chromosome gene de-repression, it is not to the same level as in a loss of DCC function mutation (Kramer *et al.,* 2015; Brejc *et al.,* 2017). An additional pathway facilitates dosage compensation by anchoring the H3K9me2/3 heterochromatin regions of the X chromosome to the nuclear periphery via the nuclear lamina-localized chromo-domain protein CEC-4. Mutants for *cec-4* as well as double mutants for the H3K9me2/3 methyltransferases *met-2 set-25* exhibit modest but significant X-linked gene de-repression (Snyder *et al.,* 2016).

RNAi pathways are a distinct mechanism of controlling gene expression utilizing small interfering RNAs (siRNAs) complexed with Argonaute (AGO) proteins. This RNAi machinery targets mRNAs in the cytoplasm for post-transcriptional silencing or nascent transcripts in the nucleus for co-transcriptional silencing at a gene locus (For a review see Almeida *et al.,* 2019). The AGO family proteins are widely conserved and vary in number across metazoans (Höck and Meister, 2008). As the human genome encodes 8 AGO genes, *Drosophila* have 5, and a fission yeast harbor just one, the striking expansion to 27 AGO genes in *C. elegans* begs the question of their role in gene regulation and relevance to physiology.

The exogenous RNAi pathway in *C. elegans* functions in the silencing of invading viral sequences through the detection of foreign dsRNA, while the endogenous RNAi pathway

silences endogenous mRNA transcripts. The piRNA pathway has a conserved role in promoting germline fertility and silencing transposable elements. However the high mismatch pairing capacity for piRNAs and their sheer abundance suggest the piRNA pathway function in *C. elegans* is not fully understood (Lee *et al.,* 2012; Pharad and Theurkauf, 2019). All three branches of the RNAi pathways in *C. elegans* involve several distinct short RNA pools (Ruby *et al,* 2006; Pak and Fire 2007). In the endogenous RNAi silencing pathway, mRNA transcripts for target genes serve as templates for the RNA-dependent RNA Polymerase RRF-3 to generate dsRNA. DICER homolog DCR-1 cleaves this dsRNA into Primary siRNAs which are 26 nucleotides in length with a 5' bias for guanosine monophosphate (26Gs) (Gent *et al.,* 2009; Han *et al.,* 2009). The primary siRNAs complex with either the ERGO-1(soma and oogenic germline) or ALG-3/4 (spermatogenic gonad) AGOs to target additional mRNA transcripts for the same target gene, upon which many secondary siRNAs are produced (Han *et al.,* 2009; Conine *et al.,* 2010; Vasale *et al.,* 2010). The exogenous RNAi pathway utilizes some of the same machinery, such as DCR-1, which cleaves viral dsRNAs to produce exogenous 26G primary siRNAs. However, exogenously derived primary siRNAs are bound to a distinct AGO called RDE-1, which functions solely in the exogenous RNAi pathway. The primary AGO of the piRNA pathway in *C. elegans* is PRG-1 (Batista *et al.,* 2008; Das *et al.,* 2008). Genomically encoded RNA pol II-transcribed piRNAs are complexed with PRG-1 and target transcripts which are subsequently utilized to generate secondary siRNAs. The exogenous, endogenous and piRNA pathways converge at the synthesis of their respective secondary siRNAs, which complex with a subset of worm-specific Argonautes (WAGOs) to effect post-transcriptional silencing in the cytoplasm, and/or recruit the *nrde* complex to target loci in the nucleus in instances of co-

transcriptional silencing (Gent *et al.,* 2010). Secondary siRNAs are 22 nucleotides in length with a 5' bias for guanosine monophosphate (22Gs) (Ruby *et al,* 2006; Pak and Fire 2007).

The RNAi machinery responsible for co-transcriptional silencing in the nucleus is also required for the accumulation of H3K9me3 and H3K27me3 heterochromatin marks at target loci (Guang *et al.,* 2010; Burkhart *et al.,* 2011; Mao *et al.,* 2015). The corresponding nuclear WAGO genes are *nrde-3* and *hrde-1,* which silence target genes in somatic cells and the germline respectively (Guang *et al.,* 2008; Buckley *et al.,* 2012). The NRDE-3 and HRDE-1 proteins lack the catalytic triad responsible for cleaving mRNAs that is typical of AGO proteins (Yigit *et al.,* 2006). However, both proteins contain an NLS sequence which localizes the WAGO to the nucleus in an siRNA-dependent manner (Guang *et al.,* 2008; Buckley *et al.,* 2012). Mutants for *hrde-1* and *prg-1* show progressive transgenerational sterility at 20 and 25 degrees and are thus designated with the mortal germ line (Mrt) phenotype (Buckley *et al.,* 2012, Simon *et al.,* 2014). Mutants for *prg-1* however, do not exhibit widespread transposable element de-repression. Rather, the transgenerational sterility is likely due to mis-regulation of the downstream WAGOs, which inappropriately re-allocate their silencing capacity to histone mRNAs (Reed *et al.,* 2020).

Here we show that the AGOs *prg-1, hrde-1* and *nrde-3* perform dual roles in *C. elegans* dosage compensation*,* both in the repression of *xol-1* in hermaphrodites as well as a *xol-1*-independent role. Our FISH experiments indicate that *nrde*-3, *hrde-1,* and *prg-1* mutants exhibit an X chromosome decondensation phenotype and our XO rescue experiments indicate that these genes contribute physiologically to dosage compensation. We demonstrate that while both the AGO-mediated XO rescue and X chromosome compaction are *xol-1*-independent, the effects of these mutations on hermaphrodite viability are largely *xol-1*-dependent. We present a model whereby *nrde-3* and *hrde-1* facilitate the transcriptional repression of *xol-1* possibly as the

effectors of *prg-1*-21UX1 piRNA pathway, and downstream of *xol-1* these nuclear AGOs promote the compaction of X chromosomes in a separate but physiologically relevant role.

MATERIALS AND METHODS

C. elegans strains and maintenance

Strains were grown under standard conditions as described (Brenner, 1974). Worm strains include: N2; SX922 *prg-1(n4357)* I*;* EKM 200 *prg-1(n4357)* I *lon-2(e678) xol-1(y70)* X; WM157 *wago-11(tm1127)* II; YY470 *dcr-1(mg375)* III; EKM 89 *hrde-1(tm1200)* III*;* EKM 101 *him-8(e1489)* III *mIs11* IV; EKM 152 *hrde-1(tm1200)* III *lon-2(e678) xol-1(y70)* X; EKM 117 *hrde-1(tm1200)* III *mIs11* IV; EKM 177 *mIs11* IV *nrde-3(tm1116)* X; EKM 178 *nrde-3(tm1116) lon-2(e678) xol-1(y70)* X; EKM 176 *mIs11* IV *him-5(21490)* V *nrde-3(tm1116)* X; WM191 MAGO12 *sag-2(tm894) ppw-1(tm914) wago-2(tm2686) wago-1(tm1414)* I, *wago-11(tm1127) wago-5(tm1113) wago-4(tm1019)* II, *hrde-1(tm1200) sago-1(tm1195)* III, *wago-10(tm1186)* V, *nrde-3(tm1116)* X; CB1489 *him-8(e1489)*IV; TY4403 *him-8(e1489) xol-1(y9) sex-1(y263)*; WM158 *ergo-1(tm1860)* V; WM27 *rde-1(ne219)* V; WM156 *nrde-3(tm1116)* X; EKM 125 *lon-2(e678) xol-1(y70)* X. Worms were fed OP50. In all FISH experiments (Figure 3.1 and 3.4), Hermaphrodite viability (Figure 3.5) and XO rescue (Figure 3.6) experiments, worms for every genotype were grown at 15°C for all experiments. This measure was taken to control for temperature-sensitive effects in strains containing *hrde-1* and *prg-1* mutations.

Male rescue and hermaphrodite viability assays

RNAi-based male rescue assay: Worms with the genotype *him-8(e1489); xol-1(y9) sex-1(y263)* were fed *E. coli* strain HT115 expressing double stranded RNAi for each gene of interest. Bacteria were picked from a single colony and grown overnight for 8-10 hours at 37°C.

150ul of bacteria were seeded on NMG plates with IPTG (0.2%w/v) and Carbenicillin (1ug/ml) and worms were transferred to plates after one day. The male rescue assay in Figure 3.2 was conducted as outlined in (Petty *et al.,* 2009). *him-8(e1489) xol-1(y9) sex-1(y263)* L1 hatchlings were transferred to RNAi plates and allowed to grow until L4 before (2-3) worms were transferred to new RNAi plates. Worms were allowed to lay eggs for 24 hours at 20°C before parents (P0) were removed. Embryos were counted and the presence of males (in the F1) was scored after 2-4 days of growth at 20°C. As a hermaphrodite with the *him-8(e1489)* mutation produces a population of 38% males, the % of males rescued was calculated by dividing the number of males observed by the number of males expected (expected males = total eggs laid X 0.38) (Philips *et al.,* 2005). Statistical significance was evaluated using Chi square tests for each comparison of two conditions. The null hypothesis was that no significant difference in male rescue would be found between each condition measured. The expected 'viable male worms' was calculated by taking the summed % viable male worms between the two groups being tested and multiplying that proportion by the total male worm number for each corresponding condition.

XO rescue assay: For the XO rescue assays on Figure 3.6B, crosses were set up between *lon-2 xol-1* hermaphrodites with the appropriate additional mutation (*nrde-3* or *hrde-1*) and *mIs11* males with the appropriate additional mutation. F1 cross progeny were identified by the presence of the GFP transgene. XX cross progeny were *lon-2/+,* and therefore developed as non-Lon hermaphrodites. XO cross progeny were hemizygous for *lon-2*, and developed as Lon males or hermaphrodites. F1 progeny were scored for the presence of GFP+ males and/or GFP+ Lon hermaphrodites (XO cross-progeny), as well as the presence of GFP+ non-Lon hermaphrodites (XX cross-progeny). The % of XO rescued animals was calculated by dividing the number of

rescued XO animals (GFP+ males and GFP+ Lon hermaphrodites) observed by the number of XX (GFP+ non-Lon) hermaphrodites. This calculation assumes that equal numbers of XX and XO cross-progeny are produced from a mating of a male to a hermaphrodite.

For the XO rescue on empty vector (EV) or *sex-1(RNAi), lon-2 xol-1* mutants with the appropriate additional mutation (*nrde-3* or *hrde-1*) were moved to *sex-1(RNAi)* or (EV) plates as hatchlings. Simultaneously, *mIs11* worms with the appropriate additional mutation (*nrde-3* or *hrde-1*) were also moved to *sex-1(RNAi)* plates as hatchlings. After approximately two days of growth at 15°C, L4's were selected from both genotypes to initiate crosses on new *sex-1(RNAi)* or *EV* plates. F1 progeny were scored as above. Statistical significance was evaluated using Chi square tests for each comparison of two conditions. The null hypothesis was that no significant difference in XO rescue would be found between each condition measured. The expected 'viable XO worms' calculation was formulated by taking the summed % viable XO worms between the two groups being tested and multiplying that proportion by the total XO worm number for each corresponding condition.

Hermaphrodite viability assay: For the hermaphrodite viability assays, strains of the appropriate genotype were moved to *sex-1(RNAi)* or *EV* plates at the L1 stage. After two days of growth at 15°C L4's were picked and transferred to new RNAi plates and allowed to lay embryos for 24 hours before being transferred again to new plates. Following the removal of parents each day the number of embryos on each plate was counted and after two full days at 15°C viability was scored based on the (number of live worms) divided by the (number of eggs laid). Statistical significance was evaluated using Chi square tests for each comparison of two conditions. The null hypothesis was that no significant difference in hermaphrodite viability would be found between each condition measured. The expected 'alive' calculation was

formulated by taking the summed % viability between the two groups being tested and multiplying that proportion by the sample size (*n*) for each corresponding condition.

Fluorescence In Situ Hybridization (FISH)

FISH probe DNA templates were created through degenerate oligonucleotide-primed PCR reactions to amplify purified yeast artificial chromosome (YAC) DNA corresponding to either the X chromosome or chromosome I (Csankovszki *et al.,* 2004, Nabeshima *et al.,* 2011). dCTP-Cy3 (GE) was incorporated along with standards dNTPs for visualization purposes using random priming (Labeling 5X Buffer Promega). For the fixation, worms were dissected in 1X sperm salts (50 mM Pipes pH 7, 25 mM KCl, 1 mM MgSO4, 45 mM NaCl and 2 mM CaCl2) and fixed in 1.6% PFA on slides for 5 minutes at RT. Subsequently slides were frozen on dry ice to 20 minutes before a series of 3X 10 minute washes in PBST. Slides were then washed in an ethanol series: 70%, 80%, 95%, 100% for 2 minutes each. After allowing slides to dry for 5 minutes, 10ul of Cy-3-labelled probe was applied with a coverslip and heated to 95°C for 3 minutes. Slides were then incubated in a humidity chamber overnight at 37°C. The following day slides were washed in 2X SSC + 50% formamide (3X 5-minute washes); 2X SSC (3X 5 minute washes); 1X SSC (10 minutes); 4X SSC+DAPI (10 minutes). Slides were then mounted with Vectashield (Vector Labs).

Imaging and Quantification

Images were taken with a Hamamatsu ORCA-ER digital camera mounted on an Olympus BX61 epi-fluorescence microscope with a motorized Z drive. The 60X APO oil immersion objective was used for all images. Series of Z stack images were collected (stack size 0.2um) and all images shown are projection images summed from ~3 microns. Quantification was conducted

in the Slidebook 5 program (Intelligent Imaging Innovations). Using the mask function, segment masks were drawn individually for the DAPI signal and Cy3 signal for each nucleus. Within the statistics menu the mask statistics function as selected with DAPI as the primary mask and Cy3 as the secondary mask. The morphometrix (voxels) and crossmask (voxels) were selected for the analysis. These procedures generated a number for the overlap corresponding to the volume of the Cy3 and DAPI masks from which chromosome volume was calculated using Cy3 volume/DAPI volume. The average volume of Cy3/DAPI for all worms of a given genotype was calculated and an unpaired (2-sample) Student's T-test was performed to compare the means of each genotype to the appropriate control. At least 20 nuclei per condition were quantified and identical probe batches were used for each experiment with a wild type (N2) control.

qRT-PCR

Synchronous culture of gravid adult worms was grown at 25°C to induce temperature-dependent gene expression changes in the temperature sensitive mutants. Worms were then bleached to obtain embryos. Embryos were lysed using a bead beater with 0.1mm zirconia/silica beads (BioSpec Products cat. no. 11079101z). TRIzol-chloroform (Invitrogen, Fisher Scientific) separation of the samples was followed by RNA extraction using the QIAGEN RNeasy Mini Kit with on-column DNase I digestion. cDNA was generated from extracted RNA using random hexamers with SuperScript III Reverse Transcriptase (Invitrogen). RT-qPCR reaction mix was prepared using Power SYBR Green Master Mix (Applied Biosystems) with 10µl SYBR master mix, 0.8µl of 10µM primer mix, 2µl sample cDNA, and 7.2µl H_2O. Samples were run on the Bio-Rad CFX Connect Real-Time System. Log2 fold change was calculated relative to control (*cdc-42*). Control primers were taken from Hoogewijs *et al.,* (2008). Statistical significance was calculated using two-tailed unpaired Student's t-test. Error bars represent standard deviation.

Primer sequences: *xol-1* forward GGTCCCACCAGAAATGCAG, *xol-1* reverse – CTGTTTCCATGTAAGTTAAGACTGG, *cdc-42* forward – ctgctggacaggaagattacg, *cdc-42* reverse – ctcggacattctcgaatgaag.

Immunofluorescence

Immunofluorescence experiments were performed as described (Csankovszki *et al.,* 2009). One day post-L4 worms were dissected in 1X sperm salts (50 mM Pipes pH 7, 25 mM KCl, 1 mM MgSO4, 45 mM NaCl and 2 mM CaCl2) and fixed in 2% paraformaldehyde in 1X sperm salts for 5 minutes with a coverslip. Slides were frozen on dry ice for at least 15 minutes. Coverslips were removed and slides were washed in PBS with 0.1% Triton X-100 (PBST) (3X 10 minutes each) and subsequently incubated with primary rabbit anti-H3K9me3 (Active Motif #39765) antibodies (at 1:500 dilution) with a square parafilm. Slides were then moved to a humidity chamber overnight at room temperature. Slides were then washed in PBST (3X 10 minutes each) and secondary donkey anti-rabbit-FITC (Jackson Immunoresearch) antibody at 1:100 dilution was added with a square parafilm slip. Slides were incubated for 2 hours at 37°C before another series of washes in PBST (3X 10 minutes each). The final PBST wash included DAPI. Slides were mounted with Vectashield (Vector Labs). Significance for H3Kme3 signal pattern differences between genotypes was calculated by Chi square tests conducted between two conditions for each comparison under the null hypothesis of no significant difference in H3K9me3 pattern between genotypes.

RESULTS

X chromosome decondensation in RNAi mutants

A hallmark phenotype of mutants for DCC genes and additional genes influencing dosage compensation is a decondensed X chromosome territory (Lau *et al.,* 2014; Snyder *et al.,* 2016; Brejc *et al.,* 2017). We previously found that heterochromatin proteins, including the H3K9 methyltransferases MET-2 and SET-25, and the chromodomain-containing protein CEC-4 that bind H3K9me, promote dosage compensation and X chromosome compaction (Snyder *et al.,* 2016). Since nuclear RNAi can lead to deposition of H3K9me3 and heterochromatin formation, we wondered whether nuclear RNAi genes would have similar effects. In a previous study, we reported that in nuclear RNAi mutants *morc-1* and *hrde-1* the X chromosomes were decondensed (Weiser *et al.,* 2017). To determine which RNAi pathways influence X chromosome compaction, we conducted X chromosome paint fluorescence in situ hybridization (FISH) experiments with loss of function mutants for various genes in the *C. elegans* RNAi pathways (Figure 3.1A). Our analysis included mutants for genes eliminating function specifically in each branch of the RNAi pathways (exogenous, endogenous and piRNA) as well as mutants for downstream AGO genes which are shared by multiple pathways. The exogenous RNAi pathway was represented by *rde-1(ne219)*, a mutation for the primary AGO which disrupts silencing in the pathway (Tabara *et al.,* 1999). Endogenous RNAi pathway mutations included: a mutation in DICER homolog *dcr-1(mg375),* a helicase domain mutant impairing the production of primary 26G siRNAs specifically in the endogenous RNAi pathway, as well as *ergo-1(tm1860)*, a null mutant for the primary AGO of the endogenous RNAi pathway which eliminates 26G primary siRNAs (Bernstein *et al.,* 2001; Yigit *et al.,* 2006; Pavelec *et al.,* 2009; Welker *et al.,* 2010). The piRNA pathway mutation included *prg-1(n4357)*, a null mutant for the primary AGO of the pathway

(Batista *et al,* 2008; Das *et al,* 2008). Downstream AGO mutations included *hrde-1(tm1200), nrde-3(tm1116)* and *wago-11(tm1127)*, which represent null mutants for three of the four nuclear AGO encoding genes, as well as the MAGO-12 (Multiple AGO) mutant bearing loss of function mutations in all 12 of the WAGO genes (*C. elegans* deletion consortium *et al.,* 2002; Guang *et al,* 2008; Buckley *et al,* 2012; Gu *et al.,* 2009).

In intestinal cells of wild type hermaphrodites with intact dosage compensation, the X chromosomes occupied about 10% of the nuclear volume on average, consistent with previous studies (Figure 3.1B) (Lau *et al.,* 2014; Snyder *et al.,* 2016; Brejc *et al.,* 2017). The *hrde-1, nrde-3, prg-1,* and MAGO-12 mutants displayed significantly decondensed X chromosome volumes, occupying about 15-16% of nuclear volume, and in the range of what was previously reported for heterochromatin mutants (Figure 3.1B) (Snyder *et al.,* 2016). The X chromosome decondensation phenotype was absent from the *rde-1, dcr-1,* and *ergo-1* mutants, which suggests the effect is not mediated through the exogenous or the endogenous RNAi pathway. The less-characterized nuclear AGO mutant *wago-11* was also not significantly different from wild type. While the *hrde-1, nrde-3, prg-1,* and MAGO-12 mutants exhibit significantly increased X chromosome volume compared to wild type animals, they were not significantly different in X chromosome volume from each other (Figure 3.1B). Moreover, the MAGO-12 mutant exhibited the same degree of X chromosome decondensation as the single AGO mutants. Based on these results, we hypothesize that the contribution from these mutants to X chromosome compaction is likely a common pathway involving a subset of the RNAi machinery.

To identify whether the X chromosome decondensation observed in the nuclear RNAi AGO mutants was specific to the X chromosome, we also conducted FISH experiments with whole chromosome I paints in each mutant (Figure 3.1C). Each of the RNAi mutants displayed

chromosome I volumes similar to wild type (Figure 3.1D). Chromosome I occupied about 15% of the nuclear volume in wild type N2, and the volume in mutants ranged from 13.4% in *nrde-3* to about 16% in *dcr-1* (Figure 3.1D). The variation observed in each mutant was not significantly different from wild type worms, highlighting that the X chromosome volume decondensation phenotype is not a genome-wide feature of the nuclear RNAi AGO mutants.

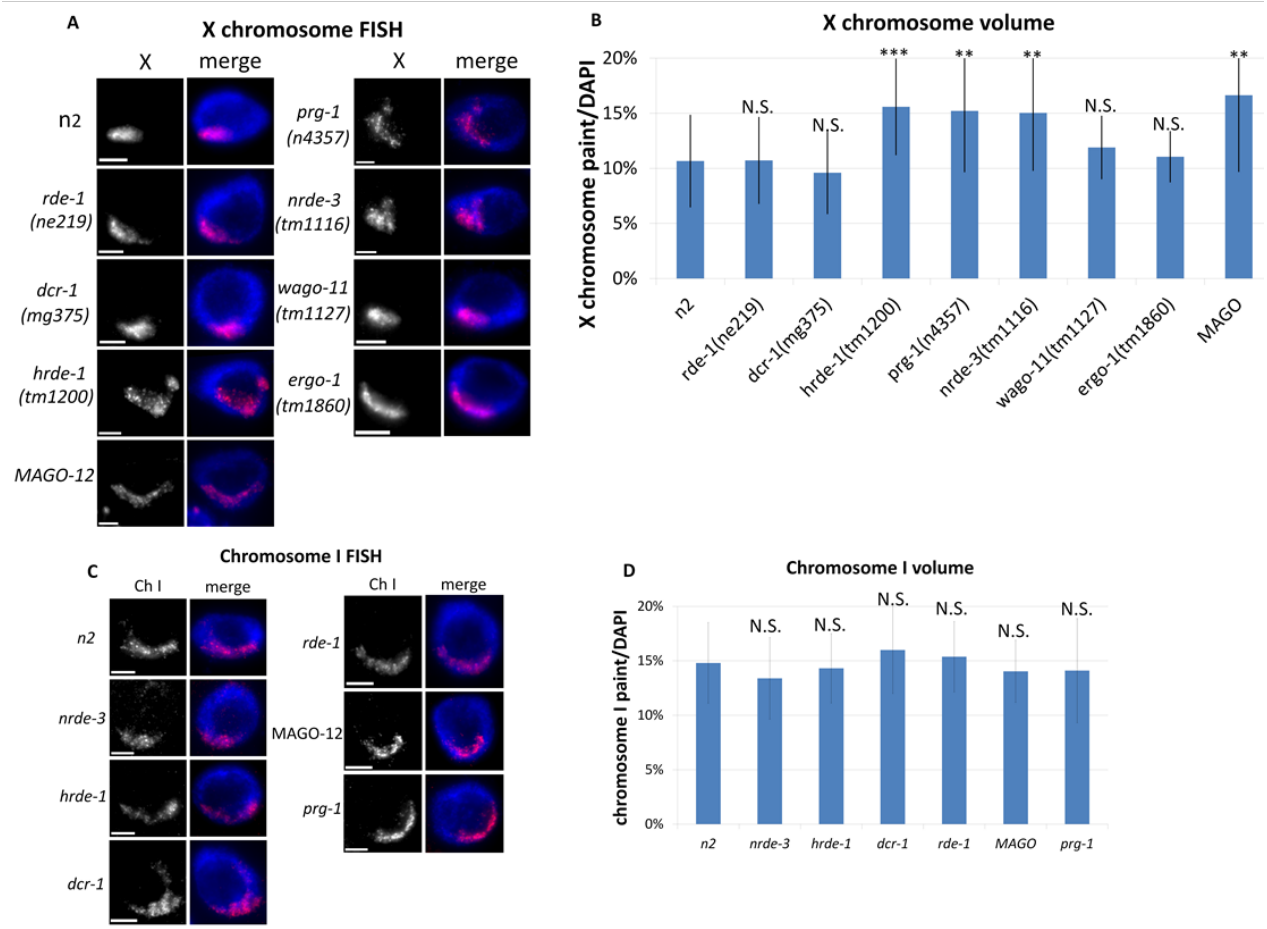

Figure 3.1. X chromosome is de-condensed in nuclear RNAi Argonaute mutants. (A) FISH X chromosome paint (red) with nuclear (DAPI) staining is shown in adult hermaphrodite intestinal cells. The X paint signal region is larger in *nrde-3, hrde-1, prg-1,* and *MAGO-12* mutants. (B) Quantification for X chromosome volume: (X chromosome paint voxels/DAPI voxels). (C) FISH chromosome I paint (red) with nuclear (DAPI) staining is shown. The Ch I paint signal region in wild type (N2) and each mutant with an X chromosome phenotype is similar for this autosome control. (D) Quantification for chromosome I volume: (chromosome I paint voxels/DAPI voxels). Significance for B and D is based on a Student's T Test: **=p<0.01, ***= p<0.001 (N2 compared to each mutant). Error bars represent SD.

Depletion of nuclear RNAi AGOs rescues *xol-1* mutant males

To further define the individual contribution of AGO mutations to dosage compensation we conducted male rescue experiments. The assay is based on the principle that dosage compensation ectopically activated in XO males is lethal (Miller *et al.,* 1988, Petty *et al.,* 2012). Mutation in the *xol-1* master switch gene bypasses the innate chromosome counting mechanism in *C. elegans,* effectively activating dosage compensation in a sex-independent manner (Rhind *et al.,* 1995). *xol-1* mutant males are 100% lethal due to the inappropriate activation of dosage compensation. However, *xol-1* mutant males can be partially rescued by the inactivation of genes required for dosage compensation (see methods for details). We previously reported that depletion nuclear RNAi genes *morc-1* and *hrde-1* led to small, but significant rescue of *xol-1* males (Weiser *et al.,* 2017). Here we report that in addition to *hrde-1,* RNAi of *prg-1* and *nrde-3* also rescued males with ectopic dosage compensation (Figure 3.2A-B). On empty vector only about 1% of males are rescued, while a positive control knockdown of DCC component *dpy-27* yielded a rescue of 52% of males. *prg-1(RNAi)* rescued 17.5% of males, *hrde-1(RNAi)* rescued 18.8% of males, and *nrde-3(RNAi)* rescued 6.1% of males (Figure 3.2A and B). Thus, the nuclear RNAi AGOs and the piRNA AGO *prg-1* promote X chromosome dosage compensation.

A **Nuclear Argonaute Male Rescue**

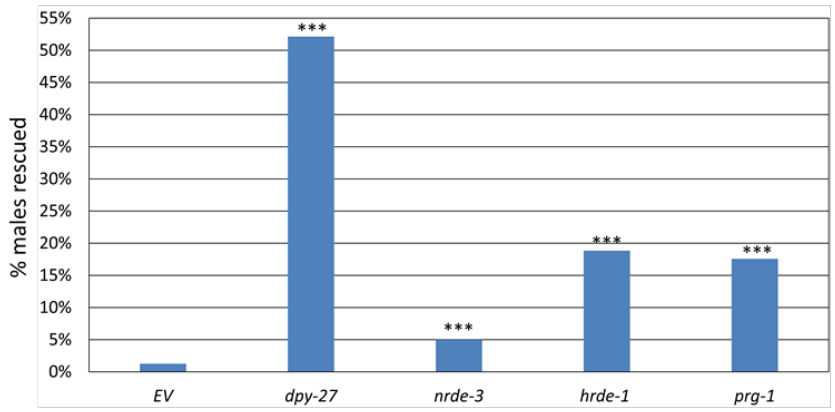

B **Nuclear Argonaute Male Rescue Chi Square Raw Data and Significance**

			OBSERVED		EXPECTED			
Condition	n	total XO worms	viable XO worms	dead XO worms	viable XO worms	dead XO worms	significance	*P* values per comparrison
EV	3130	1189	15	1174	286	904	***	0.0000000
dpy-27	2539	965	503	462	232	733		
EV	3130	1189	15	1174	35	1155	***	0.0000004
nrde-3	2475	941	47	894	27	913		
EV	3130	1189	15	1174	41	1148	***	0.0000000
hrde-1	447	170	32	138	6	164		
EV	3130	1189	15	1174	45	1145	***	0.0000000
prg-1	569	216	38	178	8	208		

Figure 3.2. RNAi screen implicates nuclear Argonautes in dosage compensation. (A) RNAi knockdown for various genes in a *him-8; xol-1 sex-1* background. Percent of rescued males is indicated. DCC component gene *dpy-27* rescues a large % of males and the other genes shown rescue a smaller but reproducible number of males. Significance is based on Chi square analysis: *= p<0.05, **=p<0.01, ***= p<0.001. (B) Raw data from the Chi Square analysis.

xol-1 is de-repressed in *hrde-1* and *nrde-3* mutants

An earlier study from Tang *et al.,* (2018) reported a role for *prg-1* in repression of *xol-1.* The study identified a piRNA *21-ux1* which, when complexed with *prg-1*, is partially responsible for repressing *xol-1* in hermaphrodites to permit dosage compensation to turn on. They showed that both *xol-1* transcripts and protein levels are de-repressed in hermaphrodites mutant for *prg-1* as well as mutants with the *21-ux1* piRNA deleted. We conducted RT-qPCR on *hrde-1* and *nrde-3* and *prg-1* mutants to determine whether *xol-1* was similarly de-repressed in the nuclear RNAi AGO mutants (Figure 3.3). *hrde-1* and *nrde-3* mutants both exhibited significant *xol-1* de-repression (Figure 3.3). The level of derepression in *nrde-3* mutants was similar to *prg-1* mutants, and somewhat less in *hrde-1* mutants. As the canonical piRNA pathway involves nuclear RNAi AGO-mediated silencing, this result suggests that repression of *xol-1* by piRNAs may be reinforced by nuclear RNAi (Ashe *et al.,* 2012; Bagijn *et al.,* 2012; Lee *et al.,* 2012; Shirayama *et al.,* 2012). Thus *nrde-3, hrde-1,* and *prg-1* contribute to dosage compensation upstream of *xol-1* through its repression. Intriguingly, however, our male rescue assay was conducted in a *xol-1* null mutant background, thus the male rescue data (Figure 3.2) suggests that these genes may play an additional *xol-1*-independent role to promote dosage compensation.

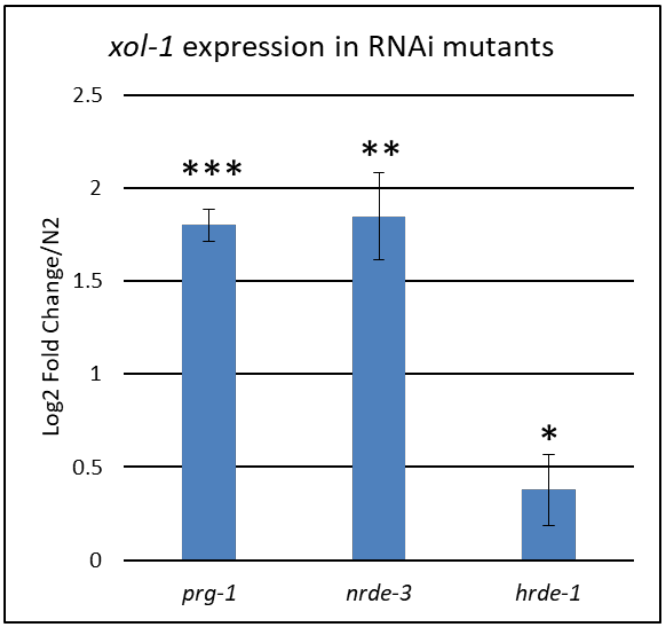

Figure 3.3. *xol-1* is de-repressed in *hrde-1* and *nrde-3* mutants. Bar graph shows qRT-PCR results. *xol-1* mRNA transcript levels normalized to wild type (N2). *prg-1* is shown as a positive control. *xol-1* transcripts are significantly more abundant in *hrde-1* and *nrde-3*. *xol-1* is de-repressed to a similar level in *prg-1* and *nrde-3* mutants, and to a lesser extent in *hrde-1*. Significance is based on a Student's T-Test: **=p<0.01, ***= p<0.001. Error bars represent SD.

X chromosome decondensation in nuclear RNAi AGO mutants is independent of *xol-1*

Since *prg-1, hrde-1 and nrde-3* contribute to the repression of *xol-1* (Figure 3.3), and our male rescue data (Figure 3.2) show that RNAi of these genes also rescues males in a *xol-1*-independent manner, the X chromosome compaction defect in the mutants (Figure 3.1) may or may not be *xol-1*-dependent. To determine if the X chromosome decondensation in *hrde-1, nrde-3,* and *prg-1* mutants (Figure 3.1) is due to *xol-1* de-repression or a *xol-1*-independent role, we conducted X chromosome FISH in double mutants for *xol-1* and each of the AGO genes (Figure 3.4A). While *xol-1* mutants did not exhibit X chromosome decondensation, in each double mutant condition, the X chromosome decondensation phenotype of *hrde-1, nrde-3* and *prg-1* persisted. These results suggest that the *xol-1* repression role of the AGO genes is separate from the X chromosome compaction role (Figure 3.4 B). We also assessed the volume of Chromosome I in each of the nuclear AGO double mutants with *xol-1* and found no significant difference from wild type animals or *xol-1* mutants (Figure 3.4 C and D). Thus the chromosome decondensation phenotype in nuclear RNAi Argonaute mutants is X-specific and *xol-1*-independent.

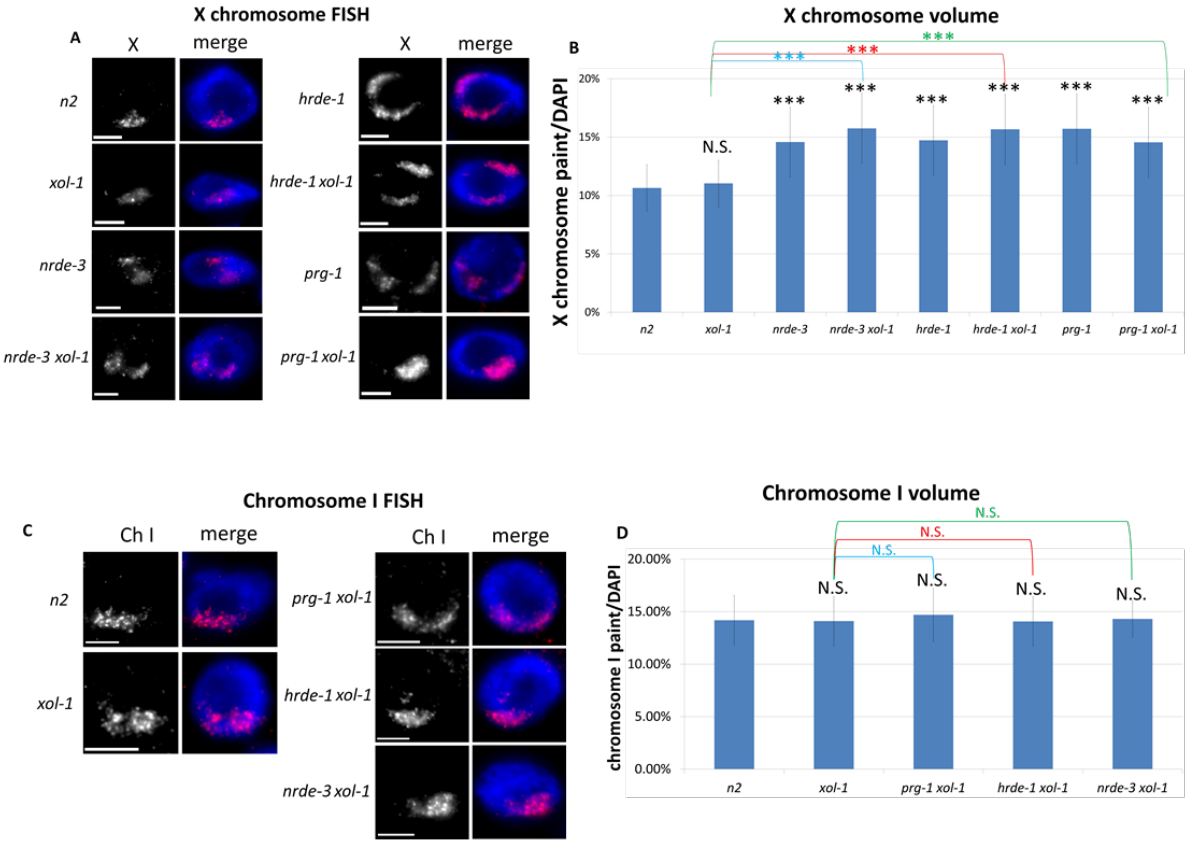

Figure 3.4. nuclear RNAi Argonaute mutant X de-condensation is independent of *xol-1* . (A) FISH X chromosome paint (red) with nuclear (DAPI) staining is shown in adult hermaphrodite intestinal cells. The X paint signal region in single mutants for each Argonaute (*nrde-3, hrde-1, prg-1*) is larger than wild type (N2) and *xol-1,* and similar to its double mutant counterpart with *xol-1.* (B) Quantification for X chromosome volume: (X chromosome paint voxels/DAPI voxels). (C) FISH chromosome I paint (red) with nuclear (DAPI) staining is shown. The Ch I paint signal region in wild type (N2) and *xol-1* negative controls are similar to each Argonaute mutant with *xol-1*. (D) Quantification for chromosome I volume: (chromosome I paint voxels/DAPI voxels). Significance for B and D is based on a Student's T Test: **=p<0.01, ***= p<0.001 (Black asterisks and labels are N2 compared to each mutant; colored asterisks and labels are *xol-1* compared to each double mutant). Error bars represent SD.

Synergistic lethality of nuclear RNAi AGO mutants with *sex-1(RNAi)*

The dual role for nuclear RNAi AGO genes is akin to that of *sex-1,* a better characterized gene in dosage compensation. *sex-1* is an X-chromosome encoded "X signal element" (XSE) which negatively regulates *xol-1* expression, while also contributing to dosage compensation downstream of *xol-1* through an uncharacterized mechanism (Gladden *et al.,* 2007). Hermaphrodite viability data indicate a high degree of lethality in *sex-1* null mutants (~20-37% viable) (Carmi *et al.,* 1998, Gladden *et al.,* 2007). This lethality is largely due to *xol-1* derepression, as x*ol-1 sex-1* double mutants largely rescue viability (~85% viability) (Gladden *et al.,* 2007). However, a mutation in *xol-1* does not completely rescue lethality, indicating that *sex-1* also plays a *xol-1*-independent role promoting hermaphrodite viability (Gladden *et al.,* 2007). In order to determine the extent to which *hrde-1* and *nrde-3* contribute to hermaphrodite viability upstream and downstream of *xol-1*, we conducted hermaphrodite viability assays with and without the *xol-1(y9)* mutation and *sex-1(RNAi)* (Figure 3.5). Briefly, mutants worms were subjected to *sex-1(RNAi)* from the L1 larval stage. For each experiment, we counted the total number of eggs laid, the number of unhatched (dead) eggs, the number of dead worms, and the number of live worms that were alive two days after the eggs were laid. The proportion of live worms is shown on Figure 3.5.

nrde-3 and *hrde-1* hermaphrodite viability was similar to wild type (N2) on control empty vector RNAi, although the viability of *nrde-3* mutants was somewhat reduced (Figure 3.5A). However on *sex-1(RNAi),* both mutants exhibited strongly enhanced lethality (Figure 3.5B, Table 3.1). Enhanced lethality in the *sex-1* mutant background is a characteristic of genes promoting dosage compensation (Gladden *et al.,* 2007). Thus, this data is consistent with a role

for *hrde-1* and *nrde-3* in dosage compensation. Much of the discrepancy between hermaphrodite viability in wild type N2 versus *nrde-3* and *hrde-1* was eliminated with the addition of *xol-1* mutation to each of the single mutants, suggesting that regulation of *xol-1* is an important component of this effect. However, there was still a small, but significant increase in lethality on *sex-1(RNAi)* for *hrde-1 xol-1* and *nrde-3 xol-1* compared to *xol-1* (Figure 3.5B, Table 3.1). These results indicate that the nuclear AGO genes contribute to hermaphrodite viability in a manner similar to *sex-1*; functioning largely upstream of *xol-1,* and to a lesser but significant extent, downstream of *xol-1.*

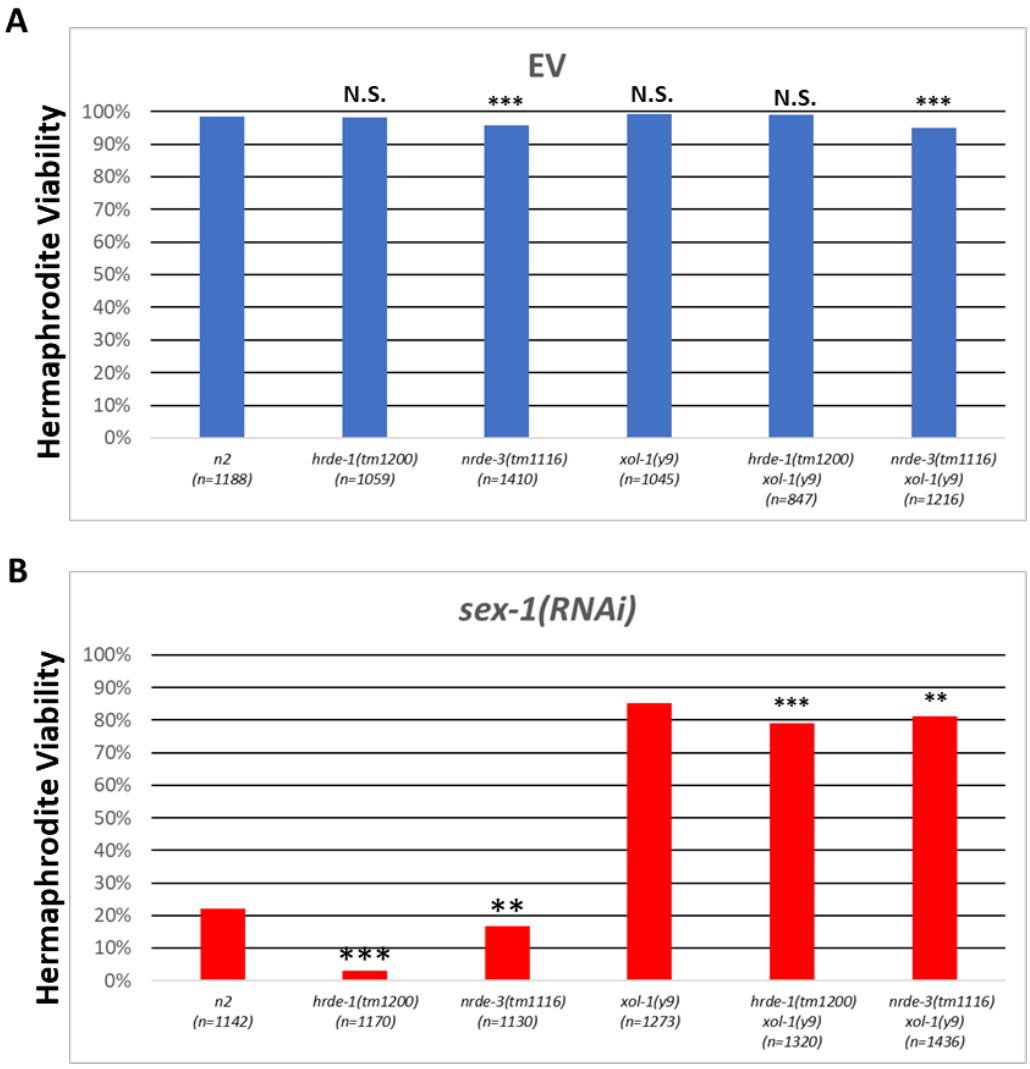

Figure 3.5. Hermaphrodite Viability of nuclear Argonaute mutants. (A) Hermaphrodite viability on empty vector RNAi. % viability (calculated as the number of live worms/total number of eggs laid) is shown. (B) Hermaphrodite viability of *hrde-1* and *nrde-3* mutants with and without *xol-1* on *sex-1(RNAi). hrde-1* mutants are only 3% viable and *nrde-3* mutants are slightly less viable than wild type (N2) worms. The lethality is *xol-1* dependent. Significance in A and B are based on comparisons of N2 to each single mutant *(hrde-1* or *nrde-3*) and *xol-1* to each double mutant. Significance is based on *p* Values from Chi Square analysis for each comparison *=p<0.05, **=p<0.01, ***= p<0.001 (See supplemental table 1).

Table 3.1: Hermaphrodite Viability Chi Square Raw Data

		observed		expected		p value	significance
condition	n	alive	dead	alive	dead		
N2 EV	1188	1169	19	725	463	-	***
N2 *sex-1(RNAi)*	1142	252	890	696	446		
xol-1 EV	1045	1036	9	956	89	0.000000000	***
xol-1 sex-1(RNAi)	1273	1084	189	1164	109		
hrde-1 EV	1059	1040	19	511	548	-	***
hrde-1 sex-1(RNAi)	1170	35	1135	564	606		
hrde-1 xol-1 EV	847	839	8	735	112	0.000000000	***
hrde-1 xol-1 sex-1(RNAi)	1320	1042	278	1146	174		
nrde-3 EV	1410	1349	61	854	556	-	***
nrde-3 sex-1(RNAi)	1130	189	941	684	446		
nrde-3 xol-1 EV	1216	1156	60	1064	152	0.000000000	***
nrde-3 xol-1 sex-1(RNAi)	1435	1164	271	1256	179		
xol-1 EV	1045	1036	9	1032	13	0.117821272	N.S.
N2 EV	1188	1169	19	1173	15		
hrde-1 EV	1059	1040	19	1041	18	0.720703389	N.S.
N2 EV	1188	1169	19	1168	20		
hrde-1 xol-1 EV	847	839	8	839	8	0.848639347	N.S.
xol-1 EV	1045	1036	9	1036	9		
nrde-3 EV	1410	1349	61	1367	43	0.000061215	***
N2 EV	1188	1169	19	1151	37		
nrde-3 xol-1 EV	1216	1156	60	1179	37	0.000000020	***
xol-1 EV	1045	1036	9	1013	32		
xol-1 sex-1(RNAi)	1273	1084	189	704	569	0.000000000	***
N2 *sex-1(RNAi)*	1142	252	890	632	510		
hrde-1 sex-1(RNAi)	1170	35	1135	145	1025	0.000000000	***
N2 *sex-1(RNAi)*	1142	252	890	142	1000		
hrde-1 xol-1 sex-1(RNAi)	1320	1042	278	1082	238	0.000038482	***
xol-1 sex-1(RNAi)	1273	1084	189	1044	229		
nrde-3 sex-1(RNAi)	1130	189	941	219	911	0.001289536	**
N2 *sex-1(RNAi)*	1142	252	890	222	920		
nrde-3 xol-1 sex-1(RNAi)	1435	1164	271	1191	244	0.005221735	**
xol-1 sex-1(RNAi)	1273	1084	189	1057	216		

Nuclear RNAi AGO mutant XO rescue with *sex-1(RNAi)*

While hermaphrodite viability defects are not a direct readout of dosage compensation, the rescue of *xol-1* mutant XO animals is a highly specific readout of dosage compensation function. To better understand the physiological contribution of *hrde-1* and *nrde-3* downstream of *xol-1,* we refined our XO rescue assay, adopting an approach modified from Gladden *et al.,* (2007) which utilizes a marker mutation to directly score for the XO karyotype, rather than the male phenotype (Figure 3.6A). In our RNAi-based *xol-1* male rescue assay (Figure 3.2) we scored the percentage of rescued worms based on the male phenotype. However, because the function of XOL-1 is also needed for male development, there could be candidate genes which yield rescued XO worms with the hermaphrodite phenotype. The strain used for the RNAi assay also has a mutation in *sex-1* which partially disrupts dosage compensation and sensitizes the strain for rescue. Our modified *xol-1* male rescue assay takes advantage of the recessive X-linked *lon-2(e678)* mutation, which renders hemizygous XO or homozygous XX mutant worms ~50% longer than wild type or *lon-2*/+ XX animals. Thus, with the *lon-2(e678)* marker we eliminate these potential false negatives by directly scoring the karyotype. The assay relies on a mating between a male and hermaphrodite which generates a theoretical yield of 50% males to 50% hermaphrodites (Figure 3.6 A). To distinguish cross-progeny from self-progeny, we include an autosomal linked GFP marker (*mIs11)* in the males of the cross, resulting in GFP+ cross progeny and GFP- self-progeny. The assay also uses loss of function mutants, rather than RNAi-based variable knockdown, which can be variable (Figure 3.6 A). The genetic background of the control cross is thus *lon-2(e678) xol-1(y9)* hermaphrodites crossed to *mIs11* males, whereby *hrde-1,* and *nrde-3* mutations were separately crossed into both of the parent strains for each experiment to ensure that the parent and progeny are homozygous mutant for the gene assessed

(for details see Methods). For controls, we analyzed the effects of mutations in the DCC subunit and H4K20 demethylase *dpy-21*. Mutations in *dpy-21* rescue a large proportion of XO animals. *hrde-1* and *nrde-3* mutations independently did not significantly rescue XO worms -*ctrl (0.00%)*; *hrde-1 (0.23%); nrde-3 (1.05%)* (Figure 3.6 B, Table 3.2). Since reduced *sex-1* function enhances rescue of *xol-1* males (Figure 3.2), we repeated the rescue matings on *sex-1(RNAi).* On *sex-1(RNAi)* we observed a significant degree of rescue in *hrde-1* and *nrde-3* mutants compared to *sex-1(RNAi)* alone: *sex-1(RNAi) (0.00%); nrde-3 (16.80%), hrde-1 (9.35%)* (Figure 3.6 C). Thus, while *nrde-3* and *hrde-1* mutations alone are insufficient to rescue XO progeny to a developmental stage that can be scored in this assay, in the sensitized background of *sex-1(RNAi)* their role becomes evident. The overwhelming majority of rescued animals were Lon male, with the Lon hermaphrodite phenotype occurring in four or fewer worms in each condition. Moreover, Lon hermaphrodites were not observed at all in the *nrde-3* and *hrde-1 sex-1(RNAi)* conditions possibly due to *sex-1's* role sex determination (Gladden *et al.,* 2007). Interestingly, the XO rescue of *hrde-1* and *nrde-3* worms slightly increased on control empty vector alone compared to standard non-RNAi food (Figure 3.6B and C). One possibility is that engagement of the RNAi machinery with empty vector in the background of nuclear AGO mutations disrupts dosage compensation to a small degree. Overall, these results suggests that in addition to regulating *xol-1*, *nrde-3* and *hrde-1* also promote dosage compensation downstream of *xol-1*. We were unable to assess the role of *prg-1* in this assay, due to the severely reduced fertility of *prg-1* mutant males. However, the RNAi-based rescue (Figure 3.2) indicates that *prg-1* likely also plays a dual role.

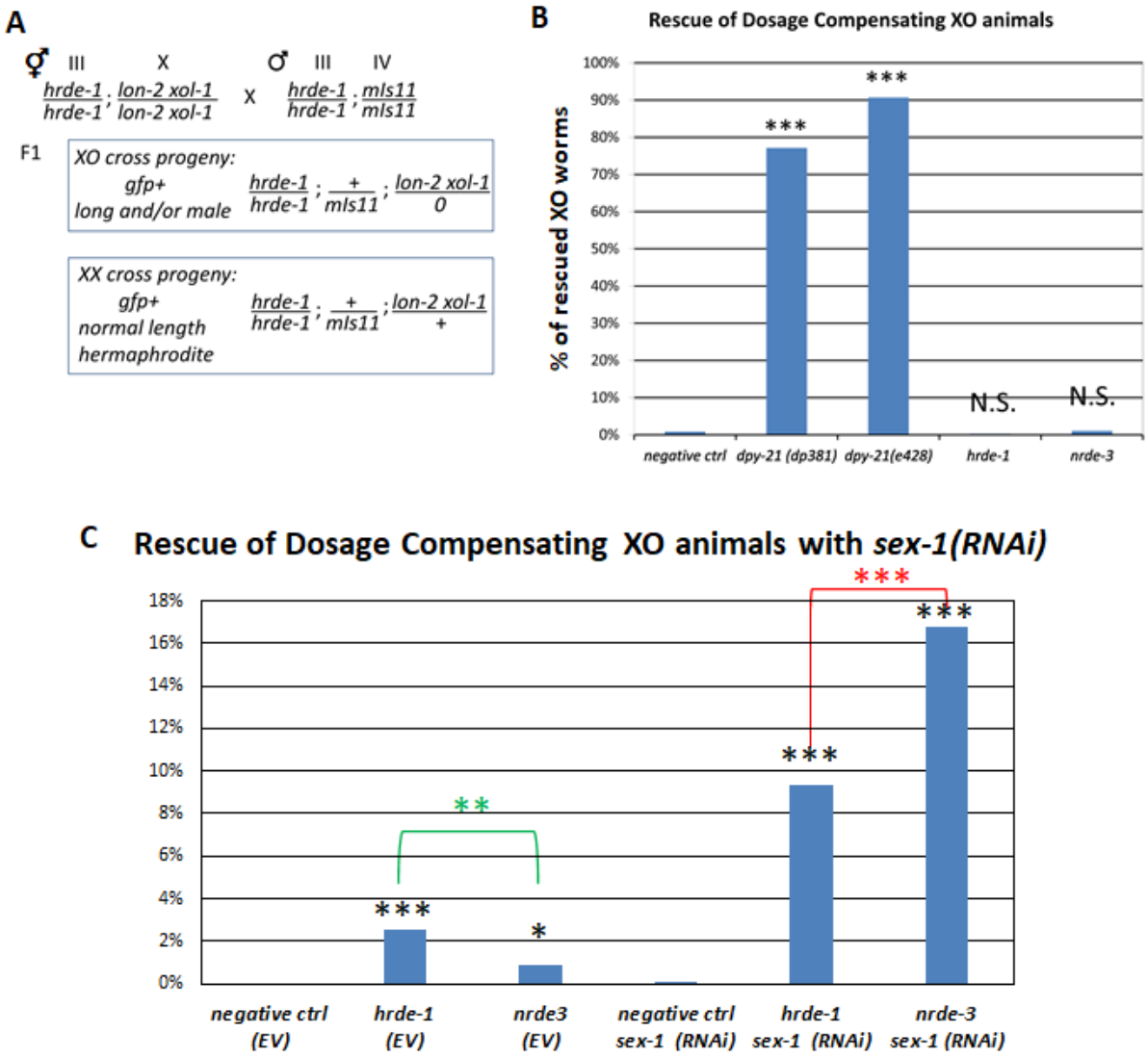

Figure 3.6. *sex-1* dependent rescue of nuclear Argonaute mutants (A) XO rescue mating cross schematic. *hrde-1* is shown as an example to highlight the experimental condition cross. *hrde-1 lon-2 xol-1* hermaphrodites are crossed to *hrde-1 mIs11* (GFP+) males. In the F1, GFP+ (*mIs11)* worms designate cross progeny. Lon worms represent XO animals hemizygous for lon-2, some of which develop as male, some as hermaphrodite. Normal length, GFP+ hermaphrodites represent XX cross progeny. (B) Percentage of XO worms rescued by various mutations are shown. *dpy-21(e428)* is a null mutation and *dpy-21(dp381)* is a partial loss of function mutation. Both positive controls rescue a large amount of XO animals and *hrde-1* and *nrde-3* on their own do not significantly rescue XO animals. Significance is based on comparison to negative control for each condition. (C) Percentage of XO worms rescued by *hrde-1* and *nrde-3* are shown with empty vector or *sex-1(RNAi)* treatment. *hrde-1 sex-1(RNAi)* and *nrde-3 sex-1(RNAi)* rescue a significant portion of XO animals. Black asterisks denote significance for comparison of each condition to negative control of the same RNAi treatment. Significance B and C are based on Chi Square analysis (See Supplemental Figure 2A/B). ***= p<0.001.

Table 3.2: Chi square Data for Mutant Rescue Experiments

A Chi Square Raw Data and Significance for Mutant Rescue

			OBSERVED		EXPECTED			
Condition	n	total XO worms	viable XO worms	dead XO worms	viable XO worms	dead XO worms	P values per comparison	significance
-control	2367	1184	20	1164	305	879	1.8473E-304	***
dpy-21(null)	820	410	390	20	105	305		
-control	2367	1184	20	1164	524	659	0	***
dpy-21(dp381)	2356	1178	1026	152	522	656		
-control	2367	1184	20	1164	16	1167	0.062035416	N.S.
hrde-1(tm1200)	855	428	2	426	6	422		
-control	2367	1184	20	1164	22	1162	0.553732128	N.S.
nrde-3(tm1116)	1351	676	14	662	12	663		
dpy-21(null)	820	410	390	20	366	44	6.68485E-06	N.S.
dpy-21(dp381)	2356	1178	1026	152	1050	128		
dpy-21(null)	820	410	390	20	192	218	8.5181E-166	***
hrde-1(tm1200)	855	428	2	426	200	227		
dpy-21(null)	820	410	390	20	153	257	1.3214E-207	***
nrde-3(tm1116)	1351	676	14	662	251	424		
dpy-21(dp381)	2356	1178	1026	152	754	424	2.8921E-224	***
hrde-1(tm1200)	855	428	2	426	274	154		
dpy-21(dp381)	2356	1178	1026	152	661	517	4.9075E-276	***
nrde-3(tm1116)	1351	676	14	662	379	296		
hrde-1(tm1200)	855	428	2	426	6	421	0.029882656	*
nrde-3(tm1116)	1351	676	14	662	10	666		

B Chi Square Raw Data and Significance for *sex-1(RNAi)* Mutant Rescue

			OBSERVED		EXPECTED			
Condition	n	total XO worms	viable XO worms	dead XO worms	viable XO worms	dead XO worms	P values per comparison	significance
-ctrl EV	690	345	0	345	0.5	345	0.344436643	N.S.
-ctrl sex-1(RNAi)	773	387	1	386	1	386		
-ctrl EV	690	345	0	345	11	334	2.70221E-05	***
hrde-1 EV	1377	689	34	655	23	666		
-ctrl EV	690	345	0	345	3	342	0.015592064	*
nrde-3 EV	714	357	6	351	3	354		
hrde-1 EV	1377	689	34	655	26	662	0.009216895	**
nrde-3 EV	714	357	6	351	14	343		
-ctrl sex-1(RNAi)	773	387	1	386	37	349	5.41073E-17	***
hrde-1 sex-1(RNAi)	982	491	84	407	48	443		
-ctrl sex-1(RNAi)	773	387	1	386	54	332	3.36059E-29	***
nrde-3 sex-1(RNAi)	723	362	104	258	51	311		
hrde-1 sex-1(RNAi)	982	491	84	407	108	383	4.94112E-05	***
nrde-3 sex-1(RNAi)	723	362	104	258	80	282		
-ctrl EV	690	345	0	345	35	310	5.48107E-16	***
hrde-1 sex-1(RNAi)	982	491	84	407	49	442		
-ctrl EV	690	345	0	345	51	294	3.91313E-27	***
nrde-3 sex-1(RNAi)	723	362	104	258	53	308		

nrde-3 and *hrde-1* modulate the structure of a heterochromatin array in somatic cells

It is interesting to note that mutations in *prg-1*, *nrde-3* and *hrde-1* led to decondensation of the X chromosomes, but not chromosome I (Figure 3.1). This observation suggests that the structure of the X chromosome is particularly sensitive to loss of nuclear RNAi function. To investigate whether non-X chromosome sequences can be affected, we sought to determine whether *nrde-3* and *hrde-1* have a structural impact on a highly heterochromatinized transgenic array (Figure 3.7). We conducted immunofluorescence staining for the H3K9me3 heterochromatin mark in intestinal cells of *hrde-1* and *nrde-3* mutants and wild type worms bearing the *mIs11* array. Note that this repetitive array is completely silent in intestinal cells. We noticed that the array formed spherical, tightly condensed structures marked by H3K9me3 accumulation in otherwise wild type worms. However, with a *nrde-3* or *hrde-1* mutation in the background, the array appeared less condensed. We characterized these structural defects by binning the heterochromatin array morphology phenotypes into one of four categories. The categories were (in order from most to least condensed): spherical, sickle/bar, starburst, spotted. In wild type, the array tended to take on one of the more compact appearances of spherical (50%) or sickle/bar (16%) H3K9me3 distribution a total of 66% frequency (Figure 3.7 A and B). In *hrde-1* mutants, the array takes on the spherical (15%) or sickle/bar (25%) H3K9me3 distribution, a total of 40% frequency, and in *nrde-3* mutants the *mIs11* array takes on the spherical (35%) or sickle/bar (18%) H3K9me3 distribution a total of 53% frequency (Figure 3.7 A and B). Among the two categories of qualitatively decondensed array, the biggest difference for both *hrde-1* and *nrde-3* mutants compared to wild type was a more than two-fold increase of the frequency of starburst H3K9me3 distribution. While the chromosome I controls from our FISH experiments did not capture differences in nuclear volume in the nuclear RNAi AGOs, the

H3K9me3 IF data indicate that on a highly heterochromatinized array, a pronounced effect on chromatin structure morphology can be observed, consistent with a previous report indicating a role for nuclear AGOs in compacting chromatin silenced by RNAi (Fields and Kennedy 2019).

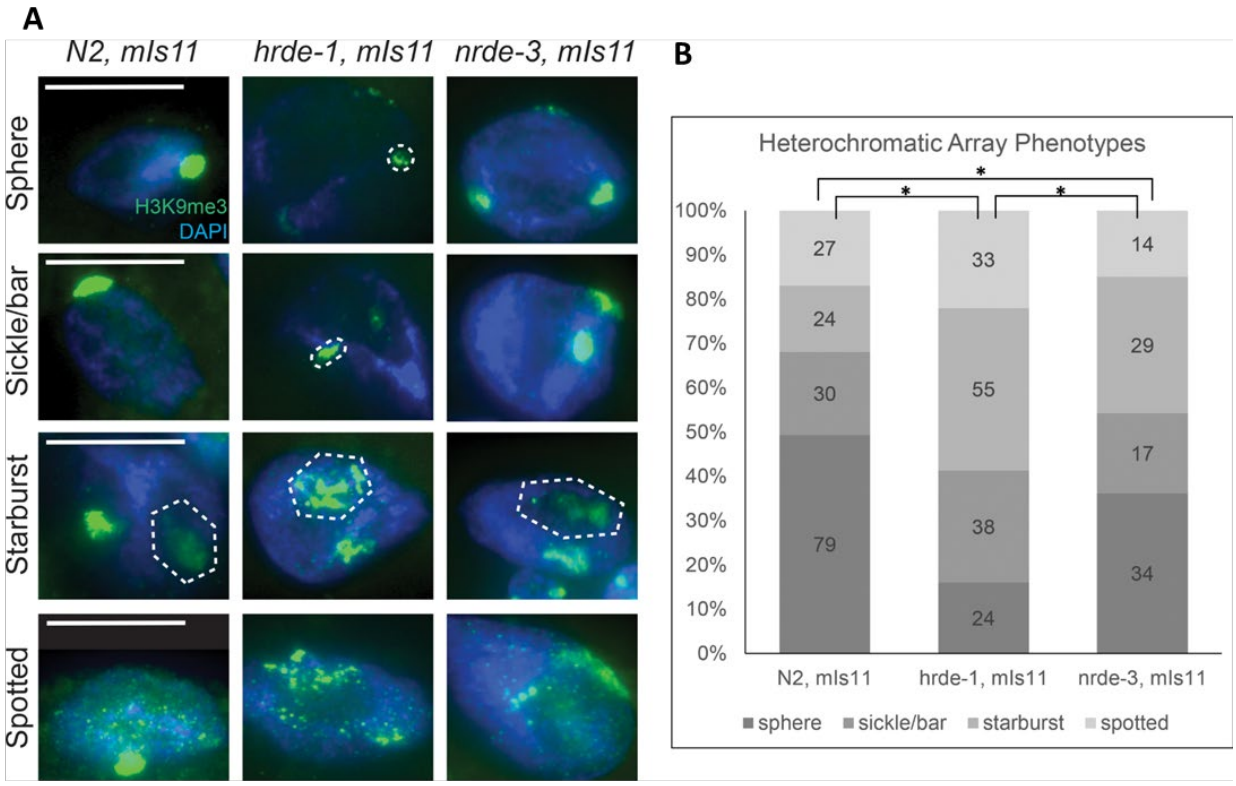

Figure 3.7. ***nrde-3*** **and** ***hrde-1*** **modulate the structure of a heterchromatin array** (A) H3K9me3 signal (green) and DAPI (blue) staining is shown in adult hermaphrodite intenstinal cells. Vertical (left) labels represent four qualitative patterns for observed H3K9me3 signal. All patterns were observed for each strain. (B) Quantification of qualitative H3K9me3 signal binned by pattern type. Number of nuclei for each pattern are shown within the bars and y-axis shows the proportion of each H3K9me3 pattern as a percentage of that observed in each genotype. *hrde-1* and *nrde-3* exhibited fewer nuclei with the compacted spherical/sickle/bar arrays and a higher proportion of the starburst/spotted arrays. Significance is based on Chi Square analysis for each comparison between genotypes. *= $P<0.05$.

DISCUSSION

We demonstrated that nuclear RNAi AGOs HRDE-1 and NRDE-3 play dual roles promoting dosage compensation. First, together with the piRNA AGO PRG-1, they repress the master sex determination and dosage compensation switch gene *xol-1*. XOL-1 promotes male development and inhibits dosage compensation, and therefore XOL-1 function must be turned off in hermaphrodites. In addition, HRDE-1, NRDE-3 and PRG-1 also promote dosage compensation downstream of *xol-1*. This downstream role is required for full compaction of dosage compensated X chromosomes, and for healthy development (Figure 3.8).

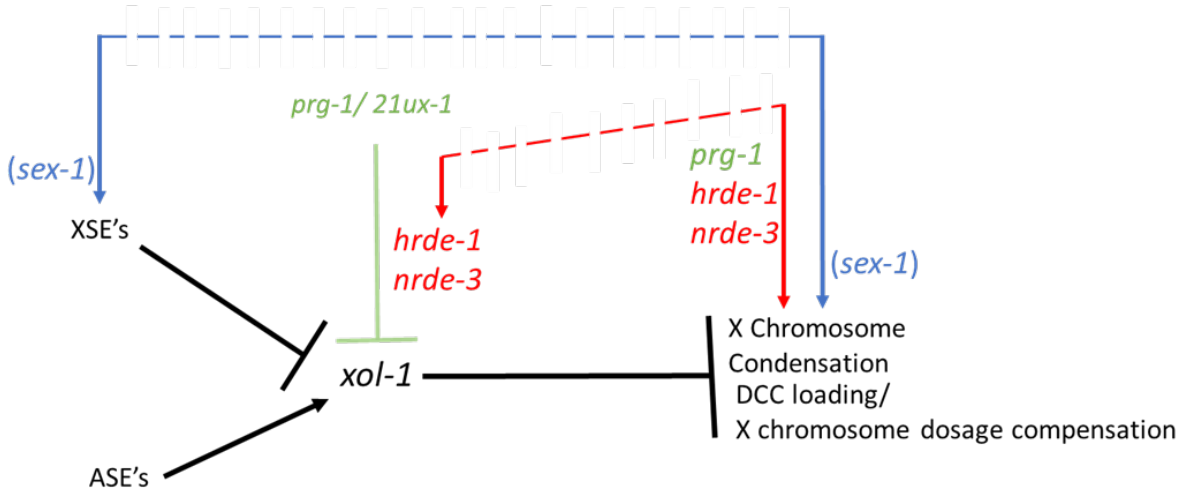

Figure 3.8. dual role for *hrde-1* and *nrde-3* in dosage compensation prg-1 and the 21ux-1 piRNA aid in the repression of xol-1 in hermaphrodites. nrde-3 and hrde-1 also contribute to xol-1 repression, and cooperate with sex-1 to contribute to hermaphrodite viability upstream of xol-1. hrde-1 and nrde-3 also promote the compaction of X chromosomes, and cooperate with sex-1 to promote physiological dosage compensation downstream of xol-1.

The dual roles of *nrde-3* and *hrde-1* in dosage compensation are similar to the dual roles *sex-1* in their *xol-1*-dependent and independent nature (Carmi *et al.,* 1998, Gladden *et al.,* 2007). While *sex-1'*s role as an X-signal element is well characterized, the *xol-1*-independent role of *sex-1* has not yet been assessed. Identifying genes targeted by *sex-1* will help elucidate how this nuclear hormone receptor homolog gene is acting in conjunction with the nuclear RNAi pathway to promote a significant degree of dosage compensation function. One possibility is that *sex-1*'s role as a nuclear hormone receptor involves recruitment of the nuclear RNAi pathway as one of the mechanism for the repression of its targets. Another possibility is that nuclear RNAi targets a different set of genes that promote dosage compensation in a *sex-1* independent manner. A third possibility is that nuclear RNAi's influence on chromatin structure augments *sex-1*'s role in promoting dosage compensation. Mutants for the pathway tethering H3K9me3 heterochromatin to the nuclear lamina also exhibit X chromosome decondensation and contribute to dosage compensation in conjunction with *sex-1.* Thus, X chromosome decondensation simultaneously with the loss of *sex-1*'s target gene repression may be what underlies the additive detriment to dosage compensation in double mutants for both *sex-1* and the nuclear RNAi pathway and *sex-1* and the heterochromatin tethering pathway.

While both AGO mutants and *prg-1* exhibit a *xol-1*-independent X chromosome decondensation phenotype to similar degree (Figure 3.4 A and B), their impacts on male rescue (Figure 3.2 A), *xol-1* de-repression (Figure 3.3), hermaphrodite viability (Figure 3.5) and rescue of XO animals (Figure 3.6) vary. One measure of the upstream, *xol-1*-dependent role is hermaphrodite viability after *sex-1(RNAi)* treatment. The *xol-1*-dependent hermaphrodite viability of *hrde-1* mutants treated with *sex-1(RNAi)* was only 3%, compared to 16% in *nrde-3 sex-1(RNAi)* (Figure 3.5 B), indicating that *hrde-1* may play a more prominent role. In contrast,

while the degree of *xol-1* de-repression is significantly stronger in both AGO mutants compared to wild type (N2), the level of de-repression is far greater in *nrde*-3 than *hrde-1* (Figure 3.3). Although impaired hermaphrodite viability is not a direct measure of dosage compensation defect, the synergistic lethality of *hrde-1 sex-1(RNAi)* is *xol-1*-dependent, suggesting that *xol-1* regulation is a major component of *hrde-1*'s function.

Rescue of *xol-1* mutant males by RNAi, rescue of *xol-1* XO animals by introducing genetic mutations, and X chromosome decompaction in *xol-1* mutants, are all measures of the downstream, *xol-1*-independent role. The *xol-1*-independent X chromosome decompaction phenotype was comparable in *prg-1*, *nrde-3* and *hrde-1* mutants (Figure 3.4). However, the level of X decompaction does not necessarily correlate with the level of X-linked gene derepression, therefore this result should not be interpreted as all genes playing comparable roles (Snyder *et al.,* 2016). The XO rescue experiments on *sex-1(RNAi)* indicate almost a two-fold greater *xol-1*-independent contribution to dosage compensation for *nrde-3* over *hrde-1* (Figure 3.6 C). However, the degree of *nrde-3* male rescue from the RNAi-based assay in Figure 3.2 is smaller than that of *hrde-1*. One potential explanation for the discrepancy is that comparisons made between different RNAi conditions are subject to varying degrees of knockdown efficacy between treatments. It is worth noting that the *sex-1(RNAi)* appears to be near (if not) a complete depletion, as the hermaphrodite viability of wild type N2 worms on *sex-1(RNAi)* is close to the published data for *sex-1(null)* mutants (Figure 3.5 B) (Gladden *et al.,* 2007). *sex-1(RNAi)* is also effective in *hrde-1* and *nrde-3* mutants as well, as evidenced by the severe effects on hermaphrodite viability (Figure 3.5). Thus, the XO rescue experiments, using loss of function mutants for each AGO and identical RNAi conditions afford a potentially more accurate comparison of contributions from each individual AGO to dosage compensation. In this vein, a

bigger role for *nrde-3* downstream of *xol-1* is consistent with its expression pattern in hermaphrodite somatic cells from the embryo through adulthood (Guang *et al.,* 2008). After DCC loading to hermaphrodite X chromosomes (~30-50 cell stage embryo) NRDE-3's presence in the soma may reinforce maintenance of dosage compensation by directing chromatin modifications (Chuang *et al.,* 1994, Dawes *et al.,* 1999). Future studies using a conditional *nrde-3* depletion to determine the phenocritical period for *nrde-3* in dosage compensation will aid in our understanding of whether *nrde-3* is maintaining and/or initiating the repressive chromatin landscape for dosage compensation.

Considering the germline-enriched expression patterns of *prg-1* and *hrde-1,* the somatic X chromosome decondensation phenotype in both mutant adults is intriguing. The fact that *prg-1* (Tang *et al.,* 2018) and *hrde-1* (Figure 3.3) repress *xol-1* and independently maintain X chromosome compaction (Figure 3.4) begs the question of when in development and how mechanistically this contribution is made. Since neither *dcr-1(mg375)* nor *ergo-1(tm1860)* mutants with impaired endogenous primary 26G siRNA accumulation exhibit X chromosome decondensation (Figure 3.1A and B), the contribution of nuclear AGOs to X chromosome compaction could originate from the piRNA pathway which bypasses the requirement for 26G primary siRNAs but utilizes the nuclear RNAi machinery for silencing (Ashe *et al.,* 2012; Lee *et al.,* 2012; Luteijn *et al.,* 2012; Shirayama *et al.,* 2012). If that were the case, *prg-1* targets may include additional genes important for maintaining the compaction of dosage compensating X chromosomes. The fact that the somatic nuclear AGO *nrde-3* also plays a role both in *xol-1* repression and in *xol-1*-independent X decompaction raises the possibility that repression of some of these *prg-1* targets are maintained by NRDE-3 in the embryo, rather than HRDE-1.

Alternatively, the capacity for these nematode-specific AGOs to direct chromatin modifications may be directly featured in X chromosome compaction. Given *hrde-1's* chromatin compaction role in the germline and soma (Fields and Kennedy, 2019), its plausible that in *sex-1* mutant hermaphrodites where *xol-1* is de-repressed and dosage compensation is impaired, the loss of *hrde-1*-mediated heterochromatin signatures on the X chromosome further exasperates DCC initiation and/or maintenance. HRDE-1 may reinforce chromatin compaction and direct some degree of heterochromatin formation in the early embryo as well, and this role may then be taken over by NRDE-3 in later stages of embryonic development. The recent discovery of MTR-4's role in the NRDE complex suggests that there may be additional important genes interacting with the nuclear RNAi machinery (Wan *et al.,* 2020). The NRDE complex is the link between nuclear RNAi target genes, histone modifications, and co-transcriptional silencing (Guang *et al.,* 2008, Guang *et al.,* 2010, Buckley *et al.,* 2011, Ashe *et al.,* 2012, Buckley *et al.,* 2012, Luteijn *et al.,* 2012). Thus, identifying the landscape of NRDE complex binding on *C. elegans* chromosomes and interactions with dosage compensation regulators will further test whether a dosage compensation role is attributed to nuclear RNAi-mediated regulation of genes functioning in dosage compensation, or to nuclear RNAi-mediated regulation of chromosome architecture.

ACKNOWLEDGEMENTS

This work was supported by the National Institute of General Medical Sciences grant NIH R01GM13385801 to G.C. M.B.D. was partially supported by Michigan Predoctoral Training in Genetics (T32 GM007544), and by the Edwards Fellowship and Okkleberg Fellowship from the Department of MCDB at the University of Michigan. Some strains were provided by the Caenorhabditis Genetics Center (CGC), which is funded by NIH Office of Research Infrastructure Programs (P40 OD010440). We thank Joshua Bembenek for the critical reading and feedback on this manuscript. We also thank all members of the Csankovszki lab for helpful discussions.

REFERENCES

Albritton, Sarah Elizabeth, and Sevinç Ercan. "Caenorhabditis Elegans Dosage Compensation: Insights into Condensin-Mediated Gene Regulation." *Trends in Genetics* 34, no. 1 (January 2018): 41–53.

Almeida, Miguel Vasconcelos, Miguel A. Andrade-Navarro, and René F. Ketting. "Function and Evolution of Nematode RNAi Pathways." *Non-Coding RNA* 5, no. 1 (2019): 8.

Ambros, Victor, Rosalind C. Lee, Ann Lavanway, Peter T. Williams, and David Jewell. "MicroRNAs and Other Tiny Endogenous RNAs in C. Elegans." *Current Biology* 13, no. 10 (2003): 807–18.

Batista, Pedro J., J. Graham Ruby, Julie M. Claycomb, Rosaria Chiang, Noah Fahlgren, Kristin D. Kasschau, Daniel A. Chaves, Weifeng Gu, Jessica J. Vasale, and Shenghua Duan, etc., *et al.,* Craig C. Mello. "PRG-1 and 21U-RNAs Interact to Form the PiRNA Complex Required for Fertility in C. Elegans." *Molecular Cell* 31, no. 1 (2008): 67–78.

Bernstein, Emily, Amy A. Caudy, Scott M. Hammond, and Gregory J. Hannon. "Role for a Bidentate Ribonuclease in the Initiation Step of RNA Interference." *Nature* 409, no. 6818 (2001): 363–66.

Billi, Allison C., Sylvia EJ Fischer, and John K. Kim. "Endogenous RNAi Pathways in C. Elegans." *WormBook: The Online Review of C. Elegans Biology [Internet]*, 2018.

Billi, Allison C., Mallory A. Freeberg, Amanda M. Day, Sang Young Chun, Vishal Khivansara, and John K. Kim. "A Conserved Upstream Motif Orchestrates Autonomous, Germline-Enriched Expression of Caenorhabditis Elegans PiRNAs." *PLoS Genetics* 9, no. 3 (2013): e1003392.

Brejc, Katjuša, Qian Bian, Satoru Uzawa, Bayly S. Wheeler, Erika C. Anderson, David S. King, Philip J. Kranzusch, Christine G. Preston, and Barbara J. Meyer. "Dynamic Control of X Chromosome Conformation and Repression by a Histone H4K20 Demethylase." *Cell* 171, no. 1 (2017): 85-102. e23.

Brenner, S. "The Genetics of Caenorhabditis Elegans." *Genetics* 77, no. 1 (May 1, 1974): 71.

Broverman, Sherryl A., and Philip M. Meneely. "Meiotic Mutants That Cause a Polar Decrease in Recombination on the X Chromosome in Caenorhabditis Elegans." *Genetics* 136, no. 1 (1994): 119–27.

Buckley, Bethany A., Kirk B. Burkhart, Sam Guoping Gu, George Spracklin, Aaron Kershner, Heidi Fritz, Judith Kimble, Andrew Fire, and Scott Kennedy. "A Nuclear Argonaute Promotes Multigenerational Epigenetic Inheritance and Germline Immortality." *Nature* 489, no. 7416 (2012): 447–51.

Burkhart, Kirk B., Shouhong Guang, Bethany A. Buckley, Lily Wong, Aaron F. Bochner, and Scott Kennedy. "A Pre-MRNA–Associating Factor Links Endogenous SiRNAs to Chromatin Regulation." *PLoS Genetics* 7, no. 8 (2011): e1002249.

Carmi, Ilil, Jennifer B. Kopczynski, and Barbara J. Meyer. "The Nuclear Hormone Receptor SEX-1 Is an X-Chromosome Signal That Determines Nematode Sex." *Nature* 396, no. 6707 (1998): 168–73.

Chuang, Pao-Tien, Donna G. Albertson, and Barbara J. Meyer. "DPY-27: A Chromosome Condensation Protein Homolog That Regulates C. Elegans Dosage Compensation through Association with the X Chromosome." *Cell* 79, no. 3 (1994): 459–74.

Conine, Colin C., Pedro J. Batista, Weifeng Gu, Julie M. Claycomb, Daniel A. Chaves, Masaki Shirayama, and Craig C. Mello. "Argonautes ALG-3 and ALG-4 Are Required for

Spermatogenesis-Specific 26G-RNAs and Thermotolerant Sperm in Caenorhabditis Elegans." *Proceedings of the National Academy of Sciences* 107, no. 8 (2010): 3588–93.

Consortium, C. elegans Deletion Mutant. "Large-Scale Screening for Targeted Knockouts in the Caenorhabditis Elegans Genome." *G3: Genes| Genomes| Genetics* 2, no. 11 (2012): 1415–25.

Crane, Emily, Qian Bian, Rachel Patton McCord, Bryan R. Lajoie, Bayly S. Wheeler, Edward J. Ralston, Satoru Uzawa, Job Dekker, and Barbara J. Meyer. "Condensin-Driven Remodelling of X Chromosome Topology during Dosage Compensation." *Nature* 523, no. 7559 (2015): 240–44.

Csankovszki, Gyorgyi, Karishma Collette, Karin Spahl, James Carey, Martha Snyder, Emily Petty, Uchita Patel, Tomoko Tabuchi, Hongbin Liu, and Ian McLeod, etc., *et al.,* Kirsten Hagstrom. "Three Distinct Condensin Complexes Control C. Elegans Chromosome Dynamics." *Current Biology* 19, no. 1 (2009): 9–19.

Csankovszki, Györgyi, Patrick McDonel, and Barbara J. Meyer. "Recruitment and Spreading of the C. Elegans Dosage Compensation Complex along X Chromosomes." *Science* 303, no. 5661 (2004): 1182–85.

Das, Partha P., Marloes P. Bagijn, Leonard D. Goldstein, Julie R. Woolford, Nicolas J. Lehrbach, Alexandra Sapetschnig, Heeran R. Buhecha, Michael J. Gilchrist, Kevin L. Howe, and Rory Stark, etc., *et al.,* Eric A Miska. "Piwi and PiRNAs Act Upstream of an Endogenous SiRNA Pathway to Suppress Tc3 Transposon Mobility in the Caenorhabditis Elegans Germline." *Molecular Cell* 31, no. 1 (2008): 79–90.

Dawes, Heather E., Dorit S. Berlin, Denise M. Lapidus, Chad Nusbaum, Tamara L. Davis, and Barbara J. Meyer. “Dosage Compensation Proteins Targeted to X Chromosomes by a Determinant of Hermaphrodite Fate.” *Science* 284, no. 5421 (June 11, 1999): 1800.

Fields, Brandon D., and Scott Kennedy. “Chromatin Compaction by Small RNAs and the Nuclear RNAi Machinery in C. Elegans.” *Scientific Reports* 9, no. 1 (2019): 1–9.

Gent, Jonathan I., Ayelet T. Lamm, Derek M. Pavelec, Jay M. Maniar, Poornima Parameswaran, Li Tao, Scott Kennedy, and Andrew Z. Fire. “Distinct Phases of SiRNA Synthesis in an Endogenous RNAi Pathway in C. Elegans Soma.” *Molecular Cell* 37, no. 5 (2010): 679–89.

Gent, Jonathan I., Mara Schvarzstein, Anne M. Villeneuve, Sam Guoping Gu, Verena Jantsch, Andrew Z. Fire, and Antoine Baudrimont. “A Caenorhabditis Elegans RNA-Directed RNA Polymerase in Sperm Development and Endogenous RNA Interference.” *Genetics* 183, no. 4 (2009): 1297–1314.

Gladden, John M., Behnom Farboud, and Barbara J. Meyer. “Revisiting the X:A Signal That Specifies *Caenorhabditis Elegans* Sexual Fate.” *Genetics* 177, no. 3 (November 2007): 1639–54.

Gu, Sam Guoping, Julia Pak, Shouhong Guang, Jay M. Maniar, Scott Kennedy, and Andrew Fire. “Amplification of SiRNA in Caenorhabditis Elegans Generates a Transgenerational Sequence-Targeted Histone H3 Lysine 9 Methylation Footprint.” *Nature Genetics* 44, no. 2 (2012): 157–64.

Gu, Weifeng, Masaki Shirayama, Darryl Conte Jr, Jessica Vasale, Pedro J. Batista, Julie M. Claycomb, James J. Moresco, Elaine M. Youngman, Jennifer Keys, and Matthew J. Stoltz, etc., *et al.,* Craig C. Mello. “Distinct Argonaute-Mediated 22G-RNA Pathways Direct

Genome Surveillance in the C. Elegans Germline." *Molecular Cell* 36, no. 2 (2009): 231–44.

Guang, Shouhong, Aaron F. Bochner, Kirk B. Burkhart, Nick Burton, Derek M. Pavelec, and Scott Kennedy. "Small Regulatory RNAs Inhibit RNA Polymerase II during the Elongation Phase of Transcription." *Nature* 465, no. 7301 (2010): 1097–1101.

Guang, Shouhong, Aaron F. Bochner, Derek M. Pavelec, Kirk B. Burkhart, Sandra Harding, Jennifer Lachowiec, and Scott Kennedy. "An Argonaute Transports SiRNAs from the Cytoplasm to the Nucleus." *Science* 321, no. 5888 (2008): 537–41.

Han, Ting, Arun Prasad Manoharan, Tim T. Harkins, Pascal Bouffard, Colin Fitzpatrick, Diana S. Chu, Danielle Thierry-Mieg, Jean Thierry-Mieg, and John K. Kim. "26G Endo-SiRNAs Regulate Spermatogenic and Zygotic Gene Expression in Caenorhabditis Elegans." *Proceedings of the National Academy of Sciences* 106, no. 44 (2009): 18674–79.

Höck, Julia, and Gunter Meister. "The Argonaute Protein Family." *Genome Biology* 9, no. 2 (2008): 1–8.

Hoogewijs, David, Koen Houthoofd, Filip Matthijssens, Jo Vandesompele, and Jacques R. Vanfleteren. "Selection and Validation of a Set of Reliable Reference Genes for Quantitative Sod Gene Expression Analysis in C. Elegans." *BMC Molecular Biology* 9, no. 1 (2008): 1–8.

Jans, Judith, John M. Gladden, Edward J. Ralston, Catherine S. Pickle, Agnès H. Michel, Rebecca R. Pferdehirt, Michael B. Eisen, and Barbara J. Meyer. "A Condensin-like Dosage Compensation Complex Acts at a Distance to Control Expression throughout the Genome." *Genes & Development* 23, no. 5 (2009): 602–18.

Kramer, Maxwell, Anna-Lena Kranz, Amanda Su, Lara H. Winterkorn, Sarah Elizabeth Albritton, and Sevinc Ercan. “Correction: Developmental Dynamics of X-Chromosome Dosage Compensation by the DCC and H4K20me1 in C. Elegans.” *PLoS Genetics* 12, no. 2 (2016): e1005899.

Kruesi, William S, Leighton J Core, Colin T Waters, John T Lis, and Barbara J Meyer. “Condensin Controls Recruitment of RNA Polymerase II to Achieve Nematode X-Chromosome Dosage Compensation.” Edited by Nick Proudfoot. *ELife* 2 (June 2013): e00808.

Lau, Alyssa C., and Györgyi Csankovszki. “Balancing up and Downregulation of the C. Elegans X Chromosomes.” *Current Opinion in Genetics & Development* 31 (2015): 50–56.

Lau, Alyssa C., Kentaro Nabeshima, and Györgyi Csankovszki. “The C. Elegans Dosage Compensation Complex Mediates Interphase X Chromosome Compaction.” *Epigenetics & Chromatin* 7, no. 1 (2014): 1–16.

Lee, Heng-Chi, Weifeng Gu, Masaki Shirayama, Elaine Youngman, Darryl Conte Jr, and Craig C. Mello. “C. Elegans PiRNAs Mediate the Genome-Wide Surveillance of Germline Transcripts.” *Cell* 150, no. 1 (2012): 78–87.

Luteijn, Maartje J, Petra van Bergeijk, Lucas J T Kaaij, Miguel Vasconcelos Almeida, Elke F Roovers, Eugene Berezikov, and René F Ketting. “Extremely Stable Piwi-Induced Gene Silencing in Caenorhabditis Elegans.” *The EMBO Journal* 31, no. 16 (August 15, 2012): 3422–30.

Mao, Hui, Chengming Zhu, Dandan Zong, Chenchun Weng, Xiangwei Yang, Hui Huang, Dun Liu, Xuezhu Feng, and Shouhong Guang. “The Nrde Pathway Mediates Small-RNA-

Directed Histone H3 Lysine 27 Trimethylation in Caenorhabditis Elegans." *Current Biology* 25, no. 18 (2015): 2398–2403.

Miller, Leilani M., John D. Plenefisch, Lawrence P. Casson, and Barbara J. Meyer. "Xol-1: A Gene That Controls the Male Modes of Both Sex Determination and X Chromosome Dosage Compensation in C. Elegans." *Cell* 55, no. 1 (1988): 167–83.

Nabeshima, Kentaro, Susanna Mlynarczyk-Evans, and Anne M. Villeneuve. "Chromosome Painting Reveals Asynaptic Full Alignment of Homologs and HIM-8–Dependent Remodeling of X Chromosome Territories during Caenorhabditis Elegans Meiosis." *PLoS Genetics* 7, no. 8 (2011): e1002231.

Ohno, S. "Sex Chromosome and Sex-Linked Genes Springer." *Chromosoma* 23, no. 1 (1967): 1–9.

Pak, Julia, and Andrew Fire. "Distinct Populations of Primary and Secondary Effectors During RNAi in *C. Elegans*." *Science* 315, no. 5809 (January 12, 2007): 241–44.

Parhad, Swapnil S., and William E. Theurkauf. "Rapid Evolution and Conserved Function of the PiRNA Pathway." *Royal Society Open Biology* 9, no. 1 (2019): 180181.

Pavelec, Derek M., Jennifer Lachowiec, Thomas F. Duchaine, Harold E. Smith, and Scott Kennedy. "Requirement for the ERI/DICER Complex in Endogenous RNA Interference and Sperm Development in Caenorhabditis Elegans." *Genetics* 183, no. 4 (2009): 1283–95.

Petty, Emily, Emily Laughlin, and Györgyi Csankovszki. "Regulation of DCC Localization by HTZ-1/H2A. Z and DPY-30 Does Not Correlate with H3K4 Methylation Levels." *PLoS One* 6, no. 10 (2011): e25973.

Pferdehirt, R. R., W. S. Kruesi, and B. J. Meyer. "An MLL/COMPASS Subunit Functions in the C. Elegans Dosage Compensation Complex to Target X Chromosomes for Transcriptional

Regulation of Gene Expression." *Genes & Development* 25, no. 5 (March 1, 2011): 499–515.

Phillips, Carolyn M., Chihunt Wong, Needhi Bhalla, Peter M. Carlton, Pinky Weiser, Philip M. Meneely, and Abby F. Dernburg. "HIM-8 Binds to the X Chromosome Pairing Center and Mediates Chromosome-Specific Meiotic Synapsis." *Cell* 123, no. 6 (2005): 1051–63.

Powell, Jennifer R., Margaret M. Jow, and Barbara J. Meyer. "The T-Box Transcription Factor SEA-1 Is an Autosomal Element of the X:A Signal That Determines C. Elegans Sex." *Developmental Cell* 9, no. 3 (2005): 339–49.

Reed, Kailee J., Joshua M. Svendsen, Kristen C. Brown, Brooke E. Montgomery, Taylor N. Marks, Tarah Vijayasarathy, Dylan M. Parker, Erin Osborne Nishimura, Dustin L. Updike, and Taiowa A. Montgomery. "Widespread Roles for PiRNAs and WAGO-Class SiRNAs in Shaping the Germline Transcriptome of Caenorhabditis Elegans." *Nucleic Acids Research* 48, no. 4 (2020): 1811–27.

Reinke, Valerie, Inigo San Gil, Samuel Ward, and Keith Kazmer. "Genome-Wide Germline-Enriched and Sex-Biased Expression Profiles in Caenorhabditis Elegans," 2004.

Rhind, Nicholas R, Leilani M Miller, Jennifer B Kopczynski, and Barbara J Meyer. "Xo1-1 Acts as an Early Switch in the C. Elegans Male/Hermaphrodite Decision." *Cell* 80, no. 1 (1995): 71–82.

Rice, William R. "Sex Chromosomes and the Evolution of Sexual Dimorphism." *Evolution*, 1984, 735–42.

Ruby, J. Graham, Calvin Jan, Christopher Player, Michael J. Axtell, William Lee, Chad Nusbaum, Hui Ge, and David P. Bartel. "Large-Scale Sequencing Reveals 21U-RNAs and

Additional MicroRNAs and Endogenous SiRNAs in C. Elegans." *Cell* 127, no. 6 (2006): 1193–1207.

Sharma, Rahul, Daniel Jost, Jop Kind, Georgina Gómez-Saldivar, Bas van Steensel, Peter Askjaer, Cédric Vaillant, and Peter Meister. "Differential Spatial and Structural Organization of the X Chromosome Underlies Dosage Compensation in C. Elegans." *Genes & Development* 28, no. 23 (2014): 2591–96.

Simon, Matt, Peter Sarkies, Kohta Ikegami, Anna-Lisa Doebley, Leonard D. Goldstein, Jacinth Mitchell, Aisa Sakaguchi, Eric A. Miska, and Shawn Ahmed. "Reduced Insulin/IGF-1 Signaling Restores Germ Cell Immortality to Caenorhabditis Elegans Piwi Mutants." *Cell Reports* 7, no. 3 (2014): 762–73.

Snyder, Martha J., Alyssa C. Lau, Elizabeth A. Brouhard, Michael B. Davis, Jianhao Jiang, Margarita H. Sifuentes, and Györgyi Csankovszki. "Anchoring of Heterochromatin to the Nuclear Lamina Reinforces Dosage Compensation-Mediated Gene Repression." *PLoS Genetics* 12, no. 9 (2016): e1006341.

Strome, Susan, William G. Kelly, Sevinc Ercan, and Jason D. Lieb. "Regulation of the X Chromosomes in Caenorhabditis Elegans." *Cold Spring Harbor Perspectives in Biology* 6, no. 3 (March 1, 2014): a018366.

Tabara, Hiroaki, Madathia Sarkissian, William G. Kelly, Jamie Fleenor, Alla Grishok, Lisa Timmons, Andrew Fire, and Craig C. Mello. "The Rde-1 Gene, RNA Interference, and Transposon Silencing in C. Elegans." *Cell* 99, no. 2 (1999): 123–32.

Tang, Wen, Meetu Seth, Shikui Tu, En-Zhi Shen, Qian Li, Masaki Shirayama, Zhiping Weng, and Craig C. Mello. "A Sex Chromosome PiRNA Promotes Robust Dosage Compensation and Sex Determination in C. Elegans." *Developmental Cell* 44, no. 6 (2018): 762-770. e3.

Torres, Eduardo M., Bret R. Williams, and Angelika Amon. “Aneuploidy: Cells Losing Their Balance.” *Genetics* 179, no. 2 (2008): 737–46.

Vasale, Jessica J., Weifeng Gu, Caroline Thivierge, Pedro J. Batista, Julie M. Claycomb, Elaine M. Youngman, Thomas F. Duchaine, Craig C. Mello, and Darryl Conte. “Sequential Rounds of RNA-Dependent RNA Transcription Drive Endogenous Small-RNA Biogenesis in the ERGO-1/Argonaute Pathway.” *Proceedings of the National Academy of Sciences* 107, no. 8 (2010): 3582–87.

Vielle, Anne, Jackie Lang, Yan Dong, Sevinc Ercan, Chitra Kotwaliwale, Andreas Rechtsteiner, Alex Appert, Q Brent Chen, Andrea Dose, Thea Egelhofer, etc., *et al.,* Julie Ahringer. “H4K20me1 Contributes to Downregulation of X-Linked Genes for C. Elegans Dosage Compensation.” *PLOS Genetics* 8, no. 9 (September 13, 2012): e1002933.

Wan, Gang, Jenny Yan, Yuhan Fei, Daniel J. Pagano, and Scott Kennedy. “A Conserved NRDE-2/MTR-4 Complex Mediates Nuclear RNAi in Caenorhabditis Elegans.” *Genetics* 216, no. 4 (2020): 1071–85.

Weiser, Natasha E., Danny X. Yang, Suhua Feng, Natallia Kalinava, Kristen C. Brown, Jayshree Khanikar, Mallory A. Freeberg, Martha J. Snyder, Györgyi Csankovszki, Raymond C. Chan, Sam G. Gu, Taiowa A. Montgomery, Steven E. Jacobsen, and John K. Kim. “MORC-1 Integrates Nuclear RNAi and Transgenerational Chromatin Architecture to Promote Germline Immortality.” *Developmental Cell* 41, no. 4 (2017): 408–23.

Welker, Noah C., Derek M. Pavelec, David A. Nix, Thomas F. Duchaine, Scott Kennedy, and Brenda L. Bass. “Dicer’s Helicase Domain Is Required for Accumulation of Some, but Not All, C. Elegans Endogenous SiRNAs.” *Rna* 16, no. 5 (2010): 893–903.

Wells, Michael B., Martha J. Snyder, Laura M. Custer, and Gyorgyi Csankovszki. "Caenorhabditis Elegans Dosage Compensation Regulates Histone H4 Chromatin State on X Chromosomes." *Molecular and Cellular Biology* 32, no. 9 (2012): 1710–19.

Yigit, Erbay, Pedro J. Batista, Yanxia Bei, Ka Ming Pang, Chun-Chieh G. Chen, Niraj H. Tolia, Leemor Joshua-Tor, Shohei Mitani, Martin J. Simard, and Craig C. Mello. "Analysis of the C. Elegans Argonaute Family Reveals That Distinct Argonautes Act Sequentially during RNAi." *Cell* 127, no. 4 (2006): 747–57.

CHAPTER 4

Conclusions and Future Directions

Condensin complexes have evolved crucial roles in coordinating the structural changes to chromosomes during cell division (Paul *et al.,* 2019). Their roles in mitosis and meiosis have been well-researched, yet several recent studies have indicated that their interphase roles may be vastly under-appreciated (Albritton and Ercan, 2018; Rosin *et al.,* 2018). However, studies seeking to identify interphase-specific condensin functions in living cells are hampered with the fact that condensin function is crucial to cell division. *in vitro* condensin studies have provided a wealth of data on how condensin is able to interact with chromatin and utilize ATP to produce DNA supercoiling, and studies conducting condensin depletions in post-mitotic cells have provided data on interphase condensin roles (Kimura *et al.,* 1997; Kimura and Hirano, 2000; Kimura *et al.,* 2001; Rawlings *et al.,* 2011; St-Pierre *et al.,* 2009; Hassan *et al.,* 2020). However, *C. elegans* provides the niche opportunity to study interphase condensin within the context of an animal which evolved its own interphase-specific condensin to conduct a chromosome-wide gene regulatory program in dosage compensation (Csankovszki *et al.,* 2009).

In the past few decades we have learned that the DCC is the condensin-containing protein complex orchestrating two-fold gene repression in dosage compensation (Lau *et al.,* 2015). The GRO-seq data shows that RNA polymerase II recruitment is the step of X-linked transcription targeted by the DCC (Kruesi *et al.,* 2013). We also know that chromatin modifications, the assembly of

TADs and X chromosome compaction are all features of *C. elegans* dosage compensation, but we have yet to understand how the DCC achieves such a broad level of repression (Lau *et al.,* 2014; Kramer *et al.,* 2015; Crane *et al.,* 2015).

With this thesis I sought to uncover additional DCC-dependent mechanisms contributing to dosage compensation. In the process, our lab identified two established and conserved chromatin and gene regulatory pathways augmenting DCC function. The genes responsible for the H3K9me3 heterochromatin mark (*met-2* and *set*-25) and nuclear lamina localized genes (*lem-2* and *cec-4*) cooperate to tether the dosage compensated X chromosomes to the nuclear lamina in a DCC-dependent manner to facilitate dosage compensation (Snyder *et al.,* 2016). The nuclear RNAi Argonaute genes *nrde-3* and *hrde-1,* and piRNA pathway Argonaute *prg-1* were also shown to contribute to dosage compensation. These Argonautes contribute to *xol-1* repression and serve a *xol-1*-independent role which includes X chromosome compaction (Tang *et al.,* 2018 and this manuscript).

RNAi depletions and loss of function mutations for the X-signal element (XSE) and nuclear hormone receptor homolog *sex-1* proved to be a crucial tool in our uncovering of the heterochromatin and Argonaute genes contributing to DCC function. The single Argonaute mutants on their own are superficially wild type, and loss of H3K9me3 in *C. elegans* is not of lethal consequence (Guang *et al.,* 2008; Buckley *et al.,* 2012; Towbin *et al.,* 2012). However, the addition of *sex-1* mutations simultaneous with depletions of our heterochromatin/Argonaute positive hits led to a significant rescue of males, and in several cases, synergistically increased hermaphrodite lethality. My work thus provides some further physiological context for the H3K9me3 methyltransferases and Argonaute proteins, whose complete endogenous roles remain an open inquiry. While *sex-1* was established as the most important XSE contributing to *xol-1*

repression in 2007, its *xol-1*-independent (down-stream) role is still unknown (Gladden *et al.,* 2007). In the context of the male rescue assay and hermaphrodite viability data presented in this thesis, the *sex-1* downstream role appears to act redundantly with the heterochromatin tethering (Chapter 2) and Argonaute (Chapter 3) pathways. Determining the downstream role of *sex-1* will likely prove to be a valuable endeavor, as it may uncover additional genes or the missing link to these pathways which appear to be augmentative to dosage compensation.

With regard to the role of the Nuclear RNAi pathway in *C. elegans* dosage compensation, future work should investigate whether the nuclear-localized NRDE complex is also involved in X chromosome compaction and dosage compensation, or test the possibility that the nuclear Argonautes HRDE-1 and NRDE-3 have co-opted a function in dosage compensation outside of the NRDE complex. In the endogenous nuclear RNAi pathway, the actual effector of silencing is the NRDE complex (Guang *et al.,* 2010; Burkhart *et al.,* 2011). In the nucleus, once NRDE-3 or HRDE-1 complexed with an siRNA bind to a target locus being actively transcribed, they recruit the worm specific proteins NRDE-1, NRDE-2, and NRDE-4. NRDE-1. NRDE-2 associates with the pre-mRNA of NRDE-3 target genes to halt transcriptional elongation. Subsequently, NRDE-1 additionally associates with chromatin of the target gene in a NRDE-4-dependent manner to promote the deposition of heterochromatin marks (Guang *et al.,* 2011; Burkhart *et al.,* 2011).

To distinguish whether the NRDE complex is involved in dosage compensation, NRDE-1, NRDE-2, or NRDE-4 mutants could be assessed for the same dosage compensation phenotypes as NRDE-3 and HRDE-1, like X chromosome decondensation or rescue of males. If the NRDE complex is involved in this dosage compensation role, the data would indicate that either silencing or the deposition of heterochromatin marks at specific loci directed by the NRDE complex are the mechanism through which nuclear RNAi promotes dosage compensation. While

the NRDE complex promotes H3K9me3 and H3K27me3 at target loci, these or additional heterochromatin marks directed by the NRDE complex could help coordinate the repressive landscape of the hermaphrodite X chromosomes in representing either an indirect or co-opted, novel role (Gu *et al.,* 2012; Mao *et al.,* 2015). The other possibility of NRDE complex involvement could directly implicate NRDE target genes either as regulators of dosage compensation-promoting genes or a minority of X-linked genes which are de-repressed in Argonaute mutants, similar to *xol-1.* However, it's important to note that while the DCC mediates downregulation of X-linked genes by limiting RNA polymerase II recruitment to the X chromosomes, NRDE silencing targets transcriptional elongation to silence genes (Guang *et al.,* 2010; Kruesi *et al.,* 2013). Thus, it would have to be a minority of genes being silenced by the NRDE complex to function in dosage compensation. In this context, a follow-up ChIP-seq analysis of NRDE complex binding patterns may uncover specific loci or even a general X chromosome enrichment pattern which would help inform the model.

Conversely, if the NRDE complex turns out to be dispensable for dosage compensation, then perhaps the HRDE-1 and NRDE-3 Argonaute proteins have adopted a non-canonical function to directly modulate chromatin in the absence of NRDE-mediated silencing. The NRDE-3 and HRDE-1 Argonaute proteins belong to a distinct Argonaute family characterized by 12 worm-specific Argonautes, thus unknown functionality within the worm-specific domains may confer some activity related to DCC function (Yigit *et al.,* 2006; Swarts *et al.,* 2014) (Figure 4.1). However, PRG-1, HRDE-1, and NRDE-3 all contain a PAZ domain with amino acid residues forming a predicted nucleic acid-binding interface (Figure 4.2) (Yigit *et al.,* 2006). This PAZ domain is a conserved and essential domain for Argonautes to target and bind siRNAs (Swarts *et al.,* 2014). Thus, in order to test the requirement of Argonaute's ability to bind RNA

for its role in compacting the X chromosomes, FISH experiments assaying the X chromosome decondensation phenotype on mutant PAZ domain Argonautes would inform the model. The NRDE-3 and HRDE-1 worm-specific Argonautes also lack a characteristic slicer motif, however the slicer motif appears to be intact in PRG-1 (Figure 4.3) (Yigit *et al.,* 2006). Similar FISH experiments to assay for X chromosome decondensation in hermaphrodites with the PRG-1 slicer motif residues from Asp, Asp, His, to a triad of residues predicted to elimate the metal coordinating which conveys enzymatic slicer activity, such as Gly, Thr, Asn, would test the requirement for PRG-1 slicer activity in its dosage compensation roles.

Its also possible that the heterochromatin tethering pathway and nuclear RNAi pathway are coordinating together in the same role for dosage compensation. This is a feasible idea because the nuclear RNAi pathway targets loci for the deposition of heterochromatin marks like H3K9me3 which are required for the anchoring of the X chromosomes to the nuclear lamina. It's possible that the nuclear RNAi pathway serves to initiate the anchoring sites for the tethering of heterochromatin, in a shared role to reinforce dosage compensation. The analysis of dosage compensation phenotypes in worm strains with mutations representing both pathways is currently under investigation in our lab to determine whether the contribution of these pathways is additive or redundant. For instance, if a *met-2 set-25 nrde-3* mutant exhibits a higher degree of male rescue than the *nrde-3* or *met-2 set-25* mutant on their own, we would hypothesize that the two pathways contribute separately. Conversely, if the two pathways show redundancy, an intriguing question of how the nuclear Argonautes and heterochromatin tethering pathway interact to promote dosage compensation would be fascinating to follow up on.

The germline-enriched expression pattern of PRG-1 in the context of its role in dosage compensation is also of interest. While we know that PRG-1 and the piRNA pathways are

responsible for contributing to *xol-1* repression in the early embryo, the *xol-1* independent X chromosome compaction mediated by PRG-1 suggests that PRG-1 may be responsible for contributing to an epigenetic chromatin signature which direct X chromosome compaction in the adult somatic tissues (Tang *et al.,* 2018). One hypothesis might involve the transgenerational inheritance of a subset of PRG-1-dependent secondary siRNAs which initiate heterochromatin on dosage compensated X chromosomes. Consistent with this hypothesis is the fact that *ergo-1* mutants do not exhibit X chromosome decondensation phenotypes. This suggests that primary siRNAs are not involved in this role, however the piRNA pathway does not utilize primary siRNAs but rather uses piRNAs as a precursor to its secondary siRNAs. Follow up experiments should be directed at assessing whether PRG-1 is required in the germline to confer somatic X chromosome compaction. With germline-deficient RNAi mutants, the knockdown of *prg-1* would test the requirement for germline enriched, PRG-1-dependent siRNAs in mediating somatic X chromosome compaction. Germline-deficient RNAi could be accomplished in a mutant background of an *rde-1(ne291)* null mutant, which is resistant to RNAi treatment, simultaneous with a wild type copy of *rde-1* expressed under the *elt-2* gut-cell specific promoter (Tabara *et al,* 1999). This would only enable RNAi knockdown of *prg-1* in the somatic gut cells which are being assayed for X chromosome compaction. Importantly, this experiment should be extended across several generations to allow for the complete loss of epigenetic signature allowing for the secondary siRNA pool to completely deplete (Ashe *et al.,* 2012). Reciprocal experiments may also be conducted with gut-cell defective RNAi strains, using the same *prg-1(RNAi)* treatment to test the requirement for PRG-1 in the somatic cells in which the X compaction is detected with our FISH assays. The gut-cell defective RNAi strains could be accomplished in a mutant background of an *rde-1(ne291)* null mutant, which is resistant to RNAi

treatment, simultaneous with a wild type copy of *rde-1* expressed under the *sun-1* germline-specific promoter (Zou *et al.,* 2019). This would only enable RNAi knockdown of *prg-1* in the germline cells to determine if *prg-1* is only required in the soma for X chromosome compaction.

Additional indirect roles for nuclear Argonautes in dosage compensation may also be related to the crosstalk of histone modifications. H3K4me3 is a chromatin modification associated with the promoters of active genes (Santos-Rosa *et al.,* 2002). In *C. elegans,* there is an antagonistic relationship between the H3K4me3 active chromatin modification, and the repressive H3K9me3 mark (Greer *et al.,* 2014). Loss of function mutations in *jmjd-2*, the gene encoding the demethylase responsible for removing methyl marks from H3K9me3, suppresses the transgenerational sterility phenotype caused by loss of function mutations in *spr-5*, the gene encoding the demethylase for H4K3me3 (Greer *et al.,* 2014). These data highlight the fact that maintaining of the proper balance of each histone modification is important for fertility in *C. elegans* over several generations. The DPY-30 protein is part of the DCC, but also maintains a distinct, independent role in the conserved MLL/COMPASS complex, which is responsible for depositing H3K4me3 at active gene promoters (Petty *et al.,* 2011). While both the heterochromatin tethering pathway and nuclear RNAi pathways are responsible for H3K9me3 at their respective target loci, we have shown that mutants for both pathways exhibit common dosage compensation phenotypes such as X chromosome decondensation. An intriguing hypothesis for the role of these pathways in dosage compensation could be that the lack of H3K9me3 in these mutant backgrounds may lead to increased H3K4me3. If ectopic MLL/COMPASS activity was detected in these mutants, where H3K4me3 is less restricted by H3K9me3, it's possible that DPY-30 is being sequestered from its DCC role and being over-represented in its MLL/COMPASS role (Figure 4.4). The lack of DPY-30 acting in its DCC role

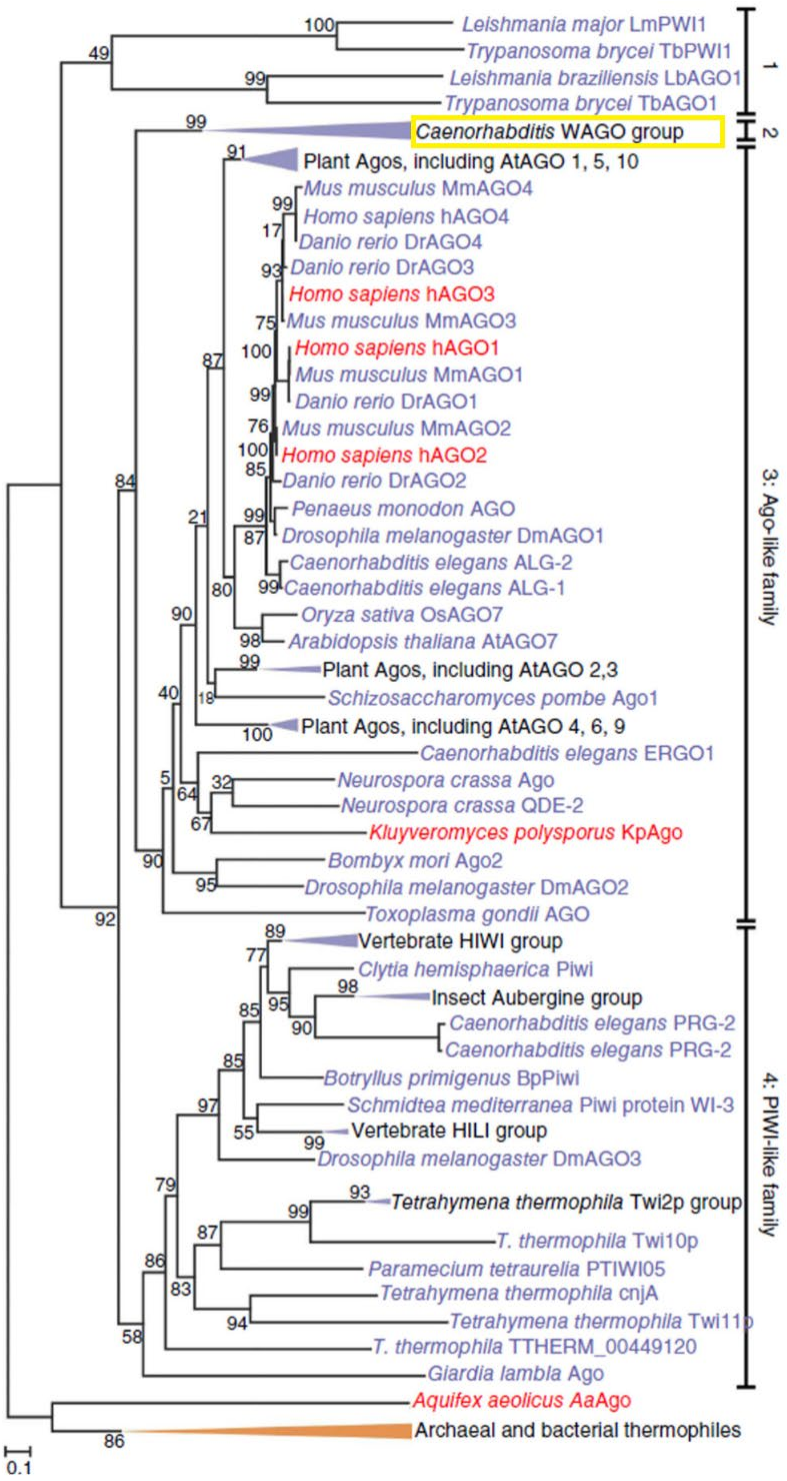

Figure 4.1 Phylogeny of Argonaute Proteins The phylogenetic tree of Argonaute proteins highlights 4 distinct families across all species of life. Worm-specific Argonautes (WAGOs) comprise 12 of the 27 Argonautes in the *C. elegans* genome and constitute a distinct Argonaute family (2). This figure is modified from Swarts *et al.,* 2014.

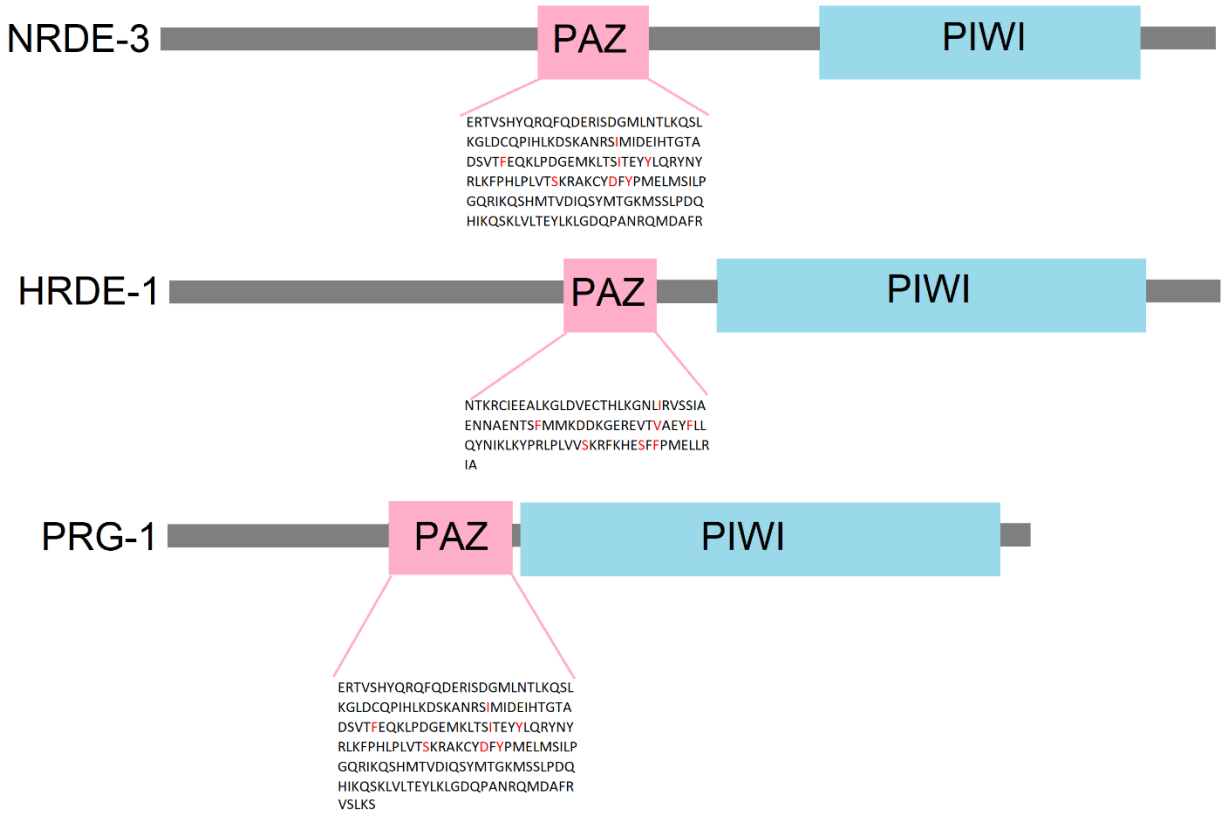

Figure 4.2 Structure of Nuclear Argonaute Proteins and piRNA Argonaute PRG-1 NRDE-3, HRDE-1, and PRG-1 all contain PAZ and PIWI domains which bind the 3' end of siRNAs and 5' end of the guide RNA respectively. The PAZ domains of each Argonaute protein contain a predicted nucleic acid binding interface (red letters).

PRG-1	TMIVGY DL...ILYR DGAG...VPAPCQYA HKLAF
NRDE-3	TQFIGF EM...VVYR VGSG...IPNVSYAA QNLAK
HRDE-1	VQFIGF EI...VIYR VGAG...VPDVLYAA ENLAK

Figure 4.3 Slicer Motifs in PIWI domain of Nuclear Argonautes and PRG-1. The Aspartic Acid (red), Aspartic Acid (red), Histidine (blue) catalytic triad which confers slicer activity in the PIWI domain of Argonaute proteins is present in PRG-1. NRDE-3 and HRDE-1 Argonautes contain Glutamic Acid (Orange) substitutes but lack a complete catalytic triad to confer predicted slicer activity. This figure is modified from Yigit *et al.,* 2006.

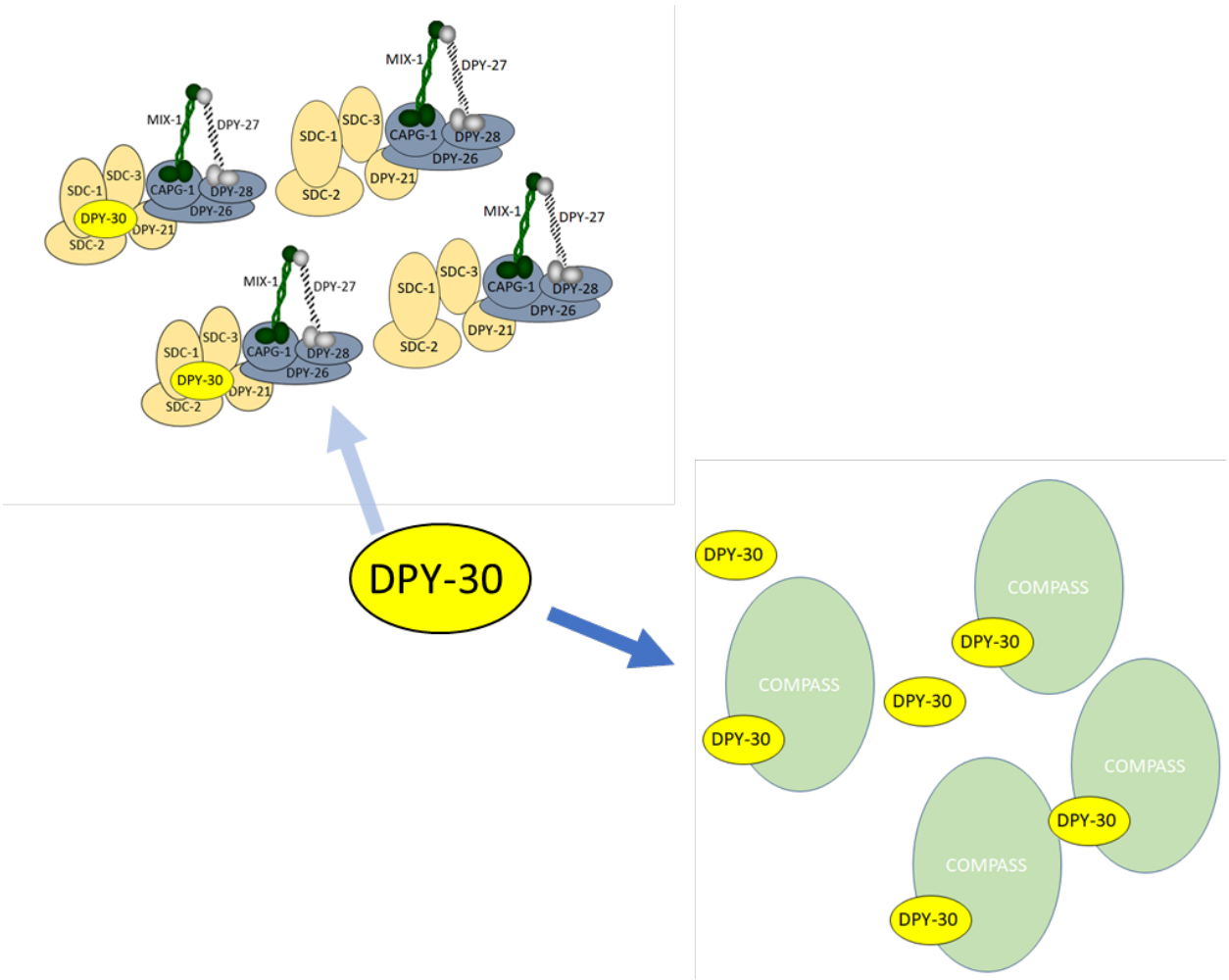

Figure 4.4 Model for DPY-30 sequestration from DCC to MLL/COMPASS role. The MLL/COMPASS complex promotes H3K4me3 at active gene promoters, which is antagonistic to H3K9me3. In nuclear RNAi and heterochromatin tethering mutants, the loss of H3K9me3 may lead to increased MLL/COMPASS activity, sequestering DPY-30 from its DCC role and partially destabilizing dosage compensation.

may cause some DCC instability, partially de-stabilizing dosage compensation. Whether or not it's correct, this DPY-30 hypothesis should spark an open inquiry into the idea that crosstalk between histone modifications could be an overarching explanation for heterochromatin pathway involvement in dosage compensation. The idea is also favorable from the standpoint that the X-linked gene repression in *C. elegans* dosage compensation is not characterized by the complete shut down of transcription, but rather a significant decrease in the accessibility of RNA polymerase II to the X chromosomes. While we understand that H4K20me1 is one chromatin modification contributing to this repressive landscape, the combinatorial effects of a complex heterochromatin signature may have been invoked for *C. elegans* to evolve a state of "tuned down" gene expression, as opposed to "turned off" as in mammalian X inactivation.

While the work of this thesis is limited to the study of *C. elegans* biology, a translational connection, if any, is that an interphase-specific condensin is interacting with multiple conserved pathways involved in chromatin and gene regulation. This is not to say that condensin is functioning similarly in humans, but rather that the capacity for these conserved condensin complexes to coordinate with other endogenous pathways is clearly there.

A common theme between the nuclear RNAi and heterochromatin tethering pathway data is that they represent small but significant contributions to X-linked gene repression. Taken at face value, this work provides insights into additional pathways contributing with the DCC to dosage compensation, however we are only seeing how these genes are contributing *today.* The existence of a 10-protein complex which spreads along the X chromosomes to robustly orchestrate two-fold genes repression clearly did not evolve overnight. And while we lack the resolution to ascertain the step-by-step evolution of dosage compensation in *C. elegans*, some of these pathways which contribute to dosage compensation may be evolutionary remnants of a

more dominant repressive mechanism from another time. It's easy to envision how one pathway is selected by nature to coordinate X-linked gene repression, and then serves as a buffer for the next, more efficient pathway to evolve and eventually become the predominant mechanism. There must be a reason for the expansion to 27 Argonautes in the *C. elegans* genome and indeed a reason why this organism today does not require the H3K9me3 chromatin modification to survive today (Yigit *et al.,* 2006; Towbin *et al.,* 2012). Perhaps these pathways were among the many previous iterations and/or buffering mechanisms on the evolutionary path which has led to the well-oiled machine that is the DCC.

REFERENCES

Albritton, Sarah Elizabeth, and Sevinç Ercan. "Caenorhabditis Elegans Dosage Compensation: Insights into Condensin-Mediated Gene Regulation." *Trends in Genetics* 34, no. 1 (2018): 41–53.

Ashe, Alyson, Alexandra Sapetschnig, Eva-Maria Weick, Jacinth Mitchell, Marloes P. Bagijn, Amy C. Cording, Anna-Lisa Doebley, Leonard D. Goldstein, Nicolas J. Lehrbach, and Jérémie Le Pen, Greta Pintacuda, Aisa Sakaguchi, Peter Sarkies, Shawn Ahmed and Eric A. Miska. "PiRNAs Can Trigger a Multigenerational Epigenetic Memory in the Germline of C. Elegans." *Cell* 150, no. 1 (2012): 88–99.

Buckley, Bethany A., Kirk B. Burkhart, Sam Guoping Gu, George Spracklin, Aaron Kershner, Heidi Fritz, Judith Kimble, Andrew Fire, and Scott Kennedy. "A Nuclear Argonaute Promotes Multigenerational Epigenetic Inheritance and Germline Immortality." *Nature* 489, no. 7416 (2012): 447–51.

Burkhart, Kirk B., Shouhong Guang, Bethany A. Buckley, Lily Wong, Aaron F. Bochner, and Scott Kennedy. "A Pre-MRNA–Associating Factor Links Endogenous SiRNAs to Chromatin Regulation." *PLoS Genetics* 7, no. 8 (2011): e1002249.

Crane, Emily, Qian Bian, Rachel Patton McCord, Bryan R. Lajoie, Bayly S. Wheeler, Edward J. Ralston, Satoru Uzawa, Job Dekker, and Barbara J. Meyer. "Condensin-Driven Remodelling of X Chromosome Topology during Dosage Compensation." *Nature* 523, no. 7559 (2015): 240–44.

Csankovszki, Gyorgyi, Karishma Collette, Karin Spahl, James Carey, Martha Snyder, Emily Petty, Uchita Patel, Tomoko Tabuchi, Hongbin Liu, and Ian McLeod, James Thompson, Ali Sarkeshik, John Yates, Barbara J. Meyer, and Kristin Hagstrom. "Three Distinct Condensin

Complexes Control C. Elegans Chromosome Dynamics." *Current Biology* 19, no. 1 (2009): 9–19.

Gladden, John M., Behnom Farboud, and Barbara J. Meyer. "Revisiting the X: A Signal That Specifies Caenorhabditis Elegans Sexual Fate." *Genetics* 177, no. 3 (2007): 1639–54.

Greer, Eric L., Sara E. Beese-Sims, Emily Brookes, Ruggero Spadafora, Yun Zhu, Scott B. Rothbart, David Aristizábal-Corrales, Shuzhen Chen, Aimee I. Badeaux, and Qiuye Jin, Wei Wang, Brian D. Strahl, Monica P. Colaiácovo, and Yang Shi. "A Histone Methylation Network Regulates Transgenerational Epigenetic Memory in C. Elegans." *Cell Reports* 7, no. 1 (2014): 113–26.

Gu, Sam Guoping, Julia Pak, Shouhong Guang, Jay M. Maniar, Scott Kennedy, and Andrew Fire. "Amplification of SiRNA in Caenorhabditis Elegans Generates a Transgenerational Sequence-Targeted Histone H3 Lysine 9 Methylation Footprint." *Nature Genetics* 44, no. 2 (2012): 157–64.

Guang, Shouhong, Aaron F. Bochner, Kirk B. Burkhart, Nick Burton, Derek M. Pavelec, and Scott Kennedy. "Small Regulatory RNAs Inhibit RNA Polymerase II during the Elongation Phase of Transcription." *Nature* 465, no. 7301 (2010): 1097–1101.

Guang, Shouhong, Aaron F. Bochner, Derek M. Pavelec, Kirk B. Burkhart, Sandra Harding, Jennifer Lachowiec, and Scott Kennedy. "An Argonaute Transports SiRNAs from the Cytoplasm to the Nucleus." *Science* 321, no. 5888 (2008): 537–41.

Hassan, Amira, Pablo Araguas Rodriguez, Stefan K. Heidmann, Emma L. Walmsley, Gabriel N. Aughey, and Tony D. Southall. "Condensin I Subunit Cap-G Is Essential for Proper Gene Expression during the Maturation of Post-Mitotic Neurons." *Elife* 9 (2020): e55159.

Kimura, Keiji, Olivier Cuvier, and Tatsuya Hirano. “Chromosome Condensation by a Human Condensin Complex InXenopus Egg Extracts.” *Journal of Biological Chemistry* 276, no. 8 (2001): 5417–20.

Kimura, Keiji, and Tatsuya Hirano. “ATP-Dependent Positive Supercoiling of DNA by 13S Condensin: A Biochemical Implication for Chromosome Condensation.” *Cell* 90, no. 4 (1997): 625–34.

Kimura, Keiji, and Tatsuya Hirano. “Dual Roles of the 11S Regulatory Subcomplex in Condensin Functions.” *Proceedings of the National Academy of Sciences* 97, no. 22 (2000): 11972–77.

Kramer, Maxwell, Anna-Lena Kranz, Amanda Su, Lara H. Winterkorn, Sarah Elizabeth Albritton, and Sevinc Ercan. “Developmental Dynamics of X-Chromosome Dosage Compensation by the DCC and H4K20me1 in C. Elegans.” *PLoS Genetics* 11, no. 12 (2015): e1005698.

Kruesi, William S., Leighton J. Core, Colin T. Waters, John T. Lis, and Barbara J. Meyer. “Condensin Controls Recruitment of RNA Polymerase II to Achieve Nematode X-Chromosome Dosage Compensation.” *Elife* 2 (2013): e00808.

Lau, Alyssa C., and Györgyi Csankovszki. “Condensin-Mediated Chromosome Organization and Gene Regulation.” *Frontiers in Genetics* 5 (2015): 473.

Lau, Alyssa C., Kentaro Nabeshima, and Györgyi Csankovszki. “The C. Elegans Dosage Compensation Complex Mediates Interphase X Chromosome Compaction.” *Epigenetics & Chromatin* 7, no. 1 (2014): 1–16.

Mao, Hui, Chengming Zhu, Dandan Zong, Chenchun Weng, Xiangwei Yang, Hui Huang, Dun Liu, Xuezhu Feng, and Shouhong Guang. “The Nrde Pathway Mediates Small-RNA-

Directed Histone H3 Lysine 27 Trimethylation in Caenorhabditis Elegans." *Current Biology* 25, no. 18 (2015): 2398–2403.

Paul, Matthew Robert, Andreas Hochwagen, and Sevinç Ercan. "Condensin Action and Compaction." *Current Genetics* 65, no. 2 (2019): 407–15.

Petty, Emily, Emily Laughlin, and Györgyi Csankovszki. "Regulation of DCC Localization by HTZ-1/H2A. Z and DPY-30 Does Not Correlate with H3K4 Methylation Levels." *PLoS One* 6, no. 10 (2011): e25973.

Rawlings, Jason S., Martina Gatzka, Paul G. Thomas, and James N. Ihle. "Chromatin Condensation via the Condensin II Complex Is Required for Peripheral T-cell Quiescence." *The EMBO Journal* 30, no. 2 (2011): 263–76.

Rosin, Leah F., Son C. Nguyen, and Eric F. Joyce. "Condensin II Drives Large-Scale Folding and Spatial Partitioning of Interphase Chromosomes in Drosophila Nuclei." *PLoS Genetics* 14, no. 7 (2018): e1007393.

Santos-Rosa, Helena, Robert Schneider, Andrew J. Bannister, Julia Sherriff, Bradley E. Bernstein, NC Tolga Emre, Stuart L. Schreiber, Jane Mellor, and Tony Kouzarides. "Active Genes Are Tri-Methylated at K4 of Histone H3." *Nature* 419, no. 6905 (2002): 407–11.

Snyder, Martha J., Alyssa C. Lau, Elizabeth A. Brouhard, Michael B. Davis, Jianhao Jiang, Margarita H. Sifuentes, and Györgyi Csankovszki. "Anchoring of Heterochromatin to the Nuclear Lamina Reinforces Dosage Compensation-Mediated Gene Repression." *PLoS Genetics* 12, no. 9 (2016): e1006341.

St-Pierre, Julie, Mélanie Douziech, Franck Bazile, Mirela Pascariu, Eric Bonneil, Véronique Sauvé, Hery Ratsima, and Damien D'Amours. "Polo Kinase Regulates Mitotic

Chromosome Condensation by Hyperactivation of Condensin DNA Supercoiling Activity." *Molecular Cell* 34, no. 4 (2009): 416–26.

Swarts, Daan C., Kira Makarova, Yanli Wang, Kotaro Nakanishi, René F. Ketting, Eugene V. Koonin, Dinshaw J. Patel, and John Van Der Oost. "The Evolutionary Journey of Argonaute Proteins." *Nature Structural & Molecular Biology* 21, no. 9 (2014): 743–53.

Tabara, Hiroaki, Madathia Sarkissian, William G. Kelly, Jamie Fleenor, Alla Grishok, Lisa Timmons, Andrew Fire, and Craig C. Mello. "The Rde-1 Gene, RNA Interference, and Transposon Silencing in C. Elegans." *Cell* 99, no. 2 (1999): 123–32.

Tang, Wen, Meetu Seth, Shikui Tu, En-Zhi Shen, Qian Li, Masaki Shirayama, Zhiping Weng, and Craig C. Mello. "A Sex Chromosome PiRNA Promotes Robust Dosage Compensation and Sex Determination in C. Elegans." *Developmental Cell* 44, no. 6 (2018): 762-770. e3.

Towbin, Benjamin Daniel. "Dynamics of Subnuclear Chromatin Organization during" C. Elegans" Development: A Role for H3K9 Methylation." University_of_Basel, 2012.

Yigit, Erbay, Pedro J. Batista, Yanxia Bei, Ka Ming Pang, Chun-Chieh G. Chen, Niraj H. Tolia, Leemor Joshua-Tor, Shohei Mitani, Martin J. Simard, and Craig C. Mello. "Analysis of the C. Elegans Argonaute Family Reveals That Distinct Argonautes Act Sequentially during RNAi." *Cell* 127, no. 4 (2006): 747–57.

Zou, Lina, Di Wu, Xiao Zang, Zi Wang, Zixing Wu, and Di Chen. "Construction of a Germline-Specific RNAi Tool in C. Elegans." *Scientific Reports* 9, no. 1 (2019): 1–10.